Title
Multi-scale Modeling of Soil Microbial Control on Terrestrial Carbon Cycle

Author
He, Liyuan

Publication Date
2022

Peer reviewed|Thesis/dissertation

Multi-scale Modeling of Soil Microbial Control on Terrestrial Carbon Cycle

By

Liyuan He

DISSERTATION

Submitted in partial satisfaction of the requirements for the degree of

DOCTOR OF PHILOSOPHY

in

Ecology

in the

OFFICE OF GRADUATE STUDIES

of the

UNIVERSITY OF CALIFORNIA DAVIS

and

SAN DIEGO STATE UNIVERSITY

Approved:

Xiaofeng Xu, Chair

Jorge L. Mazza Rodrigues

Chun-Ta Lai

David A. Lipson

Melanie A. Mayes

2022

Acknowledgments

I want to say thanks to everyone with my Ph.D. research. I would like to thank my advisor, Dr. Xiaofeng Xu, for his great patience and trust, helpful guidance, and ample inspiration. His enthusiasm, diligence, and insights in academic research motivated me to push my research forward and pursue my lifelong dream as a great scientist. Also, I want to thank my UC-Davis advisor, Dr. Jorge Rodrigues, for warmly welcoming me into his group and guiding me and continued support when I spent my second year at UC Davis and beyond. I want to thank Drs. David Lipson and Chun-Ta Lai for being on both my qualifying and dissertation committees. I would also like to thank Drs. Valerie Eviner, Fernando De Sales, and William Horwath for being on my qualifying committee and Dr. Melanie Mayes for being on my dissertation committee. Their invaluable comments on my research and edits on my writing are substantially helpful in completing this research and finalizing the dissertation.

I give thanks to members of Xu and Rodrigues labs for their academic and emotional support. Those who gave me rides and hung out with me. I want to give special thanks to Fazhu Zhao and Yihui Wang for helping me get through tough times during the pandemic by talking to me and sharing their thoughts and feelings with me. I thank the JDPE and GGE cohorts for happy memories from retreats and parties. I give special thanks to Brianne Palmer, my cohort and friend also, who helped me overcome obstacles when I first came to the United States, encouraged me to try new things, invited me to her Sparlmer trivia to help me overcome loneliness during the pandemic, and took me to national parks, baseball games, and beaches. I also want to thank Mrs. Patti Swinford, Medora Bratlien, Jamie Rhine, Cecilia Arpallan, and JoAnna Lewis for their help on program paper works.

I am deeply grateful to my parents and my brother and sister and their families for their unconditional love and support. Also, I give thanks to my friends, who came to me, talked to me, and supported me.

Abstract

Bacteria and fungi, representing two major soil microorganism groups, play an important role in the global carbon (C) cycle. Despite the critical role of fungi and bacteria in C cycling, our understanding of their roles in terrestrial C cycling was still unclear. In this dissertation, I investigated the biogeography of fungi and bacteria using a synthesized global dataset of fungal (FBC) and bacterial (BBC) biomass C of 0-30 cm. We observed clear distribution patterns of FBC, BBC, and FBC:BBC (F:B) ratio along latitude and environmental gradients including mean annual temperature, mean annual precipitation, net primary productivity, root C density, soil temperature, soil moisture, and edaphic factors. Fungal and bacterial biomass C and their ratio were dominated by different factors, with FBC and BBC predominated by edaphic properties and F:B ratio determined by climates. Combining the empirical model developed for F:B ratio with a global dataset of soil microbial biomass C, we estimated global stocks of living microbial biomass C as 12.6 (6.6~16.4) PgC for FBC and 4.3 (0.5~10.3) PgC for BBC in topsoil. To mechanistically understand microbial role in terrestrial C cycling, I first parametrized the CLM-Microbe model, a microbial-explicit model with fungal and bacterial regulatory role on soil processes represented, using the compiled time-series data of FBC and BBC from nine natural terrestrial biomes. The parameterization suggested the reasonable performance of the CLM-Microbe model in capturing the seasonal dynamics of FBC and BBC across biomes. On overage, the CLM-Microbe model explained 70% of the variation in FBC (P<0.001) and 26% of the variation in BBC (P<0.05) across biomes. Sensitivity analysis showed that microbial turnover rates, biomass carbon-to-nitrogen ratio, and assimilation efficiency were the most important parameters regulating FBC and BBC dynamics. Then, we applied the CLM-Microbe model and investigated the impacts of microbial seasonality on soil C cycling in terrestrial ecosystems. Removing soil microbial seasonality reduced model performance in simulating microbial respiration and soil respiration but led to slight differences in simulating root respiration. Removing soil microbial seasonality underestimated annual averages of soil C emission (by 0.6%-32% for microbial respiration and by 0.4%-29% for soil respiration) and overestimated soil organic C content in the top 1 m

(by 0.2%-7%) in natural biomes. Finally, we investigated the historical dynamics of terrestrial C fluxes and pools during 1901-2016 using the CLM-Microbe model. The CLM-Microbe model can reproduce the global distribution of gross (GPP; R^2=0.78) and net (NPP; R^2=0.63) primary productivity, heterotrophic (HR; R^2=0.23) and soil (SR; R^2=0.26) respiration, microbial (MBC), the sum of fungal (FBC) and bacterial (BBC), biomass C in the top 30 cm (R^2=0.22 for FBC and R^2=0.32 for BBC) and 1 m (R^2=0.21 for MBC), and dissolved (DOC; R^2=0.2 for 0-30 cm and R^2=0.22 for 0-1 m) and soil (SOC; R^2=0.36 for 0-30 cm and R^2=0.26 for 0-1 m) organic C in the top 30 cm and 1 m. The C fluxes and pool sizes increased by about 30 PgC yr^{-1} for GPP, 15 PgC yr^{-1} for NPP, 12 PgC yr^{-1} for HR, 25 PgC yr^{-1} for SR, 1.0 PgC for FBC and 0.4 PgC for BBC in 0-30 cm, 1.5 PgC for FBC, 0.8 PgC for BBC, 2.5 PgC for DOC, 40 PgC for SOC, and 5 PgC for litter C (LitC) in 0-1 m, and 40 PgC for vegetation C (VegC) from 1901 to 2016. Except for DOC in the top 1 m (increased most in Asia and North America), the absolute increases of C fluxes and pools were the largest in Asia and South America, particularly in east Asia and central and northern South America. Relative changes of C fluxes and pools exhibited different spatial patterns: the relative increase was the largest in Asia and Europe, particularly in east Asia and southern and central Europe, for GPP, NPP, HR, and SR, in South America (central and east coast of South America in particular) for FBC (0-30 cm and 0-1 m), in Europe (central and northern Europe in particular) for BBC (0-30 cm and 0-1 m), in Europe (central and northern Europe in particular) and South America (east coast of South America in particular) for DOC (0-1 m), in Arica (central and southern Africa in particular) for SOC (0-1 m), and in Europe (southern and central Europe in particular) for VegC and LitC (0-1 m). Increases in GPP, NPP, and VegC were closely related to warming and climbing precipitation, while soil C fluxes and litter, microbial, and soil C pools were jointly governed by vegetation C input and soil temperature and moisture. This study advanced our understanding of fungal and bacterial biogeography and assisted our mechanistic understanding of the microbial role in the terrestrial C cycle, providing valuable insights into the C cycle research under a changing climate.

Table of Contents

Introduction

Ongoing global climate change caused by human-induced increases in greenhouse gases, altered precipitation pattern, rising sea level, and rising air temperature has induced profound influences on global carbon (C) and nutrient cycle, representing one of the biggest challenges for the upcoming decades (Hasselmann et al. 2003, Zeng et al. 2008, Peters et al. 2012, Keohane 2015). Providing reliable estimation of the soil C cycle is critical for policymakers and communities in dealing with regional and global climate change (Heimann and Reichstein 2008, IPCC 2014). Huge uncertainties of the projection results among models challenged the current model framework (Taylor et al. 2011, Luo et al. 2015), the implicit representation of soil microbes may account for the great uncertainty in the global C cycle projection (Fang et al. 2005, Wieder et al. 2013, Wieder et al. 2015).

Soil microbes influence various ecosystem processes (Crowther et al. 2019), including C cycling (HoÈgberg et al. 2001), soil formation (Rillig and Mummey 2006), and nutrient availability (Turner et al. 2013). In addition, soil microbial groups, such as fungi and bacteria, are different in their role in soil biogeochemical processes (Boer et al. 2005). For example, bacteria and fungi have different physiological traits, e.g., bacteria prefer to decompose litter low in carbon-to-nitrogen (C:N) ratio, while fungi tend to decompose litter with higher C:N ratios (Paul 2016). Incorporating microbial role into ESMs requires a clear understanding of the distribution of soil microbes and the underlying mechanisms (Wieder et al. 2013, Xu et al. 2014). However, our knowledge of soil microbial, particularly fungal and bacterial, biogeography is still in its infancy due to the technical limitation and great heterogeneity of soil microbes.

Although the importance of soil microbes on the global C cycle has been widely recognized (Falkowski et al. 2008) and major soil microbial processes have been identified in the last decades, soil microbial processes are poorly represented in ESMs (Wieder et al. 2015). The ESMs implicitly represent biological activity in soil organic matter (SOM) mineralization as proportional to the soil C stock. The transfer of C

among different pools is regulated by environmental scalars (Jenkinson et al. 1987, Parton et al. 1987, Rodrigo et al. 1997). However, the regulatory roles of microbes in those soil processes are overlooked (Hodge et al. 2000, Talbot et al. 2008, Schimel and Schaeffer 2012). The development of soil microbial models, such as the SCAMPS model (Sistla et al. 2014), DAISY model (Svendsen et al. 1995), DAMM model (Davidson et al. 2012), and MEND model (Allison et al. 2010), proved to be powerful tools for improving our understanding of soil C processes. However, these models assumed that biological responses to environmental and edaphic conditions are invariant and microbial communities are functionally equivalent (Bradford and Fierer 2012). While soil microbial community is not static, showing strong temporal dynamics (Díaz-Raviña et al. 1995, Lipson et al. 2002, Lipson and Schmidt 2004, Cleveland et al. 2007). Recently, the further classification of soil microbes in the TRIPLEX-Microbe model (active and dormant components) and MIMICS model (K- and r-strategists) advanced the representation of soil microbial community in ESMs (Wieder et al. 2014, Wang et al. 2017). However, the distinct role of functional groups within active soil microbes in soil processes may lead to different trajectories of C responses to changing environments such as atmospheric nitrogen (N) deposition, elevated carbon dioxide (CO_2), and precipitation change (Hopkins et al. 2006, Strickland and Rousk 2010, Rousk and Bååth 2011, Bell et al. 2014). The theoretical characterization of the r-K continuum may limit using observational data to constrain the microbial parameters.

The CLM-Microbe model (available at https://github.com/email-clm) represents the soil microbial community with fungi and bacteria, two major soil microbial groups and playing distinct roles in soil processes (He et al. 2021). The CLM-Microbe model explicitly represents fungi- and bacteria-regulated processes such as SOM and litter decomposition, SOM stabilization, microbial C assimilation from SOM and litter, microbial death, and heterotrophic respiration into the CLM (He et al. 2021). Different parameters for fungi- and bacteria-regulated functions are used to distinguish the physiological traits of fungi and bacteria in soil processes. The CLM-Microbe model can simulate fungal and bacterial biomass

dynamically and can capture fine time-scale variations of the C cycle based on the fine resolution of forcing data input. Therefore, I can use the CLM-Microbe model to simulate fungal and bacterial biomass and investigate the controls of soil microbes on the terrestrial C cycle.

In this dissertation, I first synthesized fungal and bacterial biomass measurements from publications. Then, I parameterized the soil microbial biomass module and applied the parameterized CLM-Microbe model to investigate and understand effects and mechanisms of soil microbes on the C cycle. The specific research objectives of my four chapters are:

1. Identifying the biogeography of soil fungal and bacterial biomass.
2. Estimating parameters for simulating soil fungal and bacterial biomass dynamics in the CLM-Microbe model.
3. Modeling the effects of soil fungal and bacterial biomass dynamics on the C cycle at site scale using the CLM-Microbe model.
4. Investigating the historical dynamics of the terrestrial C cycle using the CLM-Microbe model.

Reference

Allison, S. D., M. D. Wallenstein, and M. A. Bradford. 2010. Soil-carbon response to warming dependent on microbial physiology. Nature Geoscience **3**:336-340.

Bell, C. W., D. T. Tissue, M. E. Loik, M. D. Wallenstein, V. A. Martinez, R. A. Erickson, and J. C. Zak. 2014. Soil microbial and nutrient responses to 7 years of seasonally altered precipitation in a Chihuahuan Desert grassland. Global change biology **20**:1657-1673.

Boer, W. d., L. B. Folman, R. C. Summerbell, and L. Boddy. 2005. Living in a fungal world: impact of fungi on soil bacterial niche development. FEMS Microbiology Reviews **29**:795-811.

Bradford, M. A., and N. Fierer. 2012. The biogeography of microbial communities and ecosystem processes: implications for soil and ecosystem models. Soil ecology and ecosystem services **18**.

Cleveland, C. C., D. R. Nemergut, S. K. Schmidt, and A. R. Townsend. 2007. Increases in soil respiration following labile carbon additions linked to rapid shifts in soil microbial community composition. Biogeochemistry **82**:229-240.

Crowther, T. W., J. v. d. Hoogen, J. Wan, M. A. Mayes, A. D. Keiser, L. Mo, C. Averill, and D. S. Maynard. 2019. The global soil community and its influence on biogeochemistry. Science **365**:eaav0550.

Davidson, E. A., S. Samanta, S. S. Caramori, and K. Savage. 2012. The Dual Arrhenius and Michaelis–Menten kinetics model for decomposition of soil organic matter at hourly to seasonal time scales. Global Change Biology **18**:371-384.

Díaz-Raviña, M., M. J. Acea, and T. Carballas. 1995. Seasonal changes in microbial biomass and nutrient flush in forest soils. Biology and Fertility of Soils **19**:220-226.

Falkowski, P. G., T. Fenchel, and E. F. Delong. 2008. The Microbial Engines That Drive Earth's Biogeochemical Cycles. Science **320**:1034-1039.

Fang, C., P. Smith, J. U. Smith, and J. B. Moncrieff. 2005. Incorporating microorganisms as decomposers into models to simulate soil organic matter decomposition. Geoderma **129**:139-146.

Hasselmann, K., M. Latif, G. Hooss, C. Azar, O. Edenhofer, C. C. Jaeger, O. M. Johannessen, C. Kemfert, M. Welp, and A. Wokaun. 2003. The Challenge of Long-Term Climate Change. Science **302**:1923-1925.

He, L., D. A. Lipson, J. L. M. Rodrigues, M. Mayes, R. G. Björk, B. Glaser, P. Thornton, and X. Xu. 2021. Dynamics of Fungal and Bacterial Biomass Carbon in Natural Ecosystems: Site-level Applications of the CLM-Microbe Model. Journal of Advances in Modeling Earth Systems **13**:e2020MS002283.

Heimann, M., and M. Reichstein. 2008. Terrestrial ecosystem carbon dynamics and climate feedbacks. Nature **451**:289-292.

Hodge, A., D. Robinson, and A. Fitter. 2000. Are microorganisms more effective than plants at competing for nitrogen? Trends in plant science **5**:304-308.

HoÈgberg, P., A. Nordgren, N. Buchmann, A. F. S. Taylor, A. Ekblad, M. N. HoÈgberg, G. Nyberg, M. Ottosson-LoÈfvenius, and D. J. Read. 2001. Large-scale forest girdling shows that current photosynthesis drives soil respiration. Nature **411**:789.

Hopkins, D. W., A. D. Sparrow, B. Elberling, E. G. Gregorich, P. M. Novis, L. G. Greenfield, and E. L. Tilston. 2006. Carbon, nitrogen and temperature controls on microbial activity in soils from an Antarctic dry valley. Soil Biology and Biochemistry **38**:3130-3140.

IPCC. 2014. Climate change 2014: impacts, adaptation, and vulnerability. IPCC Working Group II.

Jenkinson, D. S., P. B. S. Hart, J. H. Rayner, and L. C. Parry. 1987. Modelling the turnover of organic matter in long-term experiments at Rothamsted.

Keohane, R. O. 2015. The Global Politics of Climate Change: Challenge for Political Science. PS: Political Science & Politics **48**:19-26.

Lipson, D. A., C. W. Schadt, and S. K. Schmidt. 2002. Changes in soil microbial community structure and function in an alpine dry meadow following spring snow melt. Microbial ecology **43**:307-314.

Lipson, D. A., and S. K. Schmidt. 2004. Seasonal Changes in an Alpine Soil Bacterial Community in the Colorado Rocky Mountains. Applied and Environmental Microbiology **70**:2867-2879.

Luo, Y., T. F. Keenan, and M. Smith. 2015. Predictability of the terrestrial carbon cycle. Global Change Biology **21**:1737-1751.

Parton, W. J., D. S. Schimel, C. V. Cole, and D. S. Ojima. 1987. Analysis of Factors Controlling Soil Organic Matter Levels in Great Plains Grasslands 1. Soil Science Society of America Journal **51**:1173-1179.

Paul, E. A. 2016. The nature and dynamics of soil organic matter: Plant inputs, microbial transformations, and organic matter stabilization. Soil Biology and Biochemistry **98**:109-126.

Peters, G. P., R. M. Andrew, T. Boden, J. G. Canadell, P. Ciais, C. Le Quéré, G. Marland, M. R. Raupach, and C. Wilson. 2012. The challenge to keep global warming below 2 °C. Nature Climate Change **3**:4-6.

Rillig, M. C., and D. L. Mummey. 2006. Mycorrhizas and soil structure. New Phytologist **171**:41-53.

Rodrigo, A., S. Recous, C. Neel, and B. Mary. 1997. Modelling temperature and moisture effects on C–N transformations in soils: comparison of nine models. Ecological Modelling **102**:325-339.

Rousk, J., and E. Bååth. 2011. Growth of saprotrophic fungi and bacteria in soil. FEMS Microbiology Ecology **78**:17-30.

Schimel, J., and S. M. Schaeffer. 2012. Microbial control over carbon cycling in soil. Frontiers in Microbiology **3**.

Sistla, S. A., E. B. Rastetter, and J. P. Schimel. 2014. Responses of a tundra system to warming using SCAMPS: a stoichiometrically coupled, acclimating microbe–plant–soil model. Ecological Monographs **84**:151-170.

Strickland, M. S., and J. Rousk. 2010. Considering fungal: bacterial dominance in soils–methods, controls, and ecosystem implications. Soil Biology and Biochemistry **42**:1385-1395.

Svendsen, H., S. Hansen, and H. E. Jensen. 1995. Simulation of crop production, water and nitrogen balances in two German agro-ecosystems using the DAISY model. Ecological Modelling **81**:197-212.

Talbot, J. M., S. D. Allison, and K. K. Treseder. 2008. Decomposers in disguise: mycorrhizal fungi as regulators of soil C dynamics in ecosystems under global change. Functional Ecology **22**:955-963.

Taylor, K. E., R. J. Stouffer, and G. A. Meehl. 2011. An Overview of CMIP5 and the Experiment Design. Bulletin of the American Meteorological Society **93**:485-498.

Turner, B. L., H. Lambers, L. M. Condron, M. D. Cramer, J. R. Leake, A. E. Richardson, and S. E. Smith. 2013. Soil microbial biomass and the fate of phosphorus during long-term ecosystem development. Plant and Soil **367**:225-234.

Wang, K., C. Peng, Q. Zhu, X. Zhou, M. Wang, K. Zhang, and G. Wang. 2017. Modeling global soil carbon and soil microbial carbon by integrating microbial processes into the ecosystem process model TRIPLEX-GHG. Journal of Advances in Modeling Earth Systems **9**:2368-2384.

Wieder, W. R., S. D. Allison, E. A. Davidson, K. Georgiou, O. Hararuk, Y. He, F. Hopkins, Y. Luo, M. J. Smith, B. Sulman, K. Todd-Brown, Y.-P. Wang, J. Xia, and X. Xu. 2015. Explicitly representing soil microbial processes in Earth system models. Global biogeochemical cycles **29**:1782-1800.

Wieder, W. R., G. B. Bonan, and S. D. Allison. 2013. Global soil carbon projections are improved by modelling microbial processes. Nature Climate Change **3**:909-912.

Wieder, W. R., A. S. Grandy, C. M. Kallenbach, and G. B. Bonan. 2014. Integrating microbial physiology and physio-chemical principles in soils with the MIcrobial-MIneral Carbon Stabilization (MIMICS) model. Biogeosciences **11**:3899-3917.

Xu, X., J. P. Schimel, P. E. Thornton, X. Song, F. Yuan, and S. Goswami. 2014. Substrate and environmental controls on microbial assimilation of soil organic carbon: a framework for Earth system models. Ecology letters **17**:547-555.

Zeng, N., Y. Ding, J. Pan, H. Wang, and J. Gregg. 2008. Climate Change--the Chinese Challenge. Science **319**:730-731.

Chapter 1. Global Biogeography of Fungal and Bacterial Biomass Carbon in Topsoil

This chapter has already been published by Elsevier.

He, L., J. L. M. Rodrigues, N. A. Soudzilovskaia, M. Barceló, P. a. A. Olsson, C. Song, L. Tedersoo, F. Yuan, F. Yuan, and D. A. Lipson. 2020. Global biogeography of fungal and bacterial biomass carbon in topsoil. Soil Biology and Biochemistry:108024. https://doi.org/10.1016/j.soilbio.2020.108024

Abstract

Bacteria and fungi, representing two major soil microorganism groups, play an important role in global carbon (C) and nutrient biogeochemistry. Biogeographic patterns of bacterial and fungal biomass are of fundamental importance for mechanistically understanding C and nutrient cycling. We synthesized 1323 data points of phospholipid fatty acid-derived fungal biomass C (FBC), bacterial biomass C (BBC), and fungi:bacteria (F:B) ratio in topsoil, spanning 11 major biomes. The FBC, BBC, and F:B ratio display clear biogeographic patterns along latitude and environmental gradients including mean annual temperature, mean annual precipitation, net primary productivity, root C density, soil temperature, soil moisture, and edaphic factors. At the biome level, tundra has the highest FBC and BBC densities at 3684 (95% confidence interval: 1678~8084) mg kg^{-1} and 428 (237~774) mg kg^{-1}, respectively; desert has the lowest FBC and BBC densities at 16.92 (14.4~19.89) mg kg^{-1} and 6.83 (6.1~7.65) mg kg^{-1}, respectively. The F:B ratio varies dramatically, ranging from 1.8 (1.6~2.1) in savanna to 8.6 (6.7~11.0) in tundra. An empirical model was developed for the F:B ratio and it is combined with a global dataset of soil microbial biomass C to produce global maps for FBC and BBC in 0-30 cm topsoil. Across the globe, the highest FBC is found in boreal forest and tundra while the highest BBC is in boreal forest and tropical/subtropical forest, the lowest FBC and BBC are in shrub and desert. Global stocks of living microbial biomass C were estimated to be 12.6 (6.6~16.4) PgC for FBC and 4.3 (0.5~10.3) PgC for BBC in topsoil. These findings advance our understanding of the global distribution of fungal and bacterial biomass, which

facilitates the incorporation of fungi and bacteria into Earth system models. The global maps of bacterial and fungal biomass serve as a benchmark for validating microbial models in simulating the global C cycle under a changing climate.

Keywords: fungi, bacteria, F:B ratio, biogeography, pattern

Introduction

Microorganisms play an essential role in soil carbon (C) and nutrient biogeochemistry impacting on various ecosystem processes, including organic matter mineralization, soil formation, and nutrient availability (Högberg et al., 2001; Rillig and Mummey, 2006; Turner et al., 2013; Crowther et al., 2019). Eventually, the ultimate fate of soil C is driven by microbes (Schimel and Schaeffer, 2012). Although the critical roles of soil microbes in global C and nutrient cycling have been widely recognized (Falkowski et al., 2008; van der Heijden et al., 2008), the research on biogeographic distribution of fungi and bacteria is still in its infancy (Fenchel, 2002; Boer et al., 2005; Rousk and Bååth, 2011; Gougoulias et al., 2014). Furthermore, microbial community structure is an important factor controlling C and nutrient biogeochemistry as bacteria and fungi differ in enzyme production, C use efficiency, and carbon:nitrogen ratio (Caldwell, 2005; Six et al., 2006; Mouginot et al., 2014), and respond differently to multiple global change factors (Rousk and Bååth, 2007; Rousk et al., 2009). Therefore, biogeographic patterns of bacteria and fungi provide pivotal information for understanding microbial contributions to global C and nutrient biogeochemistry.

Geographic distribution of soil microbes is driven by a suite of abiotic and biotic factors (Martiny et al., 2006; Hanson et al., 2012). Previous studies have investigated the factors controlling microbial diversity and functions, including soil organic C (SOC), climate, and vegetation (de Vries et al., 2012). Soil moisture (SM), soil organic matter quality, and soil pH are among the most important factors influencing

soil microbial community composition (Fierer and Jackson, 2006; Eskelinen et al., 2009; Brockett et al., 2012; Ding et al., 2015). Although these findings provide valuable information for local to regional environmental drivers and proxies of soil microbial community structure, a holistic and quantitative understanding of soil biogeography of different microbial groups are lacking at the global scale. In particular, the lack of clear quantitative understanding of bacterial and fungal biogeography and their controls hinders the explicit incorporation of microbial mechanisms into climate models (DeLong et al., 2011; Wieder et al., 2013; Xu et al., 2014; Xu et al., 2020).

To fill the knowledge gaps in biogeographic patterns for fungi and bacteria, we compiled a global dataset of 1323 sets of phospholipid fatty acid (PLFA)-derived fungal biomass C (FBC), bacterial biomass C (BBC), and fungi:bacteria (F:B) ratio in topsoil (0-30cm). FBC and BBC derived from other approaches (primarily microscopic counting, colony forming units, substrate-induced respiration, and glucosamine and muramic acid) were excluded from this study due to large biases in reported values by various approaches. The PLFA was the most widely used and likely the most appropriate approach for estimating FBC and BBC simultaneously (Waring et al., 2013). In this study, we aimed to answer three research questions with the comprehensive dataset of FBC, BBC, and F:B ratio: 1) What are the biogeographic patterns of BBC, FBC, and F:B ratio in topsoil? 2) What are the environmental controls of the biogeographic patterns of fungal and bacterial biomass C? 3) What are the budgets of FBC and BBC at biome and global scales?

Materials and Methods

Data compilation

We used a combination of keywords, “fung*” or “bacteria*”, “ratio”, and “terrestrial” or “soil”, to search peer-reviewed papers in Google Scholar. The papers were selected via the following Criteria: 1) either concurrent fungal biomass and bacterial biomass or F:B ratio was clearly reported; 2) the data were extractable from tables (assessing the text) or figures (using Engauge Digitizer Version 10.7); 3) the study sites were not affected by disturbances such as fire, mining, and heavy metal contamination; and 4) the reported data cover 0-30 cm topsoil. Geographical information of the sampling sites was recorded and used to locate the sites on the global map (Fig. 1.1). We also collected any available data on soil pH, mean annual precipitation (MAP), mean annual temperature (MAT), SOC, total nitrogen (TN) concentration, and soil texture, and then plotted these variables against the extracted data from global datasets to test the consistency (Fig. 1.S1).

We recorded fungal and bacterial biomass C measured using methods such as phospholipid fatty acid (PLFA), direct microscopy (DM), colony forming units (CFU), substrate-induced respiration (SIR), and glucosamine and muramic acid (GMA) from peer-reviewed papers. To examine the potential biases in the measurement of fungal and bacterial biomass, we did a comparison among those methods (Table 1.1, Table 1.S1). To compare FBC and BBC measured using different methods, we used conversion factors for PLFA (Frostegård and Bååth, 1996; Klamer and Bååth, 2004), SIR (Beare et al., 1990), CFU (Aon et al., 2001), DM (Birkhofer et al., 2008), and GMA (Jost et al., 2011) reported in previous studies. Across biomes, FBC, BBC, and the F:B ratio generally followed a similar pattern among different methods. However, large variations were found in measured FBC and BBC among different methods. Specifically, compared with PLFA, SIR, and GMA, CFU reported dominant fungi over bacteria, while DM estimated a higher dominance of bacteria relative to fungi, suggesting that DM may underestimate FBC while CFU

may overestimate FBC. Meanwhile, we found overall higher FBC and BBC measured using GMA, which was largely distinct from the measurements using other methods. Using data generated from multiple methods in one analysis might be problematic. Therefore, we used PLFA data for subsequent analyses. This selection was due to two reasons: 1) the PLFA was the most widely used approach, with the PLFA-derived FBC and BBC measurements accounting for 73% of the whole dataset; 2) the PLFA method has been evaluated and proved to be the most appropriate approach for estimating FBC and BBC simultaneously (Waring et al., 2013).

The final database included the fungal and bacterial biomass data measured using PLFA from publications spanning from the late 1960s to 2018. Collectively, 1323 data points in 11 biomes (i.e., boreal forest, temperate forest, tropical/subtropical forest, grassland, shrub, savanna, tundra, desert, natural wetlands, cropland, and pasture) across the globe were included in the database (Fig. 1.1). Forest, grassland, and cropland contributed approximately 39%, 22%, and 19% of the dataset, respectively, whereas all other biomes combined accounted for 20% of the dataset. A majority of the field sites are located in North America, Europe, and Asia, and a relatively small number of observations are in South America, Africa, North Asia, Australia, and Antarctica. For data points without coordinate information being reported, we searched the geographical coordinates based on the location of the study site, city, state, and country. Then, the geographical information was used for locating the sampling points on the global map to extract climate, edaphic properties, plant productivity, and soil microclimate long-term data from global datasets.

Climate, plant, and soil data

MAT and MAP with the spatial resolution of 30 seconds during 1970-2000 were obtained from the WorldClim database version 2 (https://www.worldclim.org/data/worldclim21.html). In addition, monthly

mean SM and soil temperature (ST) during 1979-2014 were obtained from the NCEP/DOE AMIP-II Reanalysis (https://www.esrl.noaa.gov/psd/data/gridded/data.ncep.reanalysis2.gaussian.html). The global vegetation distribution data were obtained from a spatial map of 11 major biomes: boreal forest, temperate forest, tropical/subtropical forest, mixed forest, grassland, shrub, tundra, desert, natural wetlands, cropland, and pasture, which have been used in our previous publications (Xu et al., 2013; Xu et al., 2017). We also obtained the data of soil pH, sand, silt, clay, and SOC from the Harmonized World Soil Database (HWSD, https://daac.ornl.gov/cgi-bin/dsviewer.pl?ds_id=1247) at a 0.5° × 0.5° resolution grid. Soil bulk density and TN were extracted from the IGBP-DIS dataset (IGBP, https://daac.ornl.gov/SOILS/guides/igbp-surfaces.html), at a spatial resolution of 0.5′ × 0.5′. Since TN in IGBP-DIS are for the 0–100 cm soil profile as a whole, we used the factor calculated from the fraction of SOC in the top 0-30 cm in the HWSD database. Since SOC and soil TN exhibit large spatial heterogeneities, and the variation in fine-scale variation in edaphic properties are underrepresented in global datasets, we examined the relationships of FBC, BBC, and F:B ratio with SOC, TN, and C:N ratio with the data directly extracted from literature. Due to the poor correlation between bulk density extracted from HWSD and the reported bulk density values in the literature, we used the same soil bulk density values for the entire top 100 cm soil profile from IGBP, assuming no difference in bulk density between top 0-30 cm and 30-100 cm soil profiles. Root C density (C_{root}) data were extracted from global dataset of 0.5-degree resolution based on observation data (Ruesch and Gibbs, 2008; Song et al, 2017). Annual net primary productivity (NPP) for the period of 2000-2015 was obtained from the MODIS gridded dataset with a spatial resolution of 30 seconds (http://files.ntsg.umt.edu/data/NTSG_Products/). These global datasets of varied spatial resolutions were interpolated to 0.5 degree using "bilinear" method based on the GDAL library (GDAL Development Team, 2018) for generating the global maps of FBC, BBC, and F:B ratio.

Model selection and validation

For FBC, BBC, and the F:B ratio, we developed generalized linear models considering the interactive roles of climate (MAP and MAT), soil microclimate (ST and SM), plant (NPP and C_{root}), and edaphic properties (clay, sand, soil pH, bulk density, SOC, and TN) to tease apart the controlling factors on fungal and bacterial distribution. Based on the generalized linear model of climate, plant, edaphic properties, and soil microclimate for FBC, BBC, and the F:B ratio, over 70% of the variation in FBC, BBC, and the F:B ratio was explained by the generalized linear model, and FBC and BBC were better explained than the F:B ratio (Fig. 1.2).

Considering the higher proportion of missing data in FBC (14.8%) and BBC (16.3%) relative to the F:B ratio (1.9%), we built an empirical model for the F:B ratio by randomly splitting the dataset with 75% of the data used in training the model. With the generalized linear model of the F:B ratio, we performed the principal component analysis to estimate the number of the important components in explaining the variations in the F:B ratio. Based on the variations explained by each component and the cumulative variation of components, we selected 31 of the most important factors, with 33.0% of the variation in the F:B ratio explained by the empirical model (Fig. 1.S7; Table 1.S2). The selected empirical model had the formula: $\log_{10}$(F:B ratio) = 0.6789 - 0.03402 * MAT - 0.000058 * MAP + 0.003772 * ST + 1.542 * SM - 0.00099 * NPP + 0.01553 * C_{root} + 0.1226 * bulk density + 0.05991 * soil pH - 0.03631 * clay - 0.0045 * sand + 0.002878 * SOC - 0.01607 * TN + 0.000177 * MAT * ST - 0.03955 * MAT * SM - 0.000015 * MAP * ST - 0.000335 * MAP * SM + 0.000005 * MAT * NPP - 0.001615 * MAT * C_{root} + 0.000001 * MAP * NPP + 0.000007 * MAP * C_{root} + 0.02201 * MAT * bulk density - 0.003794 * MAT * soil pH + 0.002188 * MAT * clay + 0.000137 * MAT * sand - 0.000061 * MAT * SOC + 0.00513 * MAT * TN - 0.000029 * MAP * soil pH + 0.000001 * MAP * clay + 0.000003 * MAP * sand - 0.000001 * MAP * SOC - 0.000043 * MAP * TN

After the model was developed, we used 25% of the data that were not used in model development to validate the model, and we found a high consistency between model prediction and observed data (Fig. 1.S8a). We then investigated the F:B ratio model performance by comparing the model simulated values and observed data in each biome (Fig. 1.S9). We found good consistency between the simulated and observed log-transformed F:B ratio in all biomes except desert. Given the much lower BBC and FBC in deserts, this inconsistency does not introduce a large bias to the large-scale estimation of BBC and FBC. Additionally, we found some overestimation of the F:B ratio in croplands and pastures, indicating large uncertainties in managed systems.

Mapping global soil bacterial and fungal biomass carbon

We compared the soil microbial biomass C reported in Xu et al. (2013) and the sum of FBC and BBC in this study and found a strong agreement in these estimates (Fig. 1.S8b; R^2=0.91). This indicated that the sum of FBC and BBC constituted a constant proportion of microbial biomass, which provided a feasible way to estimate FBC and BBC. Based on the microbial biomass C dataset in Xu et al. (2013) and the global map of the F:B ratio generated in this study, we produced the global maps and estimated global storage of FBC and BBC. The auxiliary data used included global vegetation distribution (Xu et al., 2013) and global land area database supplied by surface data map generated by the Community Land Model 4.0 (https://svn-ccsm-models.cgd.ucar.edu/clm2/trunk_tags/clm4_5_1_r085/models/lnd/clm/tools/clm4_5/mksurfdata_map/).

Uncertainty analysis

To estimate the parameter-induced uncertainties in fungal and bacterial biomass distribution and storage, we used an improved Latin Hypercube Sampling (LHS) approach to estimate variation in F:B ratio. The LHS approach is able to randomly produce an ensemble of parameter combinations with a high efficiency. This approach has been widely used to estimate uncertainties in model output (Haefner, 2005; Xu, 2010; Xu et al., 2014). Specifically, we assumed that all parameters followed a normal distribution. Then, we used LHS to randomly select an ensemble of 3000 parameter sets using the function of "improvedLHS" in the R package "lhs" (Carnell and Carnell, 2019) (Table 1.S2). Finally, we calculated the 95% confidence interval of fungal and bacterial biomass C density and storage for reporting (Table 1.2).

Statistical analysis

We first tested the normality of data distribution using the function of "shapiro.test" in the R package "stats" (R Core Team, 2013). We found that FBC, BBC, and F:B ratio in our dataset did not follow a normal distribution. Therefore, these variables were log-transformed for subsequent statistical analysis. The mean and 95% confidence boundaries of FBC, BBC, and F:B ratio were transformed back to the original values for reporting. We constructed a generalized linear model using the function of "glm" in the R package "stats" (R Core Team, 2013) to investigate relationships between FBC, BBC, and the F:B ratio and long-term climate (MAP and MAT), soil microclimate (ST and SM), plant (NPP and C_{root}), and edaphic properties (clay, sand, soil pH, bulk density, SOC, and TN). We used Akaike information criterion (AIC) as a model selection criterion. Before conducting the generalized linear model, we tested the multicollinearity for the variables within and among each variable group, i.e., climate, soil microclimate, edaphic properties, and plant, and we found no significant multicollinearity (VIF < 5). All statistical analyses were performed and relevant figures were plotted using "agricolae" (de Mendiburu

and de Mendiburu, 2019), "multcomp" (Hothorn et al., 2016), "soiltexture" (Moeys, 2018), "VennDiagram" (Chen and Boutros, 2011), "ggplot2" (Wickham et al., 2016), and "basicTrendline" (Mei et al., 2018) packages in R version 3.5.3 for Mac OS X (https://www.r-project.org). Fig. 1.1 and Fig. 1.3 were produced with NCAR Command Language (version 6.3.0) and ArcGIS (version 10.5), respectively.

Results

Biome-level FBC, BBC, and F:B Ratio

There was a large variation in biome-level FBC, BBC, and F:B ratio (Table 1.1; $P < 0.001$ for FBC, BBC, and F:B ratio among biomes). Desert exhibited the lowest FBC of 16.9 (95% range: 14.4~19.9) mg kg^{-1} and BBC of 6.8 (6.1~7.7) mg kg^{-1}, while tundra habitats displayed the highest FBC of 3683.6 (1678.5~8083.9) mg kg^{-1} and BBC of 428.4 (237.0~774.3) mg kg^{-1}. Boreal forest had significantly higher FBC than tropical/subtropical forests and temperate forests (1234.0 mg kg^{-1} for boreal forests vs. 258.4 mg kg^{-1} for temperate forests and 451.4 mg kg^{-1} for tropical/subtropical forests). Boreal forest and tropical/subtropical forests had significantly higher BBC than temperate forests (226.4 mg kg^{-1} for boreal forest, 210.9 mg kg^{-1} for tropical/subtropical forest vs. 53.0 mg kg^{-1} for temperate forest), but no significant differences in BBC were found between boreal forests and tropical/subtropical forests (Table 1.1). Pasture had significantly higher FBC and BBC than grasslands (632.2 mg kg^{-1} soil vs. 215.2 mg kg^{-1} soil for FBC and 270.7 mg kg^{-1} soil vs. 62.7 mg kg^{-1} soil for BBC). While we did not find differences in FBC across unvegetated ground, cropland, shrub, savanna, and natural wetlands, BBC was significantly higher in wetlands than in unvegetated ground (Table 1.1).

The F:B ratio varied less across biomes, with the lowest values in savannas and highest values in tundra habitats (1.8 for savanna vs. 8.6 for tundra). We also found significantly higher F:B ratios in boreal

forests and temperate forests than in tropical/subtropical forests (5.0 for boreal forest, 4.9 for temperate forest vs. 2.2 for tropical/subtropical forest). No significant differences in F:B ratio were found among natural wetlands, unvegetated grounds, desert, and shrub (Table 1.1).

Quantitative assessment of controls on microbial biogeography

We constructed generalized linear models to disentangle the effects of climate (MAP and MAT), plant (NPP and C_{root}), soil microclimate (SM and ST), and edaphic properties (SOC, TN, soil pH, clay, sand, and bulk density) on the variation in FBC, BBC, and F:B ratio. The variance inflation factor (VIF) test showed no multicollinearity among variables. Environmental factors in total explained a large proportion of variation in microbial biomass (81.9% for FBC, 84.8% for BBC, and 71.2% for F:B ratio) (Fig. 1.2). Notably, the edaphic properties are the most important drivers in FBC and BBC, with 66.4% and 70.4% of the variation in FBC and BBC explained by edaphic properties and the interaction with other factors, respectively (Fig. 1.2a-b). Complex interactions between the groups of variables explained 23.7% of the variation in FBC (Fig. 1.2a). In contrast, variation in BBC was explained primarily by the interactions between edaphic properties and climate (13.9%), multiple interaction terms (11.9%), and edaphic properties alone (10.2%). Climate alone and climate interactions with other variables explained 11.6% and 35.5% of the variation in the F:B ratio, respectively (Fig. 1.2c).

Global carbon storage of fungal and bacterial biomass

Based on our findings of environmental controls on FBC and BBC at the biome and global scales, we further developed an empirical model for the F:B ratio considering the higher proportion of missing data in FBC (14.8%) and BBC (16.3%) relative to the F:B ratio (1.9%) (Materials and Methods; Table 1.S2). Combined with a global microbial biomass C dataset reported by Xu et al. (2013), we further produced global maps of BBC and FBC in topsoil (Fig. 1.3). The global FBC and BBC are estimated to be 12.56

(6.64~16.42) PgC and 4.34 (0.47~10.26) PgC, respectively, in 0-30 cm topsoil. Taking the global estimates of SOC (684~724 PgC in 0-30 cm), approximately 1.8% and 0.6% of SOC is stored in soil fungi and bacteria, respectively. The highest FBC density occurs in northern high-latitude regions while the lowest values are characteristic of mid-latitude regions (Fig. 1.3b). Similarly, the highest BBC is found in high-latitude and equatorial regions, and the lowest in mid-latitude regions (Fig. 1.3c).

At biome-level, boreal forest stores the largest FBC (3.60 PgC) and tropical/subtropical forests have the largest BBC storage (0.85 PgC), while shrubs contribute the least to both FBC and BBC (0.39 PgC for FBC and 0.14 PgC for BBC) (Table 1.2). Although boreal forests do not occupy the Earth's largest surface area (11.82 million km^2), the high FBC density contributes to its prominent FBC storage. The high microbial C in the pasture biome reflect its large area (27.0 million km^2). Along with the second largest area (16.44 million km^2), tropical/subtropical forests thus stored the largest BBC across the globe. The smallest FBC and BBC storage in shrub was primarily due to its small area (8.11 million km^2) and the low FBC and BBC densities (48.06 gC m^{-2} for FBC and 17.31 gC m^{-2} for BBC). The small FBC and BBC storage in deserts primarily resulted from their low FBC and BBC densities (Fig. 1.S5), while the small FBC and BBC storage in tundra and natural wetland may be due to the small area (5.75 million km^2 for tundra and 6.91 million km^2 for natural wetlands). Tundra has high densities of FBC and BBC (226.96 gC m^{-2} for FBC and 32.65 gC m^{-2} for BBC).

Discussion

Biogeographic patterns of microbial biomass

We found significant global patterns of fungi, bacteria and their balance in topsoil along latitude, climate (MAP and MAT), plant (NPP and C_{root}), soil microclimate (SM and ST), and edaphic factors (SOC, TN,

C:N ratio, soil pH, soil texture, and bulk density) (Fig. 1.S2-6) that are consistent with previous studies (Fierer et al., 2009; Waring et al., 2013; Chen et al., 2016; Bahram et al., 2018). For example, Bahram et al. (2018) reported the inverse unimodal trend of BBC and positive linear trend of F:B ratio along latitude and significant positive linear trend of F:B ratio along MAP and MAT. Fierer et al. (2009) reported significant controls of plant NPP on microbial biomass, whereas Waring et al. (2013) showed that F:B ratio increased along with the increase in C:N ratio, and de Vries et al. (2012) found that finely textured soils tend to have higher fungal and bacterial biomass. The key advantage of our study is that all these analyses are incorporated into a single study with much improved global sampling.

The discrepancies between this study and previous studies primarily lie in two aspects. First, in contrast to the inverse unimodal trend of FBC along latitude, Bahram et al. (2018) found a positive linear relationship between FBC and latitude, which we attribute to a small number of data points in the high-latitudes and the lack of data from high arctic habitats. Furthermore, the difference in overall sample size may have led to the variations in the relationships obtained among studies. The dataset in Bahram et al. (2018) was compiled using globally selected sampling plots (145 topsoil samples), while the dataset in this study is a comprehensive dataset with 1323 data points (Fig. 1.1). Second, we observed the inverse unimodal relationship between F:B ratio and soil pH, with lowest the F:B ratio at pH ~6.3, while Chen et al. (2015) reported a significant positive relationship between F:B ratio and soil pH for the Mongolian Plateau and Eskelinen et al. (2009) found a negative relationship between F:B ratio and soil pH in the alpine tundra of northern Europe. These discrepancies may result from differences in the spatial scale and range of soil pH. Soil pH values exceeded 6.5 and ranged from 4.7 to 7.0 in the studies of Chen et al. (2015) and Eskelinen et al. (2009), respectively. In their range of measurements, these F:B ratio and soil pH relationships are consistent with our study.

We found lowest FBC and BBC in deserts among biomes (Table 1.1), which was in line with precious studies. For example, Fierer et al. (2009) and Xu et al. (2013) also reported lowest soil microbial biomass in deserts, the low SOC concentration may result in low FBC and BBC in deserts (Fig. 1.S6). Furthermore, both FBC and BBC were significantly higher in tropical/subtropical forests than in temperate forests among forest biomes in this study (Table 1.1). In contrast, we found the highest soil microbial biomass in tundra, and soil microbial biomass was significantly higher in boreal forests than that in temperate forests and tropical/subtropical forests in our previous study (Xu et al., 2013). Fierer et al. (2009) reported the higher soil microbial biomass in temperate and tropical forests than that in boreal forests, which exhibited opposite patterns with this study. The seasonality of FBC and BBC could be the cause of this inconsistency. Microbial biomass showed strong seasonal dynamics, samples taken in growing and non-growing seasons are expected to have distinct microbial biomass C density (Lipson et al., 2002).

We have also detected that F:B ratio was distinct among biomes, with the smallest F:B ratio in savanna and the highest in tundra (Table 1.1). Similar to our findings, Bahram et al. (2018) found significantly higher F:B ratio in boreal-arctic biomes (e.g., tundra and boreal forests) and temperate biomes (e.g., temperate forests and grassland) than in tropical biomes (e.g., savanna and tropical/subtropical forests). The highest F:B ratio in tundra may result from several reasons. First, saprotrophic fungi have more efficient enzymatic machinery than bacteria to decompose complex organic material with high C:N ratio (de Vries et al., 2012; Chen et al., 2015). Second, highly carbon-rich soils usually display low soil pH that is relatively more stressful for bacteria compared with fungi (Eskelinen et al., 2009; Rousk et al., 2010). Third, fungi are better adapted to low-temperature conditions than bacteria (Pietikäinen et al., 2005). These three interacting mechanisms may favor fungi-dominated ecosystem C and nutrient cycling in tundra and boreal forest biomes. In contrast, Fierer et al. (2009) reported a higher F:B ratio in temperate forests than tundra, different methods used to quantify the F:B ratio may explain these differences. The

F:B ratio reported in Fierer et al. (2009) was calculated as fungal to bacterial small-subunit rRNA gene copies measured using qPCR, whereas PLFA-measured fungal to bacterial biomass C was employed in this study.

Spatial distribution and budget of FBC and BBC

Densities of both FBC and BBC were highest in arctic regions and lowest in mid-latitude regions globally (Fig. 1.3a, b). Importantly, much of the variation in FBC and BBC was determined by edaphic properties (Fig. 1.2a-b), indicating that the variation in edaphic factors along a latitudinal gradient may explain the global distribution of FBC and BBC. The predominant role of edaphic factors in regulating FBC and BBC can be ascribed to the impacts of soil pH, SOC, nutrient concentration, and soil water content on fungal and bacterial physiology (Brockett et al., 2012; de Vries et al., 2012). Our models revealed well-predicted FBC and BBC along SOC, TN, C:N ratio, bulk density, soil pH, and soil texture (Fig. 1.S6). In addition, the interactions between fungi and bacteria may affect spatial distribution of FBC and BBC. Although the taxonomic diversity of fungi and bacteria are highest in mid-latitude regions (Tedersoo et al. 2014; Bahram et al. 2018), these biomes support the lowest microbial biomass. Severe competition or substrate limitation in mid-latitude regions may reduce soil microbial biomass.

Generally, we found that the F:B ratio was low at low latitudes (Fig. 1.S2c). The decrease of soil nutrient cycling in ectomycorrhizal habitats (Fernandez and Kennedy, 2016) may result in the gradual increase of F:B ratio along latitude (Soudzilovskaia et al., 2019; Crowther et al., 2019). However, we did observe some high F:B ratios grids around equatorial regions, the high F:B ratio in these regions might be explained by several reasons. First, sand content in equator regions is much higher than other regions due to the long period of soil development and clay leaching, sandy texture soil cannot provide good protection for bacterial predators despite the relatively low bacterivore and fungivore nematode

concentration in low-latitude regions (Hassink, 1992; Hoogen et al., 2019), which will increase the proportion of bacteria being consumed. Second, well-weathered soils contain low phosphorus concentration, which is known to be an important control of initial litter decay in the tropics. Fungi are capable of decomposing recalcitrant organic matter (van der Heijden et al., 2008), and thus the poor-quality litter may in return facilitate the dominance of fungi.

We estimated FBC and BBC storage in topsoil as 12.56 PgC and 4.34 PgC, respectively (Table 1.2). This result is consistent with overall terrestrial biomass estimates of FBC and BBC storage of 12 PgC and 7 PgC, respectively, as reported by Bar-On et al. (2018). Differences in methods probably account for most of the differences between the results reported in these studies. Fungi are more sensitive to anoxic conditions, and bacteria and archaea are important components in deep soils such as subsurface environments (Bar-On et al., 2018). It is likely that the differences in the soil depths between this study (0-30 cm) and Bar-On et al. (2018) (entire soil profile) might underpin the discrepancy in estimated global budgets of BBC.

Implications for global carbon cycle

We estimated the ratio of FBC and BBC to SOC as 1.8% and 0.6%, respectively, which agrees with the findings that microbial biomass C generally comprises 0.5-13% of SOC (Insam, 1990; Sparling, 1992; Geisseler and Scow, 2014; Ananyeva et al., 2015). Soil microbes have a much faster turnover rate than soil organic carbon (Xu et al., 2017). Fungi and bacteria account for >90% of the total soil microbial biomass and are the major decomposer groups in soils (Beare, 1997). Necromass of fungi and bacteria is one of the major sources of recalcitrant organic compounds in soil (Gougoulias et al., 2014). Soil microbial necromass is about three orders of magnitude higher than soil microbial biomass (Glaser et al., 2004), and can make up more than half of SOC (Liang et al., 2019). Fungal-derived necromass was

reported to be dominant over the bacterial-derived necromass in SOC formation, which may be due to the higher recalcitrance of their cell walls, the biosynthesis of secondary metabolites, and the hyphae structure facilitated mineral protection (Li et al., 2015).

In addition to the formation of recalcitrant organic compounds in soil, soil fungal and bacterial biomass are important in conducting biochemical transformation of C and nutrients (Xu et al., 2013). For example, as litter quality decreases, fungi are expected to play more important roles (Van Der Heijden et al., 2018). Therefore, variations in F:B ratios can imply changes in the decomposer population and the changes in soil microbial community composition and function (Six et al., 2006).

However, the balance between fungal and bacterial biomass (F:B ratio) was in large variation. In addition to the natural variations due to the seasonal dynamics of fungal and bacterial biomass, fungal and bacterial growth are affected by temperature, moisture, soil pH, substrate, vegetation, and toxicity (Rousk and Bååth, 2011). Therefore, F:B ratios are highly vulnerable to changing environmental conditions such as climate change, land use change, pollution, and soil contamination. For example, Bell et al. (2014) found that a 7-year period of surplus watering increased soil F:B ratio due to the deficiency of phosphorus in watered plots. Either fungal or bacterial dominance is closely associated with the cycling pace of organic carbon from soil to atmosphere (Carvalhais et al., 2014; Crowther et al., 2019). Therefore, the F:B ratio is one critical indicator of the global C cycle under the changing environment.

Limitations and prospects

Some limitations need to be recognized when interpreting the results. First, we assumed that all samples were taken from surface soil, representing 0 - 30 cm soil profile; while the sampling depth varies between

0 and 30 cm in this study, with 76% of soil samples taken for topsoil of 0 -15 cm. Considering the vertical distribution of microbial biomass C (Xu et al., 2013), this bias might lead to a slight overestimation in BBC and FBC. Second, the disproportionate number of data points from each biome relative to its land area might lead to bias in spatial extrapolation. For example, the data points from forest, grassland, and cropland contribute approximately 80% of the dataset, while the land area of these biomes is approximately 50% of the global land area (Table 1.2). Third, the sampling date might be another reason for uncertainty; the data points were taken from various seasons and we assume the average across seasons represent the annual mean. In this aspect, future studies on seasonal variation of soil FBC and BBC should address this limitation. Fourth, actinobacteria were categorized as bacteria in a portion of studies but not in others (Andersen et al., 2010; Royer-Tardif et al., 2010). Although we reclassified bacteria based on the biomarkers used in the literature, i.e., actinobacteria were added into bacteria if the papers did not use general bacterial markers (e.g., PLFAs 14:0, 15:0, 16:0, 17:0, and 18:0) for the reported bacterial PLFA concentration, the diverse classification may introduce minor uncertainties in simulating the relationships between FBC and BBC.

Conclusions

This study reported the BBC and FBC in major biomes and produced the first global maps of BBC and FBC in 0-30 cm topsoil. The global FBC and BBC are estimated to be 12.56 (6.64 ~ 16.42) PgC and 4.34 (0.47 ~ 10.26) PgC, respectively, in 0-30 cm topsoil. The FBC, BBC, and F:B ratio showed clear distribution patterns on a global scale. Significant trends are observed along meteorological parameters (MAP, MAT, ST, and SM), vegetation productivity (C_{root} and NPP), and edaphic properties (soil texture, bulk density, soil pH, SOC, TN, and C:N ratio). The FBC and BBC were primarily determined by edaphic properties including soil texture, soil pH, bulk density, and SOC. the F:B ratio is primarily driven by climatic variables, particularly MAP and MAT. The biogeographic patterns of BBC and FBC suggest

that multiple mechanisms synergistically affect soil C and nutrient cycling at the global scale. The biogeographic patterns of BBC and FBC and their controls facilitate the development of microbial macroecology (Xu et al., 2020) and provide fundamental information for incorporating microbial mechanisms into Earth system models, and the estimated budget and maps of FBC and BBC at biome and global scales serve as a benchmark for validating the ongoing microbial modeling to enhance climate projections.

Acknowledgements

We are grateful to the Editor and two anonymous reviewers for their constructive comments that have substantially improved the manuscript. This study is partially supported by San Diego State University. Financial assistance was partially provided by the SPRUCE and NGEE Arctic projects, which are supported by the Office of Biological and Environmental Research in the Department of Energy Office of Science. This study was partially supported by the Northeast Institute of Geography and Agroecology, Chinese Academy of Sciences, and the "Top Notch" program in China. C.S. is supported by the National Natural Science Foundation of China (41125001). X.X. acknowledge the financial support from the San Diego State University and the CSU Program for Education & Research in Biotechnology. N.A.S. was supported by VIDI grant 016.161.318 issued by the Netherlands Organization of Scientific Research.

References

Ananyeva, N.D., Castaldi, S., Stolnikova, E.V., Kudeyarov, V.N., Valentini, R., 2015. Fungi-to-bacteria ratio in soils of European Russia. *Archives of Agronomy and Soil Science* 61, 427-446.

Andersen, R., Grasset, L., Thormann, M.N., Rochefort, L., Francez, A.-J., 2010. Changes in microbial community structure and function following Sphagnum peatland restoration. *Soil Biology and Biochemistry* 42, 291-301.

Bahram, M., Hildebrand, F., Forslund, S.K., Anderson, J.L., Soudzilovskaia, N.A., Bodegom, P.M., Bengtsson-Palme, J., Anslan, S., Coelho, L.P., Harend, H., 2018. Structure and function of the global topsoil microbiome. *Nature* 560, 233.

Bar-On, Y.M., Phillips, R., Milo, R., 2018. The biomass distribution on Earth. *Proceedings of the National Academy of Sciences* 115, 6506-6511.

Beare, M.H., 1997. Fungal and bacterial pathways of organic matter decomposition and nitrogen mineralization in arable soils. *Soil Ecology in Sustainable Agricultural Systems*, p. 37–70.

Bell, C.W., Tissue, D.T., Loik, M.E., Wallenstein, M.D., Martinez, V.A., Erickson, R.A., Zak, J.C., 2014. Soil microbial and nutrient responses to 7 years of seasonally altered precipitation in a Chihuahuan Desert grassland. *Global Change Biology* 20, 1657-1673.

Brockett, B.F.T., Prescott, C.E., Grayston, S.J., 2012. Soil moisture is the major factor influencing microbial community structure and enzyme activities across seven biogeoclimatic zones in western Canada. *Soil Biology and Biochemistry* 44, 9-20.

Carnell, R., Carnell, M.R., 2019. Package 'lhs'. URL http://cran. stat. auckland. ac. nz/web/packages/lhs/lhs. pdf 780.

Carvalhais, N., Forkel, M., Khomik, M., Bellarby, J., Jung, M., Migliavacca, M., Mu, M., Saatchi, S., Santoro, M., Thurner, M., 2014. Global covariation of carbon turnover times with climate in terrestrial ecosystems. *Nature* 514, 213.

Chen, D., Mi, J., Chu, P., Cheng, J., Zhang, L., Pan, Q., Xie, Y., Bai, Y., 2015. Patterns and drivers of soil microbial communities along a precipitation gradient on the Mongolian Plateau. *Landscape Ecology* 30, 1669-1682.

Chen, H., Boutros, P.C., 2011. VennDiagram: a package for the generation of highly-customizable Venn and Euler diagrams in R. *BMC Bioinformatics* 12, 35.

Chen, Y., Ding, J., Peng, Y., Li, F., Yang, G., Liu, L., Qin, S., Fang, K., Yang, Y., 2016. Patterns and drivers of soil microbial communities in Tibetan alpine and global terrestrial ecosystems. *Journal of Biogeography* 43, 2027-2039.

Crowther, T.W., Hoogen, J.v.d., Wan, J., Mayes, M.A., Keiser, A.D., Mo, L., Averill, C., Maynard, D.S., 2019. The global soil community and its influence on biogeochemistry. *Science* 365, eaav0550.

de Mendiburu, F., de Mendiburu, M.F., 2019. Package 'agricolae'. R package version, 1-2.

de Vries, F.T., Manning, P., Tallowin, J.R.B., Mortimer, S.R., Pilgrim, E.S., Harrison, K.A., Hobbs, P.J., Quirk, H., Shipley, B., Cornelissen, J.H.C., 2012. Abiotic drivers and plant traits explain landscape-scale patterns in soil microbial communities. *Ecology Letters* 15, 1230-1239.

Eskelinen, A., Stark, S., Männistö, M., 2009. Links between plant community composition, soil organic matter quality and microbial communities in contrasting tundra habitats. *Oecologia* 161, 113-123.

Fernandez, C.W., Kennedy, P.G., 2016. Revisiting the 'Gadgil effect': do interguild fungal interactions control carbon cycling in forest soils? *New Phytologist* 209, 1382-1394.

Fierer, N., Strickland, M.S., Liptzin, D., Bradford, M.A., Cleveland, C.C., 2009. Global patterns in belowground communities. *Ecology Letters* 12, 1238-1249.

GDAL Development Team. (2018). GDAL/OGR Geospatial Data Abstraction Library, Version 2.1.3.3. Open Source Geospatial Foundation. Retrieved from http://www.gdal. org

Geisseler, D., Scow, K.M., 2014. Long-term effects of mineral fertilizers on soil microorganisms–A review. *Soil Biology and Biochemistry* 75, 54-63.

Glaser, B., Turrión, M., Alef, K., 2004. Amino sugars and muramic acid—biomarkers for soil microbial community structure analysis. *Soil Biology and Biochemistry* 36, 399-407.

Gougoulias, C., Clark, J.M., Shaw, L.J., 2014. The role of soil microbes in the global carbon cycle: tracking the below-ground microbial processing of plant-derived carbon for manipulating Carbon dynamics in agricultural systems. *Journal of the Science of Food and Agriculture* 94, 2362-2371.

Haefner, J.W., 2005. *Modeling biological systems-principles and applications*. Springer, New York.

Hassink, J., 1992. Effects of soil texture and structure on carbon and nitrogen mineralization in grassland soils. *Biology and Fertility of Soils* 14, 126-134.

Hoogen, J.v.d., Geisen, S., Routh, D., Ferris, H., Traunspurger, W., Wardle, D.A., Goede, R.G.M.d., Adams, B.J., Ahmad, W., Andriuzzi, W.S., Bardgett, R.D., Bonkowski, M., Campos-Herrera, R., Cares, J.E., Caruso, T., Caixeta, L.d.B., Chen, X., Costa, S.R., Creamer, R., Castro, J.M.d.C., Dam, M., Djigal, D., Escuer, M., Griffiths, B.S., Gutiérrez, C., Hohberg, K., Kalinkina, D., Kardol, P., Kergunteuil, A., Korthals, G., Krashevska, V., Kudrin, A.A., Li, Q., Liang, W., Magilton, M., Marais, M., Martín, J.A.R., Matveeva, E., Mayad, E.H., Mulder, C., Mullin, P., Neilson, R., Nguyen, T.A.D., Nielsen, U.N., Okada, H., Rius, J.E.P., Pan, K., Peneva, V., Pellissier, L., Silva, J.C.P.d., Pitteloud, C., Powers, T.O., Powers, K., Quist, C.W., Rasmann, S., Moreno, S.S., Scheu, S., Setälä, H., Sushchuk, A., Tiunov, A.V., Trap, J., Putten, W.v.d., Vestergård, M., Villenave, C., Waeyenberge, L., Wall, D.H., Wilschut, R., Wright, D.G., Yang, J.-i., Crowther, T.W., 2019. Soil nematode abundance and functional group composition at a global scale. *Nature* 572, 194-198.

Hothorn, T., Bretz, F., Westfall, P., Heiberger, R.M., Schuetzenmeister, A., Scheibe, S., Hothorn, M.T., 2016. Package 'multcomp'. Simultaneous inference in general parametric models. Project for Statistical Computing, Vienna, Austria.

Insam, H., 1990. Are the soil microbial biomass and basal respiration governed by the climatic regime? *Soil Biology and Biochemistry* 22, 525-532.

Li, N., Xu, Y.-Z., Han, X.-Z., He, H.-B., Zhang, X.-D., Zhang, B., 2015. Fungi contribute more than bacteria to soil organic matter through necromass accumulation under different agricultural practices during the early pedogenesis of a Mollisol. *European Journal of Soil Biology* 67, 51-58.

Liang, C., Amelung, W., Lehmann, J., Kästner, M., 2019. Quantitative assessment of microbial necromass contribution to soil organic matter. *Global Change Biology* 25, 3578-3590.

Lipson, D.A., Schadt, C.W., Schmidt, S.K., 2002. Changes in soil microbial community structure and function in an alpine dry meadow following spring snow melt. *Microbial Ecology* 43, 307-314.

Mei, W., Yu, G., Lai, J., Rao, Q., Umezawa, Y., 2018. basicTrendline: Add Trendline and Confidence Interval of Basic Regression Models to Plot, 2.0.3 ed.

Moeys, J., 2018. The soil texture wizard: R functions for plotting, classifying, transforming and exploring soil texture data. CRAN. R-Project.

Pietikäinen, J., Pettersson, M., Bååth, E., 2005. Comparison of temperature effects on soil respiration and bacterial and fungal growth rates. *FEMS Microbiology Ecology* 52, 49-58.

R Core Team, 2013. R: A language and environment for statistical computing. Vienna, Austria: R Foundation for Statistical Computing. Available.

Rousk, J., Bååth, E., 2011. Growth of saprotrophic fungi and bacteria in soil. *FEMS Microbiology Ecology* 78, 17-30.

Rousk, J., Brookes, P.C., Bååth, E., 2010. Investigating the mechanisms for the opposing pH relationships of fungal and bacterial growth in soil. *Soil Biology and Biochemistry* 42, 926-934.

Royer-Tardif, S., Bradley, R., Parsons, W., 2010. Evidence that plant diversity and site productivity confer stability to forest floor microbial biomass. *Soil Biology and Biochemistry* 42, 813-821.

Ruesch, A., Gibbs, H.K., 2008. New IPCC Tier-1 global biomass carbon map for the year 2000. Available online from the Carbon Dioxide Information Analysis Center [http://cdiac. ornl. gov], Oak Ridge National Laboratory, Oak Ridge, Tennessee.

Six, J., Frey, S.D., Thiet, R.K., Batten, K.M., 2006. Bacterial and fungal contributions to carbon sequestration in agroecosystems. *Soil Science Society of America Journal* 70, 555-569.

Song, X., Hoffman, F.M., Iversen, C.M., Yin, Y., Kumar, J., Ma, C., Xu, X., 2017. Significant inconsistency of vegetation carbon density in CMIP5 Earth system models against observational data. *Journal of Geophysical Research: Biogeosciences* 122, 2282-2297.

Soudzilovskaia, N.A., van Bodegom, P.M., Terrer, C., Zelfde, M.v.t., McCallum, I., Luke McCormack, M., Fisher, J.B., Brundrett, M.C., de Sá, N.C., Tedersoo, L., 2019. Global mycorrhizal plant distribution linked to terrestrial carbon stocks. *Nature Communications* 10, 5077.

Sparling, G.P., 1992. Ratio of microbial biomass carbon to soil organic carbon as a sensitive indicator of changes in soil organic matter. *Soil Research* 30, 195-207.

Steidinger, B.S., Crowther, T.W., Liang, J., Van Nuland, M.E., Werner, G.D., Reich, P.B., Nabuurs, G., de-Miguel, S., Zhou, M., Picard, N., Herault, B., Zhao, X., Zhang, C., Routh, D., Peay, K.G., consortium, G., 2019. Climatic controls of decomposition drive the global biogeography of forest-tree symbioses. *Nature* 569, 404-408.

Tedersoo, L., Bahram, M., Põlme, S., Kõljalg, U., Yorou, N.S., Wijesundera, R., Ruiz, L.V., Vasco-Palacios, A.M., Thu, P.Q., Suija, A., Smith, M.E., Sharp, C., Saluveer, E., Saitta, A., Rosas, M., Riit, T., Ratkowsky, D., Pritsch, K., Põldmaa, K., Piepenbring, M., Phosri, C., Peterson, M., Parts, K.,

Pärtel, K., Otsing, E., Nouhra, E., Njouonkou, A.L., Nilsson, R.H., Morgado, L.N., Mayor, J., May, T.W., Majuakim, L., Lodge, D.J., Lee, S.S., Larsson, K.-H., Kohout, P., Hosaka, K., Hiiesalu, I., Henkel, T.W., Harend, H., Guo, L.-d., Greslebin, A., Grelet, G., Geml, J., Gates, G., Dunstan, W., Dunk, C., Drenkhan, R., Dearnaley, J., Kesel, A.D., Dang, T., Chen, X., Buegger, F., Brearley, F.Q., Bonito, G., Anslan, S., Abell, S., Abarenkov, K., 2014. Global diversity and geography of soil fungi. *Science* 346.

van der Heijden, M.G.A., Bardgett, R.D., Van Straalen, N.M., 2008. The unseen majority: soil microbes as drivers of plant diversity and productivity in terrestrial ecosystems. *Ecology Letters* 11, 296-310.

Van Der Heijden, M.G.A., Bardgett, R.D., Van Straalen, N.M., 2018. The unseen majority: soil microbes as drivers of plant diversity and productivity in terrestrial ecosystems. *Ecology Letters*, 296-310.

Waring, B.G., Averill, C., Hawkes, C.V., 2013. Differences in fungal and bacterial physiology alter soil carbon and nitrogen cycling: insights from meta-analysis and theoretical models. *Ecology Letters* 16, 887-894.

Wickham, H., Chang, W., Wickham, M.H., 2016. Package 'ggplot2'. Create Elegant Data Visualisations Using the Grammar of Graphics. Version 2, 1-189.

Xu, X., Wang, N., Lipson, D.L., Sinsabaugh, R.L., Schimel, J.P., He, L., Soudzilovskaia, N.A., Tedersoo, L., 2020. Microbial macroecology: in search of mechanisms governing microbial biogeographical patterns. *Global Ecology and Biogeography*. doi:10.1111/geb.13162.

Xu, X., 2010. Modeling methane and nitrous oxide exchanges between the atmosphere and terrestrial ecosystems over North America in the context of multifactor global change, School of Forestry and Wildlife Sciences. Auburn University, Auburn, p. 199.

Xu, X., Schimel, J.P., Janssens, I.A., Song, X., Song, C., Yu, G., Sinsabaugh, R.L., Tang, D., Zhang, X., Thornton, P.E., 2017. Global pattern and controls of soil microbial metabolic quotient. *Ecological Monographs* 87, 429-441.

Xu, X., Schimel, J.P., Thornton, P.E., Song, X., Yuan, F., Goswami, S., 2014. Substrate and environmental controls on microbial assimilation of soil organic carbon: a framework for Earth system models. *Ecology Letters* 17, 547-555.

Xu, X., Thornton, P.E., Post, W.M., 2013. A global analysis of soil microbial biomass carbon, nitrogen and phosphorus in terrestrial ecosystems. *Global Ecology and Biogeography* 22, 737-749.

Figures and tables

Fig. 1.1 Global distribution of data points included in this analysis. 1323 data points with geographical coordinates are shown in this map. Circles indicate study sites, with circles in different sizes showing variation in the number of data points and different colors representing different biomes

Fig. 1.2 Interactive effects of climate, plant, edaphic properties, and soil microclimate on (a) fungal biomass carbon (n=611), (b) bacterial biomass carbon (n=619), and (c) F:B ratio (n=748); Ellipses represent the different groups of factors (climate, plant, edaphic properties, and soil microclimate). Climate includes MAT and MAP; Plant represents combined information of C_{root} and NPP; Edaphic properties includes bulk density, soil pH, SOC, ST, clay, and sand. Soil microclimate represents ST and SM (red ellipse indicates the dominant group of variables). Numbers represents the variation partitioned by different sections.

Fig. 1.3 Global maps of (a) fungal biomass C, (b) bacterial biomass C, and (c) F:B ratio in topsoil

Table 1.1 Biome-level fungal biomass carbon (FBC), bacterial biomass carbon (BBC,) and fungi: bacteria (F:B) ratio

Table 1.2 Biome- and global level storage and density of soil fungal and bacterial biomass C (95% confidence interval are shown in the bracket)

Table 1.1 Biome-level fungal biomass carbon (FBC), bacterial biomass carbon (BBC,) and fungi: bacteria (F:B) ratio

Biome	FBC (mg kg^{-1} soil)	BBC (mg kg^{-1} soil)	F:B ratio
Unvegetated ground	192.74^{de} (54.79 ~ 677.99)	24.60^{d} (7.68 ~ 78.72)	3.90^{bc} (2.20 ~ 6.91)
Desert	16.92^{f} (14.40 ~ 19.89)	6.83^{e} (6.10 ~ 7.65)	3.14^{bcd} (2.20 ~ 4.49)
Grassland	215.19^{de} (168.98 ~ 274.03)	62.69^{cd} (50.44 ~ 77.92)	4.03^{b} (3.52 ~ 4.62)
Pasture	632.15^{bc} (288.99 ~ 1382.81)	270.65^{a} (129.07 ~ 567.53)	2.48^{cde} (1.62 ~ 3.80)
Cropland	212.69^{de} (150.35 ~ 300.88)	65.77^{cd} (46.30 ~ 93.42)	3.28^{bcd} (2.89 ~ 3.73)
Shrub	218.14^{cde} (106.01 ~ 448.9)	45.42^{cd} (23.48 ~ 87.85)	4.82^{b} (3.72 ~ 6.25)
Savanna	103.36^{e} (60.62 ~ 176.23)	44.37^{cd} (25.94 ~ 75.92)	1.82^{e} (1.57 ~ 2.11)
Tropical/subtropical forest	451.40^{bc} (362.32 ~ 562.39)	209.96^{ab} (179.03 ~ 246.24)	2.22^{de} (1.87 ~ 2.63)
Temperate forest	258.39^{de} (189.16 ~ 352.95)	53.05^{cd} (38.71 ~ 72.70)	4.92^{b} (4.39 ~ 5.51)
Boreal forest	1234.08^{b} (870.72 ~ 1749.08)	226.37^{ab} (172.79 ~ 296.58)	5.03^{b} (4.23 ~ 5.98)
Tundra	3683.59^{a} (1678.49 ~ 8083.94)	428.37^{a} (236.98 ~ 774.31)	8.60^{a} (6.71 ~ 11.01)
Natural wetlands	329.81^{cde} (194.80 ~ 558.4)	92.58^{bc} (50.99 ~ 168.10)	4.13^{b} (3.50 ~ 4.86)

* Values are presented as means with a 95% confidence boundary in parentheses for fungal, bacterial biomass and F:B ratio. Different superscript letters in one column mean significant difference at the significance level of P=0.05, while the same letters indicate no significant difference

Table 1.2 Biome- and global level storage and density of soil fungal and bacterial biomass C (95% confidence interval are shown in the bracket)

Biome	Area (million km^2)	Biomass C Density ($gC\ m^{-2}$)		Biomass C Storage (PgC)	
		Fungi	Bacteria	Fungi	Bacteria
Boreal forest	11.82	304.44 (191.19-356.01)	58.66 (7.02-171.86)	3.60 (2.26-4.21)	0.69 (0.08-2.03)
Temperate forest	12.89	88.89 (40.25-115.74)	29.88 (3.01-78.5)	1.15 (0.52-1.49)	0.39 (0.04-1.01)
Tropical/Subtropical forest	16.44	64.42 (2.09-115.49)	51.58 (0.51-113.82)	1.06 (0.03-1.90)	0.85 (0.01-1.87)
Grassland	12.16	88.69 (20.55-132.48)	46.14 (2.34-114.23)	1.08 (0.25-1.61)	0.56 (0.03-1.39)
Shrub	8.11	48.06 (11.40-64.78)	17.31 (0.59-53.85)	0.39 (0.09-0.53)	0.14 (0.00-0.44)
Tundra	5.75	226.96 (150.89-256.46)	32.65 (3.13-108.08)	1.31 (0.87-1.48)	0.19 (0.02-0.62)
Desert	13.51	59.04 (14.05-74.00)	15.28 (0.32-60.21)	0.80 (0.19-1.00)	0.21 (0.00-0.81)
Natural wetlands	6.91	70.44 (30.9-99.91)	32.96 (3.47-72.44)	0.49 (0.21-0.69)	0.23 (0.02-0.50)
Cropland	14.94	67.61 (18.18-95.92)	30.09 (1.73-79.35)	1.01 (0.27-1.43)	0.45 (0.03-1.19)
Pasture	27.00	62.34 (24.03-84.12)	23.68 (1.85-61.62)	1.68 (0.65-2.27)	0.64 (0.05-1.66)
Globe	129.55	96.92 (51.23-126.75)	33.50 (3.66-79.19)	12.56 (6.64-16.42)	4.34 (0.47-10.26)

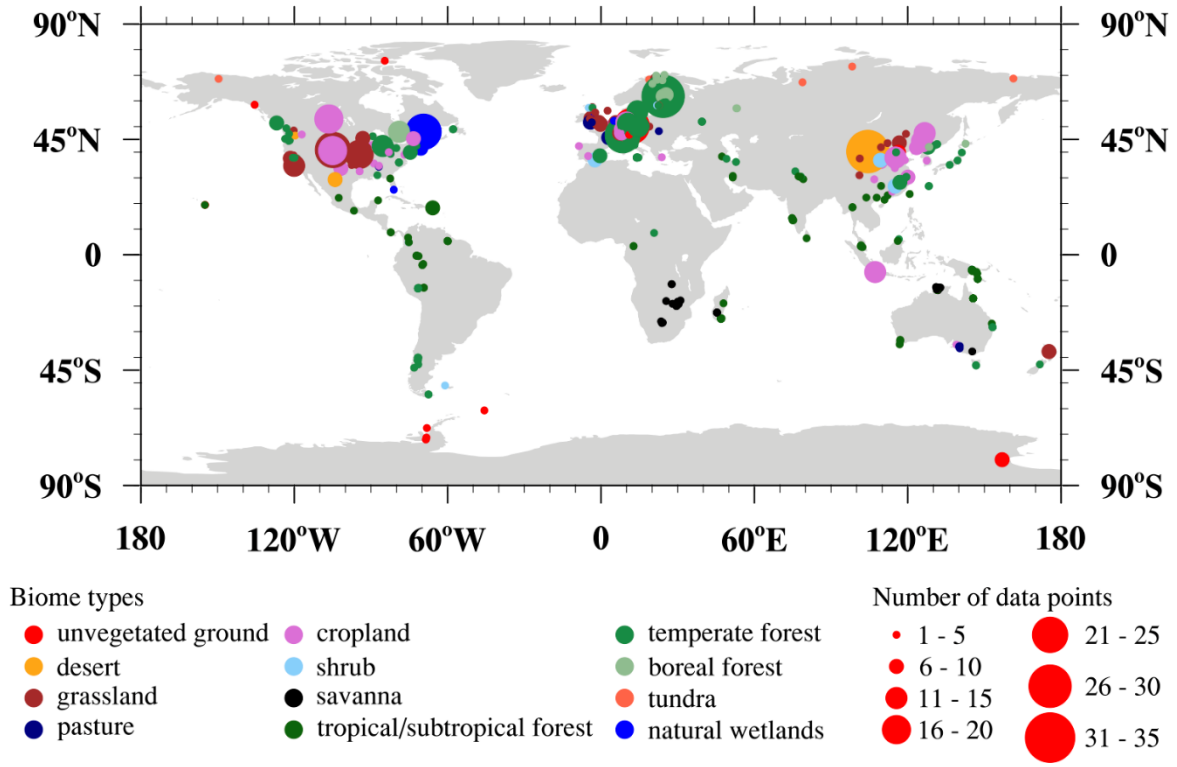

Fig. 1.1 Global distribution of data points included in this analysis. 1323 data points with geographical coordinates are shown in this map. Circles indicate study sites, with circles in different sizes showing variation in the number of data points and different colors representing different biomes

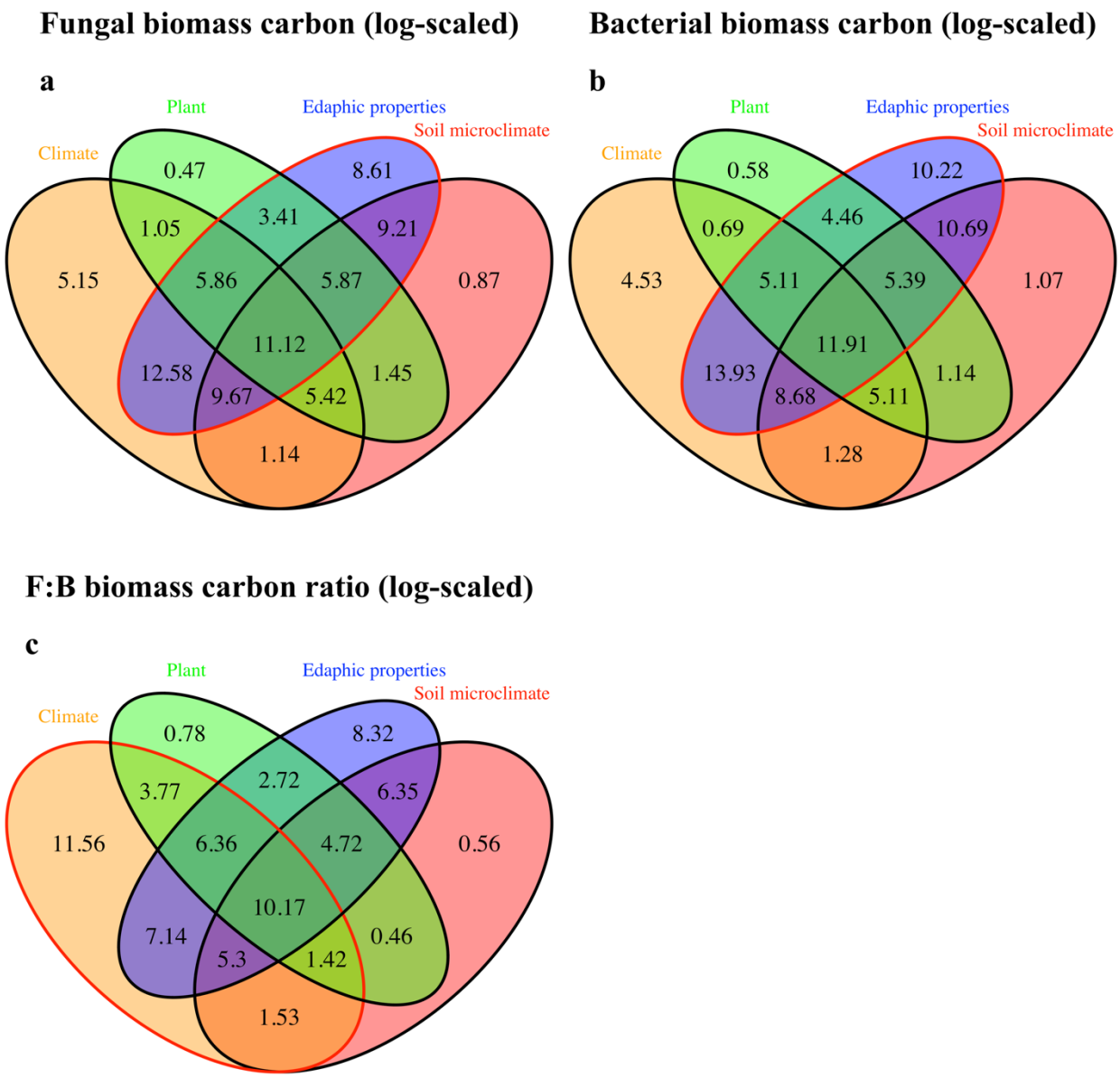

Fig. 1.2 Interactive effects of climate, plant, edaphic properties, and soil microclimate on (a) fungal biomass carbon (n=611), (b) bacterial biomass carbon (n=619), and (c) F:B ratio (n=748); Ellipses represent the different groups of factors (climate, plant, edaphic properties, and soil microclimate). Climate includes MAT and MAP; Plant represents combined information of C_{root} and NPP; Edaphic properties includes bulk density, soil pH, SOC, ST, clay, and sand. Soil microclimate represents ST and SM (red ellipse indicates the dominant group of variables). Numbers represents the variation partitioned by different sections.

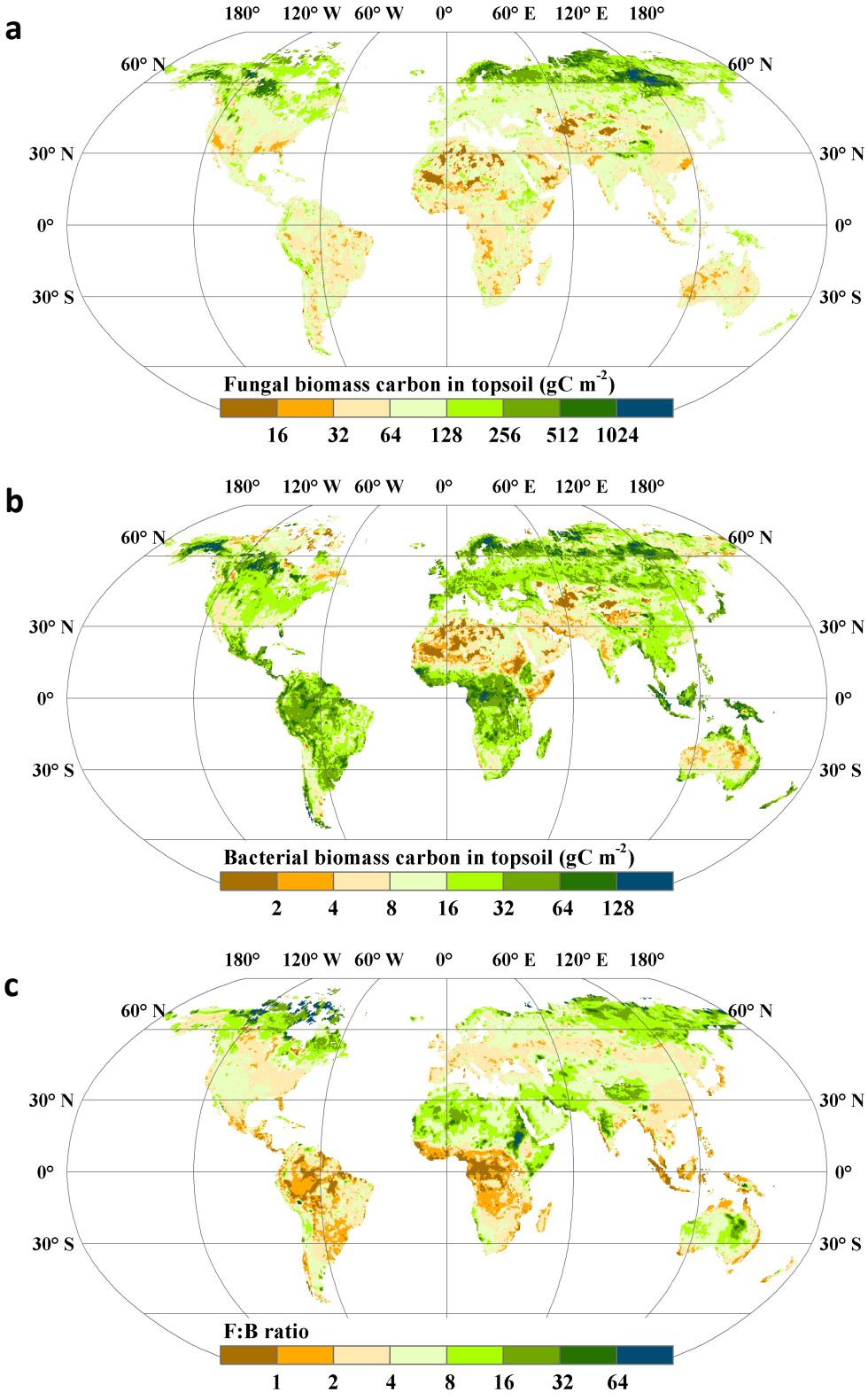

Fig. 1.3 Global maps of (a) fungal biomass C, (b) bacterial biomass C, and (c) F:B ratio in topsoil

Supplementary material for chapter 1

Fig. 1.S1. Climate variables and edaphic properties observed at for the sampling sites (obtained from the literature sources used for FBC, BBC, and F:B ratio) and those extracted from the global maps. MAT: mean annual temperature; MAP: mean annual precipitation. SOC: soil organic carbon; TN: total nitrogen. MAT and MAP with the spatial resolution of 30s during 1970-2000 were obtained from the WorldClim database version 2 (http://worldclim.org/version2). Soil pH, sand, silt, clay, and SOC data were from the Harmonized World Soil Database (https://daac.ornl.gov/cgi-bin/dsviewer.pl?ds_id=1247), while soil bulk density and TN data are from the IGBP-DIS dataset (https://daac.ornl.gov/SOILS/guides/igbp-surfaces.html).

Fig. 1.S2. Latitudinal distribution of fungal (a), bacterial (b) biomass C and F:B ratio (c). Regressions are: $Y=0.00073X^2-0.048X+3$ with N=1122 for **a**; $Y=0.00055X^2-0.044X+2.6$ with N=1140 for **b**; $Y=0.0061X+0.32$ with N=1300 for **c**.

Fig. 1.S3. Fungal, bacterial biomass and F:B ratio across MAT (a-c) and MAP (d-f). MAT, mean annual temperature; MAP, mean annual precipitation. Regressions are: $Y=0.0021X^2-0.062X+2.7$ with N=1054 for **a**; $Y=0.0057X+1.8$ with N=1069 for **b**; $Y=-0.017X+0.75$ with N=1229 for **c**; $Y=-1.5\times10^{-7}X^2+0.00065X+2$ with N=1054 for **d**; $Y=-1.1\times10^{-7}X^2+0.00067X+1.4$ with N=1069 for **e**; $Y=-0.00015X+0.74$ with N=1229 for **f**.

Fig. 1.S4. Association between fungal and bacterial biomass C and F:B ratio and soil moisture (a-c) and soil temperature (d-f). SM, soil moisture; ST, soil temperature. Regressions are: $Y=-5.3X^2+6.6X+0.83$ with N=1054 for **a**; $Y=X+1.5$ with N=1069 for **b**; $Y=-2.2X^2+2.2X+0.14$ with N=1229 for **c**; $Y=0.0046X+2.4$ with N=1054 for **d**; $Y=5.6\times10^{-5}X^2+0.011X+1.8$ with N=1069 for **e**; $Y=-0.0066X+0.62$ with N=1229 for **f**.

Fig. 1.S5. Fungal, bacterial biomass and F:B ratio across the C_{root} (a-c) and NPP (d-f). C_{root}: root carbon density; NPP: net primary productivity. Regressions are: $Y=-0.00017X^2+0.012X+2.3$ with N=1037 for **a**; $Y=0.011X+1.7$ with N=1052 for **b**; $Y=-0.00018X^2+0.0025X+0.6$ with N=1212 for **c**; $Y=0.00025X+2.3$ with N=1054 for **d**; $Y=0.00052X+1.6$ with N=1069 for **e**; $Y=-0.00033X+0.78$ with N=1229 for **f**.

Fig. 1.S6. Fungal, bacterial biomass and F:B ratio across the SOC (a-c), TN (d-f), C:N ratio (g-i), bulk density (a-c), soil pH (d-f), and Soil texture (p-r). SOC, soil organic carbon; TN, soil total nitrogen; C:N ratio, SOC:TN ratio. Regressions are: $Y=7.4\times10^{-6}X^2-0.021X+2.4$ with N=882 for **a**; $Y=6.7\times10^{-6}X^2-0.003X+1.9$ with N=900 for **b**; $Y=0.0012X+0.5$ with N=1002 for **c**; $Y=0.03X+2.4$ with N=647 for **d**; $Y=0.017X+1.9$ with N=662 for **e**; $Y=-0.00073X^2+0.037X+0.48$ with N=725 for **f**; $Y=-0.0016X^2+0.065X+2$ with N=647 for **g**; $Y=-0.0018X^2+0.063X+1.6$ with N=662 for **h**; $Y=0.00024X^2-0.0035X+0.53$ with N=728 for **i**; $Y=2.3X^2-7X+7.6$ with N=1054 for **j**; $Y=1.7X^2-4.9X+5.3$ with N=1069 for **k**; $Y=-0.55X+1.3$ with N=1229 for **l**; $Y=0.086X^2-1.3X+7$ with N=1054 for **m**; $Y=0.05X^2-0.78X+4.7$ with N=1069 for **n**; $Y=-0.071X^2-0.89X+3.3$ with N=1229 for **o**.

Fig. 1.S7. Scree plots for the proportion of variance explained by components from the generalized mixed linear model of F:B ratio.

Fig. 1.S8. Empirical model validation using randomly sampled data of F:B ratio (a) and the relationship between microbial biomass and the sum of fungal and bacterial biomass (b). Sum of fungal and bacterial biomass and microbial biomass. were calculated based on fungal and bacterial biomass in this study, while microbial biomass carbon data were from Xu et al., (2013).

Fig. 1.S9. Comparison between model simulated and observed F:B ratio for major biomes (boreal forest, temperate forest, tropical/subtropical forest, grassland, shrubland, tundra, desert, natural wetland, cropland, and pasture). F:B ratio shown in the figures were log-scaled.

Table 1.S1. Biome-level fungal and bacterial biomass carbon and fungi:bacteria biomass ratio measured with various approaches (direct microscopy, substrate-induced respiration, colony forming units, and glucosamine and muramic acid) (mean and 95% confidence interval are reported); the values in the bracket are the number of data points

Table 1.S2. Parameters for estimating global map of F:B ratio

Table 1.S1. Biome-level fungal and bacterial biomass carbon and fungi:bacteria biomass ratio measured with various approaches (direct microscopy, substrate-induced respiration, colony forming units, and glucosamine and muramic acid) (mean and 95% confidence interval are reported); the values in the bracket are the number of data points

Method	Biome	Fungal biomass C (mg kg^{-1} soil)	Bacterial biomass C (mg kg^{-1} soil)	Fungi:bacteria biomass ratio
Direct microscopy	unvegetated ground	22.8 (11.80 ~ 44.08) [6]	49.75 (34.39 ~ 71.98) [6]	0.46 (0.26 ~ 0.80) [6]
	desert	23.03 (8.36 ~ 63.43) [1]	243.88 (109.74 ~ 541.96) [1]	0.09 (0.02 ~ 0.47) [1]
	grassland	22.72 (16.72 ~ 30.86) [4]	65.79 (43.73 ~ 98.99) [4]	0.35 (0.23 ~ 0.52) [4]
	cropland	99.94 (83.92 ~ 119.01) [36]	79.25 (69.56 ~ 90.29) [36]	1.22 (1.06 ~ 1.40) [36]
	shrub	317.26 (15.51 ~ 6491.55) [245]	116.28 (21.80 ~ 620.10) [245]	2.73 (0.03 ~ 297.72) [248]
	temperate forest	317.05 (186.80 ~ 538.12) [2]	29.14 (14.99 ~ 56.65) [2]	7.44 (5.11 ~ 10.83) [2]
	natural wetlands	158.74 (158.74 ~ 158.74) [34]	696.6 (696.60 ~ 696.60) [34]	0.23 (0.23 ~ 0.23) [35]
Substrate-induced respiration	grassland	80.31 (80.31 ~ 80.31) [6]	176.68 (176.68 ~ 176.68) [6]	0.91 (0.64 ~ 1.30) [6]
	pasture	160.12 (137.78 ~ 186.09) [1]	274.02 (239.30 ~ 313.77) [1]	0.58 (0.44 ~ 0.77) [5]
	cropland	106.72 (77.62 ~ 146.73) [3]	59.85 (56.82 ~ 63.04) [3]	1.78 (1.37 ~ 2.33) [3]
	temperate forest	282.28 (276.66 ~ 288.01) [2]	207.65 (204.77 ~ 210.58) [2]	1.71 (0.97 ~ 3.02) [2]
	boreal forest	531.35 (260.85 ~ 1082.36) [2]	292.63 (154.44 ~ 554.45) [2]	1.82 (1.47 ~ 2.25) [14]
Colony forming units	unvegetated ground	30.52 (30.52 ~ 30.52) [1]	0.54 (0.54 ~ 0.54) [1]	56.26 (56.26 ~ 56.26) [1]
	grassland	11.79 (0.32 ~ 432.06) [12]	0.16 (0.00 ~ 15.03) [12]	73.48 (28.74 ~ 187.89) [12]
	cropland	144.66 (81.66 ~ 256.28) [9]	2.31 (1.36 ~ 3.91) [9]	62.72 (46.63 ~ 84.37) [9]
	shrub	30.28 (22.56 ~ 40.64) [2]	2.37 (1.04 ~ 5.40) [2]	12.76 (7.52 ~ 21.65) [2]
	temperate forest	366.99 (13.67 ~ 9850.78) [68]	2.95 (0.23 ~ 37.29) [68]	124.41 (31.98 ~ 483.93) [68]
	boreal forest	2513.23 (1722.27 ~ 3667.45) [2]	7.1 (3.57 ~ 14.15) [2]	353.79 (195.44 ~ 640.44) [2]
	natural wetlands	317.29 (209.49 ~ 480.58) [4]	2.21 (1.61 ~ 3.02) [4]	143.66 (89.48 ~ 230.64) [4]
Glucosamine and muramic acid	grassland	5458.25 (1911.4 ~ 15586.77) [4]	2180.41 (618.65 ~ 7684.83) [4]	2.46 (1.96 ~ 3.09) [4]
	cropland	6595.22 (4519.58 ~ 9624.10) [3]	3316.23 (1992.13 ~ 5520.41) [3]	1.95 (1.68 ~ 2.27) [3]

* Values are presented as means with a 95% confidence boundary reported in parentheses and number of data points for fungal, bacterial biomass and F:B ratio in brackets.

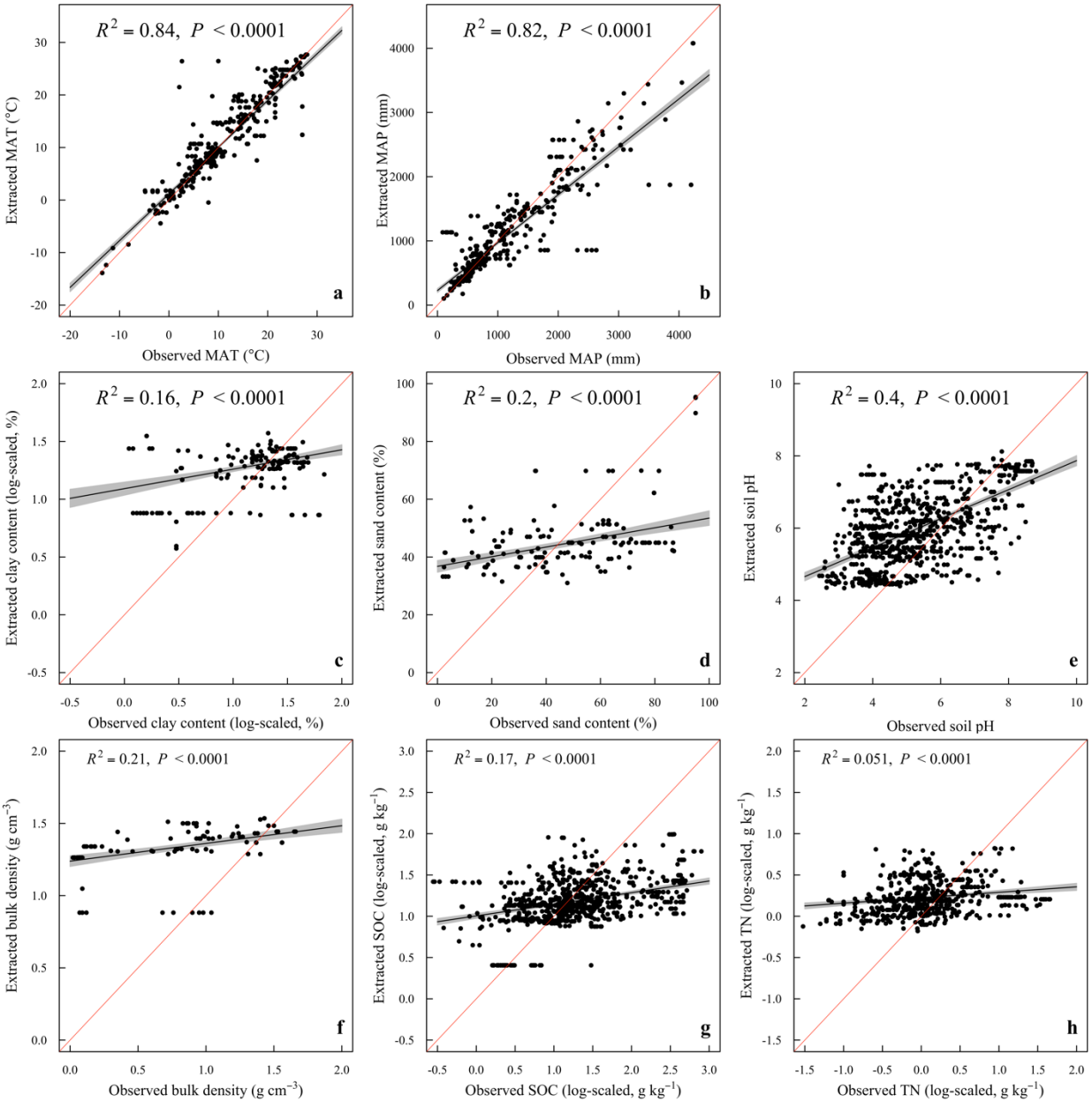

Fig. 1.S1. Climate variables and edaphic properties observed at for the sampling sites (obtained from the literature sources used for FBC, BBC, and F:B ratio) and those extracted from the global maps. MAT: mean annual temperature; MAP: mean annual precipitation. SOC: soil organic carbon; TN: total nitrogen. MAT and MAP with the spatial resolution of 30s during 1970-2000 were obtained from the WorldClim database version 2 (http://worldclim.org/version2). Soil pH, sand, silt, clay, and SOC data were from the Harmonized World Soil Database (https://daac.ornl.gov/cgi-bin/dsviewer.pl?ds_id=1247), while soil bulk density and TN data are from the IGBP-DIS dataset (https://daac.ornl.gov/SOILS/guides/igbp-surfaces.html).

Both FBC and BBC exhibited inverse unimodal relationships with latitude, with lowest values in the mid-latitudes (Fig. 1.S2a-b; $P < 0.0001$ for both FBC and BBC along latitude), whereas the F:B ratio was positively correlated with latitude (Fig. 1.S2c; $P < 0.0001$). Of climatic predictors, MAT showed an inverse unimodal relationship with FBC, with the lowest at 14-15°C (Fig. 1.S3a; $P < 0.0001$). Conversely, BBC showed no significant correlation with MAT (Fig. 1.S3b; $P = 0.19$). The F:B ratio showed a significantly negative linear relationship with MAT (Fig. 1.S3c; $P < 0.0001$).

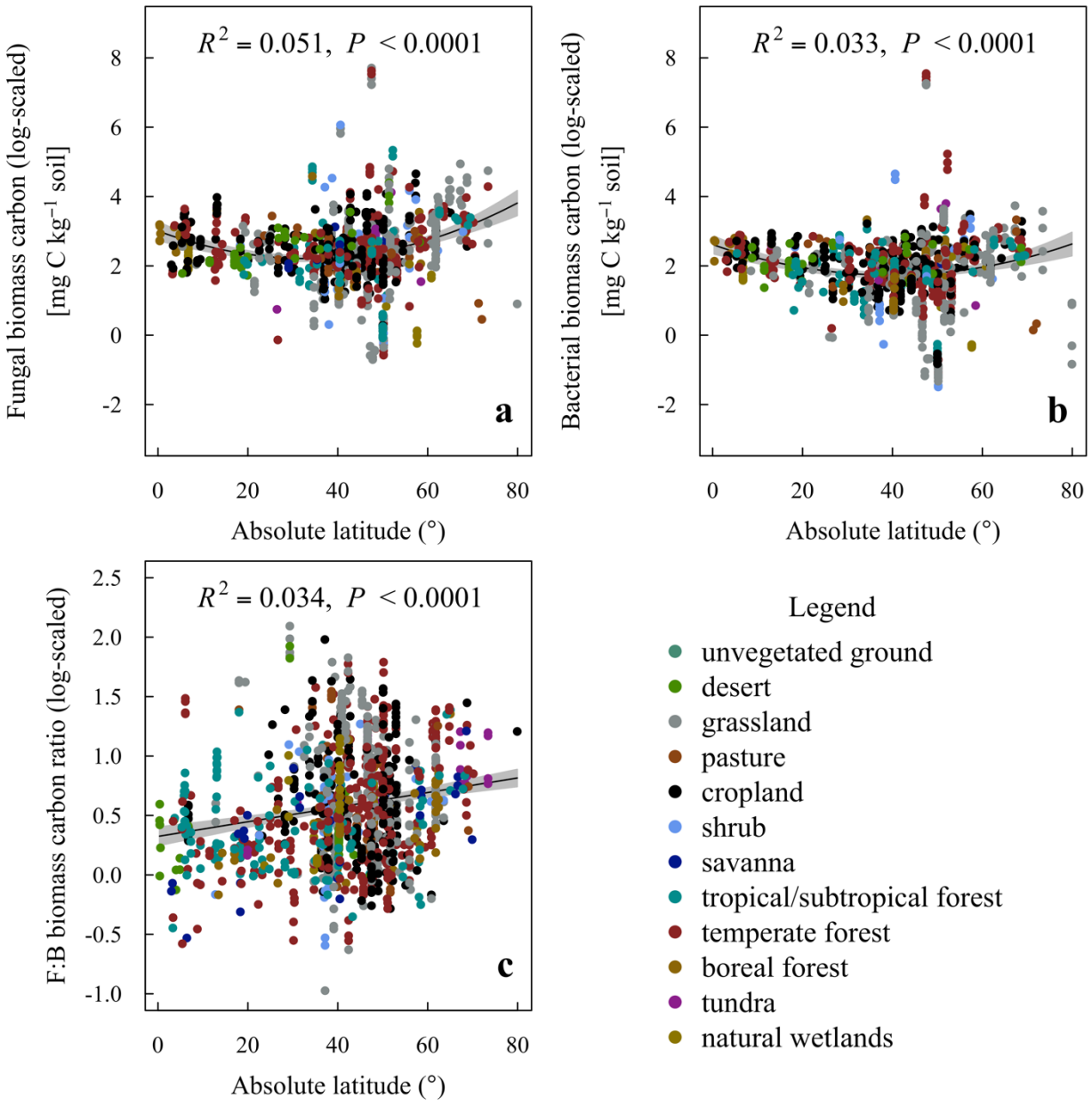

Fig. 1.S2. Latitudinal distribution of fungal (a), bacterial (b) biomass C and F:B ratio (c). Regressions are: Y=0.00073X^2-0.048X+3 with N=1122 for **a**; Y=0.00055X^2-0.044X+2.6 with N=1140 for **b**; Y=0.0061X+0.32 with N=1300 for **c**.

Both FBC and BBC showed unimodal relationships with MAP, with peak FBC and BBC at approximately 2100-mm y^{-1} and 3000-mm y^{-1}, respectively. While F:B ratio linearly decreased with MAP (Fig. 1.S3d-f; $P_{FBC} < 0.0001$, $P_{BBC} < 0.0001$, $P_{F:B\ ratio} < 0.0001$). The FBC increased in a non-linear manner with SM, while BBC linearly increased with SM (Fig. 1.S4a-b; $P_{FBC} < 0.0001$, $P_{BBC} < 0.0001$). Both FBC and BBC linearly increased with ST (Fig. 1.S4d-e; $P_{FBC} < 0.0001$, $P_{BBC} < 0.0001$). The F:B ratio increased with SM (Fig. 1.S4c; $P < 0.0001$) but decreased with ST (Fig. 1.4Sf; $P < 0.0001$).

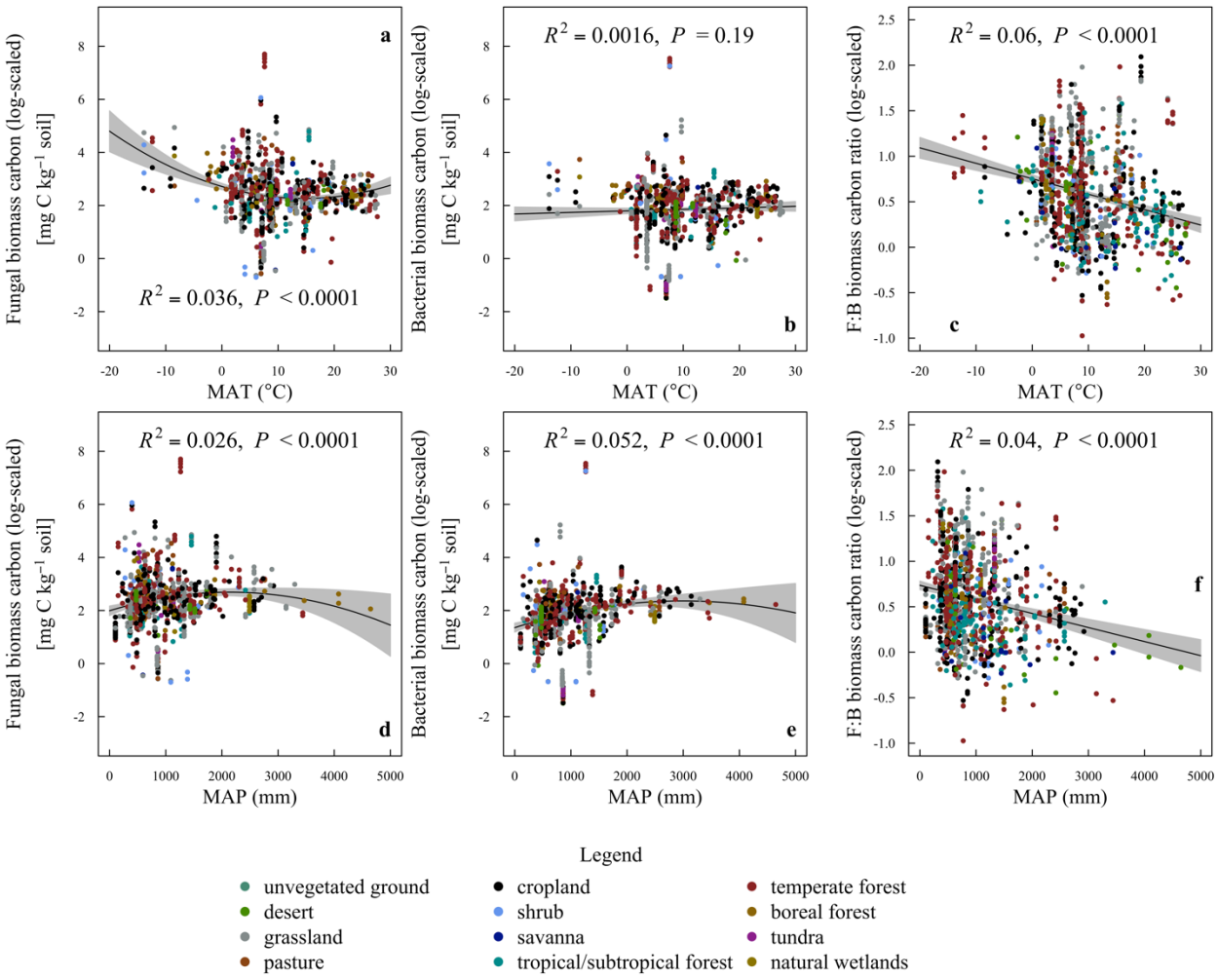

Fig. 1.S3. Fungal, bacterial biomass and F:B ratio across MAT (a-c) and MAP (d-f). MAT, mean annual temperature; MAP, mean annual precipitation. Regressions are: $Y=0.0021X^2-0.062X+2.7$ with N=1054 for **a**; $Y=0.0057X+1.8$ with N=1069 for **b**; $Y=-0.017X+0.75$ with N=1229 for **c**; $Y=-1.5\times10^{-7}X^2+0.00065X+2$ with N=1054 for **d**; $Y=-1.1\times10^{-7}X^2+0.00067X+1.4$ with N=1069 for **e**; $Y=-0.00015X+0.74$ with N=1229 for **f**.

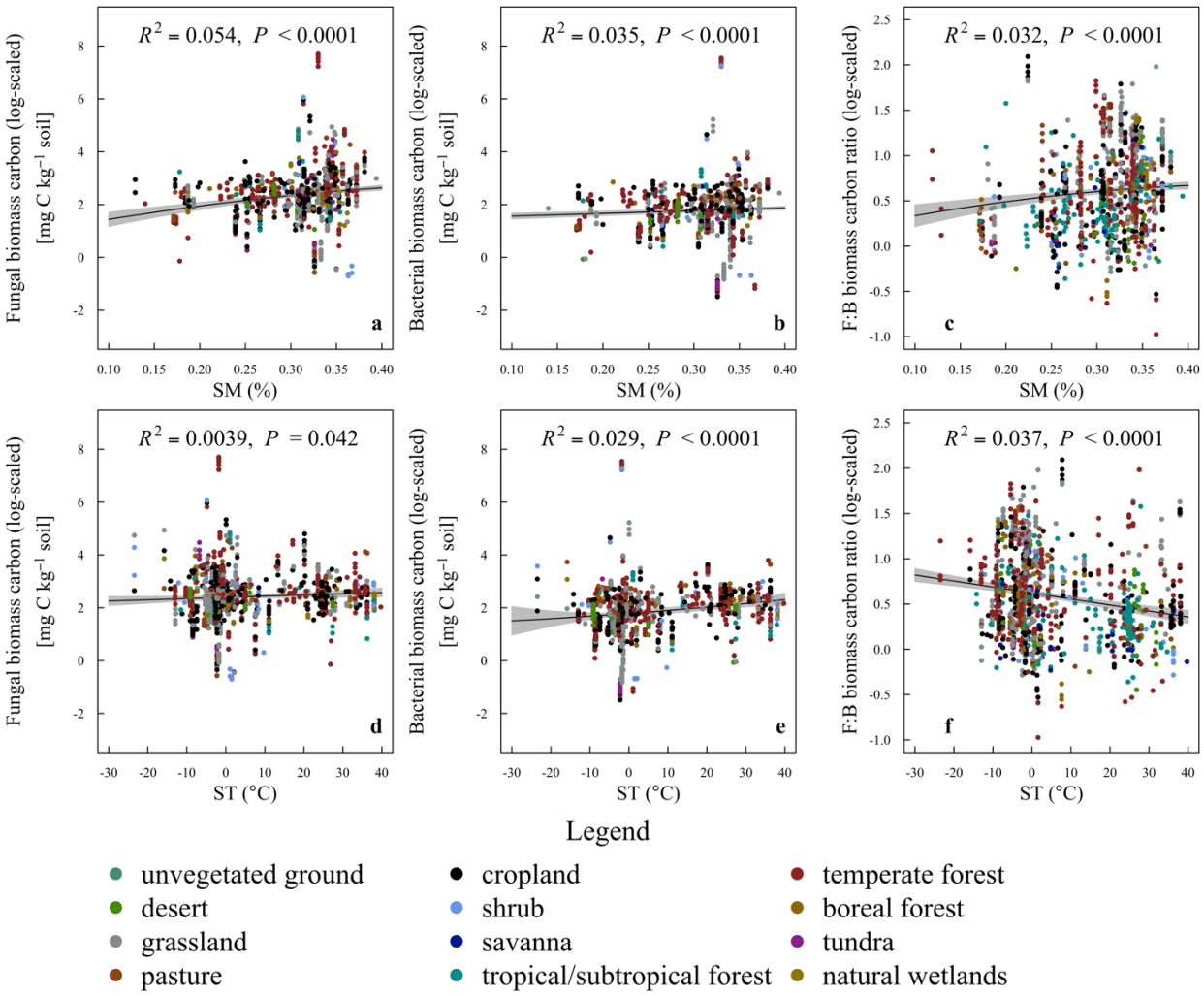

Fig. 1.S4. Association between fungal and bacterial biomass C and F:B ratio and soil moisture (a-c) and soil temperature (d-f). SM, soil moisture; ST, soil temperature. Regressions are: $Y=-5.3X^2+6.6X+0.83$ with N=1054 for **a**; $Y=X+1.5$ with N=1069 for **b**; $Y=-2.2X^2+2.2X+0.14$ with N=1229 for **c**; $Y=0.0046X+2.4$ with N=1054 for **d**; $Y=5.6\times10^{-5}X^2+0.011X+1.8$ with N=1069 for **e**; $Y=-0.0066X+0.62$ with N=1229 for **f**.

Vegetation controls on microbial biomass C differed in fungi and bacteria. While BBC significantly increased with C_{root} (Fig. 1.S5a-b; $P_{FBC} = 0.2$, $P_{BBC} = 0.00035$), no significant correlation between FBC and C_{root} occurred. The F:B ratio exhibited a unimodal correlation with C_{root}, with the peak F:B ratio associated with the C_{root} of 6.9 kg m^{-2} (Fig. 1.S5c; $P < 0.0001$). Both FBC and BBC linearly increased with NPP, while F:B ratio linearly decreased with NPP (Fig. 1.S5d-f; $P_{FBC} = 0.011$, $P_{BBC} < 0.0001$, $P_{F:B\ ratio} < 0.0001$).

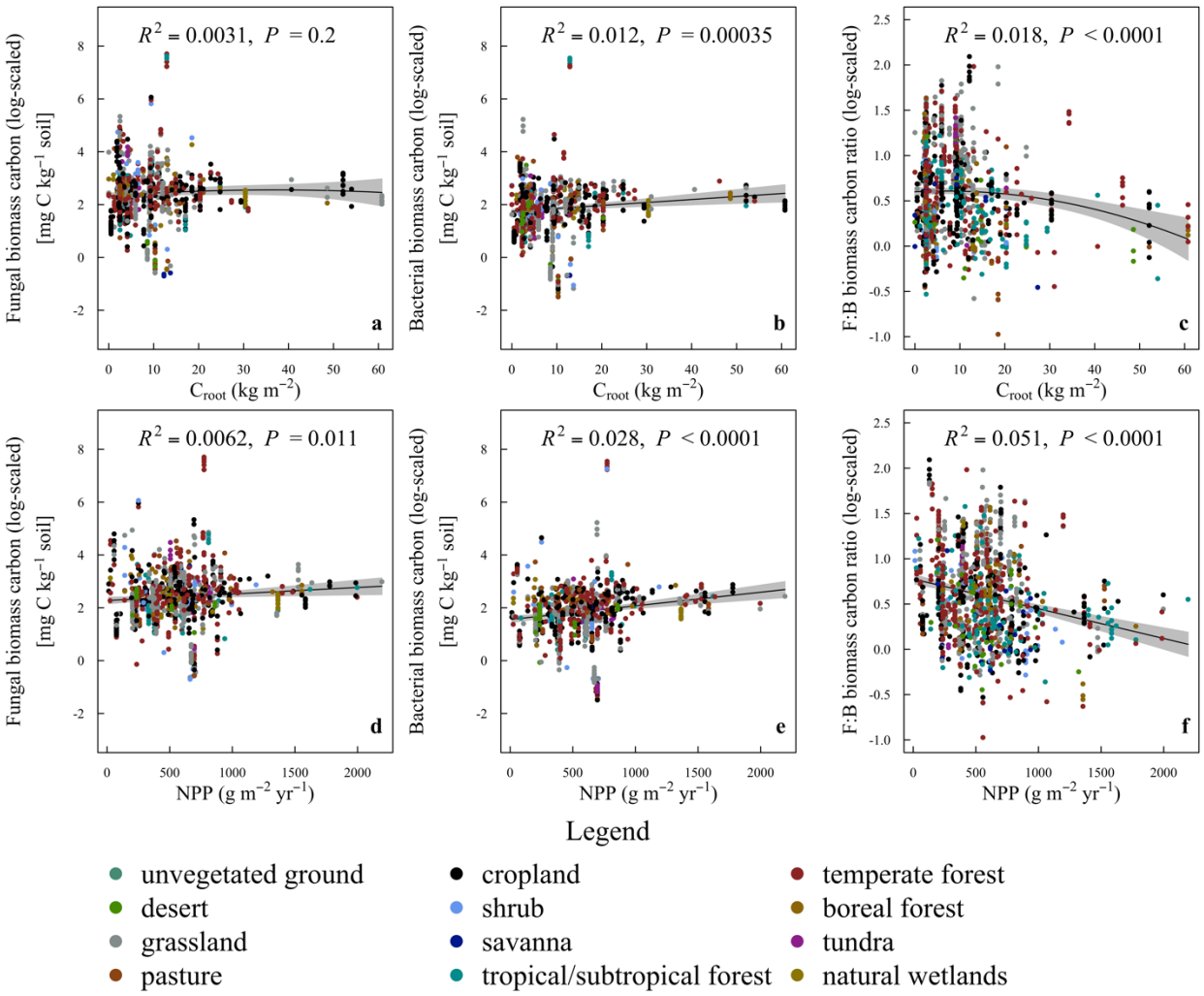

Fig. 1.S5. Fungal, bacterial biomass and F:B ratio across the C_{root} (a-c) and NPP (d-f). C_{root}: root carbon density; NPP: net primary productivity. Regressions are: $Y=-0.00017X^2+0.012X+2.3$ with N=1037 for **a**; $Y=0.011X+1.7$ with N=1052 for **b**; $Y=-0.00018X^2+0.0025X+0.6$ with N=1212 for **c**; $Y=0.00025X+2.3$ with N=1054 for **d**; $Y=0.00052X+1.6$ with N=1069 for **e**; $Y=-0.00033X+0.78$ with N=1229 for **f**.

Microbial biomass was well correlated with edaphic factors. Both FBC and BBC exhibited inverse unimodal relationships with SOC, with minimum FBC and BBC at SOC of 142.1 and 222.7 g kg^{-1}, respectively (Fig. 1.S6a-b; $P_{FBC} < 0.0001$, $P_{BBC} = 0.0017$), while F:B ratio linearly increased with SOC (Fig. 1.S6c; $P < 0.0001$). Both FBC and BBC linearly increased with TN, while F:B ratio exhibited unimodal relationship with TN, with the maximum F:B ratio at TN of 25.4 g kg^{-1} (Fig. 1.S6d-f; $P_{FBC} < 0.0001$, $P_{BBC} = 0.011$, $P_{F:B\ ratio} < 0.0001$). Both FBC and BBC showed unimodal relationships with SOC:TN (C:N) ratio, with the maximum FBC and BBC at C:N ratio of 20.1 and 17.7, respectively (Fig. 1.S6g-h; $P_{FBC} < 0.0001$, $P_{BBC} < 0.0001$), while F:B ratio showed inverse unimodal relationship with C:N ratio, with minimum F:B ratio at C:N ratio of 7.1 (Fig. 1.S6i; $P_{F:B\ ratio} < 0.0001$). In addition, both FBC and BBC showed inverse unimodal relationships with soil bulk density, with minimum FBC and BBC at bulk density of 1.5 and 1.4 gC m^{-3}, respectively, while F:B ratio linearly decreased with bulk density (Fig. 1.S6j-l; $P_{FBC} < 0.0001$, $P_{BBC} = 0.00035$, $P_{F:B\ ratio} < 0.0001$). Furthermore, we found that FBC, BBC, and F:B ratio all showed inverse unimodal relationships with soil pH, with minimum FBC, BBC, and F:B ratio at soil pH of 7.5, 7.4 and 6.3, respectively (Fig. 1.S6m-o; $P_{FBC} < 0.0001$, $P_{BBC} < 0.0001$, $P_{F:B\ ratio} < 0.0001$). We also found the highest FBC and BBC in clayey s, but the highest F:B ratio in sandy soil (Fig. 1.6Sp-r; $P_{FBC} < 0.0001$, $P_{BBC} < 0.0001$, $P_{F:B\ ratio} < 0.0001$).

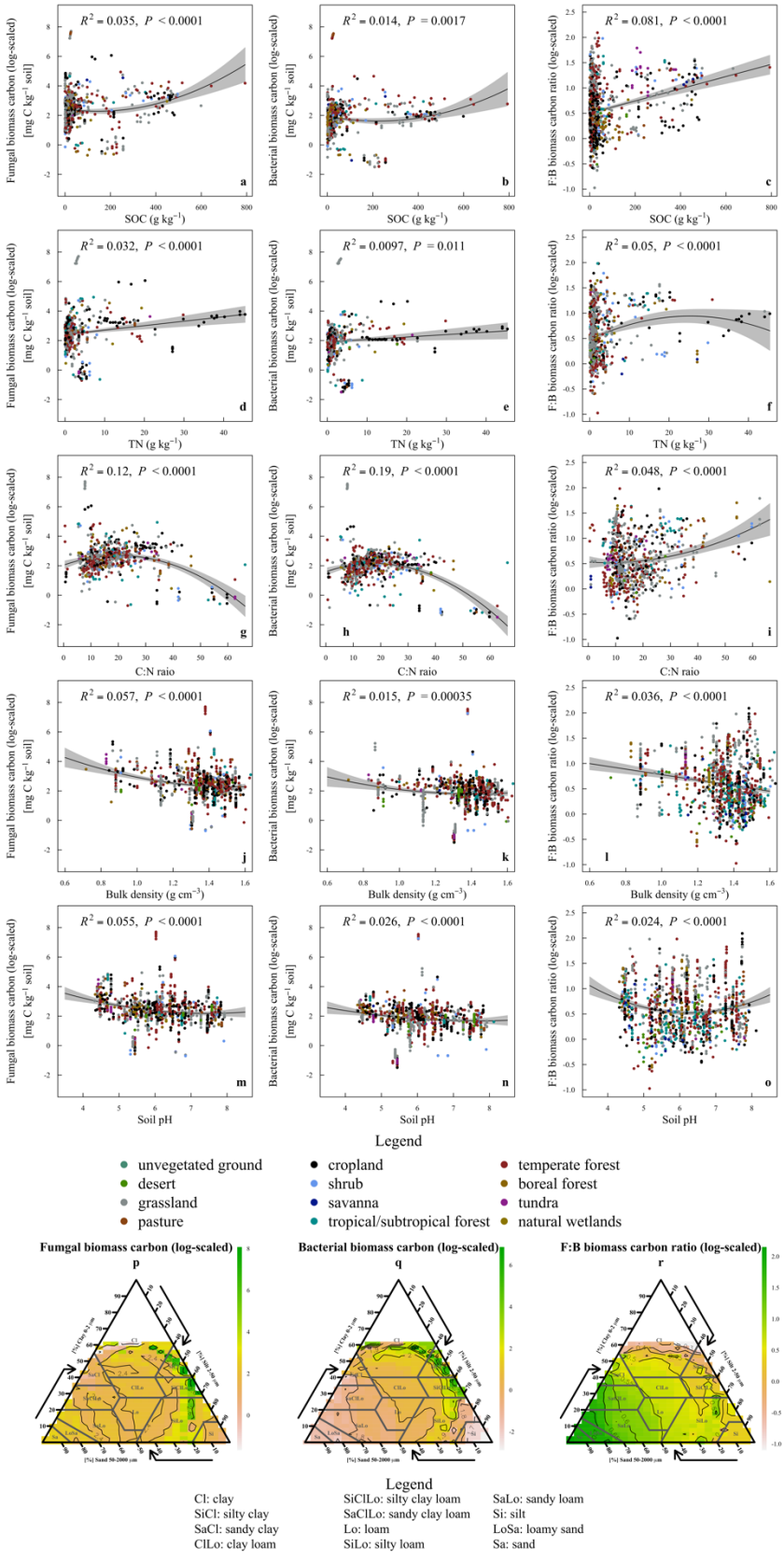

Fig. 1.S6. Fungal, bacterial biomass and F:B ratio across the SOC (a-c), TN (d-f), C:N ratio (g-i), bulk density (a-c), soil pH (d-f), and Soil texture (p-r). SOC, soil organic carbon; TN, soil total nitrogen; C:N ratio, SOC:TN ratio. Regressions are: $Y=7.4\times10^{-6}X^2-0.021X+2.4$ with N=882 for **a**; $Y=6.7\times10^{-6}X^2-0.003X+1.9$ with N=900 for **b**; $Y=0.0012X+0.5$ with N=1002 for **c**; $Y=0.03X+2.4$ with N=647 for **d**; $Y=0.017X+1.9$ with N=662 for **e**; $Y=-0.00073X^2+0.037X+0.48$ with N=725 for **f**; $Y=-0.0016X^2+0.065X+2$ with N=647 for **g**; $Y=-0.0018X^2+0.063X+1.6$ with N=662 for **h**; $Y=0.00024X^2-0.0035X+0.53$ with N=728 for **i**; $Y=2.3X^2-7X+7.6$ with N=1054 for **j**; $Y=1.7X^2-4.9X+5.3$ with N=1069 for **k**; $Y=-0.55X+1.3$ with N=1229 for **l**; $Y=0.086X^2-1.3X+7$ with N=1054 for **m**; $Y=0.05X^2-0.78X+4.7$ with N=1069 for **n**; $Y=-0.071X^2-0.89X+3.3$ with N=1229 for **o**.

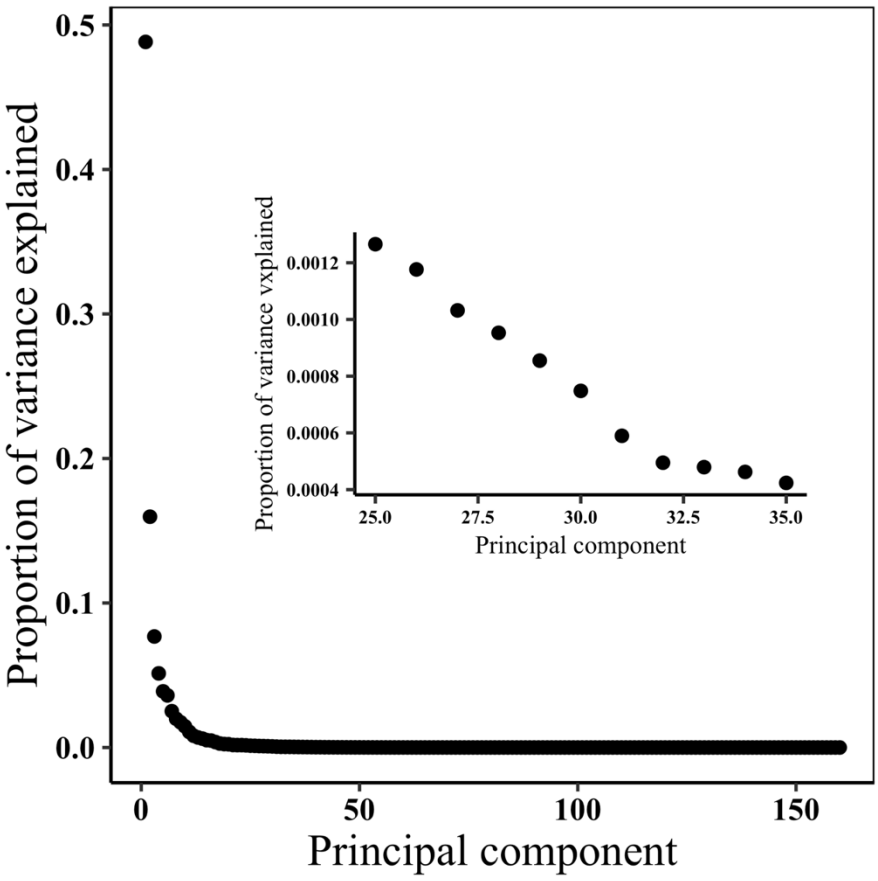

Fig. 1.S7. Scree plots for the proportion of variance explained by components from the generalized mixed linear model of F:B ratio.

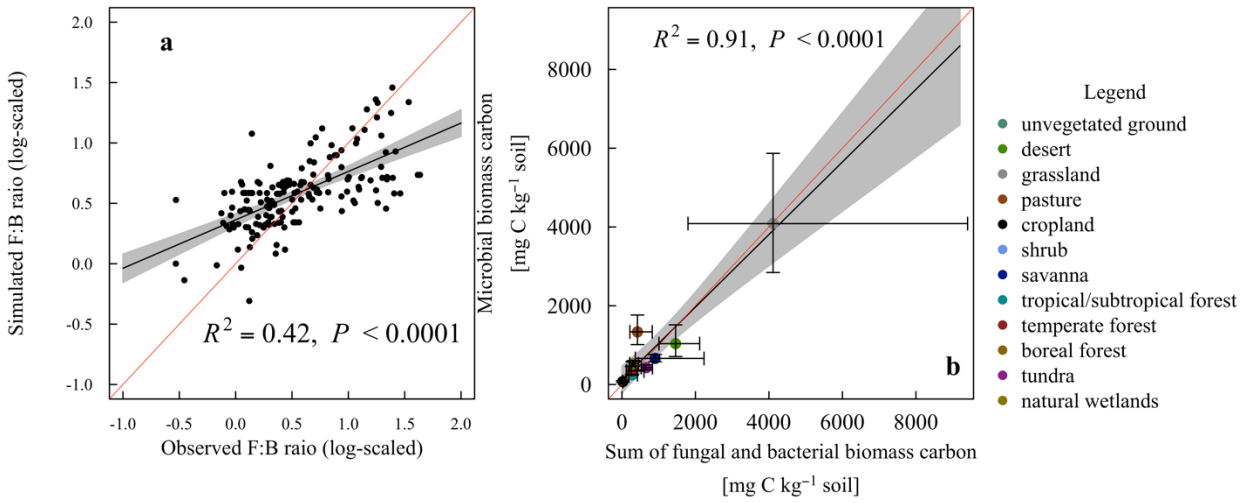

Fig. 1.S8. Empirical model validation using randomly sampled data of F:B ratio (a) and the relationship between microbial biomass and the sum of fungal and bacterial biomass (b). Sum of fungal and bacterial biomass and microbial biomass. were calculated based on fungal and bacterial biomass in this study, while microbial biomass carbon data were from Xu et al., (2013).

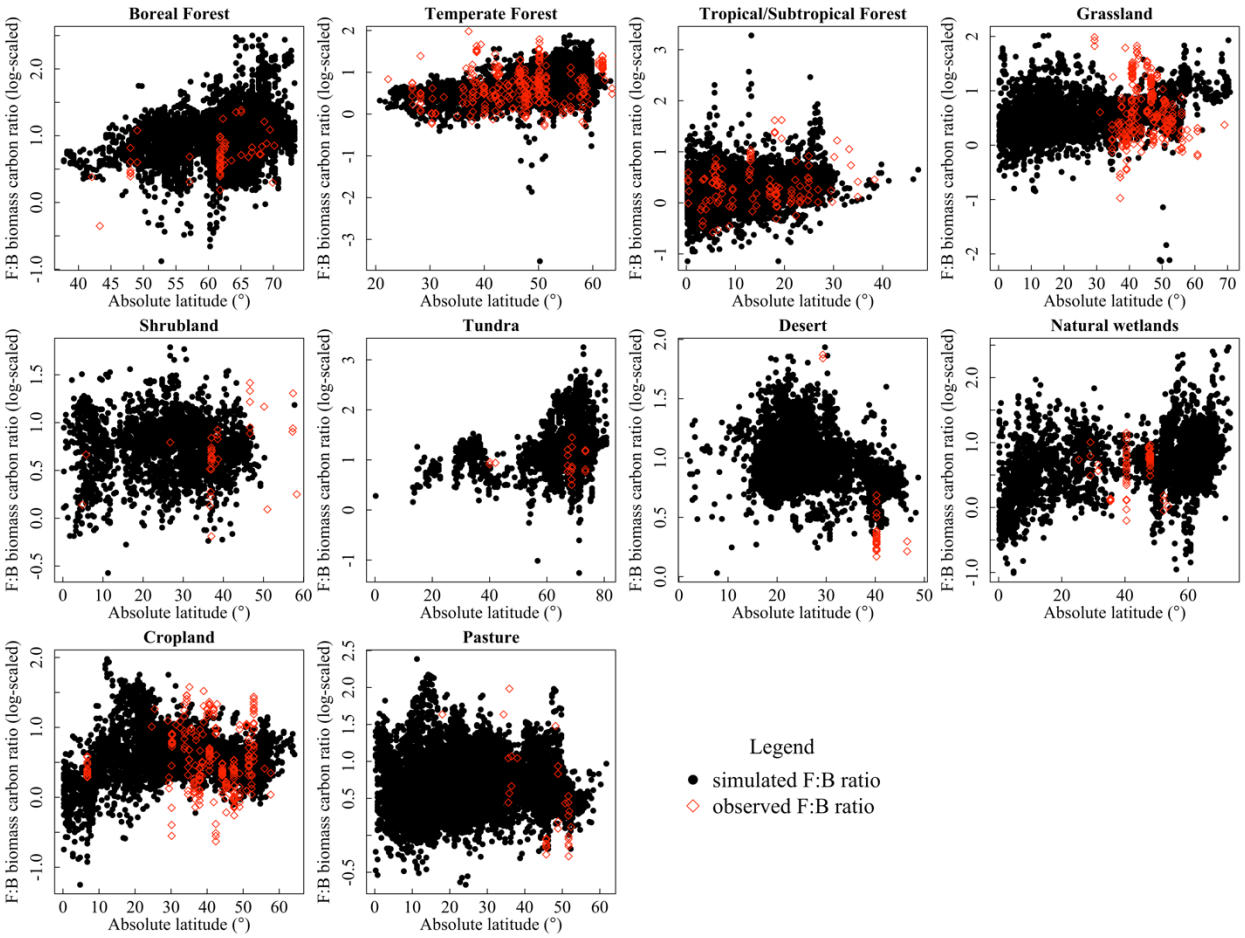

Fig. 1.S9. Comparison between model simulated and observed F:B ratio for major biomes (boreal forest, temperate forest, tropical/subtropical forest, grassland, shrubland, tundra, desert, natural wetland, cropland, and pasture). F:B ratio shown in the figures were log-scaled.

Table 1.S2. Parameters for estimating global map of F:B ratio

	Variables	Estimate	Standard error	P value
	Intercept	0.678900	0.622000	0.275455
Climate	MAT	-0.034020	0.049210	0.489551
	MAP	-0.000058	0.000614	0.925047
Soil microclimate	ST	0.003772	0.005602	0.500997
	SM	**1.542000**	**0.421200**	**0.000272**
Plant	**NPP**	**-0.000990**	**0.000192**	**0.000000**
	C_{root}	**0.015530**	**0.006976**	**0.026334**
Edaphic properties	bulk density	0.122600	0.206900	0.553724
	pH	0.059910	0.054370	0.270924
	clay	**-0.036310**	**0.009657**	**0.000185**
	sand	-0.004500	0.004813	0.350152
	SOC	**0.002878**	**0.000755**	**0.000150**
	TN	-0.016070	0.011010	0.145044
Climate * Soil microclimate	MAT * ST	0.000177	0.000360	0.623217
	MAT * SM	-0.039550	0.022240	0.075823
	MAP * ST	**-0.000015**	**0.000004**	**0.000873**
	MAP * SM	-0.000335	0.000200	0.094909
Climate * Plant	MAT * NPP	0.000005	0.000014	0.746016
	MAT * C_{root}	**-0.001615**	**0.000485**	**0.000911**
	MAP * NPP	**0.000001**	**0.000000**	**0.000019**
	MAP * C_{root}	**0.000007**	**0.000003**	**0.032850**
Climate * Edaphic properties	MAT * bulk density	0.022010	0.021550	0.307570
	MAT * pH	-0.003794	0.004407	0.389535
	MAT * clay	**0.002188**	**0.000624**	**0.000485**
	MAT * sand	0.000137	0.000399	0.730738
	MAT * SOC	-0.000061	0.000086	0.475806
	MAT * TN	**0.005130**	**0.001546**	**0.000957**
	MAP * pH	-0.000029	0.000060	0.633060
	MAP * clay	0.000001	0.000009	0.906910
	MAP * sand	0.000003	0.000005	0.593044
	MAP * SOC	-0.000001	0.000001	0.581057
	MAP * TN	**-0.000043**	**0.000014**	**0.001652**

* MAT, mean annual temperature; MAP, mean annual precipitation; SM, soil moisture; ST, soil temperature; C_{root}, root carbon density; NPP, net primary productivity; SOC, soil organic carbon; TN, total nitrogen; C:N ratio, SOC:TN ratio. Characters and numbers in bold indicate that the estimated coefficients are significant at the 0.05 level.

Chapter 2. Dynamics of Fungal and Bacterial Biomass Carbon in Natural Ecosystems: Site-level Applications of the CLM-Microbe Model

This chapter has already been published by John Wiley and Sons, with a License Number of 5302640557831 for dissertation use.

He, L., D. A. Lipson, J. L. M. Rodrigues, M. Mayes, R. G. Björk, B. Glaser, P. Thornton, and X. Xu. 2021. Dynamics of Fungal and Bacterial Biomass Carbon in Natural Ecosystems: Site-level Applications of the CLM-Microbe Model. Journal of Advances in Modeling Earth Systems **13**:e2020MS002283.

Abstract

Explicitly representing microbial processes has been recognized as a key improvement to Earth system models for the realistic projections of soil carbon (C) and climate dynamics. The CLM-Microbe model builds upon the CLM4.5 and explicitly represents two major soil microbial groups, fungi and bacteria. Based on the compiled time-series data of fungal (FBC) and bacterial (BBC) biomass C from nine biomes, we parameterized and validated the CLM-Microbe model, and further conducted sensitivity analysis and uncertainty analysis for simulating C cycling. The model performance was evaluated with mean absolute error (MAE), root mean square error (RMSE), and coefficient of determination (R^2) for relative change in FBC and BBC. The CLM-Microbe model is able to reasonably capture the seasonal dynamics of FBC and BBC across biomes, particularly for sites in tropical/subtropical forest, temperate broadleaf forest, and grassland, with MAE < 0.49 for FBC and <0.36 for BBC and RMSE <0.52 FBC and <0.39 for BBC, while R^2 values are relatively smaller in some biomes (e.g., shrub) due to small sample sizes. We found good consistencies between simulated and observed FBC (R^2=0.70, P<0.001) and BBC (R^2=0.26, P<0.05) on average across biomes, but the model is not able to fully capture the large variation in observed FBC and BBC. Sensitivity analysis shows the most sensitive parameters are turnover rate, carbon-to-nitrogen ratio of fungi and bacteria, and microbial assimilation efficiency. This study confirms that the explicit representation of soil microbial mechanisms enhances model performance in simulating

C variables such as heterotrophic respiration and soil organic C density. The further application of the CLM-Microbe model would deepen our understanding of microbial contributions to the global C cycle.

Key words: bacteria, biomass dynamics, fungi, model, sensitivity

Introduction

Global climate change is primarily caused by human-induced increases in atmospheric greenhouse gases, modulated by terrestrial ecosystems through a multitude of climate–ecosystem feedbacks (Gruber & Galloway, 2008; Keohane, 2015; Peters et al., 2012; Zaehle et al., 2010). Heterotrophic respiration, the second largest carbon (C) flux in terrestrial ecosystems, is primarily driven by soil microbes (Gougoulias et al., 2014; Sulman et al., 2014; Van Der Heijden et al., 2018). Although progress has been made in understanding how microbes affect C cycling, more research is needed on how to accurately project microbial feedbacks to climate change. Large uncertainties in global C projections challenge the current model framework (Luo et al., 2015; Taylor et al., 2011), and the implicit representation of soil microbes may account for parts of those uncertainties (Fang et al., 2005; Wieder et al., 2015; Wieder et al., 2013; Xu et al., 2014).

The importance of soil microbes in governing the terrestrial C cycle has received growing attention, and soil microbial processes have been partially represented in ecosystem models (Schimel & Weintraub, 2003; Treseder et al., 2012). The development of soil microbial models, such as the SCAMPS model (Sistla et al., 2014), DAMM model (Davidson et al., 2012), microbial-enzyme model (Allison et al., 2010), and MEND model (Wang et al., 2013), proved to be valauble in simulating microbial feedbacks to soil C processes. Soil microbial traits such as enzyme production, temperature sensitivity, carbon use efficiency (CUE), microbial and abiotic interaction, and priming effects were incorporated into soil microbial models (Allison, 2012; Allison et al., 2010; Tang & Riley, 2015). Recently, soil microbes and

microbial traits have increasingly been incorporated into Earth system models (ESMs), such as the CORPSE model (Sulman et al., 2014). However, these models assumed that biological responses of soil microbial community are functionally equivalent and exert invariant effects on soil processes (Bradford & Fierer, 2012). Given the large temporal variations in soil microbial community (Cleveland et al., 2007; Díaz-Raviña et al., 1995; Lipson et al., 2002; Lipson & Schmidt, 2004), the assumption of a static soil microbial community is increasingly questioned (Wang et al., 2015; Wieder et al., 2015; Wieder et al., 2014).

Developing models that explicitly represent soil microbial processes poses an important challenge for ESMs. Recently, the classification of soil microbes in the TRIPLEX-Microbe model (active and dormant components) and the MIMICS model (K- and r-strategists) advanced the representation of the soil microbial community and its functions in ESMs (Wang et al., 2017; Wieder et al., 2014). However, the distinct roles of broad soil microbial groups (e.g., fungi and bacteria) have not yet been considered in models. Bacteria and fungi have different physiological traits, e.g., bacteria prefer to decompose litter low in carbon-to-nitrogen (C:N) ratio, while fungi tend to decompose litter with higher C:N ratio (Paul, 2016). These differences may cause considerable distinct trajectories of C responses to changing environments such as atmospheric nitrogen (N) deposition, elevated carbon dioxide (CO_2), and precipitation change (Bell et al., 2014; Hopkins et al., 2006; Rousk & Bååth, 2011; Strickland & Rousk, 2010). The classification of the soil microbial community into K- and r-strategists based on functional traits improved the representation of distinct roles of soil microbial groups in biogeochemical processes; however, this characterization is largely theoretical and may therefore limit the effort of directly applying observational data to constrain the microbial parameters.

Fungi and bacteria, two major measurable soil microbial groups playing distinct roles on soil processes, comprise over 90% of the total soil microbial biomass and are the major agents responsible for decomposition in soils (Beare, 1997). Although fungi are widely believed to decompose low quality compounds such as lignin, bacterial ligninases are also commonly found, both fungi and bacteria decompose plant residues and soil organic matter (Burns et al., 2013). For example, as litter quality decreases, fungi are expected to play more important roles (Van Der Heijden et al., 2018). Soil fungal and bacterial biomass are important components of soil microbial community (He et al., 2020), representing the microbial ability to conduct biochemical transformation of C and nutrients (Xu et al., 2013). Therefore, variations in fungal:bacterial (F:B) biomass ratio can imply changes in the population of decomposers as well as changes in soil microbial community composition and function (Six et al., 2006).

To fill the research gap of explicitly representing soil microbial community functions in ESMs, we developed the CLM-Microbe model based on the framework in Xu et al. (2014). Fungi- and bacteria-regulated processes such as the decomposition of plant and microbial residues were added into the CLM4.5 to mechanistically represent major soil microbial processes (Fig. 2.1). To distinguish the physiological traits of fungi and bacteria in soil processes, different parameters for fungal- and bacterial-regulated processes were developed and tested. In this study, we reported the model parameterization, sensitivity analysis, and uncertainty analysis at the site level for nine different biomes, and we emphasized on interpreting and explaining the simulated results. The key objectives were to: 1) parameterize the CLM-Microbe model using observed time-series data of fungal (FBC) and bacterial (BBC) biomass C in diverse biomes, 2) evaluate the performance of the CLM-Microbe model in simulating FBC and BBC dynamics, and 3) identify the key parameters and processes controlling variations in FBC and BBC.

Methodology

Data sources

Due to the large variation in soil microbial community among biomes, we parameterized the model by biome (Xu et al., 2014). We selected time-series observed data of FBC and BBC from nine natural biomes (i.e., tropical/subtropical forest, temperate coniferous forest, temperate broadleaf forest, boreal forest, shrub, grassland, desert, tundra, and wetland), with at least two sites in each biome. Then, we randomly selected one site for model calibration and the others for model validation. Finally, nine sites were used for model calibration and twelve sites for model validation for nine natural biomes. Site information, including geographic location, biome type, site name, site ID, sampling years, and the measurement methods, was presented in Table 2.1.

The FBC and BBC were derived from multiple approaches, such as direct microscopy using optical microscope (DMO) or fluorescence microscope (DMF), plate count (PC), chloroform fumigation (CF), fatty acid methyl ester (FAME), and phospholipid fatty acid (PLFA). Based on our previous study, large variations exist in measured fungal and bacterial biomass among different approaches (He et al., 2020). The PLFA was the most widely used in field observed data (Table 2.2), and likely the most appropriate approach for estimating FBC and BBC simultaneously (He et al., 2020; Waring et al., 2013). To reduce the biases introduced by various approaches, we converted the reported FBC and BBC measured using DMO (Balser et al., 2005; Olsson & Wallander, 1998), DMF (Frostegård & Bååth, 1996; Stahl & Parkin, 1996), PC (Bai et al., 2013; Priha et al., 1999), CF (Bailey et al., 2002), and FAME (Miura et al., 2017) to PLFA measured values using the conversion factors reported by previous studies, which measured the FBC and BBC using at least two methods simultaneously. Then, we performed the conversion from the measured fungal and bacterial PLFA concentration to FBC and BBC using conversion factors reported by Frostegård and Bååth (1996) and Klamer and Bååth (2004).

Model improvements

The CLM-Microbe model was developed based on the default CLM4.5 with vertical profiles of biogeochemistry, and we specifically incorporated soil microbial processes into the decomposition subroutines (Koven et al., 2013; Thornton et al., 2007; Thornton & Rosenbloom, 2005). The key algorithm for simulating microbial controls on C processes is based on the model framework in Xu et al. (2014). The CLM4.5 classified litter into three pools, i.e., litter 1 (labile), litter 2 (cellulose) and litter 3 (lignin), and soil organic matter (SOM) into four pools, i.e., SOM 1, SOM 2, SOM 3, and SOM 4. The three litter and four SOM pools differ in base decomposition rate (τ), with turnover time of litter pools ranging from 20 hours to 71 days and SOM pools ranging from 14 days to 27 years (Fig. 2.1). Coarse woody debris (CWD) is fragmented, decomposed, and gradually transferred into litter pools, and further from litter to SOM pools (Koven et al., 2013).

One critical improvement in the CLM-Microbe model is the representation of the pools of dissolved organic matter (DOM), fungal and bacterial biomass into the biogeochemistry cascade in the default CLM4.5 (Fig. 2.1). The DOM pool is further linked with a microbial functional group-based methane module (Wang et al., 2019; Xu et al., 2015). In the decomposition subroutine, we changed the original transfers from litter to SOM to mechanisms that were mediated by soil fungi and bacteria. Specifically, we added the C transfer from litter and SOM pools to fungal and bacterial biomass pools and DOM, from DOM pool to fungal and bacterial biomass and SOM pools, and from fungal and bacterial biomass pools to DOM and SOM pools. A certain proportion of C, defined by fraction factors in fungal and bacterial biomass pools, will be respired as CO_2 into the atmosphere. In total, the CLM-Microbe model included 41 transitions mediated by fungi and bacteria, which largely increased the accuracy of simulating the complex soil processes relative to 9 transitions in the default CLM4.5. In each soil layer, these transitions

are regulated by environmental factors (e.g., temperature, moisture, and oxygen) in the soil. We defined 26 parameters related to fungi and bacteria related processes in the CLM-Microbe model, with the range and description of each parameter to be found in Table 2.2. The code for the CLM-Microbe model has been archived at https://github.com/email-clm/clm-microbe, since 2015. The model version used in this study was checked out from GitHub on June 18, 2018.

Vegetation effects on soil microbial community

Vegetation also has a significant influence on soil microbial growth through litter input and root exudation (Blagodatskaya & Kuzyakov, 2008). Labile C from litter and root exudates, in the form of DOM, can be readily used to enhance fungal and bacterial growth (Göttlicher et al., 2006). Therefore, in addition to the slow breakdown of SOM and litter, the DOM pool is refreshed by a rapid release from living roots and fresh litter, playing an important role in soil microbial activity (Sulman et al., 2014). In the CLM-Microbe model, we incorporated the DOM input from fine roots and litter, and the quantity of DOM input from these pools are determined by a parameter quantifying the labile C release from pools of fine roots and litter and their pool size. The incorporation of DOM input from litter and fine roots represents the vegetation effects on soil microbial community.

Decomposition

The decomposition of SOM, DOM, and litter was controlled by both their potential decomposition rates and environmental conditions. The decomposition processes in the CLM-Microbe model were defined following the equations as below,

$$D_C = k \times r_{oxygen} \times r_{depth} \times r_{tsoil} \times r_{water}$$

$$r_{depth} = \exp\left(-\frac{z}{z_\tau}\right)$$

$$r_{tsoil} = Q_{10}^{\frac{T_{soil,j}-T_{ref}}{10}}$$

$$r_{water} = \begin{cases} 0 & for\ \varphi_j < \varphi_{min} \\ \dfrac{log\left(\varphi_{min}/\varphi_j\right)}{log\left(\varphi_{min}/\varphi_{max}\right)} & for\ \varphi_{min} \leq \varphi_j \leq \varphi_{max} \\ 1 & for\ \varphi_j > \varphi_{max} \end{cases}$$

where D_C is the rate of substrate (e.g., SOM, DOM, and litter) breakdown; k is the potential decomposition rate; r_{oxygen} represents environmental modifier determined by soil oxygen concentration, which is set as 1 for the single layer model; r_{depth} is environmental modifier determined by soil depth, which is set as 1 for the single layer model; r_{water} is environmental modifier determined by soil moisture; r_{tsoil} means environmental modifier determined by soil temperature; z means soil depth; z_τ is the e-folding depth for decomposition; $T_{soil,j}$ is soil temperature at layer j; T_{ref} is the reference temperature for decomposition, which is set as 25°C; Q_{10} indicates the temperature dependence of decomposition, it is the ratio of the rate at a specific temperature to that at 10°C lower; Ψ_j is the soil water potential in layer j; Ψ_{min} is a lower limit for soil water potential control on decomposition rate (set to -10 MPa), r_{water} will be set as 0 if Ψ_j is lower than Ψ_{min}; Ψ_{max} is the upper limit for soil water potential control on decomposition, which equals to the saturated soil matric potential, r_{water} will be set as 1 if Ψ_j is higher than Ψ_{max}; $w_{soil,j}$ means soil water content in layer j.

Although there are variations in Q_{10} of substrate mineralization under various land use types, nutrient concentrations, moisture contents, property of substrates, and temperature gradients for measurement (Fierer et al., 2003; Hopkins et al., 2006; Larionova et al., 2007), the Q_{10} value is confined close to 1.5 at ecosystem-level, which is set as default Q_{10} value in CLM4.5. There is no difference in decomposition between aboveground and belowground substrate, Q_{10} values of the decomposition of three litter pools (Litter 1, Litter 2, and Litter 3) and two less stable SOM pools (SOM 1 and SOM 2) were set as 1.5 in the CLM-Microbe model, which is consistent with the default CLM4.5. Stable SOM in deep soils is believed

to have higher Q_{10} value than that in surface soils (Fierer et al., 2003; von Lützow & Kögel-Knabner, 2009), indicating that the decomposition of stable SOM in subsurface soil is more sensitive to temperature change than that in surface soil. Therefore, to differentiate the Q_{10} of SOM decomposition in different soil depths, Q_{10} values of 3rd SOM pool and 4th SOM pool are set as 2 and 2.5, respectively, in the CLM-Microbe model. Due to the simple chemical structure and low activation energy of DOM, Q_{10} value of DOM is expected to be lower than SOM and litter (Davidson & Janssens, 2006). Consequently, we set the Q_{10} value of DOM as 1.25 in the CLM-Microbe model.

Microbial lysis

The microbial biomass turnover is closely associated with the SOM formation, while the contribution of microbial biomass residues to the formation of SOM has been largely underestimated (Liang et al., 2019). However, growing evidence showed that the soil microbial community made a relatively high contribution to soil organic carbon (SOC) due to its large pool size (Xu et al., 2013) and fast turnover rate (Glaser et al., 2004). Sinsabaugh et al. (2016) estimated a global mean biomass turnover time of 67 ± 22 days based on a negative linear relationship between CUE and microbial biomass turnover time, with the mean microbial CUE estimated as 0.25-0.30. Xu et al. (2017) also quantified the microbial biomass turnover time as 23 and 28 days based on the area-weighted global average of the metabolic quotient in soils (1.8 μmol C·mmol microbial biomass $C^{-1}\cdot h^{-1}$) and reference metabolic quotient (1.5 μmol C·mmol microbial biomass $C^{-1}\cdot h^{-1}$), respectively, from a global microbial metabolic quotient dataset. These estimates in soil microbial biomass turnover are generally in the same order and vary slightly; however, the turnover rates of different soil microbial groups (e.g., fungi and bacteria) were distinct and in a wide range of variation, with fungal and bacterial biomass turnover rate reported as 0.00143 to 2 d^{-1} (Moore et al., 2005; Rousk & Bååth, 2007, 2011) and 0.00027 to 0.05 d^{-1} (Moore et al., 2005; Rousk & Bååth, 2011; Strickland & Rousk, 2010; Wallander et al., 2004), respectively.

In addition, bacterial and fungal growth are highly sensitive to environmental conditions, such as soil moisture and temperature. As a result, in the CLM-Microbe model, fungal and bacterial biomass lysis process is mechanistically represented as the interactive effects of lysis rate constant and environmental factors, i.e., r_{oxygen}, r_{water}, r_{tsoil}, and r_{depth}, described above.

Soil microbial respiration

Bacteria and fungi assimilate DOM, SOM, and litter to form their biomass, and a proportion of the assimilated C is respired (Fig. 2.1). The proportion of C used for fungal and bacterial respiration is determined by the factors indicated in Table 2.2 and Table 2.3. In addition, heterotrophic respiration (HR) is widely affected by multiple abiotic and biotic factors, such as substrate concentration and availability, soil moisture, and soil temperature (Gomez-Casanovas et al., 2012; Zhang et al., 2013). Therefore, fungal and bacterial respiration in the CLM-Microbe model are defined as the interactive effects of substrate (i.e., DOM, SOM, and litter), fraction factors quantifying C being respired by fungi and bacteria, and environmental factors (i.e., r_{oxygen}, r_{water}, r_{tsoil}, and r_{depth}) regulating the respiration process.

Carbon use efficiency

The CUE of soil microbes for three litter pools in the CLM-Microbe model are determined following the equation in Sinsabaugh et al. (2013). In addition, CUE is reported to vary with temperature, showing a coefficient of -0.012 with increasing temperature (Devêvre & Horwáth, 2000; Xu et al., 2014). Therefore, we assumed that CUE decreased compared with the ambient thermal regime of microbes' habitats following the equation as below,

$$\mathrm{CUE} = \left(\mathrm{CUE}_{\max} - CUE_T \times \left(T - T_{CUEref}\right)\right) \times \left({M_{\mathrm{C:N}}}/{S_{\mathrm{C:N}}}\right)^{0.6}$$

where *CUE* is C use efficiency, which is defined as the growth-to-assimilation ratio for soil microbes; CUE_{max} is the maximum value of C use efficiency; CUE_T is the coefficient indicating the dependence of C use efficiency on temperature; T_{CUEref} is the reference temperature of C use efficiency, which is defined as 15°C in the CLM-Microbe model; $M_{C:N}$ means the C:N ratio of soil microbial biomass, which is defined as 8 in the CLM-Microbe model; $S_{C:N}$ represents C:N ratio of substrate (e.g., litter).

The C flow from litter and SOM pools to soil microbes will be partitioned by fungal and bacterial biomass pools based on the C:N ratio of fungal and bacterial biomass. The fraction factor quantifying bacteria C gain from litter and SOM is calculated based on the weighted average of assimilation efficiency of fungi and bacteria following the equation as below,

$$fb = \frac{\left(B_{\mathrm{C:N}}/S_{\mathrm{C:N}}\right)^{0.6}}{\left(F_{\mathrm{C:N}}/S_{\mathrm{C:N}}\right)^{0.6} + \left(F_{\mathrm{C:N}}/S_{\mathrm{C:N}}\right)^{0.6}}$$

$$ff = 1 - fb$$

where *fb* is the fraction of C flowing into bacteria; *ff* is the fraction of C flowing into fungi; $B_{C:N}$ means the C:N ratio of BBC; $F_{C:N}$ means the C:N ratio of FBC; $S_{C:N}$ represents C:N ratio of substrates (e.g., litter and SOM).

Model forcing data

The forcing data for this model include meteorological data such as air temperature, relative humidity, incoming solar radiation, longwave radiation, precipitation rate, surface pressure, and surface winds. Since the sampling year of the sites spans from 1973 to 2018, which was not fully covered by any commonly used forcing datasets of CLM. After examining the data distribution, we found that sites

sampling later than 2014 are in North America (Table 2.1). Therefore, for sites sampled before 2014, we extracted the forcing data during 1 January 1971 through 31 December 2014 from CRUNCEP Version 4 provided by Climate Data Gateway at the National Center for Atmospheric Research (https://www.earthsystemgrid.org). The forcing data for sites sampled later than 2014 were extracted from the Global Land Data Assimilation System Version 2 (https://ldas.gsfc.nasa.gov). Using the latitude and longitude information of study sites in each biome (Table 2.2), we extracted the meteorological variables for all sites. Since the standardized input forcing data are in half-hourly time steps, the extracted 6-hourly data for each study site was interpolated to half-hourly step using linear interpolation via na.approx function in R (R for Mac OS X version 3.5.3).

Model implementation

We used default parameters for the subroutine of soil hydrological properties and methane module (Koven et al., 2013; Xu et al., 2015), and we focused on the parameterization for soil microbial mechanisms related to FBC and BBC dynamics (Table 2.2). To parameterize the model, we set up model simulations separately for nine sites (TSF-HS, TCF-NJ, TBF-VA, BRF-WC, SHB-OB, GRS-IA, DST-CH, TUN-MH, and WET-EM) in the phase of calibration and twelve sites (TUN-ES, TCF-NT, DST-GB, DST-JN, BRF-AL, TSF-OS, GRS-BC, TBF-SH, TBF-MS, TBF-TL, SHB-AC, and WET-EF) in the phase of validation (Table 2.1).

The model implementation for all sites was carried out in three stages. First, we ran the accelerated decomposition spin-up to make the system reach steady state (Thornton & Rosenbloom, 2005). Due to the differences in the length of time to reach steady state among biomes, we set the model run as 1500 years for tropical and temperate biomes (i.e., tropical/subtropical forest, temperate coniferous forest, temperate broadleaf forest, shrub, grassland, and desert), 2000 years for boreal and arctic biomes (i.e., boreal forest

and tundra), and 3000 years for wetlands. Then, we ran a final spin-up of 100 years to make the system ready for transient simulations during 1850 - 2018. Since observational FBC and BBC are reported at daily scale, we set the output resolution of transient simulations as a daily time step.

To guarantee the reasonable soil and vegetation conditions in each site at the same standard, we extracted the SOC of the top 1 m soil profile from the Harmonized World Soil Database (HWSD, https://daac.ornl.gov/cgi-bin/dsviewer.pl?ds_id=1247) and net primary productivity (NPP) from MODIS gridded dataset with a spatial resolution of 30 seconds during 2000-2015 (http://files.ntsg.umt.edu/data/NTSG_Products/) for each site using their latitude and longitude information. Before parameterizing the CLM-Microbe model, we adjusted the parameters related to plant photosynthesis (e.g., *flnr*), C allocation (e.g., *froot_leaf*), and e-folding depth for decomposition (e.g., *decomp_depth_efolding*) to make all the sites have soil and vegetation conditions reported by global datasets. Since soil and vegetation are in high spatial heterogeneity, the global datasets may not be able to capture the variation at fine scale. If the SOC and NPP extracted from global datasets were extremely high or low for the biome, we used the values reported in the literature. If the SOC and NPP were not available from literature, we used the biome average instead (Chapin et al., 2011; Jobbágy & Jackson, 2000). For tropical/subtropical forest, we had a site specified as needleleaf trees, whereas tropical needleleaf tree is not available in default plant function types. Therefore, we modified the parameters for needleleaf_evergreen_temperate_tree following the parameters featuring tropical trees such as minimum and upper limit of temperature for growth and monthly temperature. Also, we altered the longevity for needleleaf_evergreen_temperate_tree following the trend of needle tree leaf longevity reported by Xiao (2003).

Based on the current knowledge of mechanisms for FBC and BBC dynamics, we primarily focused on parameters related to microbial lysis (*m_bdom_f*, *m_bs1_f*, *m_bs2_f, m_bs3_f*, *m_fdom_f*, *m_fs1_f, m_fs2_f*, *m_fs3_f*, *k_bacteria*, and *k_fungi*), microbial respiration (*m_batm_f* and *m_fatm_f*), decomposition of litter, DOM and SOM *(k_dom*, *m_domb_f*, *m_domf_f*, *m_doms1_f*, *m_doms2_f*, and *m_doms3_f*), and stoichiometric traits of fungal and bacterial biomass (*cn_bacteria* and *cn_fungi*). We first ran the model for each biome using the average values reported by previous studies, then we empirically calibrated the parameters based on the observed FBC and BBC of sites selected in calibration phase (Table 2.3). The calibration was based on the model behavior in capturing the seasonal variations in FBC and BBC when plotting them against the time axis. Next, we validated the model using the parameters in Table 2.3 to test the model simulation performance by plotting simulated FBC and BBC against the observed data.

Model evaluation

We used three metrics to evaluate model performance, including:

1. Mean absolute error (MAE), a measure of model error, was computed as

$$MAE = \frac{1}{N}\sum_{i=1}^{N}|y_i - \hat{y}|$$

where y_i is the simulated value; $\hat{y}$ means the observed value; *N* is the number of data points. The MAE indicates the mean error of the model simulation, and thus lower MAE values are preferred.

2. Root mean square error (RMSE), indicating the model accuracy, was calculated as:

$$RMSE = \sqrt{\frac{1}{N}\sum_{i=1}^{N}(y_i - \hat{y})^2}$$

where y_i is the simulated value; $\hat{y}$ means the observed value; *N* is the number of data points. Similar with MAE, RMSE also indicates the mean error of the model simulation, and the lower values indicate the higher model accuracy. The RMSE estimation is equal or larger than MAE estimation in most cases, and the degree to which RMSE estimation exceeds MAE estimation depend on the outliers in the simulated and observed data.

3. The coefficient of determination (R^2), representing the variation in the observations explained by the model, was calculated following the equation as below,

$$R^2 = 1 - \frac{\sum(y_i - \hat{y})^2}{\sum(y_i - \bar{y})^2}$$

where y_i is the simulated value; $\hat{y}$ means the observed value; $\bar{y}$ is the mean of the observed value. Higher R^2 values indicate better performance of the model, while lower R^2 values mean the worse model performance and smaller proportion of variation being explained by the model. It is noteworthy that R^2 is not suitable for assessing the goodness-of-fit for a small number of data points due to the large bias in small samples.

Sensitivity analysis and uncertainty analysis

To identify the key processes and parameters for FBC and BBC dynamics across biomes, we conducted sensitivity analysis using one site in each biome. We selected 25 parameters related to the decomposition of SOM, litter and DOM, fungal and bacterial respiration, CUE, and microbial lysis for identifying key processes and parameters in regulating FBC and BBC dynamics, which were also used for uncertainty

analysis (Table 2.5). Eventually, nine sites, i.e., DST-CH, GRS-IA, SHB-OB, TUN-MH, BRF-WC, TBF-VA, TCF-NJ, TSF-HS, WET-EM, were used for sensitivity analysis, and these sites were also used for subsequent uncertainty analysis (Fig. 2.7, Table 2.6). For each parameter, we set up model simulations with +20% or -20% change in the parameter, and thus we set up 50 model simulations in total for sensitivity analysis in each site. Next, we investigated the responses of the simulated FBC, BBC, F:B ratio, SOC, and HR in surface soil (0-30 cm) during sampling period of each site. The index *S*, comparing the change in the model output relative to the model response for a nominal set of parameters, was calculated based on the equation following Xu et al. (2015).

$$S = \frac{(Ra - Rn)/Rn}{(Pa - Pn)/Pn}$$

where *S* is the ratio of the standardized change in model response to the standardized change in parameter values; R_a and R_n are model responses for altered and nominal parameters, respectively; P_a and P_n are the altered and nominal parameters, respectively. Negative *S* values indicate the opposite direction of model response with the regards of the direction of parameter change, and vice versa. We visualized the sensitivity analysis results using the "ComplexHeatmap" package developed by Gu et al. (2016) in R 3.5.3 for Mac OS X (R Development Core Team, 2018).

The uncertainties in FBC, BBC, F:B ratio, SOC, and HR in surface soil (0-30 cm) during the sampling period of each site were quantified using improved Latin Hypercube Sampling (LHS) approach. The LHS approach can randomly produce an ensemble of parameter combinations with high efficiency. This approach has been widely used in the modeling community to estimate uncertainties in model output (Haefner, 2005; Xu, 2010; Xu et al., 2014). First, we assumed that all parameters follow normal distribution, then we used LHS to randomly select an ensemble of 300 parameter sets using the function of "improvedLHS" in the R package "lhs" (Carnell & Carnell, 2019). Second, we computed the inverse of the standard normal cumulative distribution of 300 parameter sets using "norminv" function in MATLAB

2018b (The MathWorks Inc., Natick, Massachusetts, USA), with the standard deviation of each parameter set as 20% of its optimal value. Third, we added the filter of setting parameters featuring fraction factors (*m_rf_s1m*, *m_rf_s2m*, *m_rf_s3m*, *m_rf_s4m*, *m_batm_f*, *m_bdom_f*, *m_bs1_f*, *m_bs2_f*, *m_bs3_f*, *m_fatm_f*, *m_fdom_f*, *m_fs1_f*, *m_fs2_f*, *m_fs3_f*, *m_domb_f*, *m_domf_f*, *m_doms1_f*, *m_doms2_f*, *m_doms3_f*) larger than 1 or smaller than 0 or the sum of an array of parameters (*m_batm_f*, *m_bdom_f*, *m_bs1_f*, *m_bs2_f*, and *m_bs3_f*, or *m_fatm_f*, *m_fdom_f*, *m_fs1_f*, *m_fs2_f*, and *m_fs3_f*, or *m_domb_f*, *m_domf_f*, *m_doms1_f*, *m_doms2_f*, and *m_doms3_f*) larger than 1 as their optimal values. Finally, we implemented the 300 model runs for each biome, and we then calculated the 95% confidence interval of FBC, BBC, F:B ratio, SOC, and SR in surface soil (0-30 cm) during experimental period of each site for reporting (Table 2.6).

Results

Model parameterization and validation against observational data

The comparison between modeled and observed data showed that the CLM-Microbe model can capture the average and seasonal variation of FBC and BBC across biomes (Fig. 2.6, Table 2.4). On average, the simulated FBC and BBC were consistent with the observed values, with FBC and BBC showing R^2 values of 0.70 (P<0.001) and 0.26 (P<0.05), respectively (Fig. 2.6). However, FBC and BBC were underestimated by the CLM-Microbe model. For example, the simulated FBC was approximately 50% lower than the observed FBC in BRF-AL (boreal forest, BRF-) and SHB-OB (shrub, SHB-), and 40% lower than the observed FBC in DST-GB (desert, DST-) and TBF-VA and TBF-MS (temperate broadleaf forest, TBF-). Simulated BBC was 55% lower than the observed BBC in TUN-ES and TUN-MH (tundra, TUN-) and GRS-BC (grassland, GRS-), and 45% lower than the observed BBC in BRF-AL and TCF-NT (temperate coniferous forest, TCF-). The CLM-Microbe model overestimated FBC compared to the observed values in some sites; specifically, the simulated FBC was higher than the observed FBC in

WET-EF and WET-EM (wetland, WET-), DST-JN, and GRS-IA. The simulated BBC was higher than the observed BBC in WET-EF, WET-EM, DST-CH, BRF-WC, SHB-AC, and TSF-HS and TSF-OS (tropical/subtropical forest, TSF-) (Fig. 2.6). To compare the seasonal dynamics between observed and simulated FBC and BBC, y axes in Fig. 2.5 were adjusted to facilitate the visualization of modeling results due to the systematic underestimation of FBC and BBC.

Additionally, we found relatively smaller variation (indicated as standard error, SE) in simulated FBC (SE ranging from 0.04 to 0.90 gC m^{-2}) and BBC (SE ranging from 0.02 to 0.91 gC m^{-2}) compared with the observed FBC (SE ranging from 0.26 to 99.11 gC m^{-2}) and BBC (SE ranging from 0.07 to 12.48 gC m^{-2}) (Fig. 2.6). On average, the SE of simulated FBC and BBC was approximately 160 and 40 times smaller than the SE of observed FBC and BBC, respectively. The difference of SE in observed FBC and BBC among biomes was largely dependent on the magnitude of observed FBC and BBC (Fig. 2.6). The highest SE of observed FBC was observed in TBF-MS (99 gC m^{-2}), BRF-AL (55 gC m^{-2}), and TUN-MH (57 gC m^{-2}). The lowest SE of observed FBC were observed in WET-EF (0.93 gC m^{-2}), WET-EM (0.26 gC m^{-2}), and DST-JN (0.26 gC m^{-2}). Compared with SE of observed FBC, SE of observed BBC was much smaller. However, SE of observed BBC were distinct among sites. We observed the highest SE of observed BBC in TUN-MH (12 gC m^{-2}), and TBF-MS (12 gC m^{-2}). The SE of observed BBC was lowest in TBF-SH (0.40 gC m^{-2}), WET-EF (0.24 gC m^{-2}), TSF-HS (0.18 gC m^{-2}), and WET-EM (0.07 gC m^{-2}).

Due to the large difference in variations of simulated and observed FBC and BBC, we estimated the simulated FBC and BBC dynamics using relative change in FBC and BBC, i.e., the difference between individual and the average of biomass over the average of biomass during the study period (Table 2.4). In the calibration phase, MAE ranged from 0.06 to 1.16 for FBC and from 0.06 to 1.04 for BBC, while RMSE ranged from 0.07 to 1.43 for FBC and from 0.07 to 1.11 for BBC. In the validation phase, MAE

ranged from 0.01 to 0.73 for FBC and from 0.04 to 1.18 for BBC, while RMSE ranged from 0.02 to 0.79 for FBC and from 0.04 to 2.02 for BBC. Although the model explained the FBC and BBC dynamics well in most sites, particularly TBF-MS (R^2=0.94 for FBC and R^2=0.95 for BBC) and TSF-OS (R^2=0.98 for FBC and R^2=0.52 for BBC), the simulation in some sites for FBC (GRS-IA, SHB-OB, GRS-BC, SHB-AC, TBF-TL, TBF-SH, TCF-NT, and WET-EF) and BBC (TSF-HS, GRS-BC, TUN-ES, and WET-EF) was relatively poor, with R^2 smaller than 0.1. It is noteworthy that the number of data points ranges from 2 to 13 for FBC and BBC data across sites, which is much smaller than 30, the threshold for a large sample. The R^2 may not be suitable for assessing the goodness-of-fit for a small number of data points due to the large bias in small samples, although it is widely used in model performance estimation. For example, R^2 was 0.005 for FBC and 0.299 for BBC in SHB-OB, while MAE (0.06 for FBC and BBC) and RMSE (0.07 for FBC and BBC) were small, indicating small biases in the simulated FBC and BBC.

Sensitivity analysis

We found high sensitivity of FBC and BBC dynamics to parameters that related to microbial turnover and C:N ratio of fungal and bacterial biomass across biomes (Fig. 2.7). Fungal biomass turnover rate (*k_fungi*) had negative effects on FBC and F:B ratio across biomes, while bacterial biomass turnover rate (*k_bacteria*) had negative and positive effects on BBC and F:B ratio, respectively, across biomes. The C:N ratio of bacterial biomass (*cn_bacteria*) had negative, positive, and negative effects on FBC, BBC, and F:B ratio, respectively. In contrast, C:N ratio of fungal biomass (*cn_fungi*) had positive, negative, and positive effects on FBC, BBC, and F:B ratio, respectively. A 20% increase or decrease in *k_fungi* and *k_bacteria* led to different magnitudes of negative effects on FBC and BBC, respectively, across biomes. While a 20% decrease in *k_fungi* and *k_bacteria* led to the S values around -1.25 and -1.30 for FBC and BBC, a 20% increase in *k_fungi* and *k_bacteria* resulted in S values around -0.85 and -0.84 for FBC and BBC, respectively. Changes in *k_bacteria* had similar magnitudes of positive effects on F:B ratio, with S values around 1.00 for both 20% increase and decrease in *k_bacteria*. While a 20% increase or decrease

in *k_fungi* had different magnitudes of negative effects on F:B ratio, with a 20% decrease or increase in *k_fungi* leading to S values around -1.27 and -0.85, respectively, across biomes. The higher S values suggested that FBC and BBC were more sensitive to decreases in *k_fungi* and *k_bacteria*, which would induce larger increases in FBC and BBC; in particular, a 20% decrease in *k_fungi* led to higher sensitivity of F:B ratio.

In addition, FBC and BBC were closely correlated with the decomposition of SOM and DOM and microbial respiration (Fig. 2.7). Fraction factors quantifying C flow from SOM to soil microbes (*m_rf_s1m*, *m_rf_s2m*, *m_rf_s3m*, and *m_rf_s4m*) were positively correlated with FBC and BBC. However, the magnitude of the *m_rf_s4m* on FBC and BBC were different among biomes. The highest response was in TSF-HS (S=1.03 for FBC and S=1.08 for BBC with -20% change vs. S=1.42 for FBC and S=1.49 for BBC with +20% change), while the lowest response was in BRF-WC (S=0.28 for FBC and S=0.26 for BBC with -20% change vs. S=0.28 for FBC and S=0.24 for BBC with +20% change). In addition, we found a positive correlation between the fraction factor quantifying C flow from DOM to fungal biomass (*m_domf_f*) and FBC and F:B ratio and a positive correlation between fraction factor quantifying C flow from DOM to bacterial biomass (*m_domb_f*) and BBC, and a negative correlation between *m_domb_f* and F:B ratio. However, the magnitudes varied among biomes, with FBC being most sensitive to *m_domf_f* in GRS-IA (S=0.432), BBC being most sensitive to *m_domb_f* in TBF-VA (S=0.593), and F:B ratio being most sensitive to *m_domf_f* in GRS-IA (S=0.415) and *m_domb_f* in TBF-VA (S=-0.630) with -20% change. In contrast, FBC, BBC, and F:B ratio were insensitive to *m_domb_f* and *m_domf_f* in BRF-WC, with the absolute S values close to 0.001. Moreover, we found weak positive effects of fraction factors quantifying C flow from DOM to SOM (*m_doms1_f*, *m_doms2_f*, and *m_doms3_f*) on FBC and BBC across biomes. Across biomes, FBC, BBC, F:B ratio, SOC, and HR in surface soil (0-30 cm) were insensitive to maximum microbial CUE (CUE_{max}). We observed a higher negative correlation between fraction factor quantifying C being respired by fungi (*m_fatm_f*) and FBC

and between the fraction factor quantifying C being respired by bacteria (*m_batm_f*) and BBC in GRS-IA, TSF-SH, and TCF-NJ, with S values ranging from -0.104 to -0.044 of *m_fatm_f* for FBC and from -0.615 to -0.023 of *m_batm_f* for BBC, while FBC and BBC in other biomes were insensitive to *m_batm_f* and *m_fatm_f* change.

The SOC was positively correlated with fraction factors quantifying C flow from SOM to soil microbes (*m_rf_s1m*, *m_rf_s2m*, *m_rf_s3m*, or *m_rf_s4m*), while SOC was negatively correlated with fraction factor quantifying C being respired by bacteria (*m_batm_f*) and fungi (*m_fatm_f*), but the magnitudes varied among biomes (Fig. 2.7). We found highly positive correlations between *m_rf_s1m*, *m_rf_s2m*, *m_rf_s3m*, or *m_rf_s4m* and SOC across biomes except for tundra and boreal forest. Also, *m_batm_f* and *m_fatm_f* were negatively correlated with SOC, but the magnitudes varied among biomes. Specifically, we found higher negative correlation between *m_batm_f* and SOC in TBF-VA (S=-0.10 with -20% and +20% change), TCF-NJ (S=-0.08 with -20% and +20% change), and TSF-HS (S=-0.10 with -20% and +20% change). While *m_fatm_f* was more negatively correlated with SOC in GRS-IA (S=-0.12 with -20% and +20% change), TCF-NJ (S=-0.10 with -20% and +20% change), and TSF-HS (S=-0.17 with -20% and +20% change). The SOC in other biomes were relatively insensitive to changes in *m_batm_f* (S values ranging from -0.06 to -0.02) and *m_fatm_f* (S values ranging from -0.05 to -0.03). Across biomes, we only found strong negative correlations between *m_doms1_f*, *m_doms2_f*, and *m_doms3_f* and SOC in TCF-NJ (S=-0.08 for m_doms1, S=-0.12 for m_doms2, and S=-0.18 for m_doms3).

The HR widely responded of to all parameters listed for soil microbial mechanisms, but in low sensitivity (Fig. 2.7). Specifically, the HR in sites such as DST-CH, GRS-IA, TBF-VA, TCF-NJ, and TSF-HS showed a weak response to changes in all parameters. However, we also found relatively stronger

negative correlations between *m_batm_f* and HR in BRF-WC (S=-0.09 with -20% change and S=-0.12 with +20% change) and WET-EM (S=-0.08 with -20% change and S=-0.11 with +20% change).

Simulated FBC, BBC, F:B ratio, SOC, and HR at annual scale

Annual estimation of FBC, BBC, F:B ratio, SOC, and HR in the top 30 cm soils derived from the CLM-Microbe model showed large variations among biomes (Table 2.6). The simulated FBC was the highest in TCF-NJ (380 gC m^{-2}), followed by TBF-VA (259 gC m^{-2}), BRF-WC (205 gC m^{-2}), and TUN-MH (180 gC m^{-2}), while it was lowest in WET-EM (24 gC m^{-2}) with a range of 14-40 gC m^{-2}. The simulated FBC in the top 30 cm of soils in DST-CH, GRS-IA, SHB-OB, TUN-MH, BRF-WC, TBF-VA, TCF-NJ, TSF-HS, and WET-EM was 1.6 (0-15 cm), 5.9 (0-10 cm), 0.9 (0-10 cm), 1.7 (0-10 cm), 4.0 (5-20 cm), 2.1 (0-5 cm), 14.0 (0-2.3 cm), 1.7 (0-10 cm), and 22.6 (0-20 cm) times of the observed FBC (at varying soil depths), respectively. Compared with the global dataset of FBC and BBC (He et al., 2020), the simulated FBC in the top 30 cm of soils was generally consistent with the biome-averaged FBC in the top 30 cm of the soils. The model simulated FBC in DST-CH, GRS-IA, TUN-MH, BRF-WC, and TSF-HS was similar with the biome-averaged FBC in the top 30 cm of soils. However, we detected extreme FBC simulated by the model in some sites compared with the biome-averaged FBC. The CLM-Microbe model simulated higher FBC in SHB-OB, TBF-VA, and TCF-NJ and lower FBC in WET-EM relative to their corresponding the biome-averaged FBC in the top 30 cm soils.

The simulated BBC was the highest in TCF-NJ (100 gC m^{-2}), followed by TBF-VA (70 gC m^{-2}), BRF-WC (40 gC m^{-2}), and TUN-MH (30 gC m^{-2}), while the simulated BBC was the lowest in WET-EM (7 gC m^{-2}) and DST-CH (9 gC m^{-2}). The simulated BBC in the top 30 cm of soils in DST-CH, GRS-IA, SHB-OB, TUN-MH, BRF-WC, TBF-VA, TCF-NJ, TSF-HS, and WET-EM was 5.0 (0-15 cm), 2.1 (0-10 cm), 2.2 (0-10 cm), 1.0 (0-10 cm), 4.1 (5-20 cm), 2.3 (0-5 cm), 13.5 (0-2.3 cm), 6.3 (0-10 cm), and 25.4 (0-20

cm) times of the observed BBC (at varying soil depths), respectively. Compared with the global dataset of FBC and BBC (He et al., 2020), the simulated BBC in DST-CH, GRS-IA, TUN-MH, and BRF-WC was similar with their corresponding biome-averaged BBC in the top 30 cm soils. However, the simulated BBC was higher in SHB-OB, TBF-VA, and TCF-NJ and lower in TSF-HS and WET-relative to their corresponding biome-averaged BBC in the top 30 cm soils.

The simulated F:B ratio was the highest in TUN-MH (6.30), followed by BRF-WC (5.39), DST-CT (4.54), SHB-OB (4.16), and TCF-NJ (3.96), the F:B ratio was the lowest in TSF-HS (2.31). The observed F:B ratio was highly variable, with the highest F:B ratio in DST-CH (14.1, 0-15 cm), followed by SHB-OB (9.1, 0-10 cm) and BRF-WC (5.3, 5-20 cm), while GRS-IA (1.1, 0-10 cm) featured the lowest F:B ratio among biomes. Compared with the global dataset of FBC and BBC (He et al., 2020), the CLM-Microbe model simulated F:B ratio was generally consistent with the biome-averaged F:B ratio in the top 30 cm soils. Similar with the CLM-Microbe model simulated F:B ratio, the highest biome-averaged F:B ratio was found in tundra (8.6), followed by boreal forests (5.0), temperate forests (4.9), and shrub (4.8), while the lowest biome-averaged F:B ratio was found in tropical/subtropical forests (2.2).

Large variations were found in the simulated SOC of top 30 cm among biomes, with SOC highest in WET-EM (13204 gC m^{-2}), which was 5.3 times of that in the site with the lowest values, i.e., TSF-HS (2509 gC m^{-2}). BRF-WC (8685 gC m^{-2}) has the second largest SOC, followed by TCF-NJ (7990 gC m^{-2}), TBF-VA (5873 gC m^{-2}), and TUN-MH (3604 gC m^{-2}) (Table 2.6). Similar as the CLM-Microbe model, CLM4.5-simulated SOC in the top 30 cm was high in WET-EM (9951 gC m^{-2}) and low in SHB-OB (1598 gC m^{-2}) and TUN-MH (2086 gC m^{-2}). In contrast, CLM4.5-simulated SOC in the top 30 cm was much higher in GRS-IA (11991 gC m^{-2}), TBF-VA (11239 gC m^{-2}), and TSF-HS (6628 gC m^{-2}) compared with that simulated by the CLM-Microbe model. It is worthwhile to note that DST-CH (0 gC m^{-2})

featured the lowest SOC in the top 30 cm simulated by CLM4.5 among sites owing to the vegetation mortality. The simulated SOC in the top 30 cm was slightly lower than the average derived from a global dataset of SOC (Jobbágy & Jackson, 2000). However, the simulated SOC in BRF-WC was slightly higher than that of biome-averaged SOC in the top 30 cm. Excluding wetlands due to lack of available data, the biome-averaged SOC is consistent with the simulated SOC in the top 30 cm. The SOC is higher in temperate broadleaf forest (10875 gC m^{-2}), temperate coniferous forest (8483 gC m^{-2}), and tundra (7739 gC m^{-2}). In contrast to the lowest simulated SOC in the top 30 cm in TSF-HS (2509 gC m^{-2}), the biome-averaged SOC in the top 30 cm was lowest in the desert (2728 gC m^{-2}).

The fraction of SOC in microbial biomass (FBC and BBC combined) showed a large variation among biomes, with the proportion ranging from 0.2% to 6.0% (Table 2.6). The proportion was the highest in TCF-NJ (6.0%), followed by TUN-MH (5.80%), TBF-VA (5.60%), SHB-OB (5.50%), and GRS-IA (5.40%), WET-EM (0.23%) featured the lowest proportion between the sum of FBC and BBC and SOC among biomes. Similarly, the biome-averaged proportion between the sum of FBC and BBC and SOC ranged from 1.1% to 6.2% among biomes. However, the rank of the biome-averaged proportion between the sum of FBC and BBC and SOC was different with that simulated by the CLM-Microbe model. The proportion between the sum of FBC and BBC and SOC was highest in boreal forests (6.2%) and lowest in temperate broadleaf forests (1.1%). Tundra had the second highest proportion between the sum of FBC and BBC and SOC (3.4%), followed by desert (2.7%), grassland (2.2%), shrub (1.5%), and then tropical/subtropical forest and temperate coniferous forest (1.4%).

The CLM-Microbe-model-simulated annual estimation of HR was the highest in TCF-NJ (811 gC m^{-2} yr^{-1}), which was about 9 times of that in the lowest site, i.e., TUN-MH (93 gC m^{-2} yr^{-1}) (Table 2.6). We found second highest HR in TBF-VA (560 gC m^{-2} yr^{-1}), followed by WET-EM (540 gC m^{-2} yr^{-1}), BRF-

WC (420 gC m^{-2} yr^{-1}), and TSF-HS (401 gC m^{-2} yr^{-1}). Compared with the CLM-Microbe model, CLM4.5 simulated highly consistent HR in TBF-VA, WET-EM, TSF-HS, SHB-OB, and TUN-MH. However, we observed much higher HR in GRS-IA simulated by CLM4.5 (757 gC m^{-2} yr^{-1}), which was 2.4 times of that simulated by the CLM-Microbe model (313 gC m^{-2} yr^{-1}).

Simulated time-series C flow for fungi and bacteria

The dynamics and magnitude of C flow related to the decomposition of litter, SOM, and DOM, HR, and microbial lysis for FBC and BBC were different among biomes, while the seasonal patterns of those C flows were similar for fungi and bacteria in each biome (Figs. 2.8-9). In the CLM-Microbe model, FBC and BBC receive C from the decomposition of litter, SOM, and DOM, the dominance of these C flows varied temporally and among biomes. The C flow from litter decomposition predominated fungal and bacterial C gain year-round at a few sites such as DST-CH (Figs. 2.8a and 2.9a), TUN-MH (Figs. 2.8i and 2.9i), and TSF-HS (Figs. 2.8h and 2.9h). We also observed the dominant role of litter decomposition for fungi and bacteria C gain in GRS-IA (Figs. 2.8b and 2.9b), TBF-VA (Figs. 2.8f and 2.9f), and WET-EM during the non-growing season (Figs. 2.8i and 2.9i). The fungal and bacterial C gain in sites such as BRF-WC (Figs. 2.8e and 2.9e), SHB-OB (Figs. 2.8c and 2.9c), and TCF-NJ (Figs. 2.8g and 2.9g) were co-dominated by the decomposition of litter and SOM. The decomposition of DOM is the least important pathway for fungal and bacterial C gain across biomes; however, we observed the predominant role of the DOM decomposition for fungal and bacterial C gain in TBF-VA (Figs. 2.8f and 2.9f) and WET-EM (Figs. 2.8i and 2.9i) during the whole year, and second largest C gain pathway of DOM decomposition in TUN-MH (Figs. 2.8d and 2.9d), and temporarily dominant role of DOM decomposition during winter and spring in SHB-OB (Figs. 2.8c and 2.9c).

The C loss from fungal and bacterial biomass was primarily represented as microbial respiration and microbial lysis in the CLM-Microbe model. The C flow from fungal and bacterial biomass to SOM during microbial lysis was the predominant mechanism of C loss in DST-CH (Figs. 2.8a and 2.9a), SHB-OB (Figs. 2.8c and 2.9c), BRF-WC (Figs. 2.8e and 2.9e), TBF-VA (Figs. 2.8f and 2.9f), and TCF-NJ (Figs. 2.8g and 2.9g). However, we also observed the co-dominance of C flow from fungal and bacterial biomass to SOM and microbial respiration in GRS-IA (Figs. 2.8b and 2.9b), and TUN-MH (Figs. 2.8d and 2.9d) in controlling fungal and bacterial C loss. In WET-EM, fungal and bacterial C loss were co-determined by C flow from fungal and bacterial biomass to SOM and DOM and microbial respiration (Figs. 2.8i and 2.9i). While we found the predominant role of microbial respiration in regulating fungal and bacterial C loss in TSF-HS, microbial lysis contributed less to fungal and bacterial C loss (Figs. 2.8h and 2.9h).

Discussion

Model performance and comparison with existing models

The CLM-Microbe model simulated FBC and BBC are consistent with the observed FBC and BBC, with a slight underestimation (Fig. 2.6; Table 2.4), indicating that the CLM-Microbe model can capture fungal and bacterial biomass dynamics. Similar with our findings, Wang et al. (2015) reported that the MEND model can adequately capture the soil microbial biomass C dynamics with the representation of soil microbial processes such as microbial dormancy, microbial enzyme production, and enzyme catalyzing effects on decomposition. The TRIPLEX-MICROBE model can also estimate the global- and biome-level soil microbial biomass C with reasonable accuracy (Wang et al., 2017). Meanwhile, studies found that soil microbial traits play a key role in soil microbial biomass accumulation. Wang et al. (2015) compared the simulated soil microbial biomass C by MEND with and without dormancy, and they found that MEND model without dormancy largely underestimated the soil microbial biomass C. In the CLM-

Microbe model, the soil microbial community, represented by active fungi and bacteria, is directly related to many biogeochemical processes such as decomposition of litter, DOM, and SOM and soil microbial respiration. The increase in FBC and BBC could largely affect soil respiration and soil C pools such as SOM. To ensure reasonable soil conditions, we finalized the parameters related to soil microbial processes by comparing model simulated SOC with the global datasets of SOC. Therefore, the missing representation of dormancy may be responsible for the slight underestimation of FBC and BBC in the CLM-Microbe model.

Additionally, the CLM-Microbe model simulated FBC and BBC showed smaller variation compared with the observed FBC and BBC, respectively (Fig. 2.6). Soil microbial communities are not static, with microbial biomass showing temporal dynamics (Björk et al., 2008; Lipson et al., 2002; Lipson & Schmidt, 2004). This variation is highly associated with changing environmental factors such as soil temperature and soil moisture (Devi & Yadava, 2006). In addition to environmental factors, C inputs derived from plants also control soil microbial growth, and soil microbial biomass is positively affected by aboveground litter input (Feng et al., 2009) and root exudates (Göttlicher et al., 2006). Although we incorporated the vegetation effects in soil microbial biomass in the form of DOM released into soil, the decomposition of DOM will enhance the C availability for soil microbes, the stimulating effects of DOM on microbial activity was not included into the CLM-Microbe model. In addition, soil food web was not explicitly incorporated into the CLM-Microbe model, even the turnover rate of soil microbial biomass was probably regulated by their predators such as nematodes, mites, and protozoa (CPD et al., 1995; Ingham et al., 1986). The increasing predator activity can induce abrupt changes in soil microbial biomass; for example, Buckeridge et al. (2013) observed seasonal variation in soil microbial community structure, and the decline in FBC from winter to late winter, and then again in spring, was closely associated with the high abundance of protozoa. Furthermore, only a small proportion of the soil microbial community is active, while the majority is dormant, i.e., a reversible state of low to zero

metabolic activity (Cole, 1999). Soil microbes can determine whether the environmental conditions are suitable for staying viable within short time periods (Garcia-Pichel & Pringault, 2001). Therefore, the rapid change in soil microbial state can lead to abrupt changes in soil microbial biomass (He et al., 2015). However, in the CLM-Microbe model, we assumed that the activity of fungi and bacteria are regulated by soil environmental conditions such as soil temperature, soil moisture, and soil oxygen concentration (Decomposition section in Methodology), the dormant soil fungi and bacteria were not incorporated into the model.

Controls on soil microbial community composition

Turnover rates of FBC and BBC are the most important factors regulating FBC and BBC dynamics across biomes, respectively, with increasing turnover rate of fungi decreased FBC and F:B ratio, and increasing turnover rate of bacteria decreased BBC and increased F:B ratio (Fig. 2.7). Turnover rate, the inverse of lifespan, can be mathematically calculated by dividing the production by the biomass pool size. In the microbial world, biomass turnover is much faster relative to that of plants and animals in natural environments, microbial related biogeochemical fluxes are closely linked to turnover and succession of microbial communities (Schmidt et al., 2007). Higher estimates for biomass production consequently correspond to lower turnover times, and vice versa (Pritchard et al., 2008; Rousk & Bååth, 2007). Therefore, the increase in turnover rate of fungi and bacteria is expected to induce declining FBC and BBC, respectively. The increasing turnover rate of fungi will decrease the dominance of fungi, and thus narrowed F:B ratio. In contrast, the increasing bacterial turnover rate would suppress the bacterial dominance and thus a broadening F:B ratio.

In addition, we observed the important role of fungal and bacterial biomass C:N ratio in regulating FBC, BBC, and F:B ratio, with rising fungal biomass C:N ratio increased FBC and F:B ratio and rising bacterial

biomass C:N ratio increased BBC and decreased F:B ratio (Fig. 2.7). The C cycle is closely coupled with that of other essential elements, and the proportion of substrate C being respired by soil microbes is closely related to substrate C:N ratio, with more C being respired when substrate has high C:N ratio or low N concentration (Spohn, 2015). In addition, the ratio between the substrate and the microbial biomass C:N ratio determines the proportion of C being assimilated by soil microbes (Sinsabaugh et al., 2013), which was directly reflected as CUE and adopted into the CLM-Microbe model. Fungi and bacteria have distinct C and nutrient compositions, with C:N ratio averaged around 5 for bacteria and 12 for fungi (Strickland & Rousk, 2010), their C:N ratios specifically determine the partitioning coefficient of C between fungi and bacteria in the CLM-Microbe model. Increasing fungal biomass C:N ratio will thus increase the proportion of C assimilated by fungi and promote the dominance of fungi, while increasing bacterial biomass C:N ratio stimulates the C flow towards bacteria and suppresses the fungal C gain, and thereby decreasing F:B ratio.

The FBC, BBC, and F:B ratio were also positively affected by the C flow from SOM to soil microbes. We observed higher sensitivity of FBC and BBC in desert and tropical/subtropical sites to changes in C flow from SOM to soil microbes (Fig. 2.7). The increase in microbial C gain from SOM will enhance the C and energy availability for soil microbial growth, which is thus reflected as an increase in soil microbial biomass. In the model, fungal and bacterial C gain from SOM is first expressed as the C input from SOM to soil microbes as a whole, then the C was partitioned by FBC and BBC pools based on the C:N ratio of their biomass, the biomass pool with higher C:N ratio is expected to gain higher proportion of C (Fig. 2.1). In other words, the C flow from SOM to soil microbes will determine the overall received C from SOM for both fungi and bacteria. Although there are large variations in fungal (3-60) and bacterial (3-12) biomass C:N ratio, indicating that a large proportion of fungi and bacteria overlap with regards to biomass C:N ratio, fungi tend to have higher mean C:N ratio (Strickland & Rousk, 2010). Accordingly, we assigned higher C:N ratio for fungal (*cn_fungi*) relative to bacterial (*cn_bacteria*) biomass, and the

reasonability of these parameters were validated and tested by observed FBC and BBC dynamics (Table 2.3). As a result, the increase in microbial C gain from SOM will enhance FBC and BBC; however, FBC increase will be promoted more due to its higher C:N ratio, thereby exhibiting an increase in F:B ratio.

The FBC, BBC, and F:B ratio in DST-CH and TSF-SH showed relatively higher sensitivity to soil microbial C assimilation from SOM decomposition, which is likely result from the favorable soil moisture and temperature for decomposition. Tropical and subtropical forests are known to have higher decomposition rate due to the high annual precipitation and temperature, while decomposition in deserts is widely reported to be limited by soil moisture (Chapin et al., 2011). Despite the general recognition of water limitation in deserts, the desert site (DST-CH) in this study has a mean annual precipitation of 380 mm, which is pretty high compared to "common" deserts (Bell et al., 2014). Given the high sensitivity of SOM decomposition to soil moisture condition, the higher water availability may enhance SOM decomposition in TSF-SH and DST-CH (Chapin et al., 2011). Furthermore, DST-CH is vegetated by herbaceous plant species, the higher proportion of non-woody components will improve the decomposability of substrates (Koven et al., 2013). In addition, although water limitation decreases the activity of soil microbes, primarily bacteria, fungi are more tolerant to drought due to their hyphal water uptake capability and dominate SOM decomposition in dry environmental conditions such as deserts (Yuste et al., 2011). Therefore, the decomposition of SOM plays an important role for fungal and bacterial C turnover, and fungal growth tends to be promoted more due to higher biomass C:N ratio and tolerance to water stress, leading to an increase in F:B ratio.

Controls on soil organic C density and HR

The C flow from SOM to soil microbes enhanced SOC, but this enhancement is weak in tundra and boreal forest; soil microbial respiration strongly decreased SOC in forests except for boreal forest (Fig.

2.7). In addition to processing SOM from other organic C forms, soil microbes contribute to the formation of persistent SOM via necromass (Gougoulias et al., 2014). Soil microbial necromass is about three orders of magnitude higher than soil microbial biomass (Glaser et al., 2004), and can make up more than half of SOC (Liang et al., 2019). Soil microbial necromass is directly related to soil microbial biomass turnover rate, the slow biomass turnover rate in boreal forests and tundra might be one of the important reasons for low SOC sensitivity to soil microbial biomass C gain from SOM (Table 2.3). Moreover, boreal forests and tundra are known to have low soil temperature, indicating smaller temperature effects on soil microbial community lysis. As a result, low biomass turnover rate of fungi and bacteria as well as low soil temperature may lead to the long persistence of organic C in soil microbial biomass, resulting in the lower contribution of soil microbial necromass to SOM. Compared with boreal forests, soil moisture and soil temperature in temperate and tropical forests are relatively desirable for soil microbial activity, and thus the decomposition process is more favorable in temperate and tropical forests. Higher decomposition in temperate and tropical forests is indicated by the C released as CO_2 by fungi and bacteria in the CLM-Microbe model (Table 2.6). Therefore, in temperate and tropical forests, the higher proportion of C respired by fungi and bacteria will more prominently decrease C remaining in the ecosystem, leading to a reduction in SOC content.

The HR was generally responsive to all the parameters related to soil microbial processes but in low sensitivity (Fig. 2.7). The HR is widely affected by multiple abiotic and biotic conditions, such as substrate concentration, soil moisture, and soil temperature (Gomez-Casanovas et al., 2012; Zhang et al., 2013). In the CLM-Microbe model, HR is explicitly represented as soil microbial respiration under the influences of environmental factors (i.e., soil moisture, soil temperature, and oxygen concentration). Meanwhile, fungal and bacterial respiration is not only related to C gain through the decomposition of DOM, SOM, and litter and microbial DOM uptake, but also to soil microbial lysis (Fig. 2.1). Therefore, HR is directly determined by the microbial activities and substrate availability, and indirectly affected by

a wide range of environmental factors and parameters. For example, parameters defining C transfer from litter and SOM pools to fungal and bacterial biomass pools and DOM, from DOM pool to fungal and bacterial biomass and SOM pools, and from fungal and bacterial biomass pools to DOM and SOM pools are closely related to soil microbial C gain and loss.

In general, the CLM-Microbe model simulated comparable SOC and HR in grasslands, tundra, temperate broadleaf forests, tropical/subtropical forests, and wetlands, but much higher SOC and HR in shrub, boreal forests, and temperate coniferous forests compared with CLM4.5 (Table 2.6). This may be due to two reasons. First, to produce reasonable vegetation status, we adjusted the parameters related to plant photosynthesis (e.g., *flnr*) and C allocation (e.g., *froot_leaf*) in the CLM-Microbe model to guarantee reasonable vegetation productivity indicated by MODIS dataset. However, when running the CLM4.5, we used the default parameters for each plant functional type. Therefore, the difference in vegetation condition may induce the discrepancy in simulated SOC and HR. For example, we documented a SOC pool of 2568 gC m^{-2} and HR flux of 277 gC m^{-2} yr^{-1}, but both SOC and HR were zeros in desert site (DST-CH) because of vegetation mortality. Litterfall from vegetation serves as the C source for SOM formation (Thornton & Rosenbloom, 2005), the difference in vegetation condition may be one of the important reasons for the difference in simulated SOC and HR between CLM4.5 and the CLM-Microbe model. Second, to produce comparable SOC in the CLM-Microbe model with HSWD dataset, we adjusted active soil depth for decomposition (*decomp_depth_efolding*) to reach the goal. While we used the default value of *decomp_depth_efolding* (0.5) for the CLM4.5 simulation in all sites. *decomp_depth_efolding* determines the vertical distribution of SOC in the soil profile, changes in *decomp_depth_efolding* may account for the differences in simulated SOC, and possibly HR, between CLM4.5 and the CLM-Microbe model (Bonan et al., 2013).

Limitations and improvements

The CLM-Microbe model is capable of simulating FBC and BBC dynamics across biomes; a few improvements are identified as our future research needs. First, the dormant portion of fungi and bacteria were not considered in the CLM-Microbe model. Dormant soil microbes can become viable in short time periods due to their capability of rapidly sensing limiting resources change (Garcia-Pichel & Pringault, 2001). Therefore, dormant soil microbes are able to survive environmental stresses and serve as "seed banks" for the soil microbial community (Lennon & Jones, 2011). Representing the dormant portion of soil microbes would enhance the model capability in simulating microbial resilience to stressful conditions (Wang et al., 2015). Second, fresh C input-induced priming effects is an important pathway affecting microbial activity, which needs to be considered in future studies. In addition to environmental factors such as temperature, soil moisture, and oxygen concentration, the addition of organic or mineral substances available for soil microorganisms may stimulate microbial activities, causing priming effects (Blagodatskaya & Kuzyakov, 2008). However, we did not test the model in simulating the priming impact within current model structure. Given the different physiology of bacteria and fungi, it would be worthwhile to robustly test the model behavior in simulating the priming effect, and further improve the model as needed.

Third, the soil food web regulates fungal and bacterial biomass dynamics, thus the inclusion of soil trophic interactions would help better understand the effects of soil food web on soil microbial biomass dynamics. Soil microbial growth is strongly shaped by predation, Buckeridge et al. (2013), for example, observed the seasonal variation in soil microbial community structure, and the decline in FBC from winter to late winter, and then again in spring, which was closely associated with the abundance of protozoa. Therefore, FBC and BBC may not only be controlled by abiotic factors such as soil temperature, soil moisture, oxygen concentration, and C availability, but the seasonal variation in their predator communities (Schadt et al., 2003). Fourth, the FBC and BBC data compiled were measured

using a wide range of methods, while different methods may introduce a variety of biases (He et al., 2020). For example, direct microscopy was widely used in early stage of soil microbial studies, but the approach has inevitably included dead biomass of soil microbes, especially for fungi, into the estimated biomass (Buckeridge et al., 2013). Amino sugars such as glucosamine and muramic acid are used to estimate FBC and BBC, respectively; however, this method measures both living and dead microbial biomass due to the high stability of amino sugars in soil (Glaser et al., 2004). Therefore, comparing FBC and BBC data measured by multiple methods will suffer from uncertainties in data quality due to various biases introduced by the different methods. Although data-model integration has been proposed for more than four decades, the intimate collaboration between experimentalists and modelers is still needed for model development. A standardized microbial data system that contains primary microbial variables with consistent measurement approach or after conversion is critical to reduce the bias associated with distinct methods (Xu et al., 2020). Last but not least, the observed data for bacterial and fungal biomass C commonly vary by more than five orders of magnitude (Guo et al., 2020; He et al., 2020; Sinsabaugh et al., 2016; Xu et al., 2017; Xu et al., 2013), while ecosystem-level variables commonly vary by less than three orders of magnitude. This large discrepancy makes the validation approach applied to ecosystem-level C pools and fluxes less robust in microbial models, as shown in this study of model validation (Model parameterization section in Results). The CLM-Microbe is able to reasonably capture the seasonality of key microbial variables but less robust in simulating the magnitude of microbial variables. We call for community-level efforts to develop a new model validation approach that is more applicable to microbial models.

Conclusions

This study reported the model parameterization, validation, uncertainty analysis, and sensitivity analysis of the CLM-Microbe model in simulating fungal and bacterial biomass at the site level. The CLM-

Microbe model could simulate the seasonal variation of FBC and BBC, but the model tended to underestimate the magnitude of the observed biomass for most biomes. Sensitivity analysis showed that the turnover rates of FBC and BBC are the most important parameters regulating FBC and BBC, respectively. Meanwhile, C flow from SOM to soil microbes during decomposition and the C:N ratio of fungal and bacterial biomass are also important for FBC and BBC dynamics. We observed an enhancement of soil microbial C gain from SOM on SOC, but the enhancement is weak in tundra and boreal forests. The simulated HR was responsive to all parameters related to soil microbial processes across biomes but exhibited low sensitivity.

The CLM-Microbe model represents the first attempt to simulate the soil microbial effects on the C cycle by differentiating fungi and bacteria and their physiology in assimilating C in soils. Along with the emerging microbial macroecology (Xu et al., 2020), the improvements in modeling microbial mechanisms will likely bring more robust abilities to ESMs to better simulate and project the climate system. The explicit representation of soil microbial processes into the CLM-Microbe model will improve our mechanistic understanding of ecosystem-level C cycling and improve predictability of microbial community structure at regional to global scales, thereby reducing uncertainties in global C projection.

Acknowledgements

The authors are grateful to Dr. Yimei Huang from Northwest A&F University, and Drs. Qian Zhao and Weijun Shen from South China Botanical Garden, Chinese Academy of Sciences for providing the exact sampling date of fungal and bacterial biomass. We thank Dr. Jörg Rinklebe from University of Wuppertal for providing the time-series data of fungal and bacterial biomass data. L.H. thanks Dr. Fenghui Yuan for the discussion about sensitivity analysis. This study is partially supported by San Diego State University and the CSU Program for Education & Research in Biotechnology. Partial support for this work was provided by an Early Career Award through the U.S. Department of Energy (DOE) Biological and Environmental Research Program ORNL is managed by UT-Battelle, LLC, under contract DE-AC05-00OR22725 with the U.S. DOE.

References

Aguilera, L. E., Armas, C., Cea, A. P., Gutiérrez, J. R., Meserve, P. L., & Kelt, D. A. (2016). Rainfall, microhabitat, and small mammals influence the abundance and distribution of soil microorganisms in a Chilean semi-arid shrubland. *Journal of Arid Environments, 126*, 37-46. https://www.sciencedirect.com/science/article/pii/S0140196315300999

Allison, S. D. (2012). A trait-based approach for modelling microbial litter decomposition. *Ecology Letters, 15*(9), 1058-1070. https://onlinelibrary.wiley.com/doi/full/10.1111/j.1461-0248.2012.01807.x

Allison, S. D., Wallenstein, M. D., & Bradford, M. A. (2010). Soil-carbon response to warming dependent on microbial physiology. *Nature Geoscience, 3*(5), 336-340. https://www.nature.com/articles/ngeo846

Bai, Z., Xu, H.-J., He, H.-B., Zheng, L.-C., & Zhang, X.-D. (2013). Alterations of microbial populations and composition in the rhizosphere and bulk soil as affected by residual acetochlor. *Environmental Science and Pollution Research, 20*(1), 369-379. https://link.springer.com/article/10.1007/s11356-012-1061-3

Bailey, V. L., Peacock, A. D., Smith, J. L., & Bolton Jr, H. (2002). Relationships between soil microbial biomass determined by chloroform fumigation–extraction, substrate-induced respiration, and phospholipid fatty acid analysis. *Soil Biology and Biochemistry, 34*(9), 1385-1389. https://www.sciencedirect.com/science/article/pii/S0038071702000706

Balser, T. C., Treseder, K. K., & Ekenler, M. (2005). Using lipid analysis and hyphal length to quantify AM and saprotrophic fungal abundance along a soil chronosequence. *Soil Biology and Biochemistry, 37*(3), 601-604. https://www.sciencedirect.com/science/article/pii/S0038071704003116

Beare, M. H. (1997). Fungal and bacterial pathways of organic matter decomposition and nitrogen mineralization in arable soils. *Soil Ecology in Sustainable Agricultural Systems*, p. 37–70. https://agris.fao.org/agris-search/search.do?recordID=US1997058729

Bell, C. W., Tissue, D. T., Loik, M. E., Wallenstein, M. D., Martinez, V. A., Erickson, R. A., & Zak, J. C. (2014). Soil microbial and nutrient responses to 7 years of seasonally altered precipitation in a Chihuahuan Desert grassland. *Global Change Biology, 20*(5), 1657-1673. https://onlinelibrary.wiley.com/doi/abs/10.1111/gcb.12418

Bittman, S., Forge, T. A., & Kowalenko, C. G. (2005). Responses of the bacterial and fungal biomass in a grassland soil to multi-year applications of dairy manure slurry and fertilizer. *Soil Biology and Biochemistry, 37*(4), 613-623. https://www.sciencedirect.com/science/article/pii/S0038071704002913

Björk, R. G., Björkman, M. P., Andersson, M. X., & Klemedtsson, L. (2008). Temporal variation in soil microbial communities in Alpine tundra. *Soil Biology and Biochemistry, 40*(1), 266-268. https://www.sciencedirect.com/science/article/pii/S0038071707003136

Björk, R. G., Klemedtsson, L., Molau, U., Harndorf, J., Ödman, A., & Giesler, R. (2007). Linkages between N turnover and plant community structure in a tundra landscape. *Plant and Soil, 294*(1), 247-261. https://doi.org/10.1007/s11104-007-9250-4

Blagodatskaya, E., & Kuzyakov, Y. (2008). Mechanisms of real and apparent priming effects and their dependence on soil microbial biomass and community structure: critical review. *Biology and Fertility of Soils, 45*(2), 115-131. https://link.springer.com/article/10.1007/s00374-008-0334-y

Bonan, G., Drewniak, B., Huang, M., Koven, C. D., Levis, S., Li, F., et al. (2013). Technical description of version 4.5 of the Community Land Model (CLM). *NCAR Tech. Note NCAR/TN-503+ STR. Natl*.

Bradford, M. A., & Fierer, N. (2012). The biogeography of microbial communities and ecosystem processes: implications for soil and ecosystem models. *Soil Ecology and Ecosystem Services, 18*.

Buckeridge, K. M., Banerjee, S., Siciliano, S. D., & Grogan, P. (2013). The seasonal pattern of soil microbial community structure in mesic low arctic tundra. *Soil Biology and Biochemistry, 65*, 338-347. https://doi.org/10.1016/j.soilbio.2013.06.012

Burns, R. G., DeForest, J. L., Marxsen, J., Sinsabaugh, R. L., Stromberger, M. E., Wallenstein, M. D., et al. (2013). Soil enzymes in a changing environment: Current knowledge and future directions. *Soil Biology and Biochemistry, 58*, 216-234. https://doi.org/10.1016/j.soilbio.2012.11.009

Carnell, R., & Carnell, M. R. (2019). Package 'lhs'. *URL http://cran. stat. auckland. ac. nz/web/packages/lhs/lhs. pdf, 780*. https://github.com/bertcarnell/lhs

Chapin, F. S., Matson, P. A., & Vitousek, P. (2011). *Principles of terrestrial ecosystem ecology*: Springer Science & Business Media.

Cherrier, J., Bauer, J., & Druffel, E. (1996). Utilization and turnover of labile dissolved organic matter by bacterial heterotrophs in eastern North Pacific surface waters. *Marine Ecology Progress Series, 139*, 267-279. https://www.int-res.com/abstracts/meps/v139/p267-279/

Cleveland, C. C., Nemergut, D. R., Schmidt, S. K., & Townsend, A. R. (2007). Increases in soil respiration following labile carbon additions linked to rapid shifts in soil microbial community composition. *Biogeochemistry, 82*(3), 229-240. https://doi.org/10.1007/s10533-006-9065-z

Cole, J. J. (1999). Aquatic microbiology for ecosystem scientists: new and recycled paradigms in ecological microbiology. *Ecosystems, 2*(3), 215-225. https://doi.org/10.1007/s100219900069

CPD, B., R, R., Aam, N., Gc, C., H, W., Aj, K., et al. (1995). Effects of grazing, sedimentation and phytoplankton cell lysis on the structure of a coastal pelagic food web. *Marine Ecology Progress Series, 123*, 259-271. https://www.int-res.com/abstracts/meps/v123/p259-271/

Davidson, E. A., & Janssens, I. A. (2006). Temperature sensitivity of soil carbon decomposition and feedbacks to climate change. *Nature, 440*(7081), 165-173. https://www.nature.com/articles/nature04514

Davidson, E. A., Samanta, S., Caramori, S. S., & Savage, K. (2012). The Dual Arrhenius and Michaelis–Menten kinetics model for decomposition of soil organic matter at hourly to seasonal time scales.

Global Change Biology, 18(1), 371-384. https://onlinelibrary.wiley.com/doi/full/10.1111/j.1365-2486.2011.02546.x

Devêvre, O. C., & Horwáth, W. R. (2000). Decomposition of rice straw and microbial carbon use efficiency under different soil temperatures and moistures. *Soil Biology and Biochemistry, 32*(11-12), 1773-1785. https://www.sciencedirect.com/science/article/pii/S0038071700000961

Devi, N. B., & Yadava, P. S. (2006). Seasonal dynamics in soil microbial biomass C, N and P in a mixed-oak forest ecosystem of Manipur, North-east India. *Applied Soil Ecology, 31*(3), 220-227. https://www.sciencedirect.com/science/article/pii/S0929139305001058

Díaz-Raviña, M., Acea, M. J., & Carballas, T. (1995). Seasonal changes in microbial biomass and nutrient flush in forest soils. *Biology and Fertility of Soils, 19*(2), 220-226. https://doi.org/10.1007/BF00336163

Docherty, K. M., Borton, H. M., Espinosa, N., Gebhardt, M., Gil-Loaiza, J., Gutknecht, J. L. M., et al. (2015). Key edaphic properties largely explain temporal and geographic variation in soil microbial communities across four biomes. *PLoS ONE, 10*(11). https://www.ncbi.nlm.nih.gov/pmc/articles/PMC4633200/

Dornbush, M., Cambardella, C., Ingham, E., & Raich, J. (2008). A comparison of soil food webs beneath C3- and C4-dominated grasslands. *Biology and Fertility of Soils, 45*(1), 73-81. https://doi.org/10.1007/s00374-008-0312-4

Fang, C., Smith, P., Smith, J. U., & Moncrieff, J. B. (2005). Incorporating microorganisms as decomposers into models to simulate soil organic matter decomposition. *Geoderma, 129*(3), 139-146. https://www.sciencedirect.com/science/article/pii/S0016706104003581

Feng, W., Zou, X., & Schaefer, D. (2009). Above- and belowground carbon inputs affect seasonal variations of soil microbial biomass in a subtropical monsoon forest of southwest China. *Soil Biology and Biochemistry, 41*(5), 978-983. https://www.sciencedirect.com/science/article/pii/S0038071708003453

Fierer, N., Allen, A. S., Schimel, J. P., & Holden, P. A. (2003). Controls on microbial CO2 production: a comparison of surface and subsurface soil horizons. *Global Change Biology, 9*(9), 1322-1332. https://onlinelibrary.wiley.com/doi/full/10.1046/j.1365-2486.2003.00663.x

Flanagan, P. W., & Van Cleve, K. (1977). Microbial Biomass, Respiration and Nutrient Cycling in a Black Spruce Taiga Ecosystem. *Ecological Bulletins*(25), 261-273. https://www.jstor.org/Table/20112588

Frostegård, a., A. A., & Bååth, E. (1996). The use of phospholipid fatty acid analysis to estimate bacterial and fungal biomass in soil. *Biology and Fertility of Soils, 22*(1-2), 59-65. https://link.springer.com/article/10.1007/BF00384433

Garcia-Pichel, F., & Pringault, O. (2001). Cyanobacteria track water in desert soils. *Nature, 413*(6854), 380-381. https://www.nature.com/articles/35096640/

Glaser, B., Turrión, M. a.-B., & Alef, K. (2004). Amino sugars and muramic acid—biomarkers for soil microbial community structure analysis. *Soil Biology and Biochemistry, 36*(3), 399-407. https://www.sciencedirect.com/science/article/pii/S0038071703003407

Gomez-Casanovas, N., Matamala, R., Cook, D. R., & Gonzalez-Meler, M. A. (2012). Net ecosystem exchange modifies the relationship between the autotrophic and heterotrophic components of soil respiration with abiotic factors in prairie grasslands. *Global Change Biology, 18*(8), 2532-2545. https://onlinelibrary.wiley.com/doi/full/10.1111/j.1365-2486.2012.02721.x

Gommers, P. J. F., Schie, B. J. v., Dijken, J. P. v., & Kuenen, J. G. (1988). Biochemical limits to microbial growth yields: An analysis of mixed substrate utilization. *Biotechnology and Bioengineering, 32*(1), 86-94. https://onlinelibrary.wiley.com/doi/abs/10.1002/bit.260320112

Göttlicher, S. G., Steinmann, K., Betson, N. R., & Högberg, P. (2006). The dependence of soil microbial activity on recent photosynthate from trees. *Plant and Soil, 287*(1-2), 85-94. https://link.springer.com/article/10.1007/s11104-006-0062-8

Gougoulias, C., Clark, J. M., & Shaw, L. J. (2014). The role of soil microbes in the global carbon cycle: tracking the below-ground microbial processing of plant-derived carbon for manipulating carbon

dynamics in agricultural systems. *Journal of the Science of Food and Agriculture, 94*(12), 2362-2371. https://www.onlinelibrary.wiley.com/doi/abs/10.1002/jsfa.6577

Gruber, N., & Galloway, J. N. (2008). An Earth-system perspective of the global nitrogen cycle. *Nature, 451*(7176), 293-296. https://www.nature.com/articles/nature06592?draft=journal

Gu, Z., Eils, R., & Schlesner, M. (2016). Complex heatmaps reveal patterns and correlations in multidimensional genomic data. *Bioinformatics, 32*(18), 2847-2849. https://academic.oup.com/bioinformatics/article/32/18/2847/1743594

Guo, Z., Wang, Y., Wan, Z., Zuo, Y., He, L., Li, D., et al. (2020). Soil dissolved organic carbon in terrestrial ecosystems: global budget, spatial distribution and controls. *Global Ecology and Biogeography*. https://onlinelibrary.wiley.com/doi/full/10.1111/geb.13186

Haefner, J. W. (2005). *Modeling biological systems-principles and applications*. New York: Springer.

He, L., Rodrigues, J. L. M., Soudzilovskaia, N. A., Barceló, M., Olsson, P. A., Song, C., et al. (2020). Global biogeography of fungal and bacterial biomass carbon in topsoil. *Soil Biology and Biochemistry*, 108024. https://www.sciencedirect.com/science/article/pii/S0038071720303205

He, Y., Yang, J., Zhuang, Q., Harden, J. W., McGuire, A. D., Liu, Y., et al. (2015). Incorporating microbial dormancy dynamics into soil decomposition models to improve quantification of soil carbon dynamics of northern temperate forests. *Journal of Geophysical Research: Biogeosciences, 120*(12), 2596-2611. https://agupubs.onlinelibrary.wiley.com/doi/abs/10.1002/2015JG003130

Hopkins, D. W., Sparrow, A. D., Elberling, B., Gregorich, E. G., Novis, P. M., Greenfield, L. G., & Tilston, E. L. (2006). Carbon, nitrogen and temperature controls on microbial activity in soils from an Antarctic dry valley. *Soil Biology and Biochemistry, 38*(10), 3130-3140. https://www.sciencedirect.com/science/article/pii/S0038071706000940

Huang, G., Li, Y., & Su, Y. G. (2015). Effects of increasing precipitation on soil microbial community composition and soil respiration in a temperate desert, Northwestern China. *Soil Biology and Biochemistry, 83*, 52-56. https://www.sciencedirect.com/science/article/pii/S003807171500019X

Ingham, E. R., Trofymow, J. A., Ames, R. N., Hunt, H. W., Morley, C. R., Moore, J. C., & Coleman, D. C. (1986). Trophic interactions and nitrogen cycling in a semi-arid grassland soil. I. Seasonal dynamics of the natural populations, their interactions and effects on nitrogen cycling. *Journal of Applied Ecology, 23*(2), 597-614. https://www.jstor.org/Table/2404039

Jobbágy, E. G., & Jackson, R. B. (2000). The vertical distribution of soil organic carbon and its relation to climate and vegetation. *Ecological Applications, 10*(2), 423-436. https://doi.org/10.1890/1051-0761(2000)010[0423:TVDOSO]2.0.CO;2

Kaiser, C., Koranda, M., Kitzler, B., Fuchslueger, L., Schnecker, J., Schweiger, P., et al. (2010). Belowground carbon allocation by trees drives seasonal patterns of extracellular enzyme activities by altering microbial community composition in a beech forest soil. *New Phytologist, 187*(3), 843-858. https://nph.onlinelibrary.wiley.com/doi/abs/10.1111/j.1469-8137.2010.03321.x

Keohane, R. O. (2015). The global politics of climate change: challenge for political science. *PS: Political Science & Politics, 48*(1), 19-26. https://doi.org/10.1017/S1049096514001541

Kirchman, D. L., Suzuki, Y., Garside, C., & Ducklow, H. W. (1991). High turnover rates of dissolved organic carbon during a spring phytoplankton bloom. *Nature, 352*(6336), 612-614. https://www.nature.com/articles/352612a0

Klamer, M., & Bååth, E. (2004). Estimation of conversion factors for fungal biomass determination in compost using ergosterol and PLFA 18: 2ω6, 9. *Soil Biology and Biochemistry, 36*(1), 57-65. https://www.sciencedirect.com/science/article/pii/S0038071703002931

Koven, C. D., Riley, W. J., Subin, Z. M., Tang, J. Y., Torn, M. S., Collins, W. D., et al. (2013). The effect of vertically resolved soil biogeochemistry and alternate soil C and N models on C dynamics of CLM4. *Biogeosciences, 10*(11), 7109. https://bg.copernicus.org/articles/10/7109/2013/

Landesman, W. J., & Dighton, J. (2010). Response of soil microbial communities and the production of plant-available nitrogen to a two-year rainfall manipulation in the New Jersey Pinelands. *Soil Biology and Biochemistry, 42*(10), 1751-1758. https://doi.org/10.1016/j.soilbio.2010.06.012

Larionova, A. A., Yevdokimov, I. V., & Bykhovets, S. S. (2007). Temperature response of soil respiration is dependent on concentration of readily decomposable C. *Biogeosciences, 4*(6), 1073-1081. https://hal.archives-ouvertes.fr/hal-00297658/

Lennon, J. T., & Jones, S. E. (2011). Microbial seed banks: the ecological and evolutionary implications of dormancy. *Nature Reviews Microbiology, 9*(2), 119-130. https://www.nature.com/articles/nrmicro2504

Liang, C., Amelung, W., Lehmann, J., & Kästner, M. (2019). Quantitative assessment of microbial necromass contribution to soil organic matter. *Global Change Biology, 25*(11), 3578-3590. https://onlinelibrary.wiley.com/doi/abs/10.1111/gcb.14781

Lipson, D. A., Schadt, C. W., & Schmidt, S. K. (2002). Changes in soil microbial community structure and function in an alpine dry meadow following spring snow melt. *Microbial Ecology, 43*(3), 307-314. https://link.springer.com/article/10.1007%2Fs00248-001-1057-x?LI=true

Lipson, D. A., & Schmidt, S. K. (2004). Seasonal changes in an alpine soil bacterial community in the Colorado Rocky Mountains. *Applied and Environmental Microbiology, 70*(5), 2867-2879. https://aem.asm.org/content/70/5/2867

Liu, D., Huang, Y., Yan, H., Jiang, Y., Zhao, T., & An, S. (2018). Dynamics of soil nitrogen fractions and their relationship with soil microbial communities in two forest species of northern China. *PLoS ONE, 13*(5). https://www.ncbi.nlm.nih.gov/pmc/articles/PMC5967799/

Luo, Y., Keenan, T. F., & Smith, M. (2015). Predictability of the terrestrial carbon cycle. *Global Change Biology, 21*(5), 1737-1751. https://onlinelibrary.wiley.com/doi/full/10.1111/gcb.12766

Miura, T., Makoto, K., Niwa, S., Kaneko, N., & Sakamoto, K. (2017). Comparison of fatty acid methyl ester methods for characterization of microbial communities in forest and arable soil: Phospholipid fraction (PLFA) versus total ester linked fatty acids (EL-FAME). *Pedobiologia, 63*, 14-18. https://www.sciencedirect.com/science/article/pii/S0031405616301652

Moche, M., Gutknecht, J., Schulz, E., Langer, U., & Rinklebe, J. (2015). Monthly dynamics of microbial community structure and their controlling factors in three floodplain soils. *Soil Biology and Biochemistry, 90*, 169-178. https://doi.org/10.1016/j.soilbio.2015.07.006

Moore, J. C., McCann, K., & de Ruiter, P. C. (2005). Modeling trophic pathways, nutrient cycling, and dynamic stability in soils. *Pedobiologia, 49*(6), 499-510. https://www.sciencedirect.com/science/article/pii/S0031405605000545

National Ecological Observatory Network. (2020). *Data Product DP1.10104.001, Soil microbe biomass. Provisional data downloaded from http://data.neonscience.org on June 8, 2020. Battelle, Boulder, CO, USA NEON. 2020.*

Olsson, P. a. A., & Wallander, H. a. (1998). Interactions between ectomycorrhizal fungi and the bacterial community in soils amended with various primary minerals. *FEMS Microbiology Ecology, 27*(2), 195-205. https://academic.oup.com/femsec/article/27/2/195/531512

Paul, E. A. (2016). The nature and dynamics of soil organic matter: Plant inputs, microbial transformations, and organic matter stabilization. *Soil Biology and Biochemistry, 98*, 109-126. https://doi.org/10.1016/j.soilbio.2016.04.001

Peters, G. P., Andrew, R. M., Boden, T., Canadell, J. G., Ciais, P., Le Quéré, C., et al. (2012). The challenge to keep global warming below 2°C. *Nature Climate Change, 3*, 4-6. https://www.nature.com/articles/nclimate1783

Priha, O., Grayston, S. J., Pennanen, T., & Smolander, A. (1999). Microbial activities related to C and N cycling and microbial community structure in the rhizospheres of Pinus sylvestris, Picea abies and Betula pendula seedlings in an organic and mineral soil. *FEMS Microbiology Ecology, 30*(2), 187-199. https://academic.oup.com/femsec/article/30/2/187/609507?view=extract

Pritchard, S. G., Strand, A. E., McCormack, M. L., Davis, M. A., & Oren, R. (2008). Mycorrhizal and rhizomorph dynamics in a loblolly pine forest during 5 years of free-air-CO2-enrichment. *Global Change Biology, 14*(6), 1252-1264. https://onlinelibrary.wiley.com/doi/abs/10.1111/j.1365-2486.2008.01567.x

Rousk, J., & Bååth, E. (2007). Fungal biomass production and turnover in soil estimated using the acetate-in-ergosterol technique. *Soil Biology and Biochemistry, 39*(8), 2173-2177. https://doi.org/10.1016/j.soilbio.2007.03.023

Rousk, J., & Bååth, E. (2011). Growth of saprotrophic fungi and bacteria in soil. *FEMS Microbiology Ecology, 78*(1), 17-30. https://academic.oup.com/femsec/article/78/1/17/521006

Schadt, C. W., Martin, A. P., Lipson, D. A., & Schmidt, S. K. (2003). Seasonal dynamics of previously unknown fungal lineages in tundra soils. *Science, 301*(5638), 1359-1361. https://science.sciencemag.org/content/301/5638/1359

Schimel, J. P., & Weintraub, M. N. (2003). The implications of exoenzyme activity on microbial carbon and nitrogen limitation in soil: a theoretical model. *Soil Biology and Biochemistry, 35*(4), 549-563. https://doi.org/10.1016/S0038-0717(03)00015-4

Schindlbacher, A., Rodler, A., Kuffner, M., Kitzler, B., Sessitsch, A., & Zechmeister-Boltenstern, S. (2011). Experimental warming effects on the microbial community of a temperate mountain forest soil. *Soil Biology and Biochemistry, 43*(7), 1417-1425. https://doi.org/10.1016/j.soilbio.2011.03.005

Schippers, A., Neretin, L. N., Kallmeyer, J., Ferdelman, T. G., Cragg, B. A., John Parkes, R., & Jørgensen, B. B. (2005). Prokaryotic cells of the deep sub-seafloor biosphere identified as living bacteria. *Nature, 433*(7028), 861-864. https://www.nature.com/articles/nature03302

Schmidt, S. K., Costello, E. K., Nemergut, D. R., Cleveland, C. C., Reed, S. C., Weintraub, M. N., et al. (2007). Biogeochemical consequences of rapid microbial turnover and seasonal succession in soil. *Ecology, 88*(6), 1379-1385. https://esajournals.onlinelibrary.wiley.com/doi/abs/10.1890/06-0164

Sinsabaugh, R. L., Manzoni, S., Moorhead, D. L., & Richter, A. (2013). Carbon use efficiency of microbial communities: stoichiometry, methodology and modelling. *Ecology Letters, 16*(7), 930-939. https://onlinelibrary.wiley.com/doi/full/10.1111/ele.12113

Sinsabaugh, R. L., Turner, B. L., Talbot, J. M., Waring, B. G., Powers, J. S., Kuske, C. R., et al. (2016). Stoichiometry of microbial carbon use efficiency in soils. *Ecological Monographs, 86*(2), 172-189. https://esajournals.onlinelibrary.wiley.com/doi/abs/10.1890/15-2110.1

Sistla, S. A., Rastetter, E. B., & Schimel, J. P. (2014). Responses of a tundra system to warming using SCAMPS: a stoichiometrically coupled, acclimating microbe–plant–soil model. *Ecological Monographs, 84*(1), 151-170. https://esajournals.onlinelibrary.wiley.com/doi/full/10.1890/12-2119.1

Six, J., Frey, S. D., Thiet, R. K., & Batten, K. M. (2006). Bacterial and fungal contributions to carbon sequestration in agroecosystems. *Soil Science Society of America Journal, 70*(2), 555-569. https://acsess.onlinelibrary.wiley.com/doi/abs/10.2136/sssaj2004.0347

Spohn, M. (2015). Microbial respiration per unit microbial biomass depends on soil litter carbon-to-nitrogen ratio. *Biogeosciences, 12*, 817-823. https://eref.uni-bayreuth.de/17270/

Stahl, P. D., & Parkin, T. B. (1996). Relationship of soil ergosterol concentration and fungal biomass. *Soil Biology and Biochemistry, 28*(7), 847-855. https://www.sciencedirect.com/science/article/pii/0038071796000612

Strickland, M. S., & Rousk, J. (2010). Considering fungal: bacterial dominance in soils–methods, controls, and ecosystem implications. *Soil Biology and Biochemistry, 42*(9), 1385-1395. https://www.sciencedirect.com/science/article/pii/S0038071710001689

Sulman, B. N., Phillips, R. P., Oishi, A. C., Shevliakova, E., & Pacala, S. W. (2014). Microbe-driven turnover offsets mineral-mediated storage of soil carbon under elevated CO2. *Nature Climate Change, 4*(12), 1099-1102. https://www.nature.com/articles/nclimate2436

Tang, J., & Riley, W. J. (2015). Weaker soil carbon–climate feedbacks resulting from microbial and abiotic interactions. *Nature Climate Change, 5*(1), 56-60. https://www.nature.com/articles/nclimate2438

Taylor, K. E., Stouffer, R. J., & Meehl, G. A. (2011). An overview of CMIP5 and the experiment design. *Bulletin of the American Meteorological Society, 93*(4), 485-498. https://journals.ametsoc.org/doi/abs/10.1175/BAMS-D-11-00094.1

Thornton, P. E., Lamarque, J.-F., Rosenbloom, N. A., & Mahowald, N. M. (2007). Influence of carbon-nitrogen cycle coupling on land model response to CO2 fertilization and climate variability. *Global Biogeochemical Cycles, 21*(4). https://agupubs.onlinelibrary.wiley.com/doi/full/10.1029/2006GB002868

Thornton, P. E., & Rosenbloom, N. A. (2005). Ecosystem model spin-up: Estimating steady state conditions in a coupled terrestrial carbon and nitrogen cycle model. *Ecological Modelling, 189*(1-2), 25-48. https://www.sciencedirect.com/science/article/pii/S0304380005001948

Treseder, K. K., Balser, T. C., Bradford, M. A., Brodie, E. L., Dubinsky, E. A., Eviner, V. T., et al. (2012). Integrating microbial ecology into ecosystem models: challenges and priorities. *Biogeochemistry, 109*(1), 7-18. https://doi.org/10.1007/s10533-011-9636-5

Van Der Heijden, M. G. A., Bardgett, R. D., & Van Straalen, N. M. (2018). The unseen majority: soil microbes as drivers of plant diversity and productivity in terrestrial ecosystems. *Ecology Letters*, 296-310. https://doi.org/10.1111/j.1461-0248.2007.01139.x

von Lützow, M., & Kögel-Knabner, I. (2009). Temperature sensitivity of soil organic matter decomposition—what do we know? *Biology and Fertility of Soils, 46*(1), 1-15. https://link.springer.com/article/10.1007/s00374-009-0413-8

Wallander, H. a., Göransson, H., & Rosengren, U. (2004). Production, standing biomass and natural abundance of 15 N and 13 C in ectomycorrhizal mycelia collected at different soil depths in two forest types. *Oecologia, 139*(1), 89-97. https://link.springer.com/article/10.1007/s00442-003-1477-z

Wang, G., Jagadamma, S., Mayes, M. A., Schadt, C. W., Steinweg, J. M., Gu, L., & Post, W. M. (2015). Microbial dormancy improves development and experimental validation of ecosystem model. *The ISME Journal, 9*(1), 226-237. https://www.nature.com/articles/ismej2014120

Wang, G., Post, W. M., & Mayes, M. A. (2013). Development of microbial-enzyme-mediated decomposition model parameters through steady-state and dynamic analyses. *Ecological Applications, 23*(1), 255-272. https://esajournals.onlinelibrary.wiley.com/doi/full/10.1890/12-0681.1

Wang, K., Peng, C., Zhu, Q., Zhou, X., Wang, M., Zhang, K., & Wang, G. (2017). Modeling global soil carbon and soil microbial carbon by integrating microbial processes into the ecosystem process model TRIPLEX-GHG. *Journal of Advances in Modeling Earth Systems, 9*(6), 2368-2384. https://agupubs.onlinelibrary.wiley.com/doi/abs/10.1002/2017MS000920

Wang, Y., Yuan, F., Yuan, F., Gu, B., Hahn, M. S., Torn, M. S., et al. (2019). Mechanistic modeling of microtopographic impacts on CO2 and CH4 Fluxes in an Alaskan tundra ecosystem using the CLM-Microbe model. *Journal of Advances in Modeling Earth Systems, 11*, 17. https://agupubs.onlinelibrary.wiley.com/doi/full/10.1029/2019MS001771

Waring, B. G., Averill, C., & Hawkes, C. V. (2013). Differences in fungal and bacterial physiology alter soil carbon and nitrogen cycling: insights from meta-analysis and theoretical models. *Ecology Letters, 16*(7), 887-894. https://doi.org/10.1111/ele.12125

Wheeler, P. A., Gosselin, M., Sherr, E., Thibaultc, D., Kirchman, D. L., Benner, R., & Whitledge, T. E. (1996). Active cycling of organic carbon in the central Arctic Ocean. *Nature, 380*(6576), 697-699. https://www.nature.com/articles/380697a0

Wieder, W. R., Allison, S. D., Davidson, E. A., Georgiou, K., Hararuk, O., He, Y., et al. (2015). Explicitly representing soil microbial processes in Earth system models. *Global Biogeochemical Cycles, 29*(10), 1782-1800. https://agupubs.onlinelibrary.wiley.com/doi/abs/10.1002/2015GB005188

Wieder, W. R., Bonan, G. B., & Allison, S. D. (2013). Global soil carbon projections are improved by modelling microbial processes. *Nature Climate Change, 3*(10), 909-912. https://www.nature.com/articles/nclimate1951

Wieder, W. R., Grandy, A. S., Kallenbach, C. M., & Bonan, G. B. (2014). Integrating microbial physiology and physio-chemical principles in soils with the MIcrobial-MIneral Carbon Stabilization (MIMICS) model. *Biogeosciences, 11*(14), 3899-3917. https://www.biogeosciences.net/11/3899/2014/

Xiao, Y. (2003). Variation in needle longevity of Pinus tabulaeformis forests at different geographic scales. *Tree Physiology, 23*(7), 463-471. https://academic.oup.com/treephys/article/23/7/463/1665446

Xu, X. (2010). *Modeling methane and nitrous oxide exchanges between the atmosphere and terrestrial ecosystems over North America in the context of multifactor global change.* (Ph.D. Dissertation), Auburn University, Auburn.

Xu, X., Elias, D. A., Graham, D. E., Phelps, T. J., Carroll, S. L., Wullschleger, S. D., & Thornton, P. E. (2015). A microbial functional group-based module for simulating methane production and consumption: Application to an incubated permafrost soil. *Journal of Geophysical Research: Biogeosciences, 120*(7), 1315-1333. https://agupubs.onlinelibrary.wiley.com/doi/abs/10.1002/2015JG002935

Xu, X., Schimel, J. P., Janssens, I. A., Song, X., Song, C., Yu, G., et al. (2017). Global pattern and controls of soil microbial metabolic quotient. *Ecological Monographs, 87*(3), 429-441. https://esajournals.onlinelibrary.wiley.com/doi/full/10.1002/ecm.1258

Xu, X., Schimel, J. P., Thornton, P. E., Song, X., Yuan, F., & Goswami, S. (2014). Substrate and environmental controls on microbial assimilation of soil organic carbon: a framework for Earth system models. *Ecology Letters, 17*(5), 547-555. https://doi.org/10.1111/ele.12254

Xu, X., Thornton, P. E., & Post, W. M. (2013). A global analysis of soil microbial biomass carbon, nitrogen and phosphorus in terrestrial ecosystems. *Global Ecology and Biogeography, 22*(6), 737-749. https://onlinelibrary.wiley.com/doi/full/10.1111/geb.12029

Xu, X., Wang, N., Lipson, D., Sinsabaugh, R., Schimel, J., He, L., et al. (2020). Microbial macroecology: in search of mechanisms governing microbial biogeographical patterns. *Global Ecology and Biogeography*. https://doi.org/10.1111/geb.13162

Yuste, J. C., Peñuelas, J., Estiarte, M., Garcia-Mas, J., Mattana, S., Ogaya, R., et al. (2011). Drought-resistant fungi control soil organic matter decomposition and its response to temperature. *Global Change Biology, 17*(3), 1475-1486. https://onlinelibrary.wiley.com/doi/abs/10.1111/j.1365-2486.2010.02300.x

Zaehle, S., Friend, A. D., Friedlingstein, P., Dentener, F., Peylin, P., & Schulz, M. (2010). Carbon and nitrogen cycle dynamics in the O-CN land surface model: 2. Role of the nitrogen cycle in the historical terrestrial carbon balance. *Global Biogeochemical Cycles, 24*(1). https://agupubs.onlinelibrary.wiley.com/doi/abs/10.1029/2009GB003522

Zhang, Q., Lei, H.-M., & Yang, D.-W. (2013). Seasonal variations in soil respiration, heterotrophic respiration and autotrophic respiration of a wheat and maize rotation cropland in the North China Plain. *Agricultural and Forest Meteorology, 180*, 34-43. https://www.sciencedirect.com/science/article/pii/S0168192313001056

Zhao, Q., Jian, S., Nunan, N., Maestre, F. T., Tedersoo, L., He, J., et al. (2017). Altered precipitation seasonality impacts the dominant fungal but rare bacterial taxa in subtropical forest soils. *Biology and Fertility of Soils, 53*(2), 231-245. https://doi.org/10.1007/s00374-016-1171-z

Figures and tables

Fig. 2.1. Conceptual diagram showing the key processes and the roles of fungi and bacteria in the CLM-Microbe model. CWD, coarse woody debris; SOM, soil organic matter; B, bacteria; F, fungi; DOM, dissolved organic matter. In the CLM-Microbe model, number in the box means turnover time of each pool. Black solid lines indicate transitions in the CLM-Microbe model, which generally represents processes such as 1) decomposition of coarse woody debris, 2) litter 1 decomposition, 3) litter 2 decomposition, 4) litter 3 decomposition, 5) soil organic matter 1 decomposition, 6) soil organic matter 2 decomposition, 7) soil organic matter 3 decomposition, 8) soil organic matter 4 decomposition, 9) fungal and bacterial lysis, 10) dissolved organic matter decomposition, 11) dissolved organic matter uptake by fungal and bacterial, and 12) fungal and bacterial respiration. Red dash lines represent regulatory role of fungi and bacteria on the process, including fungi and bacteria regulation on 13) litter 1, 14) litter 2, 15) litter 3, 16) soil organic matter 1, 17) soil organic matter 2, 18) soil organic matter 3, and 19) soil organic matter 4 decomposition

Fig. 2.2. Calibration of fungal biomass for a) desert, b) grassland, c) shrub, d) tundra, e) boreal forest, f) temperate broadleaf forest, g) temperate coniferous forest, h) tropical/subtropical forest, and i) wetland. The blue star indicates the observed fungal biomass, and the black filled circle represents simulated fungal biomass.

Fig. 2.3. Calibration of bacterial biomass for a) desert, b) grassland, c) shrub, d) tundra, e) boreal forest, f) temperate broadleaf forest, g) temperate coniferous forest, h) tropical/subtropical forest, and i) wetland. The blue star indicates the observed bacterial biomass, and the black filled circle represents simulated bacterial biomass.

Fig. 2.4. Validation of fungal biomass for a and b) desert, c) grassland, d) shrub, e) tundra, f) boreal forest, g, h and i) temperate broadleaf forest, j) temperate coniferous forest, k) tropical/subtropical forest, and l) wetland. The blue star indicates the observed fungal biomass, and the black filled circle represents simulated fungal biomass.

Fig. 2.5. Validation of bacterial biomass for a and b) desert, c) grassland, d) shrub, e) tundra, f) boreal forest, g, h and i) temperate broadleaf forest, j) temperate coniferous forest, k) tropical/subtropical forest, and l) wetland. The blue star indicates the observed bacterial biomass, and the black filled circle represents simulated bacterial biomass.

Fig. 2.6. Comparison of the averaged observed and simulated a) fungal and b) bacterial biomass. The blue star indicates the a) fungal or b) bacterial biomass in calibration phase, and the black filled circle represents a) fungal or b) bacterial biomass in validation phase; vertical and horizontal error bars indicate standard error of simulated and observed values, respectively, for both a) fungal and b) bacterial biomass.

Fig. 2.7. Sensitivity analysis for model response of fungal biomass, bacterial biomass, F:B ratio, soil organic carbon, and soil microbial respiration in the top 30 cm to 25 parameters (m_bdom_f, m_bs1_f, m_bs2_f, m_bs3_f, m_fdom_f, m_fs1_f, m_fs2_f, m_fs3_f, k_dom, k_bacteria, k_fungi, m_rf_s1m, m_rf_s2m, m_rf_s3m, m_rf_s4m, m_batm_f, m_fatm_f, m_domb_f, m_domf_f, m_doms1_f, m_doms2_f, m_doms3_f, cn_bacteria, cn_fungi, and CUEmax) in a) desert, b) grassland, c) shrub, d) tundra, e) boreal forest, f) temperate broadleaf forest, g) temperate coniferous forest, h) tropical/subtropical forest, and i) wetland. "+" and "-" indicate 20% increase or 20% decrease of parameter values. FBC, fungal biomass carbon; BBC, bacterial biomass carbon; F:B ratio, fungal:bacterial biomass carbon ratio; SOC, soil organic carbon; HR, heterotrophic respiration; Dark red and darker blue indicate a stronger positive or negative model response of the variable to parameter change. S is negative if the direction of model response opposes the direction of parameter change during the sampling years for all sites.

Fig. 2.8. Time-series of simulated carbon flow into and out from the bacterial biomass carbon pool

Fig. 2.9. Time-series of simulated carbon flow into and out from the bacterial biomass carbon pool

Table 2.1. Site information of the observational data

Table 2.2. Key model parameters in processes involving fungal and bacterial biomass

Table 2.3. Key parameters for the different biomes

Table 2.4. Site-level evaluation of the goodness-of-fit criteria computed for the simulated fungal and bacterial biomass dynamics in the calibration and validation phases

Table 2.5. Key parameters for sensitivity analysis and uncertainty analysis

Table 2.6. Annual estimates of fungal and bacterial biomass carbon, fungal:bacterial (F:B) biomass carbon ratio, soil organic carbon (SOC), and heterotrophic respiration (HR) with the uncertainties of parameters during the sampling years for all sites

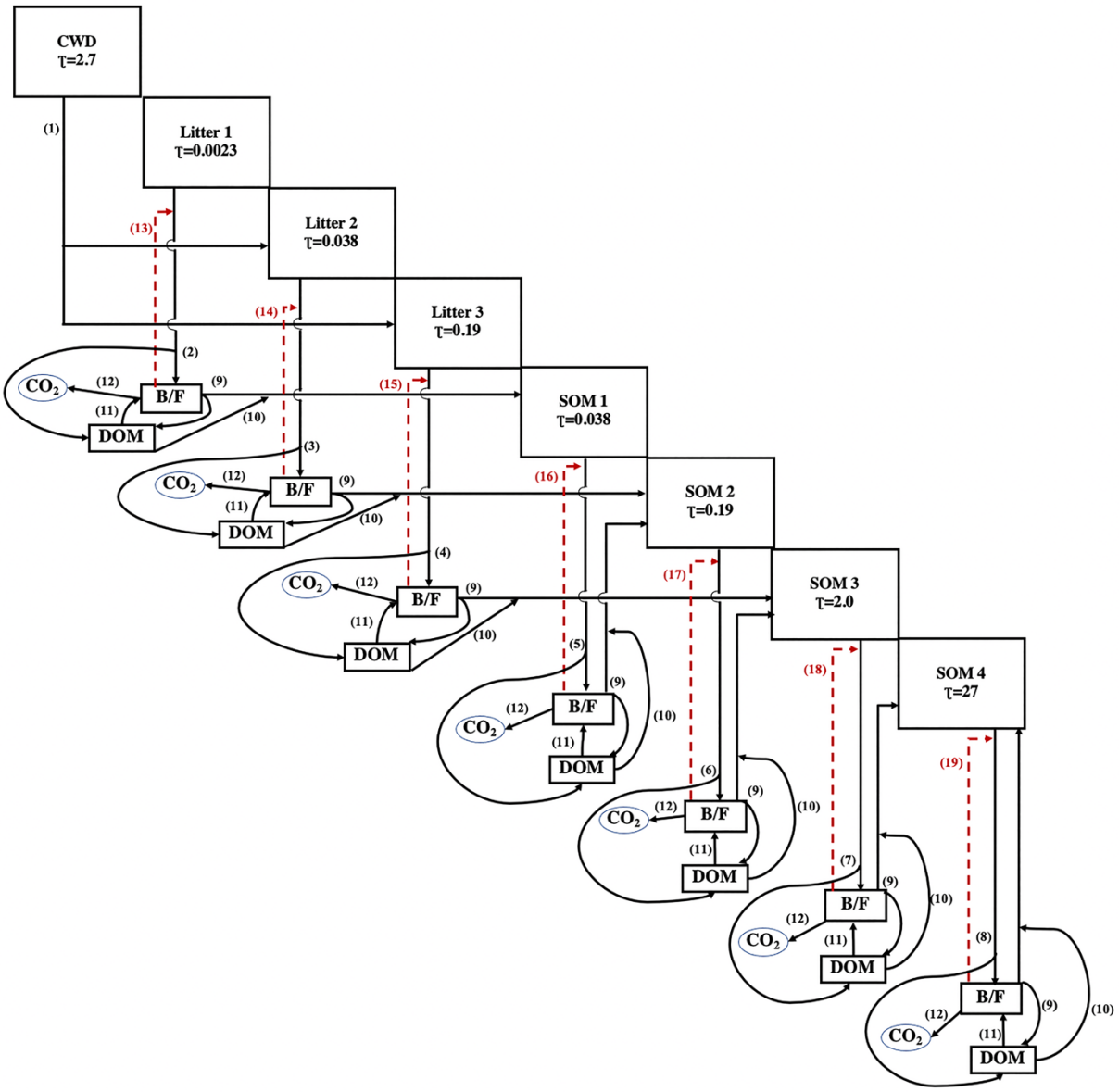

Fig. 2.1. Conceptual diagram showing the key processes and the roles of fungi and bacteria in the CLM-Microbe model. CWD, coarse woody debris; SOM, soil organic matter; B, bacteria; F, fungi; DOM, dissolved organic matter. In the CLM-Microbe model, number in the box means turnover time of each pool. Black solid lines indicate transitions in the CLM-Microbe model, which generally represents processes such as 1) decomposition of coarse woody debris, 2) litter 1 decomposition, 3) litter 2 decomposition, 4) litter 3 decomposition, 5) soil organic matter 1 decomposition, 6) soil organic matter 2 decomposition, 7) soil organic matter 3 decomposition, 8) soil organic matter 4 decomposition, 9) fungal and bacterial lysis, 10) dissolved organic matter decomposition, 11) dissolved organic matter uptake by fungal and bacterial, and 12) fungal and bacterial respiration. Red dash lines represent regulatory role of fungi and bacteria on the process, including fungi and bacteria regulation on 13) litter 1, 14) litter 2, 15) litter 3, 16) soil organic matter 1, 17) soil organic matter 2, 18) soil organic matter 3, and 19) soil organic matter 4 decomposition.

Table 2.1. Site information of the observational data

Phase	Biome	Site ID	Location	Country	Measurement	Depth (cm)	Sampling year	Reference
Calibration	tropical/subtropical forest	TSF-HS	22.57° N, 112.83° E	China	PLFA	0-10	2012-2014	(Zhao et al., 2017)
	temperate coniferous forest	TCF-NJ	39.92° N, 74.6° W	US	PLFA	0-2.3	2006-2008	(Landesman & Dighton, 2010)
	temperate broadleaf forest	TBF-VA	48.21° N, 16.36° E	Austria	PLFA	0-5	2006-2008	(Kaiser et al., 2010)
	boreal forest	BRF-WC	65.32° N, 142.31° W	US	DMO	5-20	1973	(Flanagan & Van Cleve, 1977)
	shrub	SHB-OB	40.18° N, 112.46° W	US	PLFA & FAME	0-10	2009-2010	(Docherty et al., 2015)
	grassland	GRS-IA	42.18° N, 93.5° W	US	DMO	0-10	2001-2002	(Dornbush et al., 2008)
	desert	DST-CH	29.08° N, 103.17° W	US	CF & FAME	0-15	2004-2006	(Bell et al., 2014)
	tundra	TUN-MH	68.36° N, 18.50° E	Sweden	PLFA	0-10	2006	(Björk et al., 2008)
	wetland	WET-EM	51.91° N, 11.98° E	German	PLFA	0-20	1999-2000	(Moche et al., 2015)
Validation	tundra	TUN-ES	64.83° N, 111.63° W	Canada	DMF	0-5	2007	(Buckeridge et al., 2013)
	temperate coniferous forest	TCF-NT	47.58° N, 11.64° E	Australi	PLFA	0-5	2008-2009	(Schindlbacher et al., 2011)
	desert	DST-GB	44.28° N, 87.93° E	China	PLFA	0-5	2011-2013	(Huang et al., 2015)
	Desert	DST-JN	32.59° N, 106.84° W	US	PLFA	0-30	2017	(National Ecological Observatory Network, 2020)
	boreal forest	BRF-AL	65.15° N, 147.5° W	US	PLFA & FAME	0-10	2009	(Docherty et al., 2015)
	tropical/subtropical forest	TSF-OS	29.69° N, 81.99° W	US	PLFA & FAME	0-10	2009-2010	(Docherty et al., 2015)
	grassland	GRS-BC	49.23° N, 121.77° W	Canada	DMO	0-10	1997-1999	(Bittman et al., 2005)
	temperate broadleaf forest	TBF-SH	36.02° N, 106.47° E	China	PLFA	0-11	2012-2013	(Liu et al., 2018)
	temperate broadleaf forest	TBF-MS	37.38° N, 80.52° W	US	PLFA	0-30	2018	(National Ecological Observatory Network, 2020)
	temperate broadleaf forest	TBF-TL	32.95° N, 87.39° W	US	PLFA	0-30	2017	(National Ecological Observatory Network, 2020)
	shrub	SHB-AC	30.63° S, 71.67° W	Chile	CFU	0-20	1997-2006	(Aguilera et al., 2016)
	wetland	WET-EF	51.87° N, 12.39° E	German	PLFA	0-20	1998-2000	(Moche et al., 2015)

DMO, direct microscopy using optical microscope; DMF, direct count using fluorescence microscope; PC, plate count; CF, chloroform fumigation; FAME, fatty acid methyl ester; PLFA, phospholipid fatty acid

Table 2.2. Key model parameters in processes involving fungal and bacterial biomass

Symbol	Range [a]	Uni	Description	Reference
k_dom	0.0025-0.5	d^{-1}	decomposition rate constant of DOM	(Cherrier et al., 1996; Kirchman et al., 1991; Wheeler et al., 1996)
k_bacteria	0.00143-2	d^{-1}	lysis rate constant of bacteria	(Moore et al., 2005; Rousk & Bååth, 2007, 2011; Schippers et al., 2005)
k_fungi	0.00027-0.05	d^{-1}	lysis rate constant of fungi	(Moore et al., 2005; Rousk & Bååth, 2011; Thornton & Rosenbloom, 2005; Wallander et al., 2004)
m_rf_s1m	0-1		fraction factor quantifying carbon from SOM1 to microbes	Calibrated
m_rf_s2m	0-1		fraction factor quantifying carbon from SOM2 to microbes	Calibrated
m_rf_s3m	0-1		fraction factor quantifying carbon from SOM3 to microbes	Calibrated
m_rf_s4m	0-1		fraction factor quantifying carbon from SOM4 to microbes	Calibrated
m_batm_f	0-1		fraction factor quantifying carbon respired by bacteria	Calibrated
m_bdom_f	0-1		fraction factor quantifying carbon from DOM to bacteria	Calibrated
m_bs1_f	0-1		fraction factor quantifying carbon from bacteria to SOM1	Calibrated
m_bs2_f	0-1		fraction factor quantifying carbon from bacteria to SOM2	Calibrated
m_bs3_f	0-1		fraction factor quantifying carbon from bacteria to SOM3	Calibrated
m_fatm_f	0-1		fraction factor quantifying carbon respired by fungi	Calibrated
m_fdom_f	0-1		fraction factor quantifying carbon from DOM to fungi	Calibrated
m_fs1_f	0-1		fraction factor quantifying carbon from fungi to SOM1	Calibrated
m_fs2_f	0-1		fraction factor quantifying carbon from fungi to SOM2	Calibrated
m_fs3_f	0-1		fraction factor quantifying carbon from fungi to SOM3	Calibrated
m_domb_f	0-1		fraction factor quantifying carbon from DOM to bacteria	Calibrated
m_domf_f	0-1		fraction factor quantifying carbon from DOM to fungi	Calibrated
m_doms1_f	0-1		fraction factor quantifying carbon from DOM to SOM1	Calibrated
m_doms2_f	0-1		fraction factor quantifying carbon from DOM to SOM2	Calibrated
m_doms3_f	0-1		fraction factor quantifying carbon from DOM to SOM3	Calibrated
cn_bacteria	3-12		C:N ratio of bacteria	(Strickland & Rousk, 2010)
cn_fungi	3-60		C:N ratio of fungi	(Strickland & Rousk, 2010)
cn_dom	4.2-185		C:N ratio of DOM	(Sinsabaugh et al., 2016)
CUEmax	0.46-0.9		maximum carbon use efficiency of microbes	(Gommers et al., 1988; Sinsabaugh et al., 2013; Sinsabaugh et al., 2016)

[a]The values may not be the same as those from literature sources due to unit conversion.

Table 2.3. Key parameters for the different biomes

Parameters	Biomes								
	BRF	DST	GRS	SHB	TBF	TCF	TSF	TUN	WET
m_bdom_f	0.15	0.1	0.15	0.1	0.15	0.15	0.1	0.1	0.08
m_bs1_f	0.1	0.03	0.05	0.05	0.05	0.05	0.03	0.03	0.02
m_bs2_f	0.12	0.06	0.1	0.1	0.1	0.1	0.06	0.06	0.04
m_bs3_f	0.18	0.12	0.15	0.15	0.15	0.15	0.12	0.12	0.08
m_fdom_f	0.15	0.1	0.15	0.1	0.15	0.15	0.1	0.1	0.08
m_fs1_f	0.1	0.03	0.05	0.05	0.05	0.05	0.03	0.03	0.02
m_fs2_f	0.12	0.06	0.1	0.1	0.1	0.1	0.06	0.06	0.04
m_fs3_f	0.18	0.12	0.15	0.15	0.15	0.15	0.12	0.12	0.08
k_dom	0.007	0.007	0.007	0.007	0.008	0.007	0.0005	0.007	0.007
k_bacteria	0.008	0.0178	0.005	0.0036	0.008	0.004	0.0085	0.0032	0.072
k_fungi	0.004	0.009	0.0045	0.002	0.0018	0.002	0.01	0.0012	0.032
m_rf_s1m	0.4	0.4	0.4	0.4	0.4	0.4	0.4	0.4	0.4
m_rf_s2m	0.6	0.6	0.6	0.6	0.6	0.6	0.6	0.6	0.6
m_rf_s3m	0.7	0.7	0.7	0.7	0.7	0.7	0.7	0.7	0.7
m_rf_s4m	0.8	0.8	0.8	0.8	0.8	0.8	0.8	0.8	0.8
m_batm_f	0.2	0.08	0.12	0.08	0.12	0.12	0.12	0.12	0.1
m_fatm_f	0.1	0.04	0.08	0.04	0.08	0.08	0.08	0.08	0.06
m_domb_f	0.008	0.12	0.04	0.16	0.86	0.045	0.05	0.24	0.27
m_domf_f	0.001	0.18	0.9	0.64	0.04	0.005	0.89	0.56	0.45
m_doms1_f	0.32	0.24	0.03	0.1	0.06	0.32	0.03	0.1	0.14
m_doms2_f	0.27	0.2	0.02	0.06	0.03	0.28	0.02	0.06	0.08
m_doms3_f	0.22	0.15	0.01	0.03	0.01	0.2	0.01	0.03	0.04
cn_bacteria	5	4	5	5	6	5	5	4	6
cn_fungi	15	15	15	15	12	15	15	16	12
CUEmax	0.8	0.8	0.8	0.8	0.8	0.8	0.8	0.8	0.8

BRF, boreal forest; DST, desert; GRS, grassland; SHB, shrub; TBF, temperate broadleaf forest; TCF, temperate coniferous forest; TSF, tropical/subtropical forest; TUN, tundra; WET, wetland.

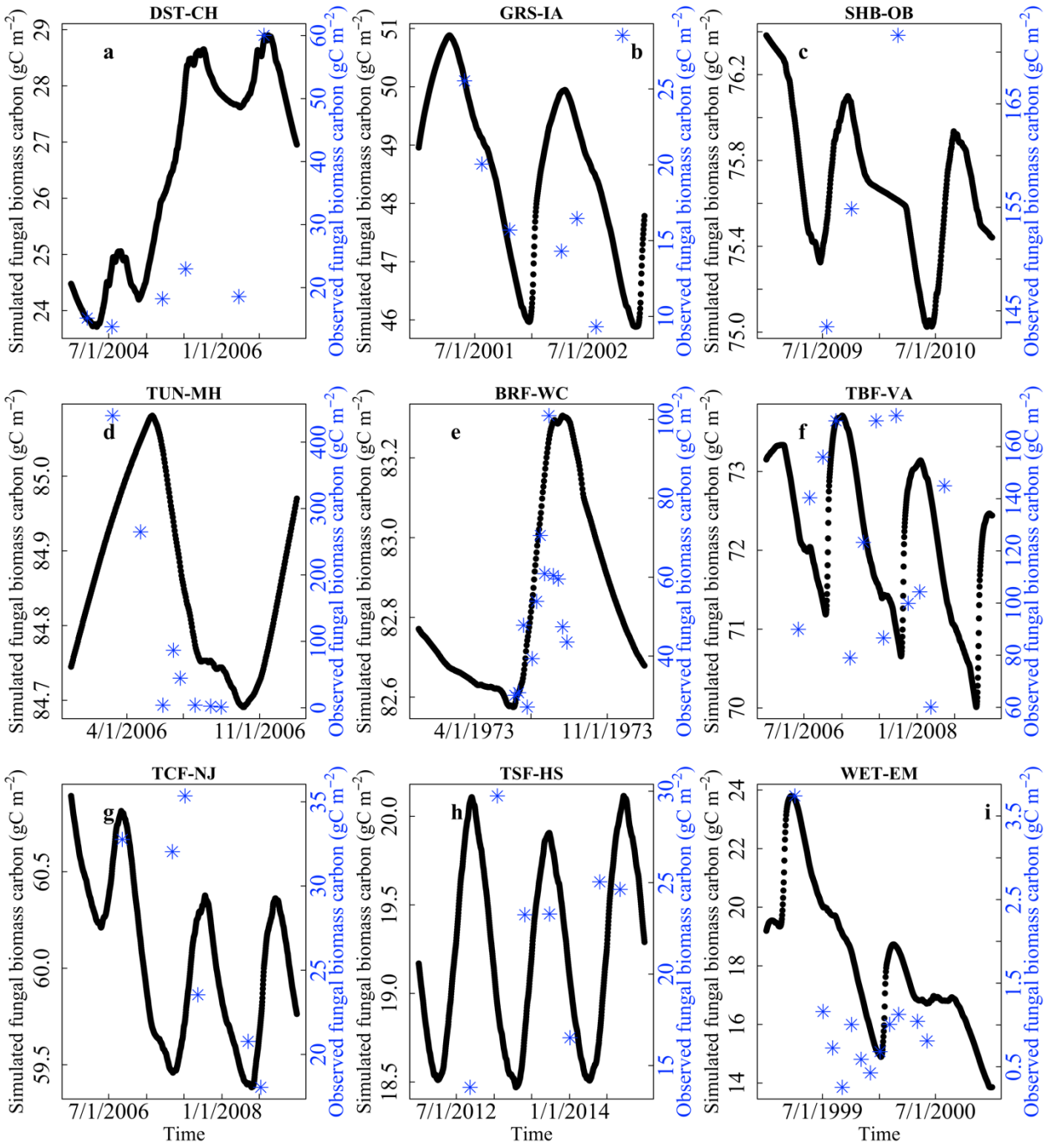

Fig. 2.2. Calibration of fungal biomass for a) desert, b) grassland, c) shrub, d) tundra, e) boreal forest, f) temperate broadleaf forest, g) temperate coniferous forest, h) tropical/subtropical forest, and i) wetland. The blue star indicates the observed fungal biomass, and the black filled circle represents simulated fungal biomass.

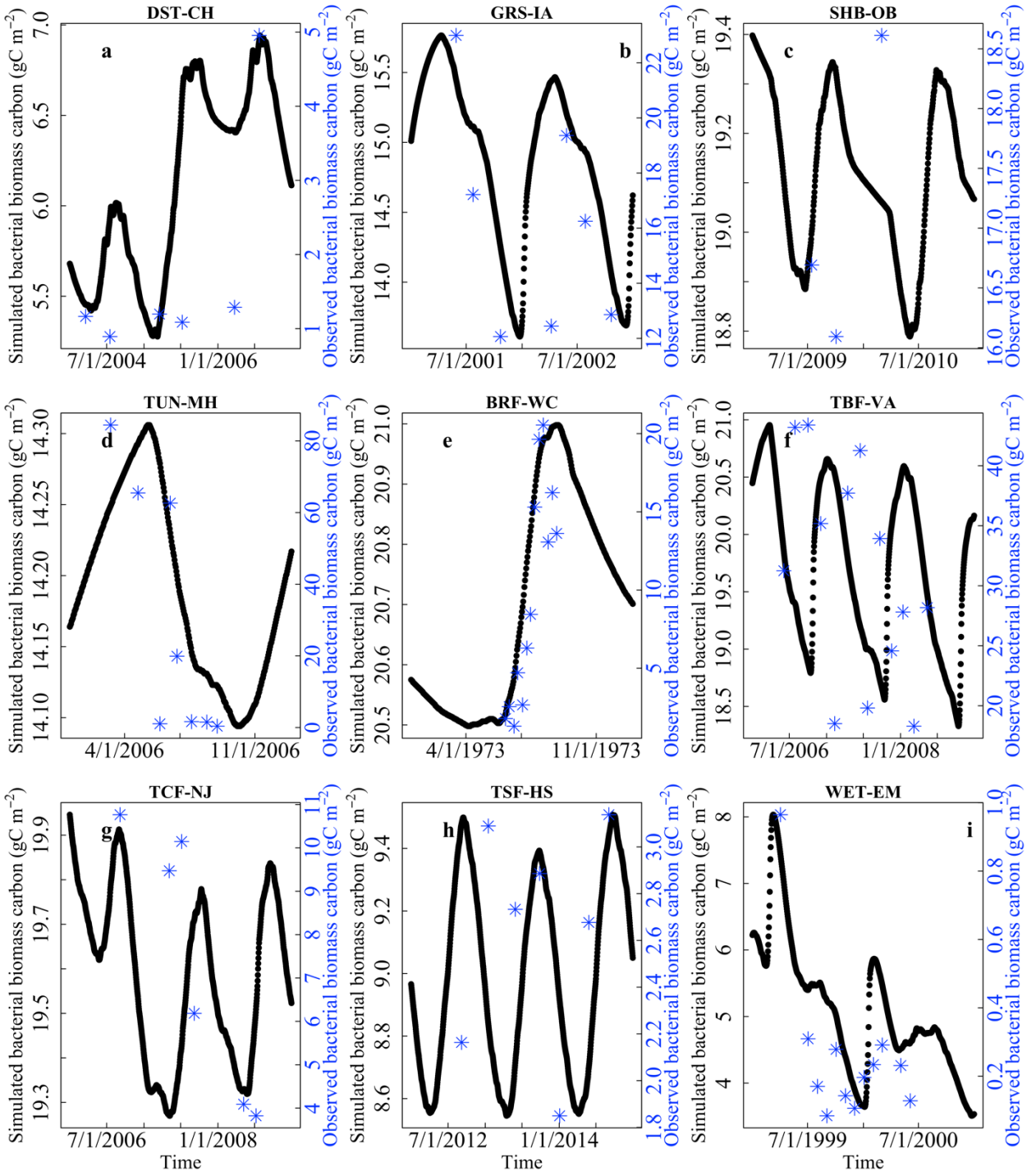

Fig. 2.3. Calibration of bacterial biomass for a) desert, b) grassland, c) shrub, d) tundra, e) boreal forest, f) temperate broadleaf forest, g) temperate coniferous forest, h) tropical/subtropical forest, and i) wetland. The blue star indicates the observed bacterial biomass, and the black filled circle represents simulated bacterial biomass.

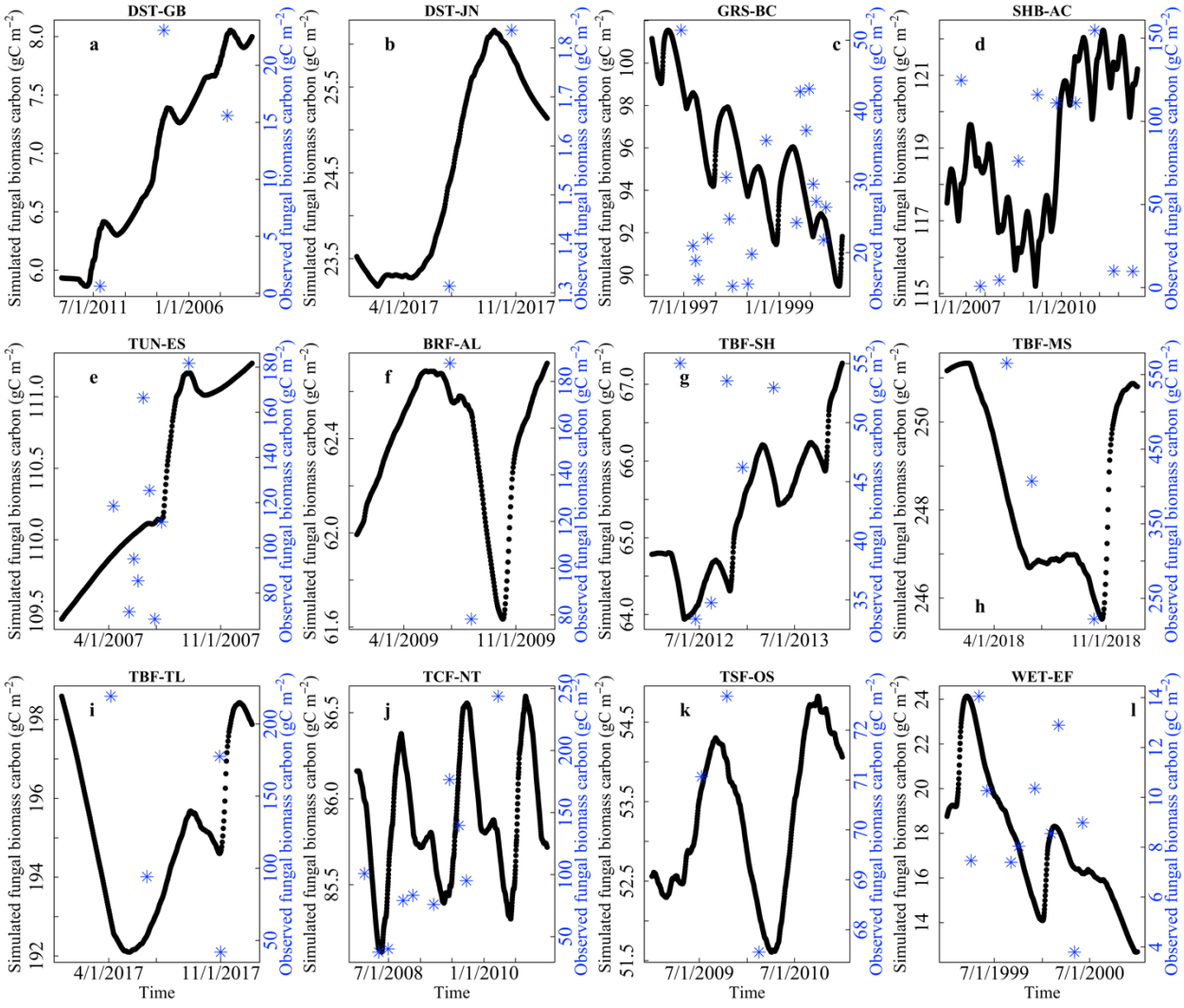

Fig. 2.4. Validation of fungal biomass for a and b) desert, c) grassland, d) shrub, e) tundra, f) boreal forest, g, h and i) temperate broadleaf forest, j) temperate coniferous forest, k) tropical/subtropical forest, and l) wetland. The blue star indicates the observed fungal biomass, and the black filled circle represents simulated fungal biomass.

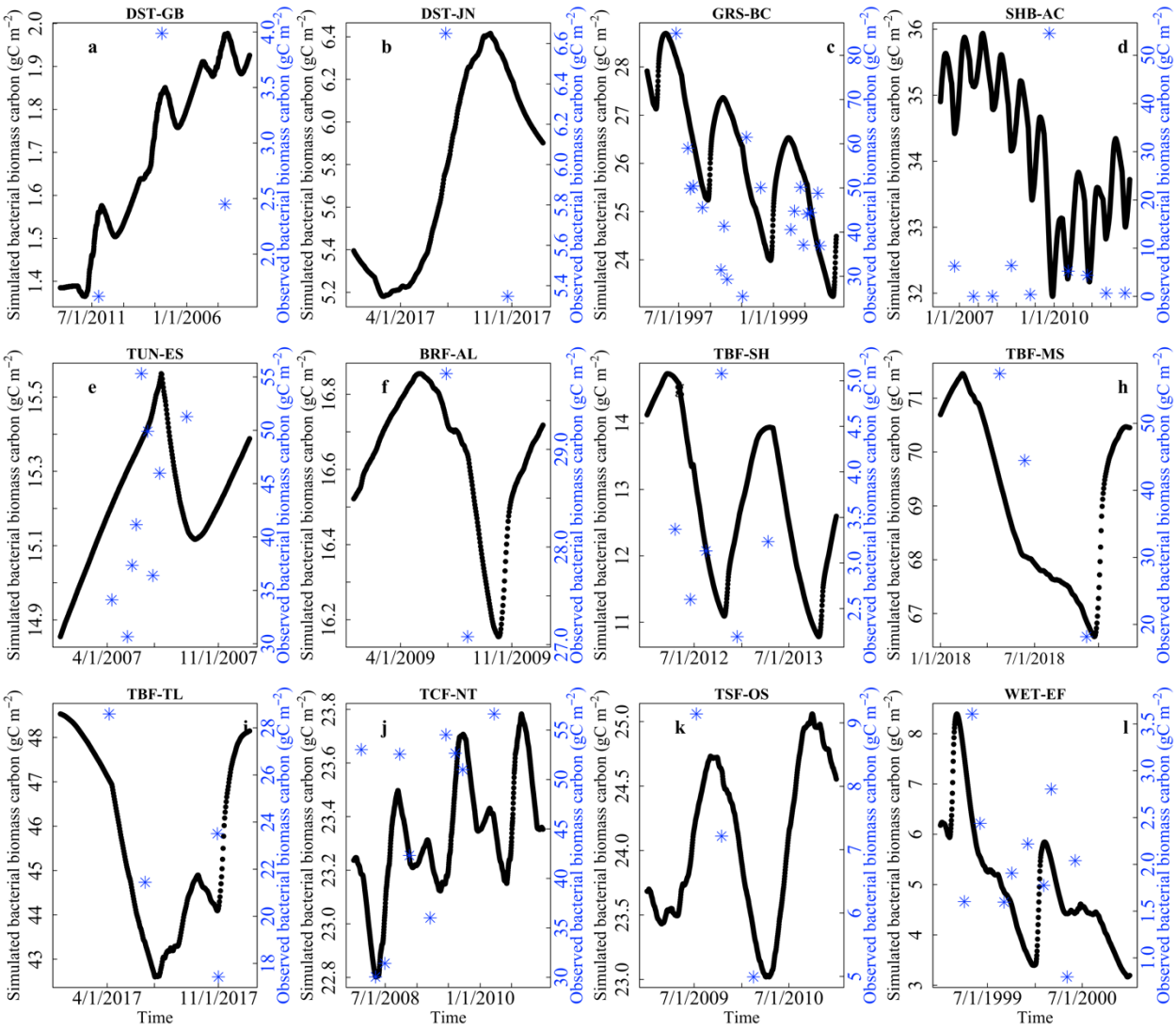

Fig. 2.5. Validation of bacterial biomass for a and b) desert, c) grassland, d) shrub, e) tundra, f) boreal forest, g, h and i) temperate broadleaf forest, j) temperate coniferous forest, k) tropical/subtropical forest, and l) wetland. The blue star indicates the observed bacterial biomass, and the black filled circle represents simulated bacterial biomass.

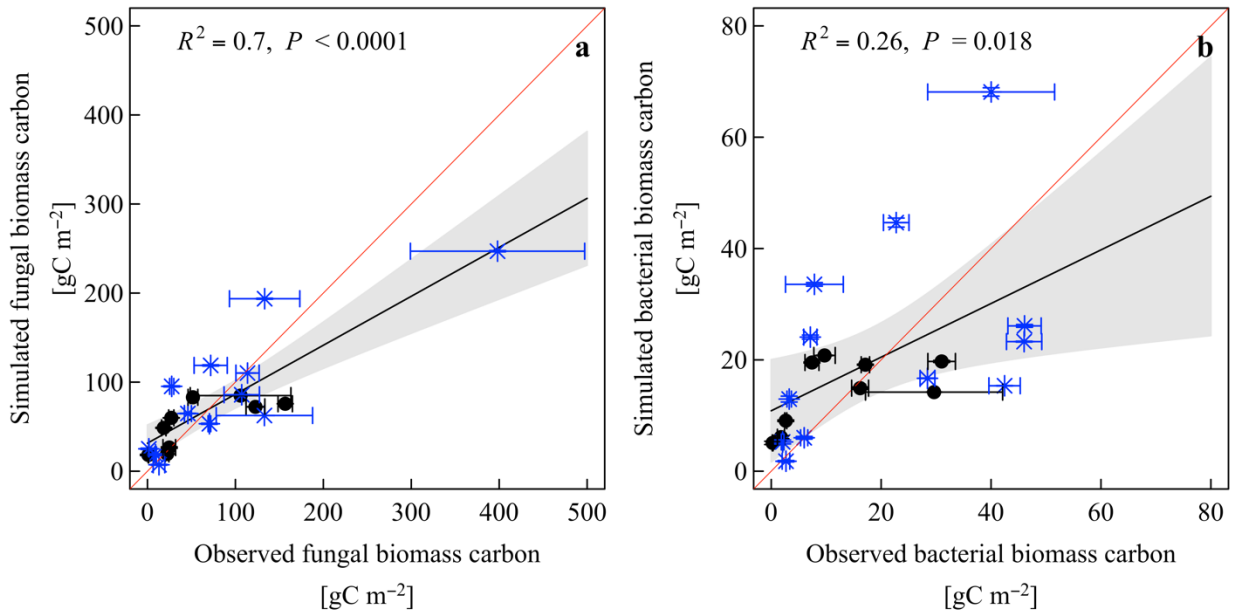

Fig. 2.6. Comparison of the averaged observed and simulated a) fungal and b) bacterial biomass. The blue star indicates the a) fungal or b) bacterial biomass in calibration phase, and the black filled circle represents a) fungal or b) bacterial biomass in validation phase; vertical and horizontal error bars indicate standard error of simulated and observed values, respectively, for both a) fungal and b) bacterial biomass.

Table 2.4. Site-level evaluation of the goodness-of-fit criteria computed for the simulated fungal and bacterial biomass dynamics in the calibration and validation phases

Phase	Site	Fungi			Bacteria		
		MAE	RMSE	R^2	MAE	RMSE	R^2
Calibration	DST-CH	0.45	0.60	0.473	0.56	0.76	0.374
	GRS-IA	0.29	0.34	0.042	0.18	0.21	0.381
	SHB-OB	0.06	0.07	0.005	0.06	0.07	0.299
	TUN-MH	1.16	1.43	0.251	1.04	1.11	0.398
	BRF-WC	0.28	0.37	0.384	0.63	0.69	0.830
	TBF-VA	0.28	0.31	0.157	0.26	0.30	0.217
	TCF-NJ	0.23	0.24	0.066	0.37	0.38	0.067
	TSF-HS	0.19	0.24	0.156	0.14	0.17	0.002
	WET-EM	0.41	0.73	0.59	0.42	0.72	0.63
Validation	DST-GB	0.54	0.65	0.513	0.32	0.33	0.269
	DST-JN	0.14	0.14	--	0.15	0.16	--
	GRS-BC	0.30	0.37	0.010	0.20	0.27	0.046
	SHB-AC	0.73	0.79	0.004	1.18	2.02	0.111
	TUN-ES	0.27	0.33	0.411	0.17	0.19	0.014
	BRF-AL	0.41	0.41	--	0.04	0.04	--
	TBF-TL	0.49	0.52	0.064	0.13	0.16	0.625
	TBF-SH	0.17	0.19	0.092	0.24	0.33	0.183
	TBF-MS	0.29	0.35	0.935	0.36	0.39	0.945
	TCF-NT	0.45	0.56	0.014	0.19	0.20	0.450
	TSF-OS	0.01	0.02	0.980	0.19	0.22	0.520
	WET-EF	0.25	0.31	0.071	0.30	0.37	0.052

MAE, mean absolute error; RMSE, root mean square error; R^2, R square. -- indicates not applicable. MAE and RMSE values indicate the mean error of the model, smaller values represent higher model performance. R^2 values mean the proportion of variation being explained by the mode, higher R^2 values indicate better model performance. Due to the difference in variations of simulated and observed fungal and bacterial biomass and our focus of estimating fungal and bacterial biomass dynamics, we did the evaluation using relative change in fungal and bacterial biomass instead, i.e., the difference between simulated/observed fungal/bacterial biomass and the average of simulated/observed fungal/bacterial biomass over the average of simulated/observed fungal/bacterial biomass; R^2 is not suitable for assessing the goodness-of-fit for a small amount of data due to the large bias in small samples.

Table 2.5. Key parameters for sensitivity analysis and uncertainty analysis

Parameters	Ecological meanings
k_dom	decomposition rate constant of dissolved organic matter
k_bacteria	lysis rate constant of bacteria
k_fungi	lysis rate constant of fungi
m_rf_s1m	fraction factor quantifying carbon from soil organic matter1 to microbes
m_rf_s2m	fraction factor quantifying carbon from soil organic matter2 to microbes
m_rf_s3m	fraction factor quantifying carbon from soil organic matter3 to microbes
m_rf_s4m	fraction factor quantifying carbon from soil organic matter4 to microbes
m_batm_f	fraction factor quantifying carbon respired by bacteria
m_bdom_f	fraction factor quantifying carbon from dissolved organic matter to bacteria
m_bs1_f	fraction factor quantifying carbon from bacteria to soil organic matter1
m_bs2_f	fraction factor quantifying carbon from bacteria to soil organic matter2
m_bs3_f	fraction factor quantifying carbon from bacteria to soil organic matter3
m_fatm_f	fraction factor quantifying carbon respired by fungi
m_fdom_f	fraction factor quantifying carbon from dissolved organic matter to fungi
m_fs1_f	fraction factor quantifying carbon from fungi to soil organic matter1
m_fs2_f	fraction factor quantifying carbon from fungi to soil organic matter2
m_fs3_f	fraction factor quantifying carbon from fungi to soil organic matter3
m_domb_f	fraction factor quantifying carbon from dissolved organic matter to bacteria
m_domf_f	fraction factor quantifying carbon from dissolved organic matter to fungi
m_doms1_f	fraction factor quantifying carbon from dissolved organic matter to soil organic matter1
m_doms2_f	fraction factor quantifying carbon from dissolved organic matter to soil organic matter2
m_doms3_f	fraction factor quantifying carbon from dissolved organic matter to soil organic matter3
cn_bacteria	C:N ratio of bacteria
cn_fungi	C:N ratio of fungi
CUEmax	maximum carbon use efficiency of microbes

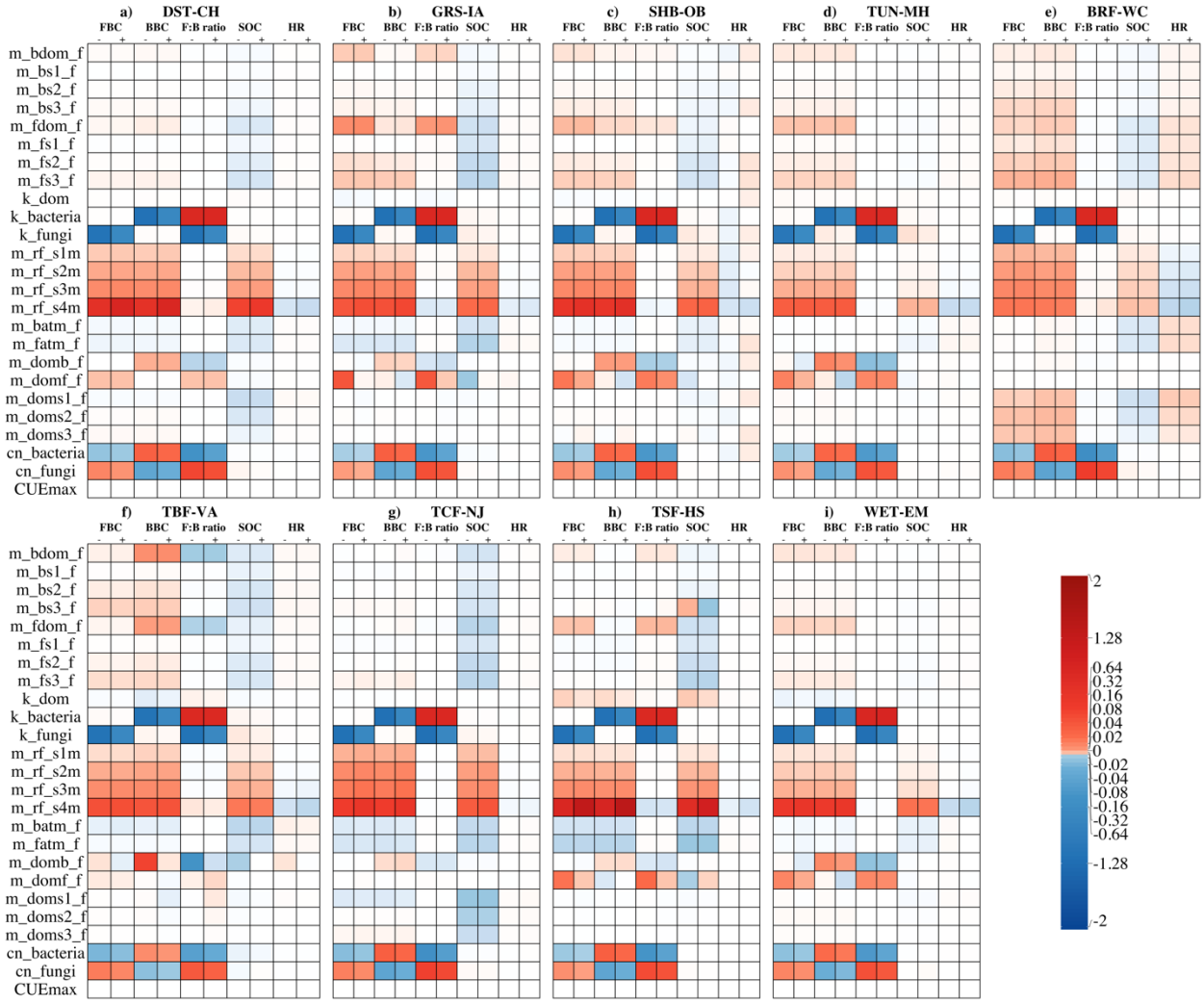

Fig. 2.7. Sensitivity analysis for model response of fungal biomass, bacterial biomass, F:B ratio, soil organic carbon, and soil microbial respiration in the top 30 cm to 25 parameters (m_bdom_f, m_bs1_f, m_bs2_f, m_bs3_f, m_fdom_f, m_fs1_f, m_fs2_f, m_fs3_f, k_dom, k_bacteria, k_fungi, m_rf_s1m, m_rf_s2m, m_rf_s3m, m_rf_s4m, m_batm_f, m_fatm_f, m_domb_f, m_domf_f, m_doms1_f, m_doms2_f, m_doms3_f, cn_bacteria, cn_fungi, and CUEmax) in a) desert, b) grassland, c) shrub, d) tundra, e) boreal forest, f) temperate broadleaf forest, g) temperate coniferous forest, h) tropical/subtropical forest, and i) wetland during the sampling years for all sites. "+" and "-" indicate 20% increase or 20% decrease of parameter values. FBC, fungal biomass carbon; BBC, bacterial biomass carbon; F:B ratio, fungal:bacterial biomass carbon ratio; SOC, soil organic carbon; HR, heterotrophic respiration; Dark red and darker blue indicate a stronger positive or negative model response of the variable to parameter change. S is negative if the direction of model response opposes the direction of parameter change.

Table 2.6. Annual estimates of fungal and bacterial biomass carbon, fungal:bacterial (F:B) ratio, soil organic carbon (SOC), and heterotrophic respiration (HR) with the uncertainties of parameters during the sampling years for all sites

Source	Site/Biome	Fungal biomass (gC m^{-2})	Bacterial biomass (gC m^{-2})	F:B ratio	SOC (gC m^{-2})	HR (gC m^{-2} yr^{-1})
CLM-Microbe simulated[a]	DST-CH	38.65 (21.69 ~ 62.97)	8.90 (5.21 ~ 15.17)	4.54 (2.15 ~ 7.94)	2567.62 (2011.82 ~ 3148.15)	277.41 (269.87 ~ 282.88)
	GRS-IA	110.25 (66.94 ~ 182.63)	33.57 (21.20 ~ 53.26)	3.44 (1.68 ~ 5.94)	2677.50 (2225.43 ~ 3104.13)	312.85 (307.67 ~ 325.92)
	SHB-OB	148.74 (86.44 ~ 253.85)	37.33 (22.44 ~ 61.57)	4.16 (2.07 ~ 7.47)	3363.62 (2908.50 ~ 3829.85)	120.69 (117.80 ~ 123.25)
	TUN-MH	180.25 (111.67 ~ 283.71)	29.89 (19.44 ~ 46.77)	6.30 (3.23 ~ 10.70)	3603.51 (3460.15 ~ 3741.94)	92.75 (90.15 ~ 95.48)
	BRF-WC	204.76 (124.98 ~ 328.30)	40.10 (27.41 ~ 63.30)	5.39 (2.61 ~ 9.45)	8685.33 (8133.04 ~ 9341.41)	420.07 (367.18 ~ 452.30)
	TBF-VA	258.79 (161.16 ~ 429.01)	70.47 (45.63 ~ 114.71)	3.83 (1.89 ~ 6.49)	5872.70 (5221.21 ~ 6540.73)	560.48 (538.93 ~ 574.73)
	TCF-NJ	379.71 (213.91 ~ 683.37)	100.15 (59.46 ~ 166.58)	3.96 (1.86 ~ 6.95)	7989.60 (6411.33 ~ 9961.35)	811.32 (800.71 ~ 818.67)
	TSF-HS	37.02 (19.70 ~ 62.50)	16.66 (9.11 ~ 29.09)	2.31 (1.14 ~ 4.19)	2509.49 (1694.83 ~ 3422.36)	400.69 (393.76 ~ 404.51)
	WET-EM	23.62 (13.52 ~ 39.54)	6.63 (4.13 ~ 11.03)	3.75 (1.85 ~ 6.67)	13203.92 (11732.67 ~ 14385.34)	540.32 (524.52 ~ 556.59)
CLM4.5 simulated[a]	DST-CH	NA	NA	NA	0.00	0.00
	GRS-IA	NA	NA	NA	11990.54	756.86
	SHB-OB	NA	NA	NA	1598.15	63.07
	TUN-MH	NA	NA	NA	2085.97	94.61
	BRF-WC	NA	NA	NA	3465.00	157.68
	TBF-VA	NA	NA	NA	11238.67	599.18
	TCF-NJ	NA	NA	NA	4920.45	315.36
	TSF-HS	NA	NA	NA	6627.84	536.11
	WET-EM	NA	NA	NA	9950.83	567.65
Observed[b]	DST-CH[d]	24.79 (13.78 ~ 60.04)	1.76 (0.89 ~ 4.95)	14.05 (12.12 ~ 21.13)	NA	NA
	GRS-IA[e]	18.55 (9.32 ~ 28.53)	16.17 (12.07 ~ 22.99)	1.15 (0.57 ~ 2.22)	NA	NA
	SHB-OB[e]	156.65 (143.46 ~ 171.62)	17.13 (16.09 ~ 18.61)	9.14 (8.60 ~ 9.62)	3559.97[e]	NA
	TUN-MH[e]	105.89 (1.10 ~ 439.88)	29.63 (0.38 ~ 84.42)	3.57 (1.38 ~ 5.21)	1945.00[ek]	NA
	BRF-WC[f]	51.71 (27.07 ~ 100.96)	9.70 (1.29 ~ 20.55)	5.33 (2.92 ~ 36.93)	NA	NA
	TBF-VA[g]	122.78 (60.12 ~ 171.88)	31.01 (18.30 ~ 43.39)	3.96 (2.88 ~ 5.15)	NA	NA
	TCF-NJ[h]	27.09 (18.05 ~ 35.35)	7.41 (3.82 ~ 10.77)	3.65 (3.04 ~ 5.08)	NA	NA
	TSF-HS[e]	22.33 (13.81 ~ 29.74)	2.65 (1.85 ~ 3.14)	8.43 (6.38 ~ 9.63)	4238.08[e]	NA
	WET-EM[i]	1.05 (0.25 ~ 3.74)	0.26 (0.08 ~ 0.97)	4.01 (3.02 ~ 6.33)	10819[j]	NA
Biome average[c]	DST	59.04 (14.05 ~ 74.00)	15.28 (0.32 ~ 60.21)	3.14 (2.20 ~ 4.49)	2728.00 (2651.58 ~ 2804.42)	NA
	GRS	88.69 (20.55 ~ 132.48)	46.14 (2.34 ~ 114.23)	4.03 (3.52 ~ 4.62)	6225.00 (5796.59 ~ 6653.41)	NA
	SHB	48.06 (11.40 ~ 64.78)	17.31 (0.59 ~ 53.85)	4.82 (3.72 ~ 6.25)	4450.00 (4207.30 ~ 4692.70)	NA
	TUN	226.96 (150.89 ~ 256.46)	32.65 (3.13 ~ 108.08)	8.60 (6.71 ~ 11.01)	7739.00 (6589.57 ~ 8888.43)	NA
	BRF	304.44 (191.19 ~ 356.01)	58.66 (7.02 ~ 171.86)	5.03 (4.23 ~ 5.98)	5812.50 (5601.96 ~ 6023.04)	NA
	TBF	88.89 (40.25 ~ 115.74)	29.88 (3.01 ~ 78.5)	4.92 (4.39 ~ 5.51)	10875.00 (9807.51 ~ 11942.49)	NA
	TCF	88.89 (40.25 ~ 115.74)	29.88 (3.01 ~ 78.5)	4.92 (4.39 ~ 5.51)	8482.50 (7974.46 ~ 8990.54)	NA
	TSF	64.42 (2.09 ~ 115.49)	51.58 (0.51 ~ 113.82)	2.22 (1.87 ~ 2.63)	8514.00 (7686.89 ~ 9341.11)	NA
	WET	70.44 (30.9 ~ 99.91)	32.96 (3.47 ~ 72.44)	4.13 (3.50 ~ 4.86)	NA	NA

a, simulated fungal and bacterial biomass, fungal:bacterial (F:B) ratio, soil organic carbon, and heterotrophic respiration of top 30 cm soil profile using either CLM-Microbe model or CLM4.5, values in the parentheses were 95% confidence interval; b, observed fungal and bacterial biomass, F:B ratio, soil organic carbon, and heterotrophic respiration from literature, values were expressed as average (range), and the values showed may not be the same as those from literature sources due to unit conversion; c, biome average of fungal and bacterial biomass and F:B ratio from He et al. (2020) of top 30 cm soil profile, and soil organic carbon of top 30 cm were from Jobbágy and Jackson (2000), assuming that 20-30 cm and 30-40 cm contribute equally to the soil organic carbon in 20-40 cm layer; BRF, boreal forest; DST, desert; GRS, grassland; SHB, shrub; TBF, temperate broadleaf forest; TCF, temperate coniferous forest; TSF, tropical/subtropical forest; TUN, tundra; WET, wetland; d, e, f, g, h, and i represent observed fungal and bacterial biomass, F:B ratio, soil organic carbon, and heterotrophic respiration of 0-15 cm, 0-10 cm, 5-20 cm, 0-5 cm, 0-2.3 cm and, 0-20 cm, respectively; j, observed soil organic carbon of 18-60 cm; k, recalculated SOC from Björk et al. (2007); NA means no data available.

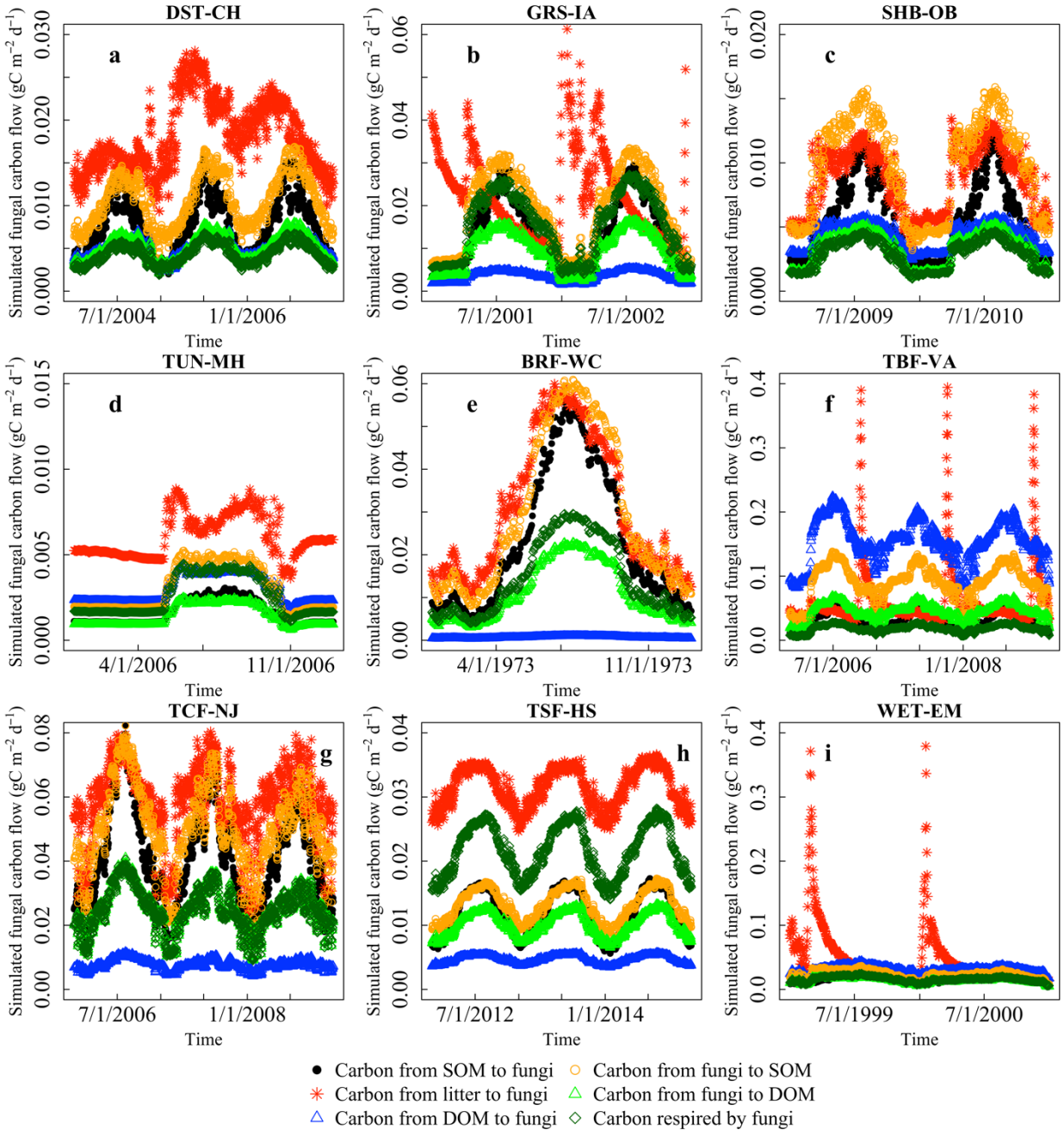

Fig. 2.8. Time-series of simulated carbon flow into and out from the fungal biomass carbon pool

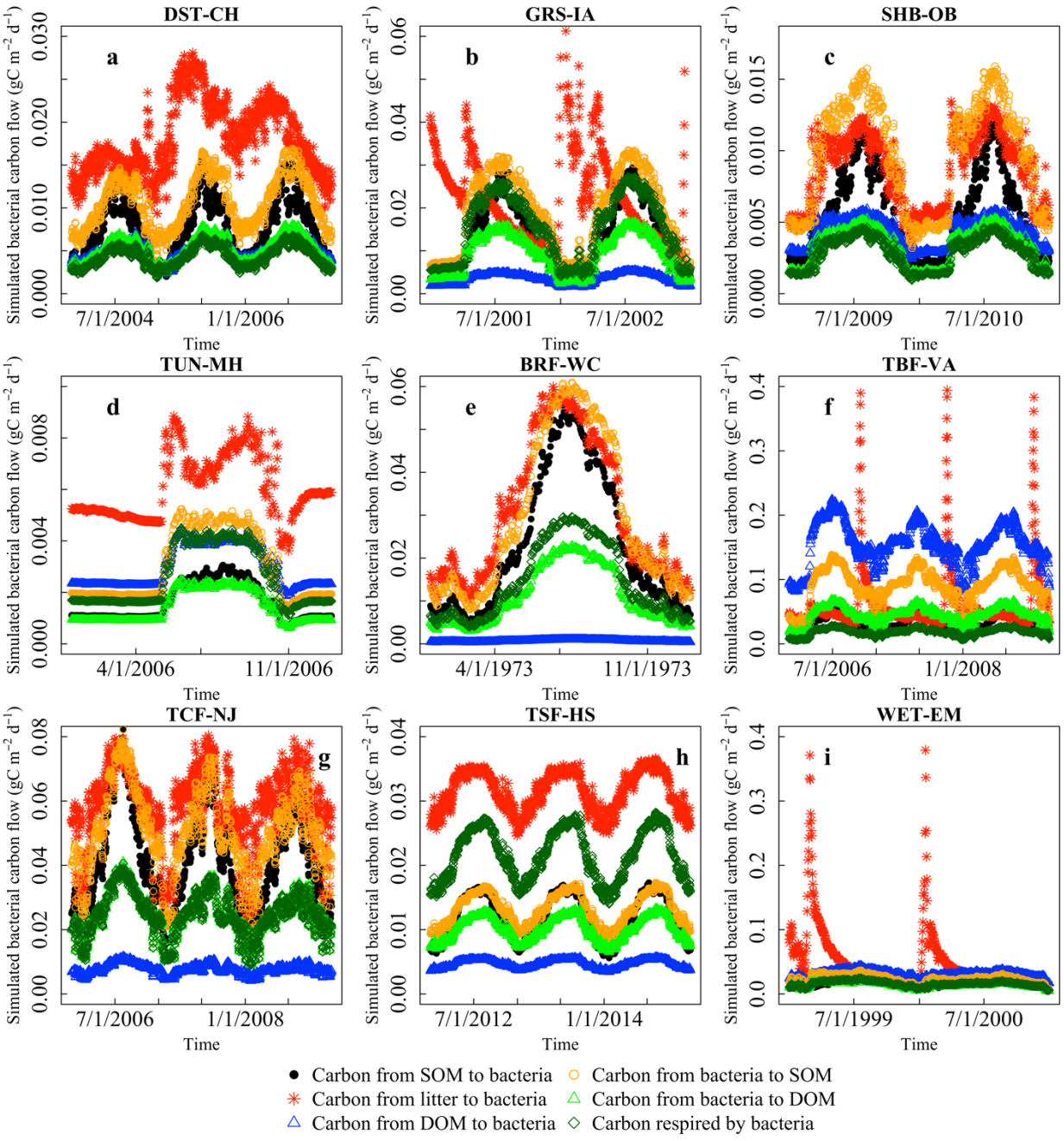

Fig. 2.9. Time-series of simulated carbon flow into and out from the bacterial biomass carbon pool

Chapter 3. Microbial Seasonality Promotes Soil Respiratory Carbon Emission in Natural Ecosystems: A Modeling Study

This chapter has already been published by John Wiley and Sons, with a License Number of 5302650019308 for dissertation use.

He, L., C.-T. Lai, M. A. Mayes, S. Murayama, and X. Xu. 2021. Microbial seasonality promotes soil respiratory carbon emission in natural ecosystems: a modeling study. Global change biology **27**:3035-3051.

Abstract

Seasonality is a key feature of the biosphere and the seasonal dynamics of soil carbon (C) emissions represent a fundamental mechanism regulating the terrestrial – climate interaction. We applied a microbial explicit model - CLM-Microbe - to evaluate the impacts of microbial seasonality on soil C cycling in terrestrial ecosystems. The CLM-Microbe model was validated in simulating belowground respiratory fluxes, i.e., microbial respiration, root respiration, and soil respiration at the site-level. On average, the CLM-Microbe model explained 72% (n=19, P<0.0001), 65% (n=19, P<0.0001), and 71% (n=18, P<0.0001) of the variation in microbial respiration, root respiration, and soil respiration, respectively. We then compared the model simulations of soil respiratory fluxes and soil organic C content in the top 1 m between the CLM-Microbe model with (CLM-Microbe) and without (CLM-Microbe_wos) seasonal dynamics of soil microbial biomass in natural biomes. Removing soil microbial seasonality reduced model performance in simulating microbial respiration and soil respiration, but led to slight differences in simulating root respiration. Compared with the CLM-Microbe, the CLM-Microbe_wos underestimated the annual flux of microbial respiration by 0.6% - 32% and annual flux of soil respiration by 0.4% - 29% in natural biomes. Correspondingly, the CLM-Microbe_wos estimated higher soil organic C content in the top 1 m (0.2% - 7%) except for the sites in Arctic and boreal regions. Our findings suggest that soil microbial seasonality enhances soil respiratory C emissions, leading to a

decline in SOC storage. An explicit representation of soil microbial seasonality represents a critical improvement for projecting soil C decomposition and reducing the uncertainties in the global C cycle projection under the changing climate.

Key words: microbial seasonality, microbial respiration, root respiration, soil respiration

Introduction

Soil respiration (SR), the second largest terrestrial C flux, has been increasing over the last five decades and is projected to further increase under a warming climate (Schlesinger and Andrews 2000; Bond-Lamberty and Thomson 2010). The SR is the sum of C emission from soil organisms and plant roots from the soil surface to the atmosphere, with approximately 2/3 contributed by soil organisms, primarily soil microbes (i.e., microbial respiration, MR), and the rest from plant roots (i.e., root respiration, RR) (Bond-Lamberty et al. 2004; Tang and Baldocchi 2005). Consequently, understanding the effects of soil microbial community on SR and its component respiration fluxes, particularly MR, is critical for accurately quantifying and projecting the terrestrial C-climate feedbacks (Schlesinger and Andrews 2000; Bond-Lamberty et al. 2004; Bond-Lamberty and Thomson 2010; Xu et al. 2013; Xu et al. 2014; Xu et al. 2017; Tang et al. 2020).

Due to the irreplaceable role of soil microbes in C biogeochemical cycling in soils, the explicit representation of soil microbial processes in Earth system models (ESMs) has been undertaken to address the large uncertainties in terrestrial C cycle projections (Wang et al. 2013a; Wieder et al. 2015; Wang et al. 2017). Although microbial traits, such as enzyme production, temperature sensitivity, dormancy, and microbial turnover, have been incorporated into ESMs (Wang et al. 2013a; Wieder et al. 2013; Xu et al. 2014; Wang et al. 2015a; Wang et al. 2017), the potential influence of seasonal variations of soil microbial community composition on ecosystem process rates is overlooked. Studies proposed close links

between microbial community composition and ecosystem function. For example, variations in soil microbial community composition could influence soil respiration rates (Cleveland et al. 2007; Monson et al. 2006; Whitaker et al. 2014). However, soil microbial community in the models is generally represented as an aggregated pool of total soil microbial biomass; the response of different soil microbial groups (e.g., fungi and bacteria) has not been explicitly represented. Fungi and bacteria, the two major soil microbial groups, respond differently to environmental change, which may lead to changes in the pool size of soil microbial biomass and further influence soil microbial community structure (Pietikäinen et al. 2005; Manzoni et al. 2012; He et al. 2020). Shifts in soil microbial community composition have profound influences on the C cycle (Lipson et al. 2002). Nevertheless, an explicit representation of variations in soil microbial community composition in ESMs is still in infancy and the influence of soil microbial seasonality on the C cycle is far from clear (Wieder et al. 2015, He et al. 2021; Xu et al., 2014).

To fill the gaps, we investigated the effects of soil microbes (fungi and bacteria in the CLM-Microbe model) on belowground respiratory fluxes using the CLM-Microbe model. The CLM-Microbe model, mechanistically represented soil microbial community dynamics by differentiating fungal and bacterial physiology, provides a feasible way to investigate the effects of soil microbial variation on C cycling (He et al. 2021). In this study, we aimed to investigate the effects of microbial seasonality on soil respiratory fluxes and annual estimation of soil respiratory fluxes and soil organic C (SOC) pool size in natural biomes. We first evaluated the performance of the CLM-Microbe model in simulating soil respiratory fluxes in major biomes. Then, we compared the simulated soil respiratory fluxes by the CLM-Microbe model with (CLM-Microbe) and without (CLM-Microbe_wos) soil microbial seasonality. Finally, we compared the annual budgets of soil respiratory fluxes and SOC in the top 1 m soil profile simulated by the CLM-Microbe and CLM-Microbe_wos to quantify the impacts of microbial seasonality on soil respiratory fluxes and soil C storage.

Materials and Methods

Model representation of fungal and bacterial biomass

The CLM-Microbe model was built on the model framework developed by Xu et al. (2014) and the default CLM4.5 (Koven et al. 2013), and it has been coupled with a microbial functional group – based methane module (Xu et al. 2015; Wang et al. 2019) and applied to quantify the fugal and bacterial biomass dynamics in natural ecosystems (He et al. 2021). The CLM4.5 classifies litter into three pools, i.e., litter 1 (labile), litter 2 (cellulose) and litter 3 (lignin), and soil organic matter (SOM), materials left during later stages of organic C decay, into four pools, i.e., SOM 1, SOM 2, SOM 3, and SOM 4. The three litter pools and four SOM pools differ in base decomposition rate (τ), with turnover time of litter pools ranging from 20 hours to 71 days and turnover time of SOM pools ranging from 14 days to 27 years (Fig. 3.S1). Coarse woody debris (CWD) is fragmented, decomposed, and gradually transferred into litter pools, and further from litter to SOM pools (Thornton et al. 2007; Koven et al. 2013). In addition to the eight soil C pools (three litter, four SOM, and CWD pools) in the CLM4.5, we introduced dissolved organic matter (DOM) and fungal and bacterial biomass pools in the CLM-Microbe model. The code for the CLM-Microbe model has been archived at https://github.com/email-clm/clm-microbe since 2015. The model version used in this study was checked out on June 18, 2018.

In the CLM-Microbe model, fungal and bacterial biomass are the balance of C input from the decomposition of SOM, DOM, and litter and C loss through the microbial lysis and microbial respiration. Specifically, fungi and bacteria receive C through the transitions from litter, DOM, and SOM pools; fungi and bacteria lose C through the transitions from fungal and bacterial biomass pools to DOM and SOM pools and the atmosphere.

The decompositions of SOM, DOM, and litter are controlled by both their potential decomposition rates and environmental conditions. The decomposition processes in the CLM-Microbe model are defined following the below equations,

$$D_C = k \times r_{depth} \times r_{tsoil} \times r_{water} \times r_{O_2} \quad \text{equation (1)}$$

$$r_{depth} = \exp\left(-\frac{z}{z_\tau}\right) \quad \text{equation (2)}$$

$$r_{tsoil} = Q_{10}^{\frac{T_{soil,j} - T_{ref}}{10}} \quad \text{equation (3)}$$

$$r_{water} = \begin{cases} 0 & for\ \varphi_j < \varphi_{min} \\ \frac{log\left(\varphi_{min}/\varphi_j\right)}{log\left(\varphi_{min}/\varphi_{max}\right)} & for\ \varphi_{min} \leq \varphi_j \leq \varphi_{max} \\ 1 & for\ \varphi_j > \varphi_{max} \end{cases} \quad \text{equation (4)}$$

$$r_{O_2} = f_r \times (1 - f_{inun}) \times max\left(O_{2_{unsat}}, O_{2_{min}}\right) + f_{inun} \times max\left(O_{2_{sat}}, O_{2_{min}}\right) \quad \text{equation (5)}$$

where D_C is the rate of substrate (e.g., SOM, DOM, and litter) breakdown; k is the potential decomposition rate; r_{O_2} represents the environmental modifier determined by soil oxygen concentration; r_{depth} is the environmental modifier determined by soil depth; r_{water} is environmental modifier determined by soil moisture; r_{tsoil} means the environmental modifier determined by soil temperature; z means soil depth; z_τ is the e-folding depth for decomposition; $T_{soil,j}$ is soil temperature at layer j; T_{ref} is the reference temperature for decomposition, which is set as 25°C; Q_{10} indicates the temperature dependence of decomposition, it is the ratio of the rate at a specific temperature to that at 10°C lower; Ψ_j is the soil water potential in layer j; Ψ_{min} is a lower limit for soil water potential control on decomposition rate (set to -10 MPa), r_{water} will be set as 0 if Ψ_j is lower than Ψ_{min}; Ψ_{max} is the upper limit for soil water potential control on decomposition, which equals to the saturated soil matric potential, r_{water} will be set as 1 if Ψ_j is higher than Ψ_{max}; $w_{soil,j}$ means soil water content in layer j; f_r is the rooting fraction by soil depth; f_{inun} means the fraction of inundated area; $O_{2_{unsat}}$ represents the oxygen available to that demanded by roots and aerobic microbes in unsaturated area; $O_{2_{min}}$ denotes the ratio between minimum anaerobic decomposition rate

and potential aerobic decomposition rate in soil (set to 0.2); $O_{2_{sat}}$ represents the oxygen available to that demanded by roots and aerobic microbes in saturated area; r_{O_2} will be set as 1 in oxic conditions, while it will be estimated as the weighted average of oxygen stress in saturated and unsaturated areas in anoxic conditions.

Bacterial and fungal growth are highly sensitive to environmental conditions, such as soil moisture and temperature. Fungi and bacteria are different in turnover time, different lysis rate constants were therefore adopted for fungi and bacteria in the CLM-Microbe model (He et al., 2021). As a result, in the CLM-Microbe model, the fungal and bacterial biomass lysis is mechanistically represented as the interactive effects of their lysis rate constants and environmental factors, i.e., r_{O_2}, r_{water}, r_{tsoil}, and r_{depth}, as described above. Microbial respiration is widely affected by multiple abiotic and biotic factors, such as substrate concentration and availability, soil moisture, and soil temperature (Gomez-Casanovas et al. 2012; Zhang et al. 2013). Therefore, in the CLM-Microbe model, fungal and bacterial respiration is represented as the interactive effects of substrate (i.e., DOM, SOM, and litter), environmental factors (i.e., r_{O_2}, r_{water}, and r_{tsoil}), and fraction factors quantifying C being respired by fungi and bacteria in transitions (Table 3.S1).

Data source

In this study, we evaluated the performance of the CLM-Microbe model in nine natural biomes, including tropical/subtropical forest, temperate coniferous forest, temperate broadleaf forest, boreal forest, shrubland, grassland, desert, tundra, and wetland. To compile the data to test the CLM-Microbe model in simulating soil respiratory fluxes, we searched peer-reviewed literatures for observational data. To investigate the contribution of soil microbes to respiratory fluxes, we selected sites that reported MR independently from other respiration components, i.e., separating MR either from SR or ecosystem respiration (ER). Due to the distinct seasonal and diurnal cycles of those respiratory fluxes, the exact

sampling time, at least the exact sampling day, needs to be clearly reported in selected sites. Given the large spatial variation in respiratory fluxes due to the heterogeneity in vegetation, abiotic factors, and the legacy effect by disturbance, we selected data from at least two sites to represent each biome.

Multiple approaches have been used to separate MR from SR or ER, and each method has its advantages and disadvantages (Hanson et al. 2000). To minimize the bias resulting from data collection methods, same method is preferred when compiling dataset for model testing. Among multiple approaches, trenching was the most widely used one for the soil profile and ecosystem-scale experiments focusing on the contribution of MR to SR (Table 3.1). Due to the similarity in methodology, trenching, root removal, and gap analysis are generally classified as root exclusion in distinguishing MR versus RR (Hanson et al. 2000). Finally, 19 studies that separated MR from soil respiratory fluxes using root exclusion (i.e., trenching, comparison, and extraction) were included in this study. Site information, including geographic location, country, biome type, site name, site ID, sampling years, measurement method, and sampling time, was summarized in Table 3.1.

Model forcing data

The forcing data for the CLM-Microbe model include meteorological variables such as air temperature, relative humidity, incoming solar radiation, longwave radiation, precipitation rate, surface pressure, and surface winds. Considering the availability of those variables from eddy covariance (EC) tower measurements and a wide array of global datasets, we searched the forcing data from multiple sources to fulfil the data needs with the emphasis on observational data for sites in diverse biomes (Table 3.1).

We first searched the FLUXNET database (https://fluxnet.org) for the site information (844 sites) to identify the closest EC station for each site presented in Table 3.1. We calculated the geographical distances between those site pairs, i.e., each selected site in Table 3.1 and its corresponding closest EC station. Site pairs with geographical distance exceeding 1 degree were excluded for further consideration. Then, we compared the plant functional type documented in the FLUXNET database and the reported vegetation type for each site. Site pairs with different vegetation types were excluded. Although a large number of EC sites are registered on FLUXNET, only a small number of sites made the data available. To generate reliable output, the length of forcing data is required to be longer than the observed soil respiratory flux and the two datasets need to be consistent in their sampling years. Therefore, we excluded site pairs without available EC data or when measurement periods were inconsistent with the FLUXNET2015 Dataset (Pastorello et al. 2020). Since data gaps are common in EC tower measurements, time periods with large gaps (more than 2 months of consecutive missing data) were not considered to drive the model. For relatively small gaps (less than 2 months of consecutive missing data), we filled the gaps by applying a 30-day running mean diurnal cycle forwards and backwards through the yearly time series. After filtering the criteria described above, the forcing data from CA-Obs (1997-2010), DE-Hai (2000-2012), and US-Prr (2011-2014) from FLUXNET2015 Dataset were selected to force the model run for sites of BRF-CA (a boreal forest site), TBF-GM (a temperate broadleaf forest site), and BRF-US (a boreal forest site), respectively, in Table 3.1. Since the EC tower height was not provided in the FLUXNET site information database, we found the instrument measurement height for CA-Obs from site location summary provided by Oak Ridge National Laboratory (https://www.ornl.gov), and we retrieved the EC tower instrument measurement height for DE-Hai and US-Prr from previous studies (Rebmann et al. 2005; Nakai et al. 2013).

For other sites without available meteorological data from the FLUXNET2015 Dataset (Pastorello et al. 2020), we chose the CRUNCEP Version 7 - Atmospheric Forcing Data for the Community Land Model,

considering the sampling year spanning from 1999 to 2015. The CRUNCEP Version 7 dataset was produced by Research Data Archive at the National Center for Atmospheric Research, Computational and Information Systems Laboratory (https://rda.ucar.edu/datasets/ds314.3/), which has been widely used to force the community land model. Finally, we extracted the forcing data during 1 January 1981 through 31 December 2016 from CRUNCEP Version 7 dataset using the latitude and longitude information of each study site (Table 3.1). Since the standard model forcing data are in half-hourly time steps, the extracted 6-hourly data for each study site were interpolated to half-hourly step using linear interpolation via na.approx function in R (R for Mac OS X version 3.5.3).

Model implementation

The model implementation was carried out in three stages. First, we ran the accelerated decomposition spin-up to allow the system to reach its steady state (Thornton and Rosenbloom 2005; Koven et al. 2013). Due to the differences in the length of time to reach steady state among biomes, we set the model simulations as 1500 years for tropical and temperate biomes (i.e., tropical/subtropical forest, temperate coniferous forest, temperate broadleaf forest, shrubland, grassland, and desert), 2000 years for boreal and Arctic biomes (i.e., boreal forest and tundra), and 3000 years for wetlands. Then, we ran a final spin-up of 100 years to ensure the system was ready for transient simulations during 1850 - 2016. Since the observational respiratory fluxes from most sites were reported at hourly intervals, we set the output resolution of transient simulations at an hourly time step. The initial setting for microbial parameters was adopted from He et al. (2021), with the parameter set same for sites from the same biome but distinct among biomes.

To produce realistic soil and vegetation conditions in the CLM-Microbe model for each site, we extracted the SOC of the top 1 m soil profile from the Harmonized World Soil Database (HWSD,

https://daac.ornl.gov/cgi-bin/dsviewer.pl?ds_id=1247) and gross primary productivity (GPP) and net primary productivity (NPP) from the MODIS gridded dataset with a spatial resolution of 30 seconds during 2000-2015 (http://files.ntsg.umt.edu/data/NTSG_Products/). For sites with GPP available from EC measurements, i.e., BRF-CA and BRF-US (boreal forest sites), TBF-GM and TBF-JP (temperate coniferous forest sites), TCF-US (a temperate coniferous forest site), and TSF-CN (a tropical/subtropical forest site), we optimized the model parameters to match with the GPP from EC measurements (Saigusa et al. 2005, Pastorello et al. 2020). We estimated NPP by multiplying the NPP/GPP ratio from the MODIS gridded dataset and GPP derived from the EC measurements, and then optimized parameters to match the estimated NPP of each site. Furthermore, we calibrated the model to match the SOC within the 1 m soil profile reported by the HWSD database. If the extracted SOC from the HWSD dataset and NPP from the MODIS dataset were 100% higher or 50% lower than the corresponding biome averages reported in Jobbágy and Jackson (2000) and Chapin et al. (2011), respectively, we calibrated model to match the recorded SOC and NPP in their source articles. If the SOC and NPP were not available from literature, we used the reported biome average instead (Jobbágy and Jackson 2000; Chapin et al. 2011).

For tropical/subtropical forests, we had a site specified as needleleaf trees, whereas tropical needleleaf tree is not a default plant function type. Therefore, we adjusted the parameters for tropical trees (e.g., minimum and upper limit of temperature for growth) to represent needleleaf_evergreen_temperate_tree. Also, we altered the longevity for needleleaf_evergreen_temperate_tree following the trend of needle tree leaf longevity reported by Xiao (2003).

The SR and RR may exhibit different seasonal patterns. We therefore calibrate both MR and RR to reproduce the seasonal variation of SR. To calibrate the model to fit the observed MR, RR, and SR, we adjusted soil microbial parameters related to microbial turnover (*k_fungi* and *k_bacteria*), microbial C

assimilation efficiency (*m_rf_s1m*, *m_rf_s2m*, *m_rf_s3m*, and *m_rf_s4m*), and the proportion of C being released as respiration (*m_batm_f* and *m_fatm_f*), decomposition temperature sensitivity (Q_{10}) of SOM, litter, and DOM decomposition, and C allocation (e.g., *froot_leaf*) to optimize the model simulations of soil respiratory fluxes. Our previous studies (Xu et al. 2014; He et al. 2020) showed a large variation in soil microbial community among biomes, we therefore performed biome-specific parameterization for microbial processes. Final adjusted soil microbial parameters for nine natural biomes were compiled and displayed in Table 3.S2.

Taken together, we optimized the model parameters based on soil and vegetation conditions reported by HWSD, MODIS, and EC measurements and soil respiratory fluxes from peer-reviewed publications. We primarily focused on the parameters related to plant photosynthesis (e.g., *flnr*), maintenance respiration (*br_mr*), C allocation (e.g., *froot_leaf*), e-folding depth for decomposition (e.g., *decomp_depth_efolding*), microbial parameters (e.g., *k_fungi*, *k_bacteria*, *m_rf_s1m*, *m_rf_s2m*, *m_rf_s3m*, *m_rf_s4m*, *m_batm_f*, *m_fatm_f*), and Q_{10} values of SOM, litter, and DOM decomposition to fit the observed data.

Removal of soil microbial seasonality

To investigate the effects of soil microbial biomass dynamics on respiratory fluxes, we set up the model simulation without soil microbial biomass dynamics (CLM-Microbe_wos). Soil temperature and moisture play an important role in regulating soil microbial growth and activity (Curiel Yuste et al. 2007, Bell et al. 2008), which represents the seasonal controls on microbial activities (He et al., 2021). In the CLM-Microbe model, top 10 soil layers are active for soil microbial and hydrological processes, extending to a depth of 3.8 m. In the CLM-Microbe_wos, we removed soil microbial biomass seasonal dynamics by setting soil temperature and water scalars to their annual averages for each layer in the biogeochemistry cascade. The temperature and water scalar constants at each site were calculated as the arithmetical mean

of temperature and water scalars during corresponding sampling period of soil respiratory fluxes by top 10 soil layers. Consequently, in the CLM-Microbe_wos, soil microbial community impacts biogeochemical processes in a soil environment without variations in temperature and moisture.

Model evaluation

To evaluate the model performance in capturing the seasonality in soil C fluxes, we compared the observed soil C fluxes with the simulated fluxes during corresponding sampling time period for each site (Table 3.1). For sites with exact sampling time reported, we did the comparison between the observed soil respiratory fluxes and the simulated values of the same sampling time. For sites with unspecified sampling time, we compared the simulations during 20:00-8:00 with measurements during nighttime and simulations during 8:00-20:00 with measurements during daytime or three times a day (morning, 10:30-12:30, and afternoon) for each respiratory flux. For sites with observed data indicated as daily average or no sampling time reported, we compared hourly averages of model outputs with the observed data in a given sampling day.

Then, we used three metrics to evaluate the model performance, including:

1. Mean absolute error (MAE), a measure of model error, was computed as

$$MAE = \frac{1}{N}\sum_{i=1}^{N}|y_i - \hat{y}_i| \qquad \text{equation (6)}$$

where y_i is the observed value; $\hat{y}_i$ means the simulated value; *N* is the number of data points. The MAE indicates the mean error of the model simulation, and thus lower MAE values are preferred.

2. Root mean square error (RMSE), indicating the model accuracy, was calculated as:

$$RMSE = \sqrt{\frac{1}{N}\sum_{i=1}^{N}(y_i - \hat{y}_i)^2} \quad \text{equation (7)}$$

where y_i is the observed value; $\hat{y}_i$ means the simulated value; *N* is the number of data points. Similar with MAE, RMSE also indicates the mean error of the model simulation, with low values indicating high model accuracy. The RMSE estimation is equal to or larger than MAE estimation in most cases, and the degree to which RMSE estimation exceeds MAE estimation depend on the outliers in the simulated and observed data.

3. The coefficient of determination (R^2), representing the variation in the observations explained by the model, was calculated following the equation as below,

$$R^2 = 1 - \frac{\sum_{i=1}^{N}(y_i - \hat{y}_i)^2}{\sum_{i=1}^{N}(y_i - \bar{y})^2} \quad \text{equation (8)}$$

where y_i is the observed value; $\hat{y}$ means the simulated value; $\bar{y}$ is the mean of the observed value; *N* is the number of data points. Higher R^2 values indicate better performance of the model, while lower R^2 values mean the worse model performance and smaller proportion of variation being explained by the model. It is noteworthy that R^2 is not suitable for assessing the goodness-of-fit for dataset with a small sample size.

Comparison between two model outputs

To test the impacts of soil microbial biomass seasonality on annual estimation of soil respiratory fluxes and SOC pool size, we calculated the arithmetic mean and 95% confidence interval of simulated MR, SR, and SOC in the top 1 m soil during 2000-2009. In addition, we used two-tailed paired *t*-tests to examine the statistical differences in average values of MR, SR, and SOC between the CLM-Microbe and CLM-Microbe_wos. These tests were applied to nine natural biomes. We therefore separately analyzed ten paired annual output of MR, SR, and SOC of top 1 m soil between the CLM-Microbe and CLM-

Microbe_wos for each biome. The statistical analyses of two-tailed paired *t*-tests were performed using the t.test function in R (R for Mac OS X version 3.5.3) at a significance level of 0.05.

Results

Model simulations of soil respiratory fluxes

The CLM-Microbe model was able to reconstruct the observed MR well (Fig. 3.1; Table 3.2). The reported R^2 values were larger than 0.40 for most sites; in particular, the comparisons produced R^2 values of 0.63 at BRF-CA (boreal forest, BRF-), 0.76 at DST-XJ (desert, DST-), 0.85 at TBT-JP (temperate broadleaf forest, TBF-), and 0.91 at TUN-RU (tundra, TUN-). However, we also observed small R^2 values at some sites. For example, the R^2 values at BRF-SW, DST-NX, GRS-HU (grassland, GRS-), TBF-GM, and WET-SJ (wetland, WET-) were smaller than 0.20. The MAE and RMSE values for MR were distinct among sites, with MAE and RMSE varying within a range of 27- and 23-fold, respectively. Similar with the R^2 values, the MAE and RMSE values for MR were smaller than 0.8 and 1.0 μmol m^{-2} s^{-1}, respectively, at most sites. However, we found relatively large MAE and RMSE values at BRF-SW, TSF-TH (tropical/subtropical forest, TSF-), WET-PY, WET-SJ, and GRS-HU.

The CLM-Microbe-simulated RR agreed well with the observed data (Fig. 3.2; Table 3.2). The R^2 values for RR were larger than 0.40 at the majority of sites; the comparisons produced R^2 values of 0.80 at BRF-CA, 0.76 at BRF-SW, 0.61 at SHB-MX (shrubland, SHB-), and 0.63 at TBT-JP, but we also observed small R^2 values at sites such as DST-NX. Both MAE and RMSE values for RR showed 11-fold variation among sites, with MAE and RMSE values for RR of most sites smaller than 0.8 and 1.0 μmol m^{-2} s^{-1}, respectively. However, we found relatively large MAE and RMSE values at WET-SJ and GRS-HU.

The CLM-Microbe model produced consistent results of SR (Fig. 3.3; Table 3.2). The R^2 values for SR were higher than 0.40 at most sites. In particular, the comparisons produced R^2 values of 0.84 at BRF-CA, 0.79 at SHB-NE, 0.85 at TBF-JP, 0.71 at TSF-CN, and 0.69 at WET-PY. However, we also observed small R^2 values at some sites such as DST-NX. The MAE and RMSE values for SR showed large variations among sites, with MAE and RMSE exhibiting 10- and 7-fold variation, respectively. Similar with the R^2 values, MAE and RMSE values for SR at most sites were smaller than 1.0 and 1.3 μmol m^{-2} s^{-1}, respectively. However, some relatively large MAE and RMSE values were found at BRF-SW, GRS-HU, GRS-US, TCF-SP (temperate coniferous forest, TCF-), TCF-US, and WET-SJ.

Taken together, the CLM-Microbe model produced MR, RR, and SR that were consistent with the observed data on average across sites (Fig. 3.4). Specifically, across-site comparisons returned R^2 values of 0.72 (n=19, P<0.0001), 0.65 (n=19, P<0.0001), and 0.71 (n=18, P<0.0001) for the linear regression models between simulated and observed means of MR, RR, and SR, respectively.

Microbial seasonality on soil respiratory fluxes

Microbial seasonality yielded impacts on soil respiratory fluxes in different magnitudes, depending on biomes and variables (Figs. 3.5 and 3.6; Table 3.S4). Among soil respiratory fluxes, MR was strongly influenced by the removal of soil microbial biomass seasonality, and the reduction of MR seasonal variation was widely observed across sites (Fig. 3.5a; Table 3.S4). Statistically, the removal of soil microbial biomass seasonality generally decreased MR across sites, with the annual range and standard deviation of MR reduced by 72.0%-99.6% and 65.5%-99.6%, respectively, across sites (Table 3.S4). In addition, the removal of soil microbial seasonality generally increased MAE and RMSE values while slightly decreased RMSE for MR at TSF-CN. The R^2 values for MR decreased for all sites (Fig. 3.6). Large variations existed in the magnitude of alterations with respect to MAE, RMSE, and R^2 values. For

example, the increases in MAE and RMSE values for MR exceeded 100% at TBF-JP and TUN-RU, while MAE and RMSE at SHB-NE and TSF-CN changed less than 15%. Similarly, the response of R^2 values to the removal of soil microbial biomass seasonality for MR varied across sites, with R^2 of GRS-US, SHB-NE, and TSF-CN decreased by >90% and that of DST-XJ decreased less than 6%.

Compared with MR, the response of RR to the removal of soil microbial biomass seasonality was much weaker, with MAE, RMSE, and R^2 values slightly changed across biomes (Figs. 3.5 and 3.6; Table 3.S4). Despite the weak response of RR to the removal of soil microbial biomass seasonality, MAE, RMSE, and R^2 values varied in direction and magnitude across biomes. The removal of soil microbial biomass seasonality increased MAE and RMSE for RR at GRS-US (+6% for MAE and +4% for RMSE) and BRF-CA (+23% for MAE and +24% for RMSE) and decreased MAE and RMSE for RR at SHB-NE (-15% for MAE and -13% for RMSE), TCF-US (-1% for MAE and -3% for RMSE), and TSF-CN (-3% for MAE and -3% for RMSE). The MAE and RMSE values for RR at DST-XJ, TBF-JP, and WET-PY changed less than 1% with the removal of soil microbial biomass seasonality. The R^2 values generally showed little change for RR without soil microbial biomass seasonality across sites except the TSF-CN, with R^2 values changed less than 2%.

The response of SR to the removal of soil microbial biomass seasonality was different across biomes with respect to MAE, RMSE, and R^2 values (Figs. 3.5 and 3.6; Table 3.S4). Similar with MR, the removal of soil microbial biomass seasonality decreased variations in SR, with the range and the standard deviation reduced by 24%-71% and 33-69%, respectively, across sites (Fig. 3.5; Table 3.S4). Removing soil microbial biomass seasonality increased MAE and RMSE values for SR at most sites, with the most pronounced increase in MAE and RMSE values at BRF-CA (+64% for MAE and +79% for RMSE). However, we also observed decreases in MAE and RMSE values for SR at SHB-NE (-16% for MAE and

-13% for RMSE) and TSF-CN (-46% for MAE and -43% for RMSE). Compared with the bias indicated by MAE and RMSE values, removing soil microbial biomass seasonality had smaller influences on R^2 values, with most R^2 values changed less than 12% despite in different directions. For example, the R^2 value for SR at TBF-JP decreased by 11%, while that at WET-PY increased by 9%. We also observed relatively large changes in R^2 values at some sites, with R^2 values of GRS-US and SHB-NE decreased by 25% and 24%, respectively.

Annual budgets of soil carbon storage and respiratory fluxes

Overall, removing soil microbial biomass seasonality largely decreased MR and SR across biomes but in different magnitudes (Table 3.3). The MR significantly decreased at boreal forest, grassland, shrubland, tropical/subtropical forest, temperate forest, and tundra sites in the absence of soil microbial biomass seasonality (P<0.05), with MR decreased by >30% at BRF-CA, >15% at GRS-US, TSF-CN, and TUN-RU, >10% at SHB-NE, and relatively small at TBF-JP (4%), and TCF-US (5%). The MR decreased the least at wetland and desert site, with MR decreased by <1% at WET-PY (P=0.11) and DST-XJ (P=0.19). Similarly, SR significantly decreased at boreal forest, grassland, shrubland, tropical/subtropical forest, temperate forest, and tundra sites (P<0.05). The SR decreased most at boreal forest and tundra sites when removing soil microbial biomass seasonality, with SR decreased by >15% at BRF-CA and TUN-RU, followed by GRS-US (14%), TSF-CN (11%), and SHB-NE (9%). The SR has a relatively small decrease in temperate forests, with SR decreased by 3% at TBF-JP and 4% at TCF-US. Wetland and desert sites exhibited the least response to the removal of soil microbial biomass seasonality, with SR decreased by 0.5% at WET-PY (P=0.09) and DST-XJ (P=0.19).

In contrast, we observed a general increase of SOC within the top 1 m soil profile, ranging from 0.2% to 7.4% (Table 3.3). The increase of SOC in the top 1 m soil profile varied across sites, with the most

pronounced increase at DST-XJ (7.4%) and WET-PY (6.8%), followed by TBF-JP (5.3%), GRS-US (3.1%), and TCF-US (1.0%). The least increase was found at SHB-NE (0.6%) and TSF-CN (0.2%). We also observed a decreased SOC in response to the removal of soil microbial seasonality. Specifically, compared with the CLM-Microbe, the CLM-Microbe_wos simulated a decrease of 1.6% at BRF-CA and <1% at TUN-RU for SOC in the top 1 m soil.

Discussion

Model performance

The CLM-Microbe model produced consistent results with the observed soil respiratory fluxes in natural ecosystems (Figs. 3.1 and 3.4; Table 3.2), as a result of the explicit representation of soil microbial processes in the model (Wang et al. 2013a; Wieder et al. 2014; Wang et al. 2017). However, we also observed a relatively poor model performance at some sites, such as MR at BRF-SW and WET-SJ and MR, RR, and SR at DST-NX (Figs. 3.1 and 3.3, Table 3.2). A few reasons may be responsible for the relatively poor performance of the CLM-Microbe model at those sites. First, the small sample size contributes to the small R^2 values observed at those sites. The R^2 is not suitable for assessing the goodness-of-fit for a small amount of data due to the large bias in small samples (Wang et al. 2015a). For example, compared with GRS-HU, we observed smaller MAE and RMSE values as well as smaller R^2 values in BRF-SW and WET-SJ. Second, the large variation in high-frequency sampling of soil C fluxes is another important factor. Although the effects of soil temperature, moisture, and vegetation DOM input have been mechanistically represented in the model, factors such as the displacement of carbon dioxide (CO_2) accumulated in soil pores with infiltrated water during a rainfall and priming effects by plant labile C input that may induce large fluctuation of CO_2 fluxes are not considered in the CLM-Microbe model (Huxman et al. 2004; Blagodatsky et al. 2010; He et al. 2021). For example, rainfall is an important factor affecting soil C fluxes not only by biologically altering soil microbial processes, but also physically

changing the porous proportion occupied by CO_2 (Huxman et al. 2004). Following a rainfall event, observations often reveal an abrupt increase in SR, which is not expected to be captured by the CLM-Microbe model.

Microbial seasonality and soil respiratory fluxes

The removal of soil moisture and temperature variation largely reduced the seasonality of fungal and bacterial biomass (Fig. 3.S2), indicating that the soil moisture and temperature had profound influence on fungal and bacterial biomass dynamics. A constant soil moisture and temperature condition is expected to weaken soil microbial community variation (Sharon 1972; Tang and Baldocchi 2005; Wang et al. 2013b). In addition, the removal of soil moisture and temperature variation largely reduced the biomass C pool sizes of fungi and bacteria (Fig. 3.S2). Similar with our findings, Salamanca et al. (1998) compared the litter decomposition between field and greenhouse microcosm implementations. They found significantly slower litter decomposition in the greenhouse than in field conditions, indicating higher soil microbial activity in field conditions. Microbial processes are strongly mediated by the intervening microclimate, and fluctuations in soil temperature and moisture were shown to increase microbial activity compared to those observed under constant conditions with the same mean values (Soulides and Allison 1961). In the CLM-Microbe model, fungal and bacterial biomass is directly controlled by the net balance between C gain through DOM uptake and the decomposition of litter and SOM and C loss through microbial lysis and microbial respiration (He et al. 2021). Despite the slight decrease in fungal and bacterial lysis with the removal of soil moisture and temperature seasonal variation, the decrease in C gain from the decomposition of litter and SOM, accompanied by the decreased uptake of DOM by fungi and bacteria can explain the decrease in fungal (FBC) and bacterial biomass C (BBC) (Figs. 3.S3-4).

The removal of soil microbial biomass seasonality generally reduced MR and SR, but had little influence on RR across sites (Figs. 3.5 and 3.6; Table 3.S4). The MR is significantly positively correlated with soil microbial biomass (Colman and Schimel 2013; Wei et al. 2019). The reduction in FBC and BBC is one of the key reasons responsible for the decrease in MR (Fig. 3.S2; Table 3.S4). The response of MR and SR to the removal of fungal and bacterial biomass seasonality varied among biomes, with large decreases in MR (10-32%) and SR (9-29%) in boreal forests, deserts, grasslands, tropical/subtropical forests, tundra, and grassland, while HR (0.4-5.7%) and SR (0.3-5.8%) slightly decreased at shrublands, temperate broadleaf forests, temperate coniferous forest, desert, and wetland sites (Table 3.S4). Soil microbial community composition has important impacts on soil C emissions (Cleveland et al. 2007; Monson et al. 2006; Whitaker et al. 2014). The shifts of soil microbial composition (i.e., F:B ratio) in response to the removal of soil microbial biomass seasonality may explain the different responses of MR and SR among sites. We observed decreases in F:B ratio in temperate broadleaf forests, temperate coniferous forests, deserts, shrubland, tundra, and wetlands compared with other biomes (Fig. 3.S2c). Fungi and bacteria are different in physiological traits. Fungi tend to have higher C use efficiency (CUE) than bacteria (Strickland and Rousk 2010). The increasing dominance of bacteria in temperate broadleaf forests, temperate coniferous forests, deserts, shrublands, and wetlands can explain the smaller decrease in MR and SR, despite the decrease in fungal and bacterial biomass with the removal of soil microbial biomass seasonality.

Annual budgets of MR, RR, and soil organic carbon storage

The removal of soil microbial seasonality generally caused the decline in annual estimation of MR and SR, and thus higher soil C storage (Table 3.3). Consistent with our findings, previous studies reported significant positive relationships between soil microbial biomass and MR or SOC decomposition rate (Colman and Schimel 2013; Wei et al. 2019). Soil microbial activity is controlled by a combination of multiple factors; substrate quality, temperatures, and water availability are reported to be critical controls

for soil microbial metabolism (Curiel Yuste et al. 2007; Zhou et al. 2007; Baumann et al. 2013; Xu et al., 2017). In the CLM-Microbe model, the decomposition of litter, DOM, and SOM are regulated by fungal and bacterial biomass, which are interactively affected by soil moisture, temperature, oxygen concentration, and the pool sizes of litter, DOM, and SOM (He et al. 2021). Removing soil microbial biomass seasonality decreased fungal and bacterial biomass C pool sizes (Fig. 3.S2), which subsequently reduced enzyme production (Nannipieri et al. 1983). Decreases in soil fungal and bacterial biomass led to declining decomposition (Figs. 3.S3-4), and thus lowered CO_2 emissions.

In contrast to the evident decline (>11%) in annual estimation of MR in most biomes, we found weak responses (<5%) in wetlands, deserts, temperate broadleaf forests, and temperate coniferous forests in annual estimation of MR with the removal of soil microbial biomass seasonality (Table 3.3). Concurrently, we observed a reduction in F:B ratios at those sites, indicating different fungal and bacterial responses to the removal of soil moisture and temperature seasonal variation (Fig. 3.S2c). Therefore, the removal of soil moisture and temperature seasonality influences the F:B ratio, while soil microbial activity and function are closely related to the soil microbial community composition (Bell et al. 2009). Fungi and bacteria have distinct physiological traits. Fungal-dominated soils tend to have higher CUE than bacterial-dominated ones (Strickland and Rousk 2010), which is believed to result from the tradeoff between growth rate and yield (Lipson 2015). The difference in CUE between fungi and bacteria has been incorporated in the CLM-Microbe model (He et al. 2021). Therefore, the increasing dominance of bacteria in soil microbial community can be responsible for the smaller decrease in MR in wetlands, temperate broadleaf forests, and temperate coniferous forests with the removal of soil microbial biomass seasonality. Similarly, we observed the overall large decrease (>9%) of SR across biomes, but weak response (<5%) in wetlands, deserts, temperate coniferous forests, and temperate broadleaf forests with respect to annual estimation of SR with the removal of soil microbial biomass seasonality (Table 3.3). As an important component of SR, MR largely dominated the response pattern of SR in response to the

removal of soil microbial biomass seasonality (Bond-Lamberty et al. 2004; Tang and Baldocchi 2005). Consequently, similar with MR, SR decreased across biomes with the removal of soil microbial biomass seasonality, but the decrease was relatively small in wetlands, deserts, temperate coniferous forests, and temperate broadleaf forests in magnitude compared with other biomes.

We observed an overall increase of SOC with the removal of soil microbial biomass seasonality across biomes. However, we also observed a decrease of SOC at the boreal forest site and neutral changes in SOC at the tundra site with the removal of soil microbial biomass seasonality (Table 3.3). Fungi and bacteria are major agents in SOM decomposition. The decreases in fungal and bacterial biomass can explain the overall increase of SOC (Fig. 3.S2). In addition to biomass, variations in soil microbial diversity and community structure seriously affect SOM turnover and thus affect the function of a given ecosystem (Stroud et al. 2007; Baumann et al. 2013; Wang et al. 2013b). Bacteria are better consumers of simple organic compounds. The increasing dominance of bacteria at tundra sites will facilitate the decomposition of SOM and increase the C and nutrient cycling, leading to a declining SOC pool size (Myers et al. 2001). In addition, the lower CUE of bacteria can also contribute to the decrease in SOC (Lipson 2015). It is expected that fungi produce more biomass C per unit of C metabolized than bacteria. Moreover, the contribution of microbial necromass to SOC pool size is also linked to the relative dominance of fungi and bacteria, with fungal necromass contributed more to the formation of recalcitrant SOM. Therefore, the increasing dominance of bacteria may alleviate C stabilization and dampen the contribution of soil microbes to SOM formation in tundra. In contrast to the increasing dominance of bacteria in tundra, the removal of soil microbial biomass seasonality increased the dominance of fungi in boreal forests (Fig. 3.S2c). Fungi are more advantageous at decomposing low-quality substrate and better adapt to low temperatures (Lipson et al. 2002; Pietikäinen et al. 2005; He et al. 2020), resulting in the increasing dominance of fungi in boreal forests. Surprisingly, the increasing dominance of fungi did not enhance the formation of SOC in boreal forests given the higher CUE and higher contribution of fungi

relative to bacteria in stabilizing SOM. The NPP is the direct determinant of organic C input in a system. Changes in organic C input can result in variations in the amount of organic C stored in soil. When removing soil microbial biomass seasonality, we observed a decrease of NPP by 33% at the boreal forest site (BRF-CA) and by 16% at the tundra site (TUN-RU), indicating that constant soil moisture and temperature conditions suppressed vegetation productivity in boreal-arctic biomes. Therefore, lower organic C input may explain the decrease of SOC in the top 1 m soil in boreal forests, while the decrease of SOC in the top 1 m soil in tundra is due to both increasing dominance of bacteria and decreasing NPP.

Future improvements

Despite the CLM-Microbe model produced comparable results between our simulated soil C fluxes (MR, RR, and SR) and field observations, a few improvements have been identified in future work. First, although the CLM-Microbe model explicitly represents fungi and bacteria that regulate C transfers among different soil C pools, and the vegetation effects on soil microbial community, the missing representation of physical replacement of CO_2 by percolating water in soil pores during precipitation events and priming effects may induce the poor performance of the CLM-Microbe model in capturing CO_2 flux variations with high-sampling frequency (Huxman et al. 2004; Blagodatsky et al. 2010). For example, in arid and semiarid regions, precipitation is a key limiting factor for ecosystem processes such as plant growth and soil microbial activity (Bell et al. 2008). Following a precipitation event, water percolated can biologically stimulate soil microbial activity and physically replace the air in soil pores, leading to the abrupt release of CO_2 and large variations in soil C fluxes (Huxman et al. 2004).

In addition, the missing representation of fungal and bacterial dormancy may have led to the overestimation of respiratory fluxes but underestimation of SOC pool size. Soil microbial activity is primarily controlled by soil moisture and temperature, and soil microbes are active within well-confined

soil temperature and moisture ranges (Pietikäinen et al. 2005; Frindte et al. 2019). In the CLM-Microbe model, soil fungal and bacterial activity are simultaneously affected by soil moisture and temperature scalars, with higher fungal and bacterial activity at more optimal soil temperature and moisture conditions, and vice versa. Nevertheless, no soil moisture and temperature thresholds were defined to classify the dormant state of fungi and bacteria in the model (He et al. 2021). An improvement in representing microbial dormancy in the CLM-Microbe is underway that will likely produce more accurate projection of microbial impacts on C cycling in extreme environments such as deserts and tundra.

Conclusion

Microbes predominately drive the SOC turnover and nutrient cycling in soils, soil microbial seasonal variation thus has profound implications on terrestrial C and nutrient cycling. The CLM-Microbe model produced good performance in capturing the seasonality in soil respiratory fluxes. Removing soil microbial biomass seasonality yielded minor impacts on RR, but significantly increased the simulation bias and reduced the goodness-of-fit in MR and SR. The model simulation without soil microbial seasonality led to lower soil respiratory fluxes across sites, leading to higher SOC pool size except for boreal-arctic sites. These lines of evidence confirmed that microbial seasonality promotes soil C emission. The different roles of bacteria and fungi in regulating C flux suggest the important regulation of soil microbial community on belowground C biogeochemistry. Our findings highlight the importance of explicit representation of microbial mechanisms at the seasonal scale on simulated C cycling in ESMs, which will both improve the simulation performance of soil respiratory fluxes and reduce the uncertainties associated with model projection in the global C cycle under the changing climate.

Acknowledgements

We are grateful to the editor and two anonymous reviewers for their constructive comments that have substantially improved the manuscript. The authors thank Drs. Hayley Peter-Contesse and Kate Lajtha from Oregon State University and Dr. Alejandro Cueva from University of California, Riverside for proving sampling time of respiration fluxes. This study is supported by San Diego State University and the CSU Program for Education & Research in Biotechnology. Partial support for this work was provided by an Early Career Award through the U.S. Department of Energy (DOE) Biological and Environmental Research Program. Oak Ridge National Laboratory is managed by UT-Battelle, LLC, under contract DE-AC05-00OR22725 with the U.S. DOE. The data used for model parameterization and validation are obtained in published literature that have been clearly cited in the Table 3.1 of the manuscript.

References

Balogh, J., M. Papp, K. Pintér, S. Fóti, K. Posta, W. Eugster, and Z. Nagy. 2016. Autotrophic component of soil respiration is repressed by drought more than the heterotrophic one in dry grasslands. *Biogeosciences* **13**:5171-5182.

Barba, J., J. C. Yuste, R. Poyatos, I. A. Janssens, and F. Lloret. 2016. Strong resilience of soil respiration components to drought-induced die-off resulting in forest secondary succession. *Oecologia* **182**:27-41.

Baumann, K., M.-F. Dignac, C. Rumpel, G. Bardoux, A. Sarr, M. Steffens, and P.-A. Maron. 2013. Soil microbial diversity affects soil organic matter decomposition in a silty grassland soil. *Biogeochemistry* **114**:201-212.

Bell, C., N. McIntyre, S. Cox, D. Tissue, and J. Zak. 2008. Soil microbial responses to temporal variations of moisture and temperature in a Chihuahuan Desert grassland. *Microbial Ecology* **56**:153-167.

Bell, C. W., V. Acosta-Martinez, N. E. McIntyre, S. Cox, D. T. Tissue, and J. C. Zak. 2009. Linking microbial community structure and function to seasonal differences in soil moisture and temperature in a Chihuahuan desert grassland. *Microbial Ecology* **58**:827-842.

Bhupinderpal, S., A. Nordgren, M. Ottosson Löfvenius, M. N. Högberg, P. E. Mellander, and P. Högberg. 2003. Tree root and soil heterotrophic respiration as revealed by girdling of boreal Scots pine forest: extending observations beyond the first year. *Plant, Cell & Environment* **26**:1287-1296.

Biasi, C., S. Jokinen, M. E. Marushchak, K. Hämäläinen, T. Trubnikova, M. Oinonen, and P. J. Martikainen. 2014. Microbial respiration in Arctic upland and peat soils as a source of atmospheric carbon dioxide. *Ecosystems* **17**:112-126.

Blagodatsky, S., E. Blagodatskaya, T. Yuyukina, and Y. Kuzyakov. 2010. Model of apparent and real priming effects: linking microbial activity with soil organic matter decomposition. *Soil Biology and Biochemistry* **42**:1275-1283.

Bond-Lamberty, B., and A. Thomson. 2010. Temperature-associated increases in the global soil respiration record. *Nature* **464**:579-582.

Bond-Lamberty, B., C. Wang, and S. T. Gower. 2004. A global relationship between the heterotrophic and autotrophic components of soil respiration? *Global Change Biology* **10**:1756-1766.

Cahoon, S. M. P., P. F. Sullivan, C. Gamm, J. M. Welker, D. Eissenstat, and E. Post. 2016. Limited variation in proportional contributions of auto-and heterotrophic soil respiration, despite large differences in vegetation structure and function in the Low Arctic. *Biogeochemistry* **127**:339-351.

Chapin, F. S., P. A. Matson, and P. Vitousek. 2011. *Principles of terrestrial ecosystem ecology*. Springer Science & Business Media.

Cleveland, C. C., Nemergut, D. R., Schmidt, S. K., and Townsend, A. R. (2007). Increases in soil respiration following labile carbon additions linked to rapid shifts in soil microbial community composition. *Biogeochemistry*, **82**:229-240.

Colman, B. P., and J. P. Schimel. 2013. Drivers of microbial respiration and net N mineralization at the continental scale. *Soil Biology and Biochemistry* **60**:65-76.

Curiel Yuste, J., D. D. Baldocchi, A. Gershenson, A. Goldstein, L. Misson, and S. Wong. 2007. Microbial soil respiration and its dependency on carbon inputs, soil temperature and moisture. *Global Change Biology* **13**:2018-2035.

Frindte, K., R. Pape, K. Werner, J. Löffler, and C. Knief. 2019. Temperature and soil moisture control microbial community composition in an arctic–alpine ecosystem along elevational and micro-topographic gradients. *The ISME Journal* **13**:2031-2043.

Gaumont-Guay, D., T. A. Black, A. G. Barr, R. S. Jassal, and Z. Nesic. 2008. Biophysical controls on rhizospheric and heterotrophic components of soil respiration in a boreal black spruce stand. *Tree Physiology* **28**:161-171.

Gomez-Casanovas, N., R. Matamala, D. R. Cook, and M. A. Gonzalez-Meler. 2012. Net ecosystem exchange modifies the relationship between the autotrophic and heterotrophic components of soil respiration with abiotic factors in prairie grasslands. *Global Change Biology* **18**:2532-2545.

Hanson, P. J., N. T. Edwards, C. T. Garten, and J. A. Andrews. 2000. Separating root and soil microbial contributions to soil respiration: a review of methods and observations. *Biogeochemistry* **48**:115-146.

He, L., D. A. Lipson, J. L. M. Rodrigues, M. Mayes, R. G. Björk, B. Glaser, P. Thornton, and X. Xu. 2021. Dynamics of Fungal and Bacterial Biomass Carbon in Natural Ecosystems: Site-level Applications of the CLM-Microbe Model. *Journal of Advances in Modeling Earth Systems*. DOI: 10.1029/2020MS002283.

He, L., J. L. M. Rodrigues, N. A. Soudzilovskaia, M. Barceló, P. A. Olsson, C. Song, L. Tedersoo, F. Yuan, F. Yuan, D. A. Lipson, and X. Xu. 2020. Global biogeography of fungal and bacterial biomass carbon in topsoil. *Soil Biology and Biochemistry*: 151, 108024 DOI: 10.1016/j.soilbio.2020.108024.

Hu, Q., Q. Wu, B. Yao, and X. Xu. 2015. Ecosystem respiration and its components from a Carex meadow of Poyang Lake during the drawdown period. *Atmospheric Environment* **100**:124-132.

Huang, G., Y. Li, and Y. G. Su. 2015. Effects of increasing precipitation on soil microbial community composition and soil respiration in a temperate desert, Northwestern China. *Soil Biology and Biochemistry* **83**:52-56.

Huxman, T. E., K. A. Snyder, D. Tissue, A. J. Leffler, K. Ogle, W. T. Pockman, D. R. Sandquist, D. L. Potts, and S. Schwinning. 2004. Precipitation pulses and carbon fluxes in semiarid and arid ecosystems. *Oecologia* **141**:254-268.

Irvine, J., B. E. Law, J. G. Martin, and D. Vickers. 2008. Interannual variation in soil CO2 efflux and the response of root respiration to climate and canopy gas exchange in mature ponderosa pine. *Global Change Biology* **14**:2848-2859.

Jobbágy, E. G., and R. B. Jackson. 2000. The vertical distribution of soil organic carbon and its relation to climate and vegetation. *Ecological Applications* **10**:423-436.

Kopittke, G. R., A. Tietema, E. E. van Loon, and D. Asscheman. 2014. Fourteen annually repeated droughts suppressed autotrophic soil respiration and resulted in an ecosystem change. *Ecosystems* **17**:242-257.

Koven, C. D., W. J. Riley, Z. M. Subin, J. Y. Tang, M. S. Torn, W. D. Collins, G. B. Bonan, D. M. Lawrence, and S. C. Swenson. 2013. The effect of vertically resolved soil biogeochemistry and alternate soil C and N models on C dynamics of CLM4. *Biogeosciences* **10**:7109.

Kutsch, W. L., T. Persson, M. Schrumpf, F. E. Moyano, M. Mund, S. Andersson, and E.-D. Schulze. 2010. Heterotrophic soil respiration and soil carbon dynamics in the deciduous Hainich forest obtained by three approaches. *Biogeochemistry* **100**:167-183.

Li, Y., C. Hou, C. Song, and Y. Guo. 2016. Seasonal changes in the contribution of root respiration to total soil respiration in a freshwater marsh in Sanjiang Plain, Northeast China. *Environmental Earth Sciences* **75**:848.

Lipson, D. A. 2015. The complex relationship between microbial growth rate and yield and its implications for ecosystem processes. *Frontiers in Microbiology* **6**:615.

Lipson, D. A., C. W. Schadt, and S. K. Schmidt. 2002. Changes in soil microbial community structure and function in an alpine dry meadow following spring snow melt. *Microbial Ecology* **43**:307-314.

Liu, Z., Y. Zhang, K. Fa, S. Qin, and W. She. 2017. Rainfall pulses modify soil carbon emission in a semiarid desert. *Catena* **155**:147-155.

Manzoni, S., J. P. Schimel, and A. Porporato. 2012. Responses of soil microbial communities to water stress: results from a meta-analysis. *Ecology* **93**:930-938.

Monson, R. K., Lipson, D. L., Burns, S. P., Turnipseed, A. A., Delany, A. C., Williams, M. W., and Schmidt, S. K. (2006). Winter forest soil respiration controlled by climate and microbial community composition. *Nature*, **439**:711-714.

Myers, R. T., D. R. Zak, D. C. White, and A. Peacock. 2001. Landscape-level patterns of microbial community composition and substrate use in upland forest ecosystems. *Soil Science Society of America Journal* **65**:359-367.

Nakai, T., Y. Kim, R. C. Busey, R. Suzuki, S. Nagai, H. Kobayashi, H. Park, K. Sugiura, and A. Ito. 2013. Characteristics of evapotranspiration from a permafrost black spruce forest in interior Alaska. *Polar Science* **7**:136-148.

Nannipieri, P., L. Muccini, and C. Ciardi. 1983. Microbial biomass and enzyme activities: production and persistence. *Soil Biology and Biochemistry* **15**:679-685.

Noh, N. J., M. Kuribayashi, T. M. Saitoh, and H. Muraoka. 2017. Different responses of soil, heterotrophic and autotrophic respirations to a 4-year soil warming experiment in a cool-temperate deciduous broadleaved forest in central Japan. *Agricultural and Forest Meteorology* **247**:560-570.

Pastorello, G., C. Trotta, E. Canfora, H. Chu, D. Christianson, Y.-W. Cheah, C. Poindexter, J. Chen, A. Elbashandy, M. Humphrey, P. Isaac, D. Polidori, A. Ribeca, C. van Ingen, L. Zhang, B. Amiro, C. Ammann, M. A. Arain, J. Ardö, T. Arkebauer, S. K. Arndt, N. Arriga, M. Aubinet, M. Aurela, D. Baldocchi, A. Barr, E. Beamesderfer, L. B. Marchesini, O. Bergeron, J. Beringer, C. Bernhofer, D. Berveiller, D. Billesbach, T. A. Black, P. D. Blanken, G. Bohrer, J. Boike, P. V. Bolstad, D. Bonal, J.-M. Bonnefond, D. R. Bowling, R. Bracho, J. Brodeur, C. Brümmer, N. Buchmann, B. Burban, S. P. Burns, P. Buysse, P. Cale, M. Cavagna, P. Cellier, S. Chen, I. Chini, T. R. Christensen, J. Cleverly, A. Collalti, C. Consalvo, B. D. Cook, D. Cook, C. Coursolle, E. Cremonese, P. S. Curtis, E. D'Andrea, H. da Rocha, X. Dai, K. J. Davis, B. De Cinti, A. de Grandcourt, A. De Ligne, R. C. De Oliveira, N. Delpierre, A. R. Desai, C. M. Di Bella, P. di Tommasi, H. Dolman, F. Domingo, G. Dong, S. Dore, P. Duce, E. Dufrêne, A. Dunn, J. Dušek, D. Eamus, U. Eichelmann, H. A. M. ElKhidir, W. Eugster, C. M. Ewenz, B. Ewers, D. Famulari, S. Fares, I. Feigenwinter, A. Feitz, R. Fensholt, G. Filippa, M. Fischer, J. Frank, M. Galvagno, M. Gharun, D. Gianelle, B. Gielen, B. Gioli, A. Gitelson, I. Goded, M. Goeckede, A. H. Goldstein,

C. M. Gough, M. L. Goulden, A. Graf, A. Griebel, C. Gruening, T. Grünwald, A. Hammerle, S. Han, X. Han, B. U. Hansen, C. Hanson, J. Hatakka, Y. He, M. Hehn, B. Heinesch, N. Hinko-Najera, L. Hörtnagl, L. Hutley, A. Ibrom, H. Ikawa, M. Jackowicz-Korczynski, D. Janouš, W. Jans, R. Jassal, S. Jiang, T. Kato, M. Khomik, J. Klatt, A. Knohl, S. Knox, H. Kobayashi, G. Koerber, O. Kolle, Y. Kosugi, A. Kotani, A. Kowalski, B. Kruijt, J. Kurbatova, W. L. Kutsch, H. Kwon, S. Launiainen, T. Laurila, B. Law, R. Leuning, Y. Li, M. Liddell, J.-M. Limousin, M. Lion, A. J. Liska, A. Lohila, A. López-Ballesteros, E. López-Blanco, B. Loubet, D. Loustau, A. Lucas-Moffat, J. Lüers, S. Ma, C. Macfarlane, V. Magliulo, R. Maier, I. Mammarella, G. Manca, B. Marcolla, H. A. Margolis, S. Marras, W. Massman, M. Mastepanov, R. Matamala, J. H. Matthes, F. Mazzenga, H. McCaughey, I. McHugh, A. M. S. McMillan, L. Merbold, W. Meyer, T. Meyers, S. D. Miller, S. Minerbi, U. Moderow, R. K. Monson, L. Montagnani, C. E. Moore, E. Moors, V. Moreaux, C. Moureaux, J. W. Munger, T. Nakai, J. Neirynck, Z. Nesic, G. Nicolini, A. Noormets, M. Northwood, M. Nosetto, Y. Nouvellon, K. Novick, W. Oechel, J. E. Olesen, J.-M. Ourcival, S. A. Papuga, F.-J. Parmentier, E. Paul-Limoges, M. Pavelka, M. Peichl, E. Pendall, R. P. Phillips, K. Pilegaard, N. Pirk, G. Posse, T. Powell, H. Prasse, S. M. Prober, S. Rambal, Ü. Rannik, N. Raz-Yaseef, D. Reed, V. R. de Dios, N. Restrepo-Coupe, B. R. Reverter, M. Roland, S. Sabbatini, T. Sachs, S. R. Saleska, E. P. Sánchez-Cañete, Z. M. Sanchez-Mejia, H. P. Schmid, M. Schmidt, K. Schneider, F. Schrader, I. Schroder, R. L. Scott, P. Sedlák, P. Serrano-Ortíz, C. Shao, P. Shi, I. Shironya, L. Siebicke, L. Šigut, R. Silberstein, C. Sirca, D. Spano, R. Steinbrecher, R. M. Stevens, C. Sturtevant, A. Suyker, T. Tagesson, S. Takanashi, Y. Tang, N. Tapper, J. Thom, F. Tiedemann, M. Tomassucci, J.-P. Tuovinen, S. Urbanski, R. Valentini, M. van der Molen, E. van Gorsel, K. van Huissteden, A. Varlagin, J. Verfaillie, T. Vesala, C. Vincke, D. Vitale, N. Vygodskaya, J. P. Walker, E. Walter-Shea, H. Wang, R. Weber, S. Westermann, C. Wille, S. Wofsy, G. Wohlfahrt, S. Wolf, W. Woodgate, Y. Li, R. Zampedri, J. Zhang, G. Zhou, D. Zona, D. Agarwal, S. Biraud, M. Torn, and D. Papale. 2020. The FLUXNET2015 dataset and the ONEFlux processing pipeline for eddy covariance data. *Scientific Data* **7**:225.

Pietikäinen, J., M. Pettersson, and E. Bååth. 2005. Comparison of temperature effects on soil respiration and bacterial and fungal growth rates. *FEMS Microbiology Ecology* **52**:49-58.

Rebmann, C., M. Göckede, T. Foken, M. Aubinet, M. Aurela, P. Berbigier, C. Bernhofer, N. Buchmann, A. Carrara, and A. Cescatti. 2005. Quality analysis applied on eddy covariance measurements at complex forest sites using footprint modelling. *Theoretical and Applied Climatology* **80**:121-141.

Saigusa, N., S. Yamamoto, S. Murayama, and H. Kondo. 2005. Inter-annual variability of carbon budget components in an AsiaFlux forest site estimated by long-term flux measurements. *Agricultural and Forest Meteorology* **134**:4-16.

Salamanca, E. F., N. Kaneko, and S. Katagiri. 1998. Effects of leaf litter mixtures on the decomposition of Quercus serrata and Pinus densiflora using field and laboratory microcosm methods. *Ecological Engineering* **10**:53-73.

Schimel, J. P., & Schaeffer, S. M. (2012). Microbial control over carbon cycling in soil. *Frontiers in Microbiology*, 3 1- 11, DOI: 10.3389/fmicb.2012.00348.

Schlesinger, W. H., and J. A. Andrews. 2000. Soil respiration and the global carbon cycle. *Biogeochemistry* **48**:7-20.

Sharon, D. 1972. The spottiness of rainfall in a desert area. Journal of Hydrology **17**:161-175.

Soulides, D. A., and F. E. Allison. 1961. Effect of drying and freezing soils on carbon dioxide production, available mineral nutrients, aggregation, and bacterial population. *Soil Science* **91**:291-298.

Strickland, M. S., and J. Rousk. 2010. Considering fungal: bacterial dominance in soils–methods, controls, and ecosystem implications. *Soil Biology and Biochemistry* **42**:1385-1395.

Stroud, J. L., G. I. Paton, and K. T. Semple. 2007. Microbe-aliphatic hydrocarbon interactions in soil: implications for biodegradation and bioremediation. *Journal of Applied Microbiology* **102**:1239-1253.

Takahashi, M., K. Hirai, P. Limtong, C. Leaungvutivirog, S. Panuthai, S. Suksawang, S. Anusontpornperm, and D. Marod. 2011. Topographic variation in heterotrophic and autotrophic

soil respiration in a tropical seasonal forest in Thailand. *Soil Science and Plant Nutrition* **57**:452-465.

Tang, J., and D. D. Baldocchi. 2005. Spatial–temporal variation in soil respiration in an oak–grass savanna ecosystem in California and its partitioning into autotrophic and heterotrophic components. *Biogeochemistry* **73**:183-207.

Tang, X., J. Du, Y. Shi, N. Lei, G. Chen, L. Cao, and X. Pei. 2020. Global patterns of soil heterotrophic respiration–A meta-analysis of available dataset. *CATENA* **191**:104574.

Thornton, P. E., J.-F. Lamarque, N. A. Rosenbloom, and N. M. Mahowald. 2007. Influence of carbon-nitrogen cycle coupling on land model response to CO_2 fertilization and climate variability. *Global Biogeochemical Cycles* **21**.

Thornton, P. E., and N. A. Rosenbloom. 2005. Ecosystem model spin-up: Estimating steady state conditions in a coupled terrestrial carbon and nitrogen cycle model. *Ecological Modelling* **189**:25-48.

Vogel, J. G., D. W. Valentine, and R. W. Ruess. 2005. Soil and root respiration in mature Alaskan black spruce forests that vary in soil organic matter decomposition rates. *Canadian Journal of Forest Research* **35**:161-174.

Wang, G., S. Jagadamma, M. A. Mayes, C. W. Schadt, J. M. Steinweg, L. Gu, and W. M. Post. 2015a. Microbial dormancy improves development and experimental validation of ecosystem model. *The ISME Journal* **9**:226-237.

Wang, G., W. M. Post, and M. A. Mayes. 2013a. Development of microbial-enzyme-mediated decomposition model parameters through steady-state and dynamic analyses. *Ecological Applications* **23**:255-272.

Wang, K., C. Peng, Q. Zhu, X. Zhou, M. Wang, K. Zhang, and G. Wang. 2017. Modeling global soil carbon and soil microbial carbon by integrating microbial processes into the ecosystem process model TRIPLEX-GHG. *Journal of Advances in Modeling Earth Systems* **9**:2368-2384.

Wang, Q., T. He, S. Wang, and L. Liu. 2013b. Carbon input manipulation affects soil respiration and microbial community composition in a subtropical coniferous forest. *Agricultural and Forest Meteorology* **178**:152-160.

Wang, Y., H. Wang, M. Xu, Z. Ma, and Z.-L. Wang. 2015b. Soil organic carbon stocks and CO_2 effluxes of native and exotic pine plantations in subtropical China. *Catena* **128**:167-173.

Wang, Y., F. Yuan, F. Yuan, B. Gu, M. S. Hahn, M. S. Torn, D. M. Ricciuto, J. Kumar, L. He, and D. Zona. 2019. Mechanistic modeling of microtopographic impacts on CO_2 and CH_4 Fluxes in an Alaskan tundra ecosystem using the CLM-Microbe model. *Journal of Advances in Modeling Earth Systems* **11**:17, 4228-4304 DOI:10.1029/2019MS001771.

Wei, H., X. Chen, J. He, L. Huang, and W. Shen. 2019. Warming but not nitrogen addition alters the linear relationship between microbial respiration and biomass. *Frontiers in Microbiology* **10**:1055.

Whitaker, J., N. Ostle, A. T. Nottingham, A. Ccahuana, N. Salinas, R. D. Bardgett, P. Meir, and N. P. McNamara. 2014. Microbial community composition explains soil respiration responses to changing carbon inputs along an Andes-to-Amazon elevation gradient. *Journal of Ecology*, **102**:1058-1071.

Widén, B., and H. Majdi. 2001. Soil CO_2 efflux and root respiration at three sites in a mixed pine and spruce forest: seasonal and diurnal variation. *Canadian Journal of Forest Research* **31**:786-796.

Wieder, W. R., , G. B. Bonan, and Allison, S. D. (2013). Global soil carbon projections are improved by modelling microbial processes. *Nature Climate Change*, **3**:909-912.

Wieder, W. R., A. S. Grandy, C. M. Kallenbach, and G. B. Bonan. 2014. Integrating microbial physiology and physio-chemical principles in soils with the MIcrobial-MIneral Carbon Stabilization (MIMICS) model. *Biogeosciences* **11**:3899-3917.

Wieder, W. R., Allison, S. D., davidson, E. A., K. Georgiou, Hararuk O., He, Y., Hopkins, F., Luo, Y., Smith, M., Sulman, B.N., Todd-Brown, K.Y., Wang, Y., Xia J., Xu, X. (2015). Explicitly

representing soil microbial processes in Earth system models. *Global Biogeochemical Cycles*, 29(10), 1781-1800. doi:10.1002/2015GB005188

Wieder, W. R., A. S. Grandy, C. M. Kallenbach, P. G. Taylor, and G. B. Bonan. 2015. Representing life in the Earth system with soil microbial functional traits in the MIMICS model. *Geoscientific Model Development* **8**:1789-1808.

Xiao, Y. 2003. Variation in needle longevity of Pinus tabulaeformis forests at different geographic scales. *Tree Physiology* **23**:463-471.

Xu, X., D. A. Elias, D. E. Graham, T. J. Phelps, S. L. Carroll, S. D. Wullschleger, and P. E. Thornton. 2015. A microbial functional group-based module for simulating methane production and consumption: Application to an incubated permafrost soil. *Journal of Geophysical Research: Biogeosciences* **120**:1315-1333.

Xu, X., J. P. Schimel, I. A. Janssens, X. Song, C. Song, G. Yu, R. L. Sinsabaugh, D. Tang, X. Zhang, and P. E. Thornton. 2017. Global pattern and controls of soil microbial metabolic quotient. *Ecological Monographs* **87**:429-441.

Xu, X., J. P. Schimel, P. E. Thornton, X. Song, F. Yuan, and S. Goswami. 2014. Substrate and environmental controls on microbial assimilation of soil organic carbon: a framework for Earth system models. *Ecology Letters* **17**:547-555.

Xu, X., P. E. Thornton, and W. M. Post. 2013. A global analysis of soil microbial biomass carbon, nitrogen and phosphorus in terrestrial ecosystems. *Global Ecology and Biogeography* **22**:737-749.

Zhang, Q., H.-M. Lei, and D.-W. Yang. 2013. Seasonal variations in soil respiration, heterotrophic respiration and autotrophic respiration of a wheat and maize rotation cropland in the North China Plain. *Agricultural and Forest Meteorology* **180**:34-43.

Zhou, X., S. Wan, and Y. Luo. 2007. Source components and interannual variability of soil CO_2 efflux under experimental warming and clipping in a grassland ecosystem. *Global Change Biology* **13**:761-775.

Figures and tables

Fig. 3.1. Observed and the CLM-Microbe simulated microbial respiration (MR) in deserts (a and b), grasslands (c and d), shrublands (e and f), boreal forests (g, h, and i), temperate broadleaf forests (j and k), temperate coniferous forests (l and m), tropical/subtropical forests (n and o), wetlands (p and q), and tundra (r and s).

Fig. 3.2. Observed and the CLM-Microbe model simulated root respiration (RR) in deserts (a and b), grasslands (c and d), shrublands (e and f), boreal forests (g, h, and i), temperate broadleaf forests (j and k), temperate coniferous forests (l and m), tropical/subtropical forests (n and o), wetlands (p and q), and tundra (r).

Fig. 3.3. Observed and the CLM-Microbe model simulated soil respiration (SR) in deserts (a and b), grasslands (c and d), shrublands (e and f), boreal forests (g, h, and i), temperate broadleaf forests (j and k), temperate coniferous forests (l and m), tropical/subtropical forests (n and o), wetlands (p and q), and tundra (r).

Fig. 3.4. Comparison of the averaged observed and simulated microbial respiration (MR) (a), root respiration (RR) (b), and soil respiration (SR) (c). Vertical and horizontal error bars indicate standard error of simulated and observed values, respectively, for a) heterotrophic respiration, b) root respiration, and c) soil respiration.

Fig. 3.5. Observed versus simulated a) microbial respiration (MR), root respiration (RR), and soil respiration (SR) by the CLM-Microbe_wos. CLM-Microbe_wos indicates the model simulation scenario without the seasonality of fungal and bacterial biomass.

Fig. 3.6. Comparison of the model goodness-of-fit in microbial respiration (MR) (a, d, and g), root respiration (RR) (b, e, and h), and soil respiration (SR) (c, f, and i). MAE, mean absolute error; RMSE, root mean square error; R^2, R square. Solid line indicates not applicable. MAE and RMSE values indicate the mean error of the model, smaller values represent higher model performance. R^2 values mean the proportion of variation being explained by the mode, higher R^2 values indicate better model performance. R^2 is not suitable for assessing the goodness-of-fit for a small amount of data due to the large bias in small samples. CLM-Microbe represents the default model simulation with the seasonality of fungal and bacterial biomass; CLM-Microbe_wos indicates the model simulation scenario without the seasonality of fungal and bacterial biomass.

Table 3.1. Site information of the observational respiration flux data

Table 3.2. Site-level evaluation of the goodness-of-fit criteria computed for the simulated microbial respiration (MR), root respiration (RR), and soil respiration (SR)

Table 3.3. Annual budgets of microbial respiration (MR), soil respiration (SR), and soil organic carbon (SOC) during 2000-2009 for the representative sites in natural biomes

Table 3.1. Site information of the observational respiration flux data

Biome	Site ID	Location	Country	Measurement	Sampling year	Sampling time	Reference
Boreal Forest	BRF-CA	54.00, -105.10	Canada	Trenching	2003-2004	nighttime	Gaumont-Guay et al. (2008)
	BRF-SW	60.08, 17.50	Sweden	Extraction	1999	daytime	Widén and Majdi (2001)
	BRF-US	64.80, -147.87	USA	Trenching	2001	10:00-12:00	Vogel et al. (2005)
Desert	DST-NX	37.70, 107.22	China	Trenching	2015	daily average	Liu et al. (2017)
	DST-XJ	44.28, 87.93	China	Extraction	2011-2013	9:00-12:00	Huang et al. (2015)
Grassland	GRS-HU	46.69, 19.60	Hungary	Trenching	2013	daily average	Balogh et al. (2016)
	GRS-US	34.98, -97.52	USA	Trenching	2002-2005	10:00-15:00	Zhou et al. (2007)
Shrubland	SHB-MX	32.03, -116.60	México	Trenching	2011-2012	12:00-14:00	Balogh et al. (2016)
	SHB-NE	52.40, 5.92	Netherlands	Comparison	2010-2012	not indicated	Kopittke et al. (2014)
Temperate broadleaf forest	TBF-GM	51.08, 10.45	Germany	Trenching	2004-2006	12:00	Kutsch et al. (2010)
	TBF-JP	36.13, 137.42	Japan	Trenching	2013-2015	morning, 10:30-12:30, and afternoon	Noh et al. (2017)
Temperate coniferous forest	TCF-SP	42.62, 2.42	Spain	Trenching	2012-2013	daily average	Barba et al. (2016)
	TCF-US	44.45, -121.56	USA	Trenching	2004-2005	daily average	Irvine et al. (2008)
Tropical/subtropical forest	TSF-CN	26.73, 115.05	China	Trenching	2008-2009	8:30-11:30 and 14:00-17:00	Wang et al. (2015b)
	TSF-TH	14.58, 98.87	Thailand	Trenching	2008-2009	9:00-14:00	Takahashi et al. (2011)
Tundra	TUN-GL	67.10, -50.27	Greenland	Trenching	2011-2013	not indicated	Cahoon et al. (2016)
	TUN-RU	67.05, 62.95	Russia	Trenching	2008	12:00-18:00	Biasi et al. (2014)
Wetland	WET-PY	28.89, 116.32	China	Trenching	2009-2011	9:00-11:00	Hu et al. (2015)
	WET-SJ	47.58, 133.52	China	Trenching	2010-2011	not indicated	Li et al. (2016)

nighttime, 20:00-8:00; daytime, 8:00-20:00; not indicated, used daily average instead; morning, 10:30-12:30, and afternoon, used daytime average.

Table 3.2. Site-level evaluation of the goodness-of-fit criteria computed for the simulated microbial respiration (MR), root respiration (RR), and soil respiration (SR)

Biome	Site	MR (μmol m^{-2} s^{-1})			RR (μmol m^{-2} s^{-1})			SR (μmol m^{-2} s^{-1})		
		MAE	RMSE	R^2	MAE	RMSE	R^2	MAE	RMSE	R^2
Boreal Forest	BRF-CA	0.41	0.49	0.63	0.46	0.72	0.80	0.67	0.82	0.84
	BRF-SW	1.30	1.53	0.02	0.18	0.22	0.76	1.16	1.38	0.32
	BRF-US	0.31	0.36	0.36	0.53	0.68	0.37	0.75	0.97	0.41
Desert	DST-NX	0.38	0.47	0.14	0.18	0.28	0.02	0.52	0.66	0.03
	DST-XJ	0.05	0.07	0.76	0.14	0.21	0.52	0.17	0.27	0.57
Grassland	GRS-HU	1.36	1.63	0.14	1.02	1.30	0.22	1.76	2.12	0.38
	GRS-US	0.66	0.88	0.36	0.60	0.95	0.29	1.15	1.54	0.53
Shrub	SHB-MX	0.69	0.80	0.29	0.09	0.12	0.61	0.74	0.84	0.19
	SHB-NE	0.45	0.53	0.56	0.25	0.31	0.39	0.68	0.74	0.79
Temperate broadleaf forest	TBF-GM	0.60	0.69	0.12	0.69	0.82	0.49	0.91	1.10	0.41
	TBF-JP	0.31	0.37	0.85	0.34	0.40	0.63	0.57	0.66	0.85
Temperate coniferous forest	TCF-SP	1.01	1.21	0.35	0.46	0.61	0.18	1.20	1.47	0.30
	TCF-US	0.39	0.47	0.47	0.78	0.99	0.14	0.95	1.26	0.36
Tropical/subtropical forest	TSF-CN	0.64	0.85	0.58	0.59	0.77	0.24	1.00	1.25	0.71
	TSF-TH	0.92	1.12	0.42	0.51	0.65	0.21	0.81	1.03	0.54
Tundra	TUN-GL	0.27	0.36	0.39	0.70	0.78	0.21	0.97	1.01	0.12
	TUN-RU	0.20	0.25	0.91	--	--	--	--	--	--
Wetland	WET-PY	0.81	1.06	0.52	0.54	0.70	0.13	1.03	1.21	0.69
	WET-SJ	1.02	1.21	0.09	0.87	1.20	0.18	1.48	1.78	0.29

MAE, mean absolute error; RMSE, root mean square error; R^2, R square. -- indicates not applicable. MAE and RMSE values indicate the mean error of the model, smaller values represent higher model performance. R^2 values mean the proportion of variation being explained by the mode, higher R^2 values indicate better model performance. R^2 is not suitable for assessing the goodness-of-fit for a small amount of data due to the large bias in small samples.

Table 3.3. Annual budgets of microbial respiration (MR), soil respiration (SR), and soil organic carbon (SOC) during 2000-2009 for the representative sites in natural biomes

Biome	MR (μmol m^{-2} s^{-1})			SR (μmol m^{-2} s^{-1})			SOC (kg C m^{-2} yr^{-1})		
	CLM-Microbe	CLM-Microbe_wos	*t*-test	CLM-Microbe	CLM-Microbe_wos	*t*-test	CLM-Microbe	CLM-Microbe_wos	*t*-test
BRF-CA	1.170 (1.097-1.226)	0.797 (0.784-0.810)	*	2.569 (2.367-2.877)	1.820 (1.640-1.978)	*	17.07 (17.05-17.08)	16.79 (16.79-16.80)	*
DST-XJ	0.170 (0.129-0.209)	0.169 (0.129-0.206)	NS	0.223 (0.169-0.276)	0.2220 (0.170-0.273)	NS	4.72 (4.72-4.72)	5.07 (5.06-5.08)	*
GRS-US	1.005 (0.813-1.148)	0.854 (0.777-0.928)	*	1.526 (1.341-1.658)	1.320 (1.246-1.399)	*	10.60 (10.58-10.61)	10.93 (10.91-10.96)	*
SHB-NE	1.527 (1.284-1.759)	1.360 (1.245-1.507)	*	2.442 (1.883-3.168)	2.212 (1.695-2.887)	*	11.36 (11.30-11.40)	11.43 (11.37-11.48)	*
TBF-JP	1.455 (1.386-1.507)	1.396 (1.371-1.433)	*	2.271 (2.169-2.342)	2.211 (2.155-2.270)	*	8.74 (8.71-8.77)	9.20 (9.14-9.26)	*
TCF-US	1.542 (1.477-1.606)	1.470 (1.410-1.551)	*	2.735 (2.572-2.889)	2.624 (2.500-2.711)	*	13.51 (13.48-13.53)	13.65 (13.63-13.67)	*
TSF-CN	1.705 (1.660-1.771)	1.436 (1.397-1.476)	*	2.961 (2.876-3.070)	2.629 (2.587-2.684)	*	14.59 (14.53-14.65)	14.62 (14.55-14.69)	*
TUN-RU	0.475 (0.441-0.567)	0.399 (0.396-0.402)	*	0.668 (0.617-0.789)	0.562 (0.551-0.575)	*	22.90 (22.88-22.92)	22.89 (22.88-22.91)	*
WET-PY	1.411 (1.379-1.459)	1.403 (1.387-1.448)	NS	1.985 (1.928-2.075)	1.976 (1.939-2.043)	NS	16.66 (16.66-16.68)	17.80 (17.75-17.88)	*

Values in parentheses indicate the 95% confidence interval. *t*-test represents the paired *t*-test (least significant difference) at $\alpha = 0.05$, and n = 10 pairs for all variables. NS means not significant; * indicates significant at the 0.05 probability level. CLM-Microbe represents the default model simulation with the seasonality of fungal and bacterial biomass; CLM-Microbe_wos indicates the model simulation scenario without the seasonality of fungal and bacterial biomass.

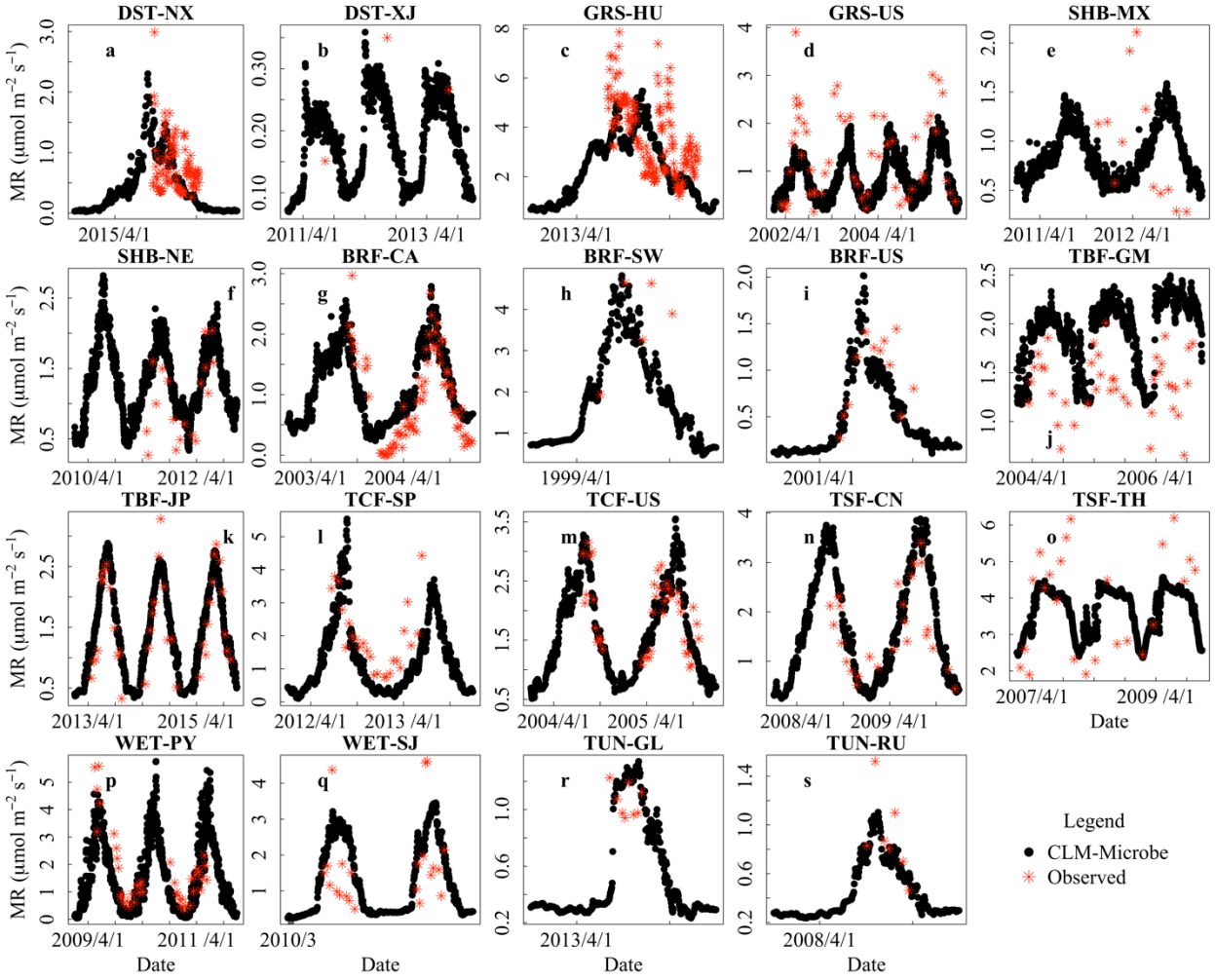

Fig. 3.1. Observed and the CLM-Microbe simulated microbial respiration (MR) in deserts (a and b), grasslands (c and d), shrublands (e and f), boreal forests (g, h, and i), temperate broadleaf forests (j and k), temperate coniferous forests (l and m), tropical/subtropical forests (n and o), wetlands (p and q), and tundra (r and s).

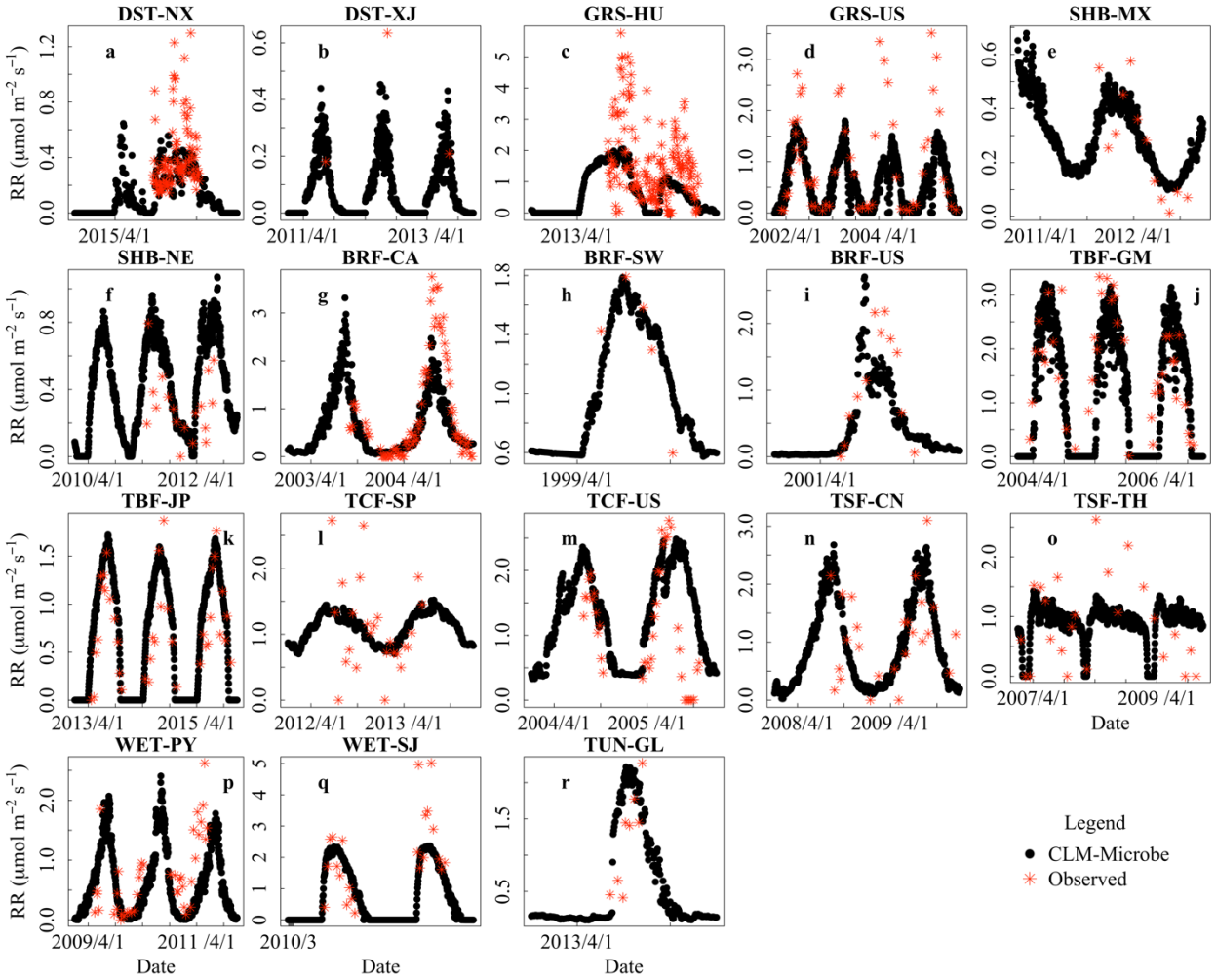

Fig. 3.2. Observed and the CLM-Microbe model simulated root respiration (RR) in deserts (a and b), grasslands (c and d), shrublands (e and f), boreal forests (g, h, and i), temperate broadleaf forests (j and k), temperate coniferous forests (l and m), tropical/subtropical forests (n and o), wetlands (p and q), and tundra (r).

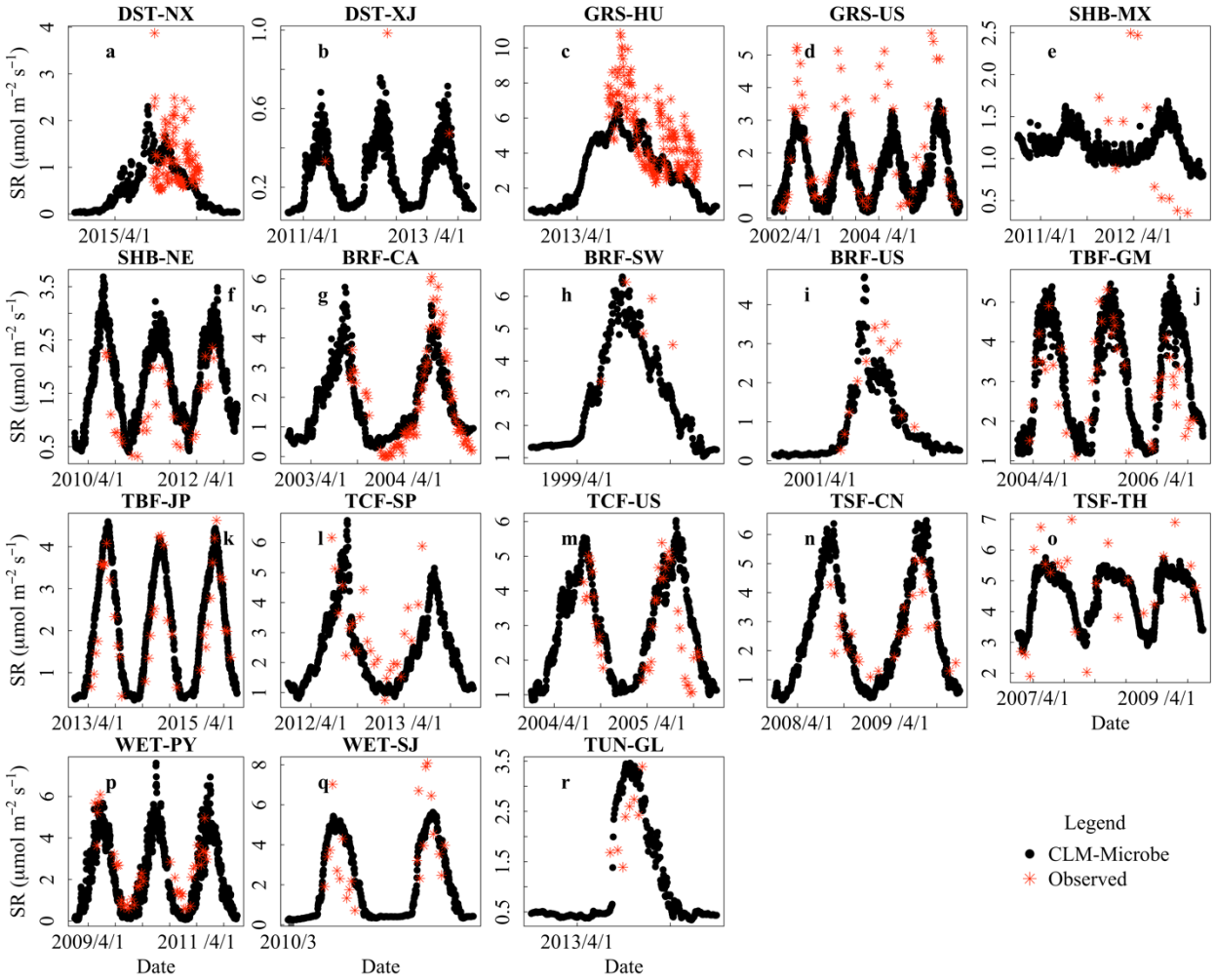

Fig. 3.3. Observed and the CLM-Microbe model simulated soil respiration (SR) in deserts (a and b), grasslands (c and d), shrublands (e and f), boreal forests (g, h, and i), temperate broadleaf forests (j and k), temperate coniferous forests (l and m), tropical/subtropical forests (n and o), wetlands (p and q), and tundra (r).

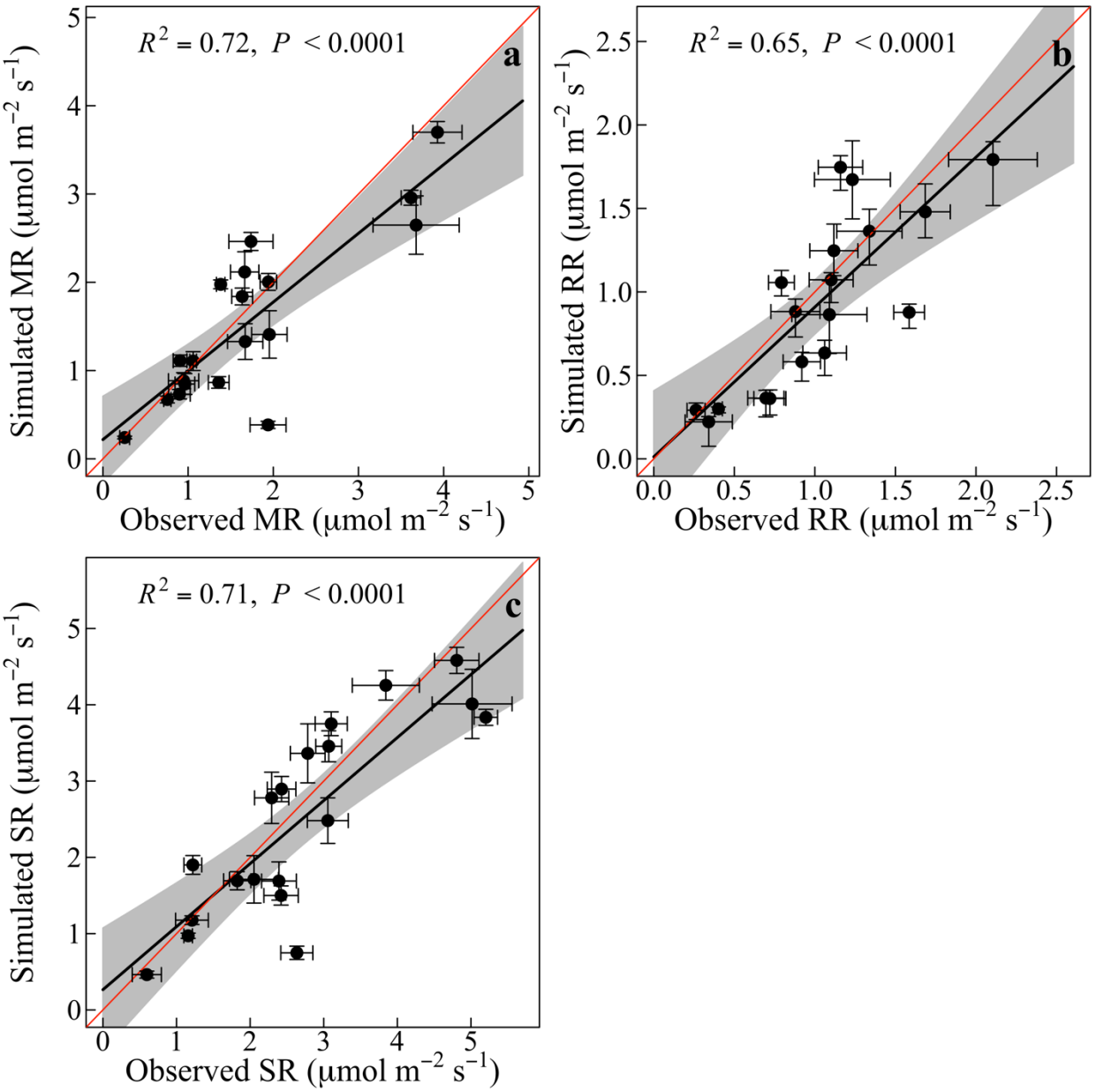

Fig. 3.4. Comparison of the averaged observed and simulated microbial respiration (MR) (a), root respiration (RR) (b), and soil respiration (SR) (c). Vertical and horizontal error bars indicate standard error of simulated and observed values, respectively, for a) heterotrophic respiration, b) root respiration, and c) soil respiration.

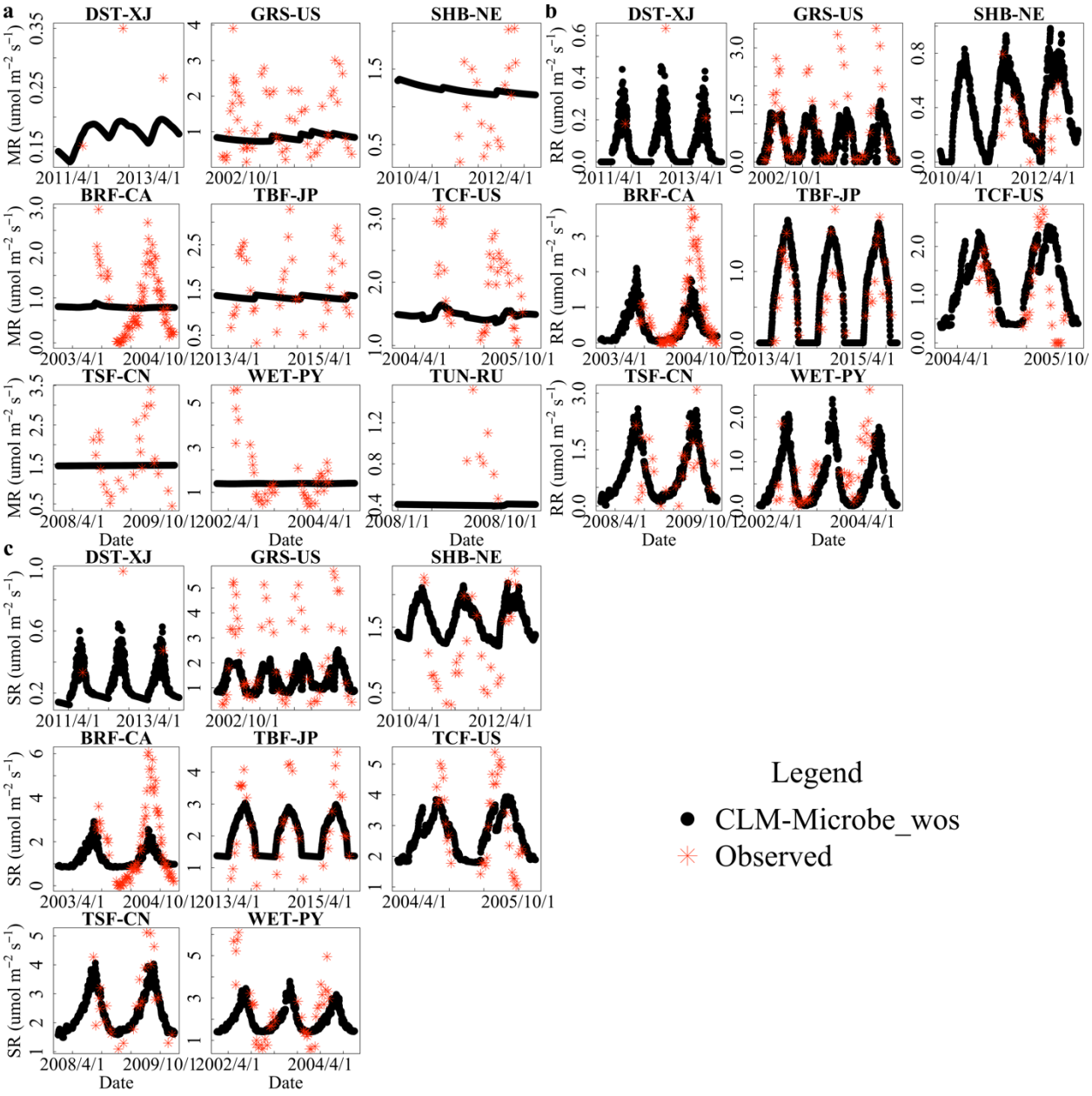

Fig. 3.5. Observed versus simulated a) microbial respiration (MR), root respiration (RR), and soil respiration (SR) by the CLM-Microbe_wos. CLM-Microbe_wos indicates the model simulation scenario without the seasonality of fungal and bacterial biomass.

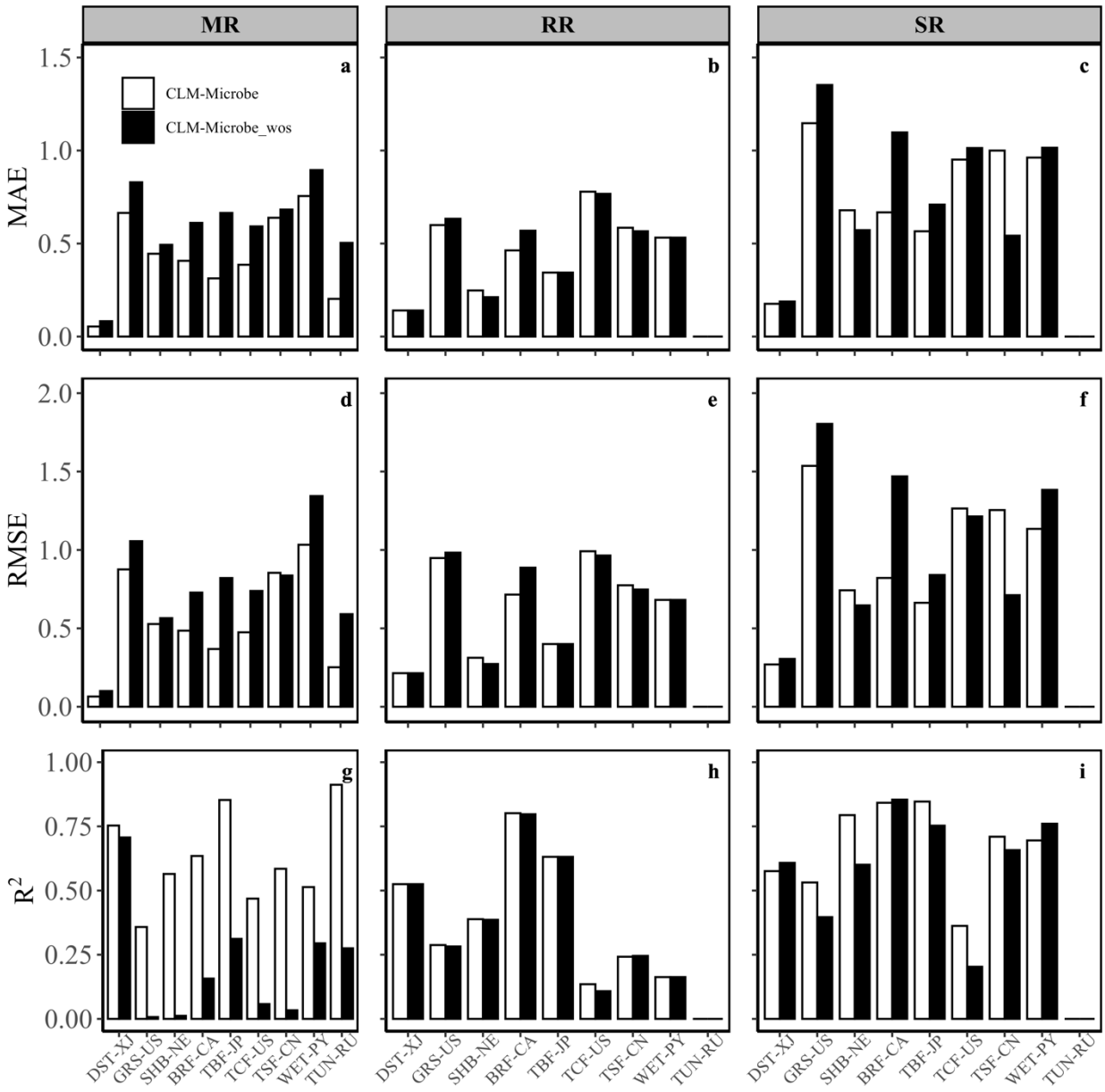

Fig. 3.6. Comparison of the model goodness-of-fit in microbial respiration (MR) (a, d, and g), root respiration (RR) (b, e, and h), and soil respiration (SR) (c, f, and i). MAE, mean absolute error; RMSE, root mean square error; R^2, R square. Solid line indicates not applicable. MAE and RMSE values indicate the mean error of the model, smaller values represent higher model performance. R^2 values mean the proportion of variation being explained by the mode, higher R^2 values indicate better model performance. R^2 is not suitable for assessing the goodness-of-fit for a small amount of data due to the large bias in small samples. CLM-Microbe represents the default model simulation with the seasonality of fungal and bacterial biomass; CLM-Microbe_wos indicates the model simulation scenario without the seasonality of fungal and bacterial biomass.

Supplementary material for chapter 3

Fig. 3.S1. Conceptual diagram showing the key processes and the roles of fungi and bacteria in the CLM-Microbe model. CWD, coarse woody debris; SOM, soil organic matter; B, bacteria; F, fungi; DOM, dissolved organic matter. In the CLM-Microbe model, number in the box means turnover time of each pool. Black solid lines indicate transitions in the CLM-Microbe model, which generally represents processes such as 1) decomposition of coarse woody debris, 2) litter 1 decomposition, 3) litter 2 decomposition, 4) litter 3 decomposition, 5) soil organic matter 1 decomposition, 6) soil organic matter 2 decomposition, 7) soil organic matter 3 decomposition, 8) soil organic matter 4 decomposition, 9) fungal and bacterial lysis, 10) dissolved organic matter adsorption, 11) dissolved organic matter uptake by fungal and bacterial, and 12) fungal and bacterial respiration. Red dash lines represent regulatory role of fungi and bacteria on the process, including fungi and bacteria regulation on 13) litter 1, 14) litter 2, 15) litter 3, 16) soil organic matter 1, 17) soil organic matter 2, 18) soil organic matter 3, and 19) soil organic matter 4 decomposition (He et al. 2021).

Fig. 3.S2. Simulated a) fungal biomass carbon (FBC), b) bacterial biomass carbon (BBC), and c) fungi:bacteria (F:B) ratio under scenarios with and without microbial biomass seasonality for representative sites. The CLM-Microbe represents the default model simulation with the seasonality of fungal and bacterial biomass; the CLM-Microbe_wos is the model without the seasonality of fungal and bacterial biomass.

Fig. 3.S3. Simulated a) fungal carbon gain from litter decomposition (Lit2Fun), b) fungal dissolved organic matter uptake (DOM2Fun), c) fungal carbon gain from soil organic matter decomposition (SOM2Fun), and d) fungal lysis under scenarios with and without microbial biomass seasonality for representative sites. The CLM-Microbe represents the default model simulation with the seasonality of fungal and bacterial biomass; the CLM-Microbe_wos is the model without the seasonality of fungal and bacterial biomass.

Fig. 3.S4. Simulated a) bacterial carbon gain from litter decomposition (Lit2Bac), b) bacterial dissolved organic matter uptake (DOM2Bac), c) bacterial carbon gain from soil organic matter decomposition (SOM2Bac), and d) bacterial lysis under scenarios with and without microbial biomass seasonality for representative sites. The CLM-Microbe represents the default model simulation with the seasonality of fungal and bacterial biomass; the CLM-Microbe_wos is the model without the seasonality of fungal and bacterial biomass.

Table 3.S1. Key model parameters in processes involving fungal and bacterial biomass

Table 3.S2. Key parameters used for constraining the model for different biomes

Table 3.S3. Statistics of fungal biomass carbon (FBC), bacterial biomass carbon (BBC), and fungal:bacterial biomass carbon (F:B) ratio with and without microbial biomass seasonality for representative sites during sampling years

Table 3.S4. Statistics of simulated microbial respiration (MR), root respiration (RR), and soil respiration (SR) with and without microbial biomass seasonality for representative sites during sampling years

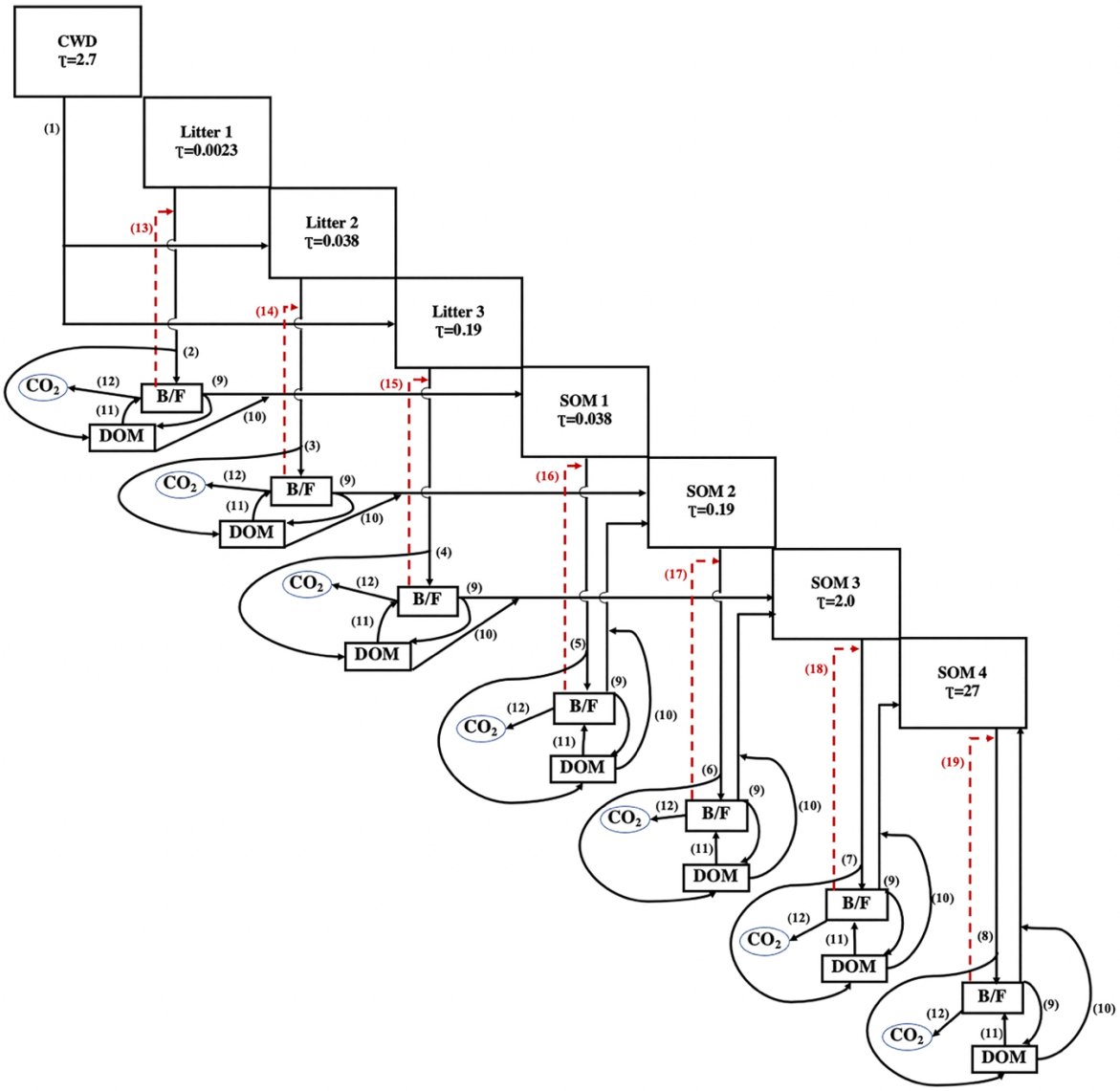

Fig. 3.S1. Conceptual diagram showing the key processes and the roles of fungi and bacteria in the CLM-Microbe model. CWD, coarse woody debris; SOM, soil organic matter; B, bacteria; F, fungi; DOM, dissolved organic matter. In the CLM-Microbe model, number in the box means turnover time of each pool. Black solid lines indicate transitions in the CLM-Microbe model, which generally represents processes such as 1) decomposition of coarse woody debris, 2) litter 1 decomposition, 3) litter 2 decomposition, 4) litter 3 decomposition, 5) soil organic matter 1 decomposition, 6) soil organic matter 2 decomposition, 7) soil organic matter 3 decomposition, 8) soil organic matter 4 decomposition, 9) fungal and bacterial lysis, 10) dissolved organic matter adsorption, 11) dissolved organic matter uptake by fungal and bacterial, and 12) fungal and bacterial respiration. Red dash lines represent regulatory role of fungi and bacteria on the process, including fungi and bacteria regulation on 13) litter 1, 14) litter 2, 15) litter 3, 16) soil organic matter 1, 17) soil organic matter 2, 18) soil organic matter 3, and 19) soil organic matter 4 decomposition (He et al. 2021).

Table 3.S1. Key model parameters in processes involving fungal and bacterial biomass

Symbol	Range [a]	Uni	Description	Reference
k_dom	0.0025-0.5	d^{-1}	decomposition rate constant of DOM	(Cherrier et al., 1996; Kirchman et al., 1991; Wheeler et al., 1996)
k_bacteria	0.00143-2	d^{-1}	lysis rate constant of bacteria	(Moore et al., 2005; Rousk & Bååth, 2007, 2011; Schippers et al., 2005)
k_fungi	0.00027-0.05	d^{-1}	lysis rate constant of fungi	(Moore et al., 2005; Rousk & Bååth, 2011; Thornton & Rosenbloom, 2005; Wallander et al., 2004)
m_rf_s1m	0-1		fraction factor quantifying carbon from SOM1 to microbes	Calibrated
m_rf_s2m	0-1		fraction factor quantifying carbon from SOM2 to microbes	Calibrated
m_rf_s3m	0-1		fraction factor quantifying carbon from SOM3 to microbes	Calibrated
m_rf_s4m	0-1		fraction factor quantifying carbon from SOM4 to microbes	Calibrated
m_batm_f	0-1		fraction factor quantifying carbon respired by bacteria	Calibrated
m_bdom_f	0-1		fraction factor quantifying carbon from DOM to bacteria	Calibrated
m_bs1_f	0-1		fraction factor quantifying carbon from bacteria to SOM1	Calibrated
m_bs2_f	0-1		fraction factor quantifying carbon from bacteria to SOM2	Calibrated
m_bs3_f	0-1		fraction factor quantifying carbon from bacteria to SOM3	Calibrated
m_fatm_f	0-1		fraction factor quantifying carbon respired by fungi	Calibrated
m_fdom_f	0-1		fraction factor quantifying carbon from DOM to fungi	Calibrated
m_fs1_f	0-1		fraction factor quantifying carbon from fungi to SOM1	Calibrated
m_fs2_f	0-1		fraction factor quantifying carbon from fungi to SOM2	Calibrated
m_fs3_f	0-1		fraction factor quantifying carbon from fungi to SOM3	Calibrated
m_domb_f	0-1		fraction factor quantifying carbon from DOM to bacteria	Calibrated
m_domf_f	0-1		fraction factor quantifying carbon from DOM to fungi	Calibrated
m_doms1_f	0-1		fraction factor quantifying carbon from DOM to SOM1	Calibrated
m_doms2_f	0-1		fraction factor quantifying carbon from DOM to SOM2	Calibrated
m_doms3_f	0-1		fraction factor quantifying carbon from DOM to SOM3	Calibrated
cn_bacteria	3-12		C:N ratio of bacteria	(Strickland & Rousk, 2010)
cn_fungi	3-60		C:N ratio of fungi	(Strickland & Rousk, 2010)
cn_dom	4.2-185		C:N ratio of DOM	(Sinsabaugh et al., 2016)
CUEmax	0.46-0.9		maximum carbon use efficiency of microbes	(Gommers et al., 1988; Sinsabaugh et al., 2013; Sinsabaugh et al., 2016)

[a]The values may not be the same as those from literature sources due to unit conversion.

Table 3.S2. Key parameters used for constraining the model for different biomes

Parameters	Biomes								
	BRF	DST	GRS	SHB	TBF	TCF	TSF	TUN	WET
k_bacteria	0.008	0.0178	0.005	0.0056	0.02	0.012	0.01	0.0042	0.072
k_fungi	0.004	0.009	0.0045	0.004	0.0048	0.006	0.01	0.0021	0.03
m_rf_s1m	0.40	0.40	0.40	0.40	0.40	0.20	0.40	0.40	0.75
m_rf_s2m	0.60	0.60	0.60	0.60	0.60	0.30	0.60	0.60	0.85
m_rf_s3m	0.70	0.70	0.70	0.70	0.70	0.40	0.70	0.70	0.95
m_rf_s4m	0.80	0.80	0.80	0.80	0.80	0.50	0.80	0.80	1.00
m_batm_f	0.20	0.08	0.12	0.08	0.12	0.12	0.12	0.12	0.10
m_fatm_f	0.10	0.10	0.08	0.04	0.08	0.08	0.08	0.08	0.08

BRF, boreal forest; DST, desert; GRS, grassland; SHB, shrub; TBF, temperate broadleaf forest; TCF, temperate coniferous forest; TSF, tropical/subtropical forest; TUN, tundra; WET, wetland.

To examine the efficiency of setting soil moisture and moisture scalars as constants in removing soil microbial biomass seasonality, we compared the model simulations of fungal (FBC) and bacterial (BBC) biomass carbon (C) between the CLM-Microbe and CLM-Microbe_wos. Compared with the CLM-Microbe, the CLM-Microbe_wos with constant soil moisture and temperature scalars produced weaker seasonality in FBC, BBC, and F:B ratio across sites (Fig. 3.S2; Table 3.S3). Compared with the CLM-Microbe, the seasonal variation of FBC, BBC, and F:B ratios simulated by the CLM-Microbe_wos were dampened, with FBC decreased by 47.0-99.6% and 51.3-99.7%, BBC decreased by 48.2-99.7% and 36.6-99.5%, and F:B ratio decreased by 9.38-100.0% and 10.0-100.0%, respectively, in range and standard deviation across biomes. In addition, the removal of soil moisture and moisture seasonal variation led to suppressed FBC and BBC. Compared with the CLM-Microbe, the CLM-Microbe_wos simulated smaller pool sizes of FBC and BBC, with the magnitude varied across biomes. For example, the decrease in FBC ranging from 5.9% at TBF-JP (temperate broadleaf forest, TBF-) and 22.7% at BRF-CA (boreal forest, BRF-) and BBC ranging from 2.3% at TBF-JP and 23.4% at BRF-CA. The response of F:B ratio to the removal of soil moisture and moisture seasonal variation were varied in magnitude and direction among biomes (Fig. 3.S2c; Table 3.S3). We found decreases in F:B ratio at DST-XJ (desert, DST-; 1.6%), TBF-JP (4.6%), TCF-US (temperate coniferous forest, TCF-; 1.3%), WET-PY (wetland, WET-; 8.1%), SHB-NE (shrubland, SHB-; 0.6%), and TUN-RU (tundra, TUN-; 4.9%). In contrast, compared with the CLM-Microbe, F:B ratios increased in the CLM-Microbe_wos at TSF-CN (tropical/subtropical forest, TSF-; 3.9%) and BRF-CA (0.7%). In addition, the removal of fungal and bacteria biomass seasonality changed the seasonal pattern of F:B ratio at some sites. For example, we detected the peak F:B ratio in summer in the CLM-Microbe and in autumn in the CLM-Microbe_wos at BRF-CA.

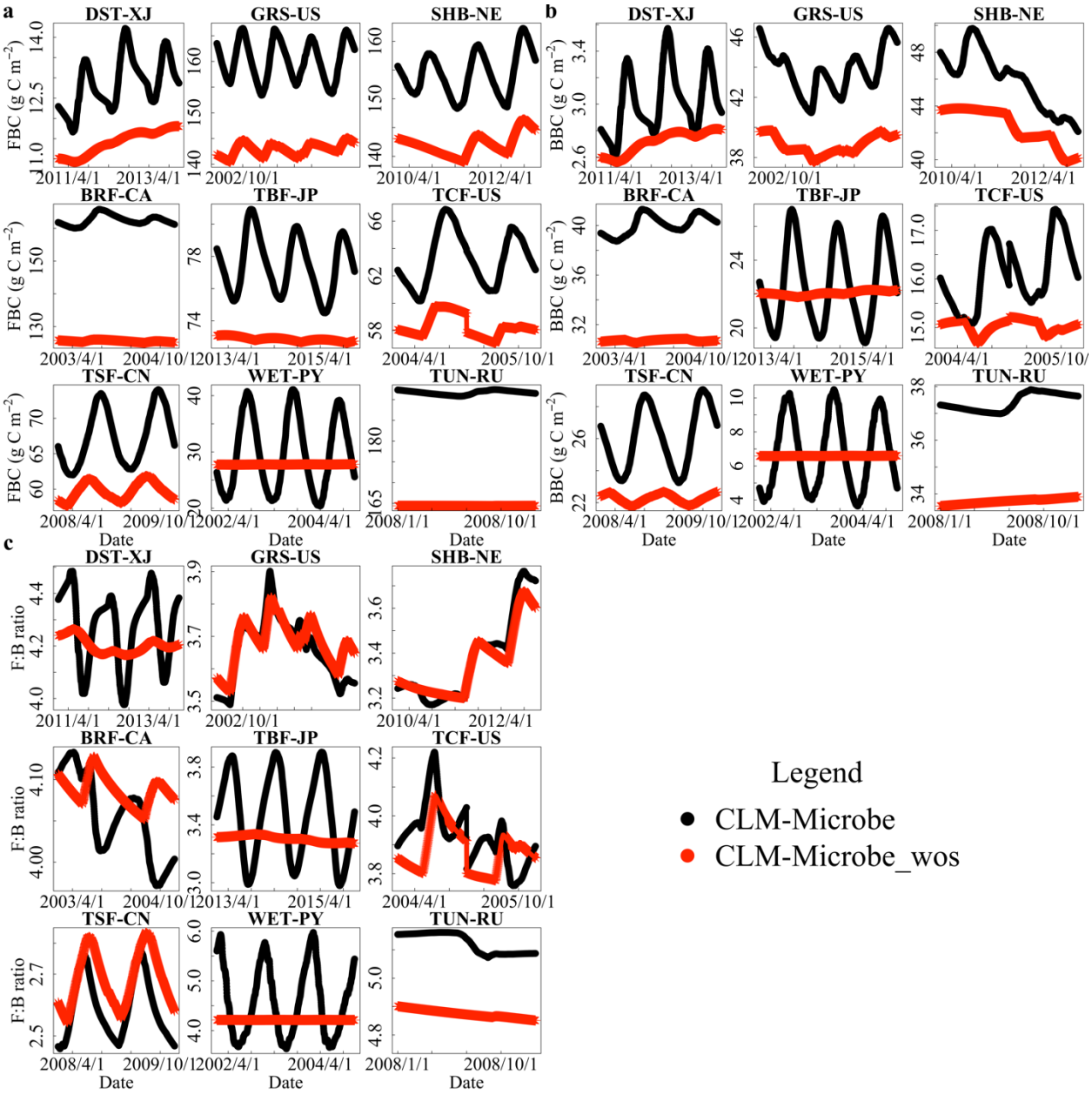

Fig. 3.S2. Simulated a) fungal biomass carbon (FBC), b) bacterial biomass carbon (BBC), and c) fungi:bacteria (F:B) ratio under scenarios with and without microbial biomass seasonality for representative sites. The CLM-Microbe represents the default model simulation with the seasonality of fungal and bacterial biomass; the CLM-Microbe_wos is the model without the seasonality of fungal and bacterial biomass.

Table 3.S3. Statistics of fungal biomass carbon (FBC), bacterial biomass carbon (BBC), and fungal:bacterial biomass carbon (F:B) ratio with and without microbial biomass seasonality for representative sites during sampling years

Variable	Biome	Mean (μmol m^{-2} s^{-1})		Range (μmol m^{-2} s^{-1})		Standard deviation (μmol m^{-2} s^{-1})	
		CLM-Microbe	CLM-Microbe_wos	CLM-Microbe	CLM-Microbe_wos	CLM-Microbe	CLM-Microbe_wos
FBC	DST-XJ	12.87	11.40	2.56	0.88	0.63	0.30
	GRS-US	160.16	142.92	13.01	4.61	3.84	1.14
	SHB-NE	154.33	142.10	13.92	7.37	3.80	1.85
	BRF-CA	162.52	125.54	5.75	1.00	1.55	0.26
	TBF-JP	77.45	72.87	6.43	0.48	1.76	0.13
	TCF-US	63.26	58.32	6.69	2.67	1.97	0.82
	TSF-CN	67.40	59.75	12.04	4.24	3.96	1.21
	WET-PY	29.78	27.77	20.68	0.09	6.70	0.02
	TUN-RU	191.70	164.40	1.60	0.06	0.47	0.02
BBC	DST-XJ	3.02	2.71	0.97	0.25	0.24	0.08
	GRS-US	43.77	38.83	5.61	2.09	1.44	0.61
	SHB-NE	45.90	42.47	7.68	3.98	2.13	1.35
	BRF-CA	40.08	30.72	2.57	0.32	0.79	0.08
	TBF-JP	22.57	22.06	7.88	0.42	2.45	0.12
	TCF-US	16.11	15.03	2.36	0.53	0.69	0.13
	TSF-CN	26.06	22.25	5.81	0.89	1.93	0.27
	WET-PY	6.77	6.59	6.84	0.02	2.18	0.01
	TUN-RU	37.42	33.73	0.90	0.34	0.32	0.09
F:B ratio	DST-XJ	4.27	4.20	0.51	0.10	0.14	0.03
	GRS-US	3.66	3.68	0.41	0.29	0.10	0.07
	SHB-NE	3.37	3.35	0.59	0.48	0.19	0.15
	BRF-CA	4.06	4.09	0.16	0.08	0.05	0.02
	TBF-JP	3.46	3.30	0.92	0.06	0.30	0.02
	TCF-US	3.93	3.88	0.46	0.29	0.10	0.08
	TSF-CN	2.59	2.69	0.32	0.29	0.10	0.09
	WET-PY	4.58	4.21	2.34	0.00	0.72	0.00
	TUN-RU	5.12	4.87	0.09	0.05	0.04	0.01

The CLM-Microbe represents the default model simulation with the seasonality of fungal and bacterial biomass; the CLM-Microbe_wos is the model without the seasonality of fungal and bacterial biomass.

To identify the pathways resulting in the shifts in soil microbial biomass and community composition, we examined the C flow in and out of fungal and bacterial biomass pools (Figs. 3.S3-4). Compared with the CLM-Microbe, the CLM-Microbe_wos with constant soil moisture and temperature scalars generally suppressed soil fungal and bacterial C gain from litter decomposition across sites (Figs. 3.S3a and 3.S4a). The decrease in fungal and bacterial C gain from litter decomposition was in different magnitudes among sites, ranging from 0.2% at TBF-JP and 27.8% at BRF-CA for both fungi and bacteria. Similarly, the removal of soil microbial seasonality decreased the DOM uptake by fungi and bacteria across sites, with the magnitude varying among sites (Figs. 3.S3b and 3.S4b). For example, the DOM uptake by fungi and bacteria decreased the most at DST-XJ (34.0% for fungi vs. 34.0% for bacteria) and the least at GRS-US (grassland, GRS-; 2.9% for fungi vs. 3.7% for bacteria). The removal of soil microbial biomass seasonality decreased fungal and bacterial C gain from SOM decomposition, but the magnitude varied among sites (Figs. 3.S3c and 3.S4c). Compared with the CLM-Microbe, the CLM-Microbe_wos simulated declines in fungal and bacterial C gain from SOM decomposition. The decreases of fungal and bacterial C gain were the most at DST-XJ (53.7% for bacteria vs. 51.5% for fungi), BRF-CA (21.8% for bacteria vs. 22.7% for fungi), TSF-CN (20.7% for bacteria vs. 18.7% for fungi), TUN-RU (13.4% for bacteria vs. 14.4% for fungi), and TBF-JP (15.1% for bacteria vs. 14.2% for fungi). The TCF-US (9.5% for bacteria vs. 9.3% for fungi) featured the least fungal and bacterial C gain from SOM decomposition when removing soil microbial biomass seasonality. The removal of soil microbial biomass seasonality generally decreased fungal and bacterial lysis rate, with the least decline at TCF-US (8.2% for bacteria vs. 8.9% for fungi) and most at DST-XJ (37.8% for bacteria vs. 37.9% for fungi) (Figs. 3.S3d and 3.S4d).

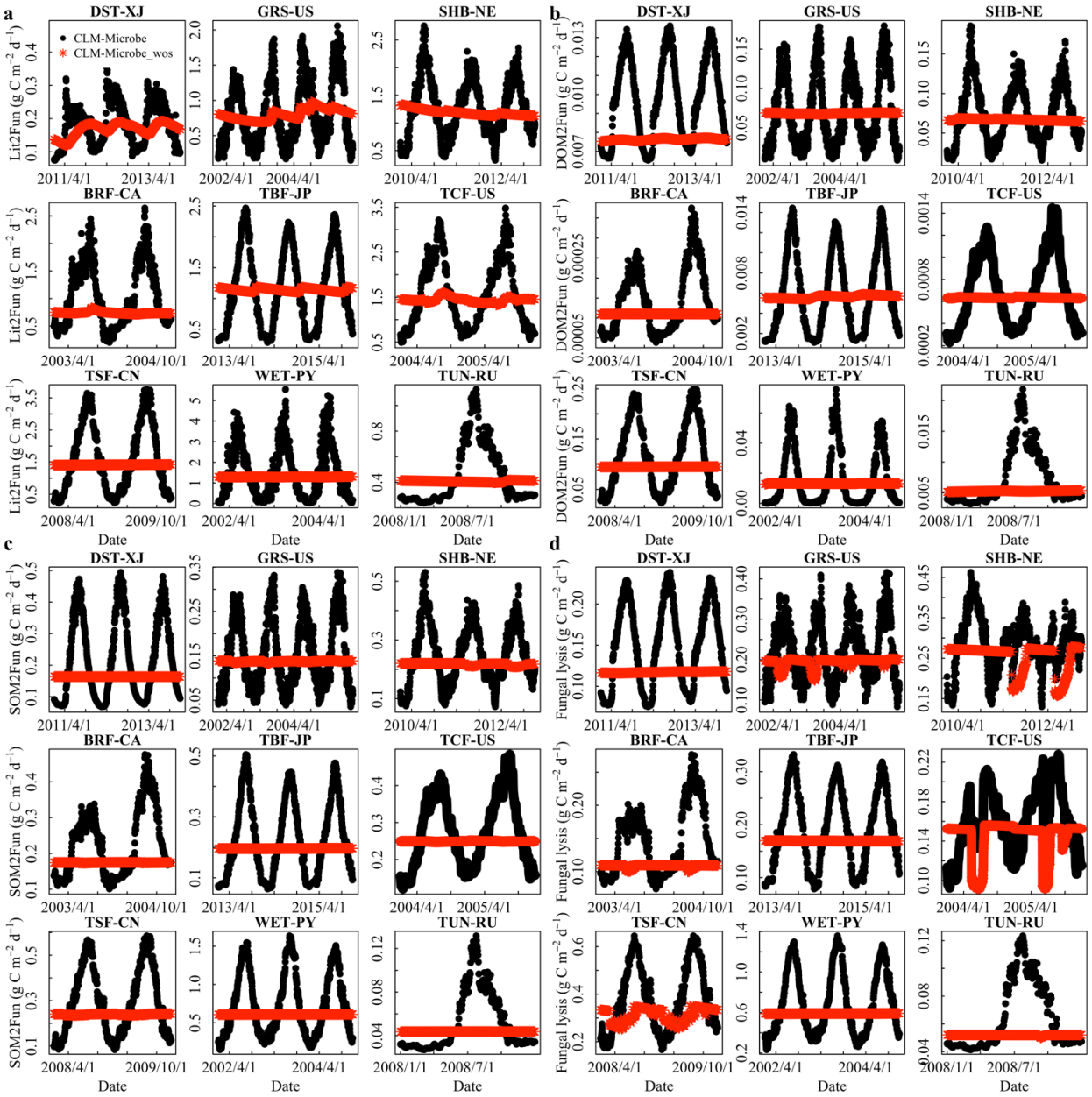

Fig. 3.S3. Simulated a) fungal carbon gain from litter decomposition (Lit2Fun), b) fungal dissolved organic matter uptake (DOM2Fun), c) fungal carbon gain from soil organic matter decomposition (SOM2Fun), and d) fungal lysis under scenarios with and without microbial biomass seasonality for representative sites. The CLM-Microbe represents the default model simulation with the seasonality of fungal and bacterial biomass; the CLM-Microbe_wos is the model without the seasonality of fungal and bacterial biomass.

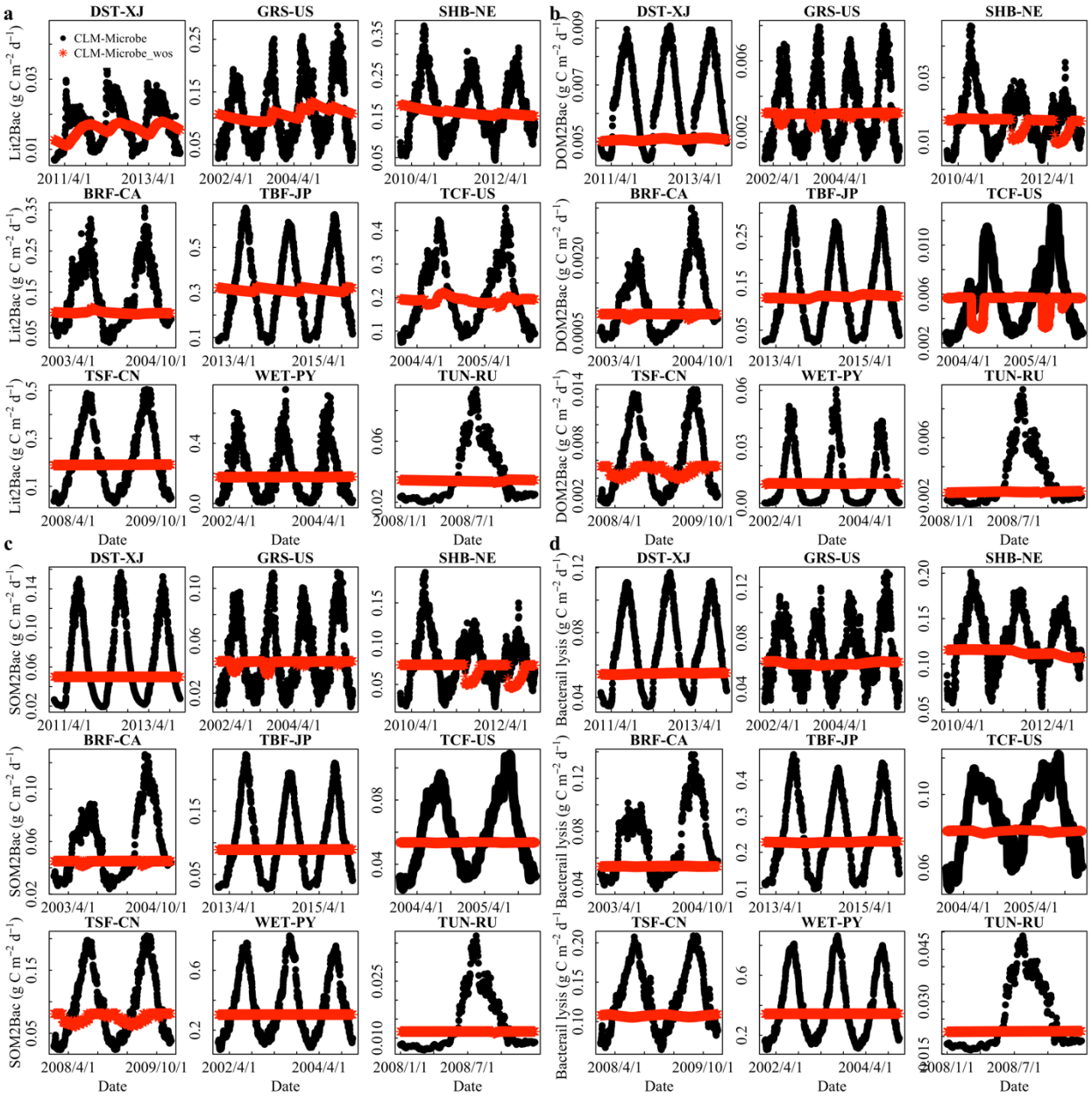

Fig. 3.S4. Simulated a) bacterial carbon gain from litter decomposition (Lit2Bac), b) bacterial dissolved organic matter uptake (DOM2Bac), c) bacterial carbon gain from soil organic matter decomposition (SOM2Bac), and d) bacterial lysis under scenarios with and without microbial biomass seasonality for representative sites. The CLM-Microbe represents the default model simulation with the seasonality of fungal and bacterial biomass; the CLM-Microbe_wos is the model without the seasonality of fungal and bacterial biomass.

Table 3.S4. Statistics of simulated microbial respiration (MR), root respiration (RR), and soil respiration (SR) with and without microbial biomass seasonality for representative sites during sampling years

Variable	Biome	Mean (μmol m^{-2} s^{-1})		Range (μmol m^{-2} s^{-1})		Standard deviation (μmol m^{-2} s^{-1})	
		CLM-Microbe	CLM-Microbe_wos	CLM-Microbe	CLM-Microbe_wos	CLM-Microbe	CLM-Microbe_wos
MR	DST-XJ	0.175	0.173	0.257	0.072	0.058	0.020
	GRS-US	0.930	0.833	2.044	0.286	0.524	0.078
	SHB-NE	1.298	1.224	2.479	0.207	0.524	0.055
	BRF-CA	1.175	0.797	2.892	0.119	0.701	0.021
	TBF-JP	1.394	1.337	2.686	0.095	0.782	0.028
	TCF-US	1.565	1.477	3.035	0.280	0.763	0.059
	TSF-CN	1.688	1.471	3.731	0.017	1.150	0.005
	WET-PY	1.394	1.389	5.276	0.026	1.161	0.007
	TUN-RU	0.446	0.402	0.903	0.032	0.246	0.006
RR	DST-XJ	0.054	0.054	0.348	0.348	0.072	0.072
	GRS-US	0.536	0.468	2.338	1.999	0.445	0.376
	SHB-NE	0.409	0.383	1.071	0.983	0.283	0.264
	BRF-CA	1.324	0.978	11.207	6.707	1.652	1.170
	TBF-JP	0.805	0.805	2.008	2.008	0.764	0.764
	TCF-US	1.257	1.206	2.154	2.104	0.686	0.656
	TSF-CN	1.231	1.192	2.828	2.742	0.776	0.665
	WET-PY	0.548	0.548	1.960	1.958	0.472	0.472
	TUN-RU	0.171	0.150	1.239	1.056	0.332	0.287
SR	DST-XJ	0.229	0.227	0.548	0.415	0.120	0.080
	GRS-US	1.466	1.302	3.842	2.003	0.883	0.373
	SHB-NE	1.706	1.607	3.287	0.964	0.781	0.256
	BRF-CA	2.498	1.775	14.099	6.727	2.307	1.173
	TBF-JP	2.199	2.142	4.590	1.974	1.527	0.740
	TCF-US	2.822	2.683	5.189	2.144	1.423	0.669
	TSF-CN	2.919	2.664	6.531	2.754	1.918	0.666
	WET-PY	1.943	1.937	6.747	1.954	1.531	0.470
	TUN-RU	0.617	0.551	2.094	1.054	0.553	0.284

The CLM-Microbe represents the default model simulation with the seasonality of fungal and bacterial biomass; the CLM-Microbe_wos is the model without the seasonality of fungal and bacterial biomass.

References for supplementary materials in chapter 3

Cherrier, J., J. Bauer, and E. Druffel. 1996. Utilization and turnover of labile dissolved organic matter by bacterial heterotrophs in eastern North Pacific surface waters. Marine Ecology Progress Series **139**:267-279.

Gommers, P. J. F., B. J. v. Schie, J. P. v. Dijken, and J. G. Kuenen. 1988. Biochemical limits to microbial growth yields: An analysis of mixed substrate utilization. Biotechnology and Bioengineering **32**:86-94.

He, L., D. A. Lipson, J. L. M. Rodrigues, M. Mayes, R. G. Björk, B. Glaser, P. Thornton, and X. Xu. 2021. Dynamics of Fungal and Bacterial Biomass Carbon in Natural Ecosystems: Site-level Applications of the CLM-Microbe Model. Journal of Advances in Modeling Earth Systems **13**:e2020MS002283.

Kirchman, D. L., Y. Suzuki, C. Garside, and H. W. Ducklow. 1991. High turnover rates of dissolved organic carbon during a spring phytoplankton bloom. Nature **352**:612-614.

Moore, J. C., K. McCann, and P. C. de Ruiter. 2005. Modeling trophic pathways, nutrient cycling, and dynamic stability in soils. Pedobiologia **49**:499-510.

Rousk, J., and E. Bååth. 2007. Fungal biomass production and turnover in soil estimated using the acetate-in-ergosterol technique. Soil Biology and Biochemistry **39**:2173-2177.

Rousk, J., and E. Bååth. 2011. Growth of saprotrophic fungi and bacteria in soil. FEMS Microbiology Ecology **78**:17-30.

Schippers, A., L. N. Neretin, J. Kallmeyer, T. G. Ferdelman, B. A. Cragg, R. John Parkes, and B. B. Jørgensen. 2005. Prokaryotic cells of the deep sub-seafloor biosphere identified as living bacteria. Nature **433**:861-864.

Sinsabaugh, R. L., S. Manzoni, D. L. Moorhead, and A. Richter. 2013. Carbon use efficiency of microbial communities: stoichiometry, methodology and modelling. Ecology Letters **16**:930-939.

Sinsabaugh, R. L., B. L. Turner, J. M. Talbot, B. G. Waring, J. S. Powers, C. R. Kuske, D. L. Moorhead, and J. J. F. Shah. 2016. Stoichiometry of microbial carbon use efficiency in soils. Ecological Monographs **86**:172-189.

Strickland, M. S., and J. Rousk. 2010. Considering fungal: bacterial dominance in soils–methods, controls, and ecosystem implications. Soil Biology and Biochemistry **42**:1385-1395.

Thornton, P. E., and N. A. Rosenbloom. 2005. Ecosystem model spin-up: Estimating steady state conditions in a coupled terrestrial carbon and nitrogen cycle model. Ecological Modelling **189**:25-48.

Wallander, H. a., H. Göransson, and U. Rosengren. 2004. Production, standing biomass and natural abundance of 15 N and 13 C in ectomycorrhizal mycelia collected at different soil depths in two forest types. Oecologia **139**:89-97.

Wheeler, P. A., M. Gosselin, E. Sherr, D. Thibaultc, D. L. Kirchman, R. Benner, and T. E. Whitledge. 1996. Active cycling of organic carbon in the central Arctic Ocean. Nature **380**:697-699.

Chapter 4. Historical Dynamics of Terrestrial Carbon during 1901-2016 as Simulated by the CLM-Microbe Model

Abstract

Environmental changes have had drastically altered global carbon (C) cycle; however, the role soil microbes play in those alterations remains unclear. In this study, we applied a microbial-explicit model – the CLM-Microbe – to investigate the dynamics of vegetation, litter, soil, and microbial C during 1901-2016. Compared with observations, the CLM-Microbe model was able to reproduce global annual averages and latitudinal trends of gross (GPP) and net (NPP) primary productivity, heterotrophic (HR) and soil (SR) respiration, microbial (MBC), the sum of fungal (FBC) and bacterial (BBC), biomass C in the top 30 cm and 1 m, and dissolved (DOC) and soil (SOC) organic C in the top 30 cm and 1 m. In addition, the CLM-Microbe model can significantly (P<0.05) capture the grid-level variation in GPP (R^2=0.78), NPP (R^2=0.63), SR (R^2=0.26), HR (R^2=0.23), DOC in 0-30 cm (R^2=0.2) and 0-1 m (R^2=0.22), SOC in 0-30 cm (R^2=0.36) and 0-1 m (R^2=0.26), FBC (R^2=0.22) and BBC (R^2=0.32) in 0-30 cm, and MBC in 0-1 m (R^2=0.21). Compared with the 1900s, C fluxes and pool sizes increased by about 30 PgC yr^{-1} for GPP, 15 PgC yr^{-1} for NPP, 12 PgC yr^{-1} for HR, 25 PgC yr^{-1} for SR, 1.0 PgC for FBC and 0.4 PgC for BBC in 0-30 cm, 1.5 PgC for FBC, 0.8 PgC for BBC, 2.5 PgC for DOC, 40 PgC for SOC, and 5 PgC for litter C (LitC) in 0-1 m, and 40 PgC for vegetation C (VegC). Except for DOC in the top 1 m (increased most in Asia and North America), the absolute increases of C fluxes and pools were the largest in Asia and South America, particularly in east Asia and central and northern South America. Relative changes exhibited different spatial patterns: the relative increase was the largest in Asia and Europe, particularly in east Asia and southern and central Europe, for GPP, NPP, HR, and SR, in South America (central and east coast of South America in particular) for FBC (0-30 cm and 0-1 m), in Europe (central and northern Europe in particular) for BBC (0-30 cm and 0-1 m), in Europe (central and northern Europe in particular) and South America (east coast of South America in particular) for DOC (0-1 m), in Arica (central and southern Africa in particular) for SOC (0-1 m), and in Europe (southern and central Europe in

particular) for VegC and LitC (0-1 m). Increases of GPP, NPP, and VegC were closely related to warming and climbing precipitation, while soil C fluxes and litter, microbial, and soil C pools were jointly governed by vegetation C input and soil temperature and moisture. Incorporating microbial roles into the terrestrial C framework assist our mechanistic understanding of the global C cycle and the insightful analysis of microbial roles in the C-climate feedback.

Key words: environmental change, carbon cycle, soil, microbial, temporal trend, global pattern

Introduction

The atmospheric concentration of carbon dioxide (CO_2) has been drastically increased due to fossil fuel combustion, cement production, and land-use change since the Industrial Revolution (IPCC 2001, Lal 2004, 2008, IPCC 2013). The cumulative radiative forcing caused by the enrichment of CO_2 in the atmosphere has led to an increase in the average global surface temperature, known as global warming (IPCC 2001). Meanwhile, the increase in gaseous forms of nitrogen (N) in the atmosphere due to anthropogenic activities, including agriculture and fossil fuel combustion, have accelerated atmospheric N inputs into terrestrial ecosystems (Galloway et al. 2008, Van Damme et al. 2021). The increase in atmospheric CO_2, surface temperature, atmospheric particles, and N deposition has induced cascading environmental issues and disrupted carbon (C) and nutrient cycles (Matson et al. 2002, Meeran et al. 2021, Soong et al. 2021).

Previous studies have assessed the effects of increasing atmospheric CO_2, global mean temperature, and N deposition on the global C cycle using Earth system models (ESMs) (Todd-Brown et al. 2013, Bonan et al. 2019). For example, Bonan et al. (2019) compared vegetation productivity, heterotrophic respiration, and vegetation and soil C stocks in the community land model forced by two climate reconstructions (CRUNCEPv7 and GSWP3v1). These models, however, were developed with the implicit representation

of microbial processes. Given the critical role that soil microorganisms play in soil biogeochemical processes and their sensitivity to environmental changes, their explicit incorporation into models is needed to improve predictions of the global C cycling (Wieder et al. 2013, Wang et al. 2015, Wang et al. 2017, He et al. 2021a). Recently, researchers have applied microbial-explicit ESMs in investigating responses of the global C cycle to environmental change. For example, Wieder et al. (2015) have examined the responses of soil, vegetation, and litter C pools to environmental change using the MIMICS model. Wang et al. (2017) also investigated the impacts of environmental change on enzyme, soil, and microbial biomass C pools in the TRIPLEX-MICROBE model. However, the rough comparison of microbial biomass at global or biome levels as the validation may introduce uncertainties in the model, particularly soil microbial biomass and microbe-mediated processes, which can further affect the soil C cycle in those models.

Fungi and bacteria, the two major soil microbial groups, respond differently to environmental change, and differences in their physiological traits concerning biogeochemical processes have been incorporated into the CLM-Microbe model (He et al. 2021a, He et al. 2021b). Therefore, validating fungal and bacterial biomass in the CLM-Microbe model at fine scales can reduce uncertainties in model predictions. Changes of fungi and bacteria can largely affect soil biogeochemical processes (Hršelová et al. 1999, Bailey et al. 2002, Boer et al. 2005). Predicting changes in the spatial pattern of fungi and bacteria at the global scale and identifying their controls are essential for understanding the impacts of environmental changes on the terrestrial C cycle (e.g., vegetation, litter, soil, and microbes).

To fill the gaps, we investigated the effects of environmental change (climate change, N deposition, rising CO_2, and aerosols) on the global C cycle using the CLM-Microbe model. The CLM-Microbe model, mechanistically representing soil microbial community dynamics by differentiating fungal and bacterial

physiology, provides a feasible way to investigate the effects of environmental change on soil C cycling mediated by soil microbes (He et al. 2021b). This study aimed to examine the effects of environmental changes on the global C cycle from 1901 to 2016. We first evaluated the performance of the CLM-Microbe model in reproducing soil, vegetation, and microbial C variables, including gross (GPP) and net (NPP) primary productivity, fungal (FBC) and bacterial (BBC) biomass C in the top 30 cm and 1 m, heterotrophic (HR) and soil (SR) respiration, and dissolved (DOC) and soil (SOC) organic C in the top 30 cm and 1 m. Then, we investigated the effects of environmental change on the temporal trend of variables related to soil, vegetation, microbial, and litter C, including GPP, NPP, HR, SR, FBC and BBC in the top 30 cm, FBC, BBC, DOC, SOC, and litter C (LitC) in the top 1 m, and vegetation C (VegC), from 1901 to 2016. Finally, we investigated changes in spatial patterns and controls of those fluxes and pools from 1901 to 2016.

Materials and Methods

Model representation of fungal and bacterial biomass

The CLM-Microbe model was built on the model framework developed by Xu et al. (2014) and the default CLM4.5 (hereafter CLM4.5) (Koven et al. 2013), and it has been coupled with a microbial functional group – based methane module (Xu et al. 2015, Wang et al. 2019) and applied to quantify the fugal and bacterial biomass dynamics in natural ecosystems (He et al. 2021b). The CLM4.5 classifies litter into three pools, i.e., litter 1 (labile), litter 2 (cellulose) and litter 3 (lignin), and soil organic matter (SOM), materials left during later stages of organic C decay, into four pools, i.e., SOM 1, SOM 2, SOM 3, and SOM 4 (low-high recalcitrance). The three litter pools and four SOM pools differ in base decomposition rate (τ), with turnover time of litter pools ranging from 20 hours to 71 days and turnover time of SOM pools ranging from 14 days to 27 years (Fig. 4.S1). Coarse woody debris (CWD) is fragmented, decomposed, and gradually transferred into litter pools, and further from litter to SOM pools

(Thornton et al. 2007; Koven et al. 2013). In addition to eight C pools (three litter, four SOM, and CWD pools) in the CLM4.5, we introduced dissolved organic matter (DOM) and fungal and bacterial biomass pools in the CLM-Microbe model. The code for the CLM-Microbe model has been archived at https://github.com/email-clm/clm-microbe. The model version used in this study was checked out on May 1, 2021.

In the CLM-Microbe model, fungal and bacterial biomass are simulated as the balance of C input from the decomposition of SOM, DOM, and litter and C loss through the microbial lysis and microbial respiration. Specifically, fungi and bacteria receive C through the transitions from litter, DOM, and SOM pools; fungi and bacteria lose C through the transitions from fungal and bacterial biomass pools to DOM and SOM pools and the atmosphere. The conceptual diagram of the CLM-Microbe model and major parameters were compiled and displayed in Fig. 4.S1 and Table 4.S1.

The decomposition rates of SOM, DOM, and litter are controlled by both their potential decomposition rates and environmental conditions. The decomposition processes in the CLM-Microbe model are defined following the below equations,

$$D_C = k \times r_{depth} \times r_{tsoil} \times r_{water} \times r_{O_2} \quad \text{equation (1)}$$

$$r_{depth} = \exp\left(-\frac{z}{z_\tau}\right) \quad \text{equation (2)}$$

$$r_{tsoil} = Q_{10}^{\frac{T_{soil,j} - T_{ref}}{10}} \quad \text{equation (3)}$$

$$r_{water} = \begin{cases} 0 & for\ \varphi_j < \varphi_{min} \\ \frac{log\left(\varphi_{min}/\varphi_j\right)}{log\left(\varphi_{min}/\varphi_{max}\right)} & for\ \varphi_{min} \leq \varphi_j \leq \varphi_{max} \\ 1 & for\ \varphi_j > \varphi_{max} \end{cases} \quad \text{equation (4)}$$

$$r_{O_2} = f_r \times (1 - f_{inun}) \times max\left(O_{2_{unsat}}, O_{2_{min}}\right) + f_{inun} \times max\left(O_{2_{sat}}, O_{2_{min}}\right) \quad \text{equation (5)}$$

where D_C is the rate of substrate (e.g., SOM, DOM, and litter) breakdown; k is the potential decomposition rate; r_{O_2} represents the environmental modifier determined by soil oxygen concentration; r_{depth} is the environmental modifier determined by soil depth; r_{water} is environmental modifier determined by soil moisture; r_{tsoil} means the environmental modifier determined by soil temperature; z means soil depth; z_τ is the e-folding depth for decomposition; $T_{soil,\,j}$ is soil temperature at layer j; T_{ref} is the reference temperature for decomposition, which is set as 25°C; Q_{10} indicates the temperature dependence of decomposition, it is the ratio of the rate at a specific temperature to that at 10°C lower; Ψ_j is the soil water potential in layer j; Ψ_{min} is a lower limit for soil water potential control on decomposition rate (set to -10 MPa), r_{water} will be set as 0 if Ψ_j is lower than Ψ_{min}; Ψ_{max} is the upper limit for soil water potential control on decomposition, which equals to the saturated soil matric potential, r_{water} will be set as 1 if Ψ_j is higher than Ψ_{max}; $w_{soil,\,j}$ means soil water content in layer j; f_r is the rooting fraction by soil depth; f_{inun} means the fraction of inundated area; $O_{2_{unsat}}$ represents the oxygen available to that demanded by roots and aerobic microbes in unsaturated area; $O_{2_{min}}$ denotes the ratio between minimum anaerobic decomposition rate and potential aerobic decomposition rate in soil (set to 0.2); $O_{2_{sat}}$ represents the oxygen available to that demanded by roots and aerobic microbes in saturated area; r_{O_2} will be set as 1 in oxic conditions, while it will be estimated as the weighted average of oxygen stress in saturated and unsaturated areas in anoxic conditions.

Bacterial and fungal growth are highly sensitive to environmental conditions, such as soil moisture and temperature. In addition, fungi and bacteria have different turnover times, hence, different lysis rate constants were adopted for fungi and bacteria in the CLM-Microbe model (He et al. 2021b). As a result, in the CLM-Microbe model, fungal and bacterial biomass lysis is mechanistically represented as the interactive effects of their lysis rate constants and environmental factors, i.e., r_{O_2}, r_{water}, r_{tsoil}, and r_{depth}, as

described above. Microbial respiration is widely affected by multiple abiotic and biotic factors, such as substrate concentration and availability, soil moisture, and soil temperature (Gomez-Casanovas et al. 2012, Zhang et al. 2013). Therefore, in the CLM-Microbe model, fungal and bacterial respirations are represented as the interactive effects of substrates (i.e., DOM, SOM, and litter), environmental factors (i.e., r_{O_2}, r_{water}, and r_{tsoil}), and fraction factors quantifying C being respired by fungi and bacteria in transitions (Table 4.S1).

Representation fungal- and bacterial-mediated processes by column

In the CLM-Microbe model, land surface heterogeneity was represented using a hierarchical data structure, which is adapted from the CLM4.5. Each land grid cell can contain multiple land units (e.g., glacier, lake, wetland, urban, vegetated land, and cropland) and each land unit can be further divided into multiple soil/snow columns. On the vegetated land units, multiple (up to 16) plant functional types (PFTs) distinct in physiology and structure from different climate zones (e.g., needleleaf-evergreen-tree-boreal vs. needleleaf-deciduous-tree-boreal, broadleaf-evergreen-tree-tropical vs. broadleaf-deciduous-tree-tropical, and c3-arctic-grass vs. c3-non-arctic-grass) can occupy space on the column. All vegetation fluxes and state variables were defined at the PFT level, while soil fluxes and state variables were defined at the column level.

In the CLM4.5 and early version of the CLM-Microbe model, microbial and decomposition parameters were assumed to be homogenous across data structure levels. Our previous work suggested the differences in microbial processes among biomes (He et al. 2021b), the implicitly accounted sub-grid microbial processes may introduce uncertainties in the estimation of soil and microbial fluxes and state variables. Since soil fluxes and state variables in the CLM-Microbe model are defined at the column level, we represented the heterogeneity of microbial-mediated processes by column. The PFTs, plant

group sharing similar physical, phylogenetic and phenological characteristics, are a good approximation of biomes. We thus assigned the parameter set of microbial properties by PFT. Furthermore, we determined the microbial properties of each column by the relative weight of PFTs occupied on the column, with the parameter set of the most dominant PFT adopted to represent the microbial and soil processes (e.g., fungal and bacterial biomass turnover rate, DOM degradation rate, and fungal and bacterial C assimilation proportion from SOM, litter, and DOM) on the column.

Model forcing data

The forcing data for the CLM-Microbe model include meteorological variables such as air temperature, relative humidity, incoming solar radiation, longwave radiation, precipitation rate, surface pressure, and surface winds. In this study, we used the CRUNCEP dataset to force the CLM-Microbe model, which has been widely used to force the community land model. The CRUNCEP dataset is a combination of two existing datasets, i.e., Climate Research Center timeseries (CRU TS) dataset of 0.5° × 0.5° at monthly scale and the National Centers for Environmental Prediction (NCEP) reanalysis dataset of 2.5° × 2.5° at 6-hourly scale. In the CRUNCEP dataset, the diurnal and daily variation of variables such as the air temperature, precipitation, humidity, solar radiation, surface pressure, downward longwave radiation, and wind speed were derived from NCEP dataset, while their monthly means are bias corrected by the CRU TS dataset. In this study, the CRUNCEP dataset version 7, with a spatial resolution of 0.5° × 0.5°, spanning from 1901 to 2016, was used to drive the model simulation (Viovy 2018). More information about the CRUNCEP dataset version 7 is available at https://rda.ucar.edu/datasets/ds314.3/.

In addition to the meteorological data, we forced the CLM-Microbe model using time-varying CO_2 concentration, N deposition, and aerosol concentration to estimate the C cycle change in the last century, which were provided by NCAR for forcing community land model offline simulations. Atmospheric N

deposition during 1849-2006 with a spatial resolution of 1.25° longitude × 0.9° latitude were applied for all simulations. The CO_2 concentrations remained fixed at 1850 levels (284.7 ppm) for accelerated decomposition and final runs, and followed with transient historical (1849-2006) changes in transient run. The aerosol concentration in accelerated decomposition and final runs for offline simulation was prescribed at 1850 level, while aerosol concentration with a spatial resolution of 1.25° longitude × 0.9° latitude during 1765-2005 was used in transient simulation.

Model implementation

The model implementation was carried out in three stages, with the spatial resolution of the simulations being 2.5° longitude × 1.9° latitude. First, we ran the accelerated decomposition spin-up to allow the system to reach its steady state (Thornton and Rosenbloom 2005, Koven et al. 2013). We set the model simulations to 1200 years for the accelerated decomposition phase. Then, we ran a final spin-up of 100 years to ensure the system was ready for transient simulations during 1850-2016. For the model years of 1850-1900 in transient simulations, we cycled atmospheric forcing during the period 1901-1910 of the CRUNCEP dataset version 7 to force the model. Then, we used the atmospheric data during 1901-2016 of the CRUNCEP dataset version 7 to drive the simulation during the period of 1901-2016. The CLM-Microbe model was initially parameterized by biome, the initial setting for microbial parameters was adopted from He et al. (2021b).

Validation data

Several datasets were employed in this study for model validation. To produce realistic soil conditions in the CLM-Microbe model at the grid level, we used datasets

of SOC in the top 1 m soil profile from the Harmonized World Soil Database (HWSD, https://daac.ornl.gov/cgi-bin/dsviewer.pl?ds_id=1247) at 0.05-degree spatial resolution archived at Oak Ridge National Laboratory and SOC in the top 30 cm from the Global Soil Organic C Map (GSOCmap) version 1.5 at a spatial resolution of 1 km provided by Food and Agriculture Organization of the United Nations, which is available at http://54.229.242.119/GSOCmap/ to validate the SOC in the top 1 m and 30 cm of the CLM-Microbe model, respectively. To guarantee the reasonability of vegetation productivity, GPP and NPP of MODIS gridded datasets with a spatial resolution of 30 seconds during 2000-2015 (http://files.ntsg.umt.edu/data/NTSG_Products/) were used to compare with the simulated GPP and NPP, respectively. To reproduce the soil C emission flux, SR and HR from Global Gridded 1-km Annual Soil Respiration Database (SRDB) version 3 available at Oak Ridge National Laboratory (https://daac.ornl.gov/CMS/guides/CMS_Global_Soil_Respiration.html) were used to validate SR and HR, respectively. For FBC and BBC in the top 30 cm, the dataset of FBC and BBC with a resolution of 0.5 degree obtained from He et al. (2020) were used to validate FBC and BBC in the top 30 cm in the CLM-Microbe model, respectively. Microbial biomass C (MBC), the sum of FBC and BBC, in the top 1 m of the CLM-Microbe model outputs were compared with Xu et al. (2013) for accuracy. The DOC (0-30 cm and 0-1 m) with a resolution of 0.5 degree derived from Guo et al. (2020) were used to compare with that in the top 30 cm and 1 m from the CLM-Microbe output for validation. Ten-year (2000-2009) averages of simulated soil, vegetation, and microbial variables from the CLM-Microbe output were calculated to compare with those from observed datasets previously described.

Taken together, we optimized the model parameters related to plant, soil, microbial processes based on SOC in the top 30 cm from GSOCmap and that in the top 1 m from HWSD dataset, vegetation GPP and NPP from MODIS, SR and HR from SRDB, FBC and BBC (0-30 cm) in He et al. (2020), MBC in Xu et al. (2013), and DOC (0-30 cm and 0-1 m) in Guo et al. (2020). We primarily focused on parameters related to plant photosynthesis (e.g., *flnr*), e-folding depth for decomposition (e.g.,

decomp_depth_efolding) to match the reported GPP, NPP, and SOC in the top 0-30 cm and 1 m. To calibrate the model to fit the observed FBC, BBC, and DOC, we adjusted soil microbial parameters related to microbial (*k_fungi* and *k_bacteria*) and DOC (*k_dom*) turnover, microbial C assimilation efficiency (*m_rf_s1m*, *m_rf_s2m*, *m_rf_s3m*, and *m_rf_s4m*), the proportion of C being released as respiration (*m_batm_f* and *m_fatm_f*), plant C allocation (froot_leaf), and the N concentration of plant tissues (*leafcn* and *frootcn*) to optimize the model simulations of FBC, BBC, MBC, DOC, SR, and HR.

To assess the efficacy of the CLM-Microbe model, the available soil and vegetation variables from the CLM4.5, including GPP, NPP, HR, SR, and SOC in the top 30 cm and 1m, were adopted for comparison. The simulation results during 1850-2014 was forced using GSWP3v1, with environmental changing factors including N deposition and rising CO_2 considered in the historical simulation. The GPP, NPP, HR, SR, and SOC in the top 30 cm and 1m were provided by Climate Data Gateway at National Center for Atmospheric Research (NCAR). The GPP, NPP, HR, SR, and SOC in the top 30 cm and 1m were from CLM land-only release, more details can be found at https://www.earthsystemgrid.org/dataset/ucar.cgd.ccsm4.CLM_LAND_ONLY.html. All variables were at a resolution of 0.9° latitude × 1.25° longitude. The temporal resolutions were different among variables; GPP, NPP, SR, and HR are of a monthly output, whereas SOC (0-30 cm and 0-1 m) are of yearly simulations. Ten-year (2000-2009) averages of the CLM4.5-simulated GPP, NPP, HR, SR, and SOC (0-30 cm and 0-1 m) were calculated to represent the long-term soil and vegetation status and for comparison with observed variables.

Since datasets and model simulations are of different resolutions and 0.5 degree is the most widely used, we used the function of linint2 in NCAR Command Language to interpolate those datasets and model outputs from their original resolutions to 0.5 degree. To make the maps comparable, we used the nibble

and extracted by mask functions provided by ArcGIS version 10.2 (ESRI, Redlands, California, USA) to make all maps consistent in geographical boundary and missing values.

Model evaluation

To evaluate the model performance in capturing the spatial variation in soil and vegetation variables, we compared GPP, NPP, HR, SR, FBC and BBC in the top 30 cm, MBC (0-1 m), and DOC and SOC (0-30 cm and 0-1 m) reported by the observational datasets and simulated averages of these variables during 2000-2009. The coefficient of determination (R^2) was used to evaluate the overall model performance for those variables. R^2, representing the variation in the observations explained by the model, was calculated following the equation as below,

$$R^2 = 1 - \frac{\sum_{i=1}^{N}(y_i - \hat{y}_i)^2}{\sum_{i=1}^{N}(y_i - \bar{y})^2} \qquad \text{equation (6)}$$

where y_i is the observed value; $\hat{y}$ means the simulated value; $\bar{y}$ is the mean of the observed value; N is the number of data points. Higher R^2 values indicate better performance of the model, while lower R^2 values mean the worse model performance and smaller proportion of variation being explained by the model. It is noteworthy that R^2 is not suitable for assessing the goodness-of-fit for datasets with a small sample size (Wang et al. 2015).

Statistical analysis

Due to the non-normality of GPP, NPP, HR, SR, FBC and BBC in the top 30 cm, MBC (0-1 m), and DOC and SOC (0-30 cm and 0-1 m), we performed a 10-base logarithm transformation for robust analyses. To examine the agreement between simulated and observed GPP, NPP, HR, SR, FBC and BBC

in the top 30 cm, MBC (0-1 m), and DOC and SOC (0-30 cm and 0-1 m) at the grid level, we performed linear regression models to examine the consistency between simulated and observed values.

To identify environmental controls of soil, vegetation, litter, and microbial variables, we examined the correlations between vegetation productivity and mean annual temperature (MAT) and precipitation (MAP) and correlations of soil temperature (ST) and moisture (SM) with soil, litter, and microbial variables with respect to their area-weighted averages at the grid level from 1901 to 2016. Considering the consistent but stronger environmental influence on soil and microbial variables in the top 30 cm than in the top 1 m, only correlations between environmental factors and soil and microbial variables in the top 1 m were assessed whether an association exists.

The correlations between environmental factors (e.g., MAP, MAT, SM, and ST) and annual averages of GPP, NPP, HR, SR, VegC, and FBC, BBC, DOC, SOC, and LitC in the top 1m at the global level during 1901-2016 were estimated using the Pearson's correlation. All statistical analyses above were performed and relevant figures (Figs. 4.1-4.8 & 4.14) were plotted using "ggcorrplot" (Kassambara and Kassambara 2019) and "basicTrendline" (Mei et al. 2018) packages in R version 3.5.3 for Mac OS X (https://www.r-project.org).

To estimate the changing rate of GPP, NPP, HR, SR, FBC and BBC in the top 30 cm, FBC, BBC, DOC, LitC, and SOC in the top 1 m, and VegC during 1901-2016, we conducted linear regression models for these variables with time at the grid level, with the changing rate indicated by the slope of the regression model. In addition, correlations between environmental factors (e.g., MAT, MAP, ST, and SM) and vegetation, soil, litter, and microbial variables including GPP, NPP, HR, SR, VegC, FBC, BBC, DOC, SOC, and LitC in the top 1m at the grid level were estimated using Pearson's correlation. Such statistical

analyses were performed using NCAR Command Language (https://www.ncl.ucar.edu). Relevant figures (Figs. 4.9-4.13 & 4.15) were produced using Matlab version 2021b (The MathWorks, Inc.).

Results

Model validation

The CLM-Microbe-model-simulated GPP, NPP, HR, SR, FBC and BBC in the top 30 cm, MBC (0-1 m), DOC (0-30 cm and 0-1 m), and SOC (0-30 cm and 0-1 m) were comparable with observed data with respect to global budget (Table 4.1), latitudinal trend (Fig. 4.1), and individual grid (Fig. 4.3). However, the performance of the CLM-Microbe model in reproducing latitudinal trends varied among variables and with soil depth (Fig. 4.1). The latitudinal trends of both GPP and NPP in the CLM-Microbe model were overestimated at northern latitudes and in equatorial regions, but NPP was underestimated while GPP was well predicted at southern latitudes (Fig. 4.1a-b). The CLM4.5 produced similar latitudinal patterns of GPP and NPP (Fig. 4.2a-b). Both HR and SR in the CLM-Microbe model agreed well with observed data at southern latitudes. Such variables were overestimated in equatorial regions and at middle and high latitudes in the Northern Hemisphere but underestimated at low latitudes in the Northern Hemisphere (Fig. 4.1c-d). The similar latitudinal trends of HR and SR were also observed in the CLM4.5 simulation (Fig. 4.1c-d). Soil pools showed similar latitudinal patterns across soil depths (Fig. 4.1e-k). Specifically, DOC (0-30 cm and 0-1 m) was overestimated in equatorial regions but underestimated in northern temperate regions (Fig. 4.1e-f). Meanwhile, we observed the overestimation of SOC (0-30 cm and 0-1 m) in equatorial and northern high-latitude regions, but underestimation in northern mid-latitude regions (Fig. 4.1g-h). As opposed to the CLM-Microbe model, the CLM4.5 consistently underestimated SOC (0-30 cm and 0-1 m) along latitudes, except for SOC (0-1 m) at latitudes of >60° N. Similarly, both FBC and BBC in the top 30 cm were overestimated in equatorial and at northern high latitudes but underestimated in northern mid-latitude regions (Fig. 4.1i-j). Overall, FBC (0-30 cm) at southern latitudes was well

predicted by the CLM-Microbe model, but BBC (0-30 cm) in that region was underestimated, while MBC (0-1 m) was overestimated across latitudinal gradients (Fig. 4.1k).

At the grid scale, the CLM-Microbe-model-simulated vegetation, soil, and microbial variables were significantly (P<0.05) consistent with the observed values (Fig. 4.3). The CLM4.5 also indicated significant (P<0.05) consistency between simulated and observed vegetation and soil variables (Fig. 4.4). Overall, both the CLM-Microbe model and CLM4.5 performed better at simulating GPP and NPP, while soil variables were relatively worse reproduced. The CLM-Microbe-model-simulated GPP (R^2=0.78) and NPP (R^2=0.63) were significantly and positively related to their observed values (Fig. 4.3a-b). The GPP (R^2=0.76) and NPP (R^2=0.6) in the CLM4.5 were also significantly and positively associated with observed values (Fig. 4.4a-b). The SR tended to be better predicted than HR in both the CLM-Microbe model (R^2=0.26 for SR vs. R^2=0.23 for HR) and the CLM4.5 (R^2=0.27 for SR vs. R^2=0.23 for HR) (Fig. 4.3c-d, Fig. 4.4c-d). The DOC in 0-1 m (R^2=0.22) was slightly better reproduced than in 0-30 cm (R^2=0.2) in the CLM-Microbe model (Fig. 4.3e-f), while both the CLM-Microbe model (R^2=0.36 for 0-30 cm vs. R^2=0.26 for 0-1 m) and CLM4.5 (R^2=0.3 for 0-30 cm vs. R^2=0.24 for 0-1 m) performed better at simulating SOC in the top 30 cm than in the top 1 m (Fig. 4.3g-h, Fig. 4.4e-f). Similarly, the CLM-Microbe model performed better in simulating FBC and BBC in the top 30 cm than MBC in the top 1 m (R^2=0.21) (Fig. 4.3i-k). In addition, BBC (R^2=0.32) was better reproduced than FBC (R^2=0.22) in the top 30 cm.

The CLM-Microbe model and the CLM4.5 overestimated the GPP by 15.7% and 7.3%, respectively (Table 4.1). However, NPP simulated by the CLM-Microbe model and the CLM4.5 was overestimated by 1.3% and underestimated by 8.1%, respectively. Similarly, SR was overestimated in both the CLM-Microbe model (15.6%) and the CLM4.5 (4.0%). While HR in the CLM-Microbe model and the CLM4.5

was overestimated by 1.7% and underestimated by 4.4%, respectively. Both the CLM-Microbe model and the CLM4.5 underestimated SOC (0-30 cm), by 8.5% and 22.4%, respectively, while SOC (0-1 m) in the CLM-Microbe model and the CLM4.5 was overestimated by 32.4% and underestimated by 21.4%, respectively. The FBC, BBC, MBC, and DOC, only available in the CLM-Microbe model, were better predicted in the top 30 cm than 1 m. The simulated FBC, BBC, and DOC in the top 30 cm were underestimated by 3.3% and overestimated by 26.7% and 24.9%, respectively, while MBC and DOC in the top 1m were overestimated by 69.5% and 75.0%, respectively.

Carbon fluxes and pools associated with vegetation, litter, microbes, and soil

The GPP, NPP, HR, and SR displayed increasing trends from 1901 to 2016 (Fig. 4.5). The magnitudes of increase were different among variables. By 2016, GPP (30 PgC yr^{-1}) increased about two times more than NPP (15 PgC yr^{-1}). Similarly, the increase of SR (25 PgC yr^{-1}) was about twice that of HR (12 PgC yr^{-1}) from 1901. Their increasing rates showed variations with time. We observed relatively modest increase in GPP, NPP, HR, and SR during 1901-1980, whereas the increase in GPP, NPP, HR, and SR were more rapid from 1981 to 2016.

Microbial, vegetation, litter, and soil C pools increased from 1901 to 2016 despite the year-to-year variability (Fig. 4.5). The VegC, FBC and BBC in the top 30 cm, and FBC, BBC, DOC, SOC, and LitC in the top 1 m increased by about 40, 1.0, 0.4, 1.5, 0.8, 2.5, 40, and 5 PgC, respectively, from 1901 to 2016. However, the temporal trends of those variables varied during 1901-2016. The VegC and LitC and SOC in the top 1 m showed steady increase during 1901-2016 (Fig. 4.2f-h), while FBC (0-30 cm and 0-1 m) decreased from 1901 to 1940 and increased since 1940 (Fig. 4.2a-b). The BBC (0-30 cm and 0-1 m) exhibited little change through 1901-1940, but increased greatly from 1940-2016 (Fig. 4.2c-d). The DOC (0-1 m) slightly decreased from 1901 to 1920, but increased since 1920 (Fig. 4.2e). Similar to vegetation

and soil C fluxes, vegetation, microbial, soil, and litter C pools showed faster rate of increase during 1981-2016 relative to 1901-1980.

During both 1901-1910 and 2007-2016, the decadal average of soil C (4527 PgC for 1901-1910 and 4564 PgC for 2007-2016) was the largest C pool in the soil-vegetation-litter system, about 15 times of the sum of vegetation (193 PgC for 1901-1910 and 230 PgC for 2007-2016) and litter (63 PgC for 1901-1910 and 68 PgC for 2007-2016) C (Table 4.3). Soil, litter, and vegetation C increased by 2007-2016 relative to 1901-1910. However, the absolute increase in those C pools were different, with soil (37.0 PgC) and vegetation (37.1 PgC) increased to a larger extent than litter (5.1 PgC). Although soil and vegetation increased to a similar extent, vegetation (19.2%) showed a much larger relative increase than soil (0.8%) due to its smaller pool size. Despite the smallest absolute increase, litter (8.0%) showed a larger increase than soil.

Spatial pattern of vegetation and soil carbon fluxes

Compared with 1901-1910, GPP, NPP, HR, and SR increased across latitudinal gradients during 2007-2016 (Fig. 4.7). However, the magnitude of increase differed among latitudinal gradients. Specifically, increases of GPP, NPP, HR, and SR were larger at northern latitudes and equatorial regions than at southern latitudes.

The ten-year averages of GPP, NPP, HR, and SR were distinct among continents during 1901-1910 and 2007-2016 (Table 4.2). However, the ranking of continents by GPP, NPP, HR, and SR were consistent between 1901-1910 and 2007-2016. Asia and South America had the largest GPP, NPP, HR, and SR during both time periods, followed by Africa, North America, and Europe, whereas Australia/Oceania had

the smallest fluxes. The absolute increases of GPP, NPP, HR, and SR from 1901-1910 to 2007-2016 were the largest in Asia and South America, followed by Africa, North America, and Europe. While Australia/Oceania witnessed the smallest absolute increases. Compared with the absolute changes, the relative changes of GPP, NPP, HR, and SR were more similar across continents. Asia and Europe displayed the largest relative changes. While North America, Africa, South America, and Australia/Oceania showed relatively smaller and comparable relative changes.

Across the globe, GPP, NPP, HR, and SR showed similar spatial patterns and evident absolute increases from 1901-1910 to 2007-2016 in east coast of North America, central and northern South America, central Africa, east Asia, and west Europe (Fig. 4.9a-b, d-e, g-h, and j-k). Correspondingly, we observed positive relative change in those regions from 1901-1910 to 2007-2016 (Fig. 4.9c, f, i, and l). The relative change was mostly positive across the globe, with >6.25% in relative change commonly observed and most prominent changes (>50%) in east Asia, southern and central Europe, central Africa, central North America, and east coast of South America. However, we also observed decreases in GPP, NPP, HR, and SR, with prominent negative relative changes found in Middle East (>50%). In addition, we also found subtle negative relative changes in grids of northeast North America.

The GPP, NPP, HR, and SR displayed similar spatial patterns of changing rates (Fig. 4.12a-d). We found the largest positive changing rates of GPP, NPP, HR, and SR in east coast of North America, central and northern South America, central Africa, east Asia, southern and central Europe, and island southeast Asia from 1901 to 2016. In addition, we also found subtle negative changing rates of GPP, NPP, HR, and SR in Greenland, South Asia, and the Sahara.

Spatial pattern of vegetation, litter, microbial, and soil carbon stocks

Similar with vegetation and soil C fluxes, vegetation, soil, microbial, and litter C pools increased across latitudinal gradients during 2007-2016 compared with those during 1901-1910 (Fig. 4.8). Overall, FBC and BBC in the top 30 cm, FBC, BBC, DOC, SOC, and LitC in the top 1 m, and VegC showed small but to a different extent of increase across latitudinal gradients. Specifically, the increases were larger at northern high latitudes and in equatorial regions than at other latitudes.

The FBC and BBC in the top 30 cm and FBC, BBC, DOC, and SOC in the top 1 m were distinct among continents during 1901-1910 and 2007-2016 (Table 4.2). However, the ranking of continents by their pool sizes was consistent between 1901-1910 and 2007-2016. Asia had the largest reservoirs of FBC (0-30 cm and 0-1 m) during both time periods. North America had the second largest FBC (0-30 cm) during both time periods, followed by South America, Africa, and Europe, and Australia/Oceania. The BBC (0-30 cm) were the largest in Asia, followed by North and South America, during both time periods. The BBC (0-30 cm) were the same in Europe and Africa during both time periods. While Australia/Oceania has the smallest and same BBC in the top 1 m during both time periods. The BBC (0-1 m) was the largest in Asia, followed by South America, North America, Africa, and Europe, during both time periods. While BBC (0-1 m) was the smallest and same in Australia/Oceania during both time periods. The DOC and SOC in the top 1 m were the largest in Asia during both time periods, followed by North America. The DOC (0-1 m) was comparable between 1901-1910 and 2007-2016 in Europe and South America, but not SOC (0-1 m). The DOC and SOC in the top 1 m were the second smallest in Africa and the smallest in Australia/Oceania. While Asia and South America had the largest ten-year averages of VegC and LitC (0-1 m) during both time periods, followed by Africa, North America, and Europe. While such pools were the smallest in Australia/Oceania during both time periods.

The FBC and BBC in the top 30 cm and FBC, BBC, DOC, and SOC in the top 1 m widely increased from 1901-1910 to 2007-2016 across continents (Table 4.2). However, we also found slight decreases of FBC (0-1 m) in Europe and decreases of FBC and BBC in the top 30 cm and 1 m and DOC (0-1 m) in Australia/Oceania. The absolute increase of FBC (0-30 cm and 0-1 m) were the largest in Asia and South America, followed by North America and Africa. The smallest absolute increase of FBC (0-30 cm) was observed in Europe. Similarly, the absolute increase of BBC (0-30 cm and 0-1 m) was the largest in Asia and South America, followed by North America, Europe, and Africa. The absolute increases in DOC and SOC in the top 1 m were the largest in Asia. However, the absolute increase in DOC (0-1 m) was the second largest in North America, followed by South America, Europe, and Africa, whereas that of SOC (0-1 m) in South America was the second largest, followed by Europe, Africa, and North America. Australia/Oceania had the smallest increase of SOC (0-1 m). The absolute increases of VegC and LitC (0-1 m) were the largest in South America and Asia, followed by North America, Africa, and Europe, whereas Australia/Oceania witnessed the smallest absolute change of VegC and LitC (0-1 m).

In contrast to the absolute changes, the magnitude of relative changes of FBC and BBC in the top 30 cm and FBC, BBC, DOC, and SOC in the top 1 m were similar from 1901-1910 to 2007-2016 (Table 4.2). The largest relative increases of FBC (0-30 cm and 0-1 m) were in South America, whereas that of BBC (0-30 cm and 0-1 m) were in Europe. The second largest relative change in FBC (0-1 m) was in Africa, while the second largest relative change in BBC (0-30 cm and 0-1 m) were found in Africa and South America. Relative changes in FBC (0-30 cm) were comparable among Asia, North America, Europe, and Africa. Asia and North America were similar in the magnitude of relative changes in FBC (0-1 m) and BBC (0-30 cm and 0-1 m). The relative change of DOC (0-1 m) was largest in Europe and South America. Such changes were of a similar magnitude among Asia, North America, and Africa, while the largest relative increase of SOC (0-1 m) was in Africa, followed by Europe, South America, and Australia/Oceania. Such relative increases were comparable between Asia and North America for SOC

(0-1 m). The relative changes of VegC and LitC (0-1 m) were to a similar extent. Europe displayed the largest relative changes in VegC and LitC (0-1 m), while Asia, North America, Africa, South America, and Australia/Oceania showed relatively smaller and comparable relative increases of VegC and LitC (0-1 m).

At the global scale, FBC and BBC in the top 30 cm and 1 m showed similar spatial patterns and widely increased from 1901-1910 to 2007-2016 (Fig. 4.10a-b, d-e, g-h, and j-k). For example, we found higher increases of FBC and BBC in the top 30 cm and 1 m at northern high latitudes of Europe and Asia, central and northern South America, east coast of South America, and central Africa. Correspondingly, we observed positive relative changes of FBC and BBC in the top 30 cm and 1 m in such regions from 1901-1910 to 2007-2016 (Fig. 4.10c, f, i, and l). Similarly, positive relative changes of FBC and BBC in the top 30 cm and 1 m were widely observed across the globe, with most prominent changes (>50%) in east Asia, central and northern Europe, and central North America. However, we also observed negative relative changes in FBC and BBC in the top 30 cm and 1 m. The largest relative decreases (>50%) were found in southern Europe and central North America. In addition, we also found grids with negative relative changes in FBC and BBC in the top 30 cm and 1 m in South Asia, southern Australia/Oceania, central Africa, and central South America.

Similarly, DOC (0-1 m) showed higher increases in central and northern Europe, east and northern Asia, east coast of South Africa, central and northern South America, and central and southern Africa from 1901-1910 to 2007-2016 (Fig. 4.11a-b). The relative changes in DOC (0-1 m) also suggested positive values in those regions from 1901-1910 to 2007-2016 (Fig. 4.11c). Positive relative changes in DOC (0-1 m) were commonly found across the globe, with most prominent changes (>50%) in east Asia, central and northern Europe, central North America, and east coast of South America. However, we also

observed negative relative changes in DOC (0-1 m) in South Asia, southern Europe, central and southern North America, southern Australia/Oceania, and central Africa. We also widely observed increases in SOC (0-1 m) by 2007-2016 relative to 1901-1910 (Fig. 4.11d-e). The highest relative increases were found in east Asia and central and northern South America, while South Asia displayed decreases in SOC (0-1 m) (Fig. 4.11f). The VegC and LitC (0-1 m) exhibited similar spatial patterns and widely increased across the globe (Fig. 4.11g-l). The most distinct absolute increases of such variables were in west North America, east Asia, central and northern South America. The relative change in both VegC and LitC (0-1 m) were mostly positive across the globe, but the magnitudes were different. The most prominent increases of VegC and LitC in the top 1 m were in central Europe, east Asia, central and northern South America, and central North America. However, the relative change of VegC was to a larger extent than of LitC (0-1 m). Despite the widely increase, both VegC and LitC (0-1 m) decreased in South Asia.

The FBC and BBC in the top 30 cm, DOC, SOC, and LitC of top1 m, and VegC showed similar spatial patterns of changing rates (Fig. 4.13a-h). Increasing temporal trends of such variables were widely observed across the globe, but weak decreasing trends were also found in Greenland, the Sahara, South Asia, and southern Australia/Oceania. However, the distribution of fastest increasing rates was different among variables. Grids with fastest increasing rates of FBC and BBC in the top 30 cm and 1 m were at northern latitudes of Northern America and Asia, east Asia, central and northern South America, and central Africa, and island southeast Asia (Fig. 4.13a-d). Similarly, DOC in the top 1 m showed the fastest increasing rates at northern latitudes of Northern America and Asia, east Asia, and some grids along the east coast of South America (Fig. 4.13e). Spatial patterns of SOC and LitC in the top 1 m and VegC changing rates were similar (Fig. 4.13f-h). The fastest increasing rates of such variables were observed in east coast of North America, central and northern Europe, east Asia, island southeast Asia, central and northern South America, and central Africa.

Environmental controls on C cycling

The area-weighted average of GPP, NPP, and VegC were significantly correlated with that of MAT and MAP (Fig. 4.14a). However, the strength of correlations varied, with MAT associated correlations stronger than MAP associated ones. The area-weighted MAP and MAT had widely significant correlations with GPP, NPP, and VegC, and the spatial patterns of those correlations were similar among GPP, NPP, and VegC. However, the spatial patterns of correlations with MAT were different with those with MAP (Fig. 4.15). The significant positive correlations of MAT with GPP, NPP, and VegC were found at middle and high latitudes of North America, Europe, and Asia, central Africa, east coast of South America, and southern edge of Asia, South America, and Australia/Oceania (Fig. 4.15a, c, and e). In addition, we also found significant negative correlations of MAT with GPP, NPP, and VegC in southeast North America, South Asia, southern Africa, and central and northern Australia/Oceania. Despite the similar spatial pattern, there were differences in the strengths and signs of those correlations. For example, both GPP and VegC had significant correlations with MAT in northeast South America, while correlations between NPP and MAT were weak negative in such regions. The GPP and NPP showed significant negative correlations with MAT in northwest South America, but the correlation between MAT and VegC was weak (P>0.05). In addition, GPP and NPP showed significant positive correlations with MAT in central Africa, while the correlation between VegC and MAT was weak in that area (P>0.05).

Significant positive correlations of GPP, NPP, and VegC with MAP were also widely found (Fig. 4.15b, d, and f). However, we also found weak negative correlations in some grids in northern and east edge of Asia and central Africa. In addition, although correlations of MAP with GPP, NPP, and VegC were similar in spatial patterns, correlations with GPP and NPP tended to be stronger than with VegC. For example, strong (r>0.5) correlations of MAP with GPP and NPP were commonly observed across the

globe, while the proportion of grids with strong correlations were to a lesser extent for VegC in central Australia/Oceania and southern Africa.

The area-weighted average of HR, SR, and FBC, BBC, DOC, SOC, and LitC in the top 1 m were significantly correlated with that of ST and SM in the top 1 m (Fig. 4.14b). However, the strengths of correlations depended on both environmental controls (ST and SM) and variables (HR, SR, FBC, BBC, DOC, SOC, and LitC in the top 1 m). For example, correlations of HR and SR with ST and SM in the top 1 m were of the same magnitude, while the FBC, BBC, DOC, SOC, and LitC were more strongly correlated with ST than with SM in the top 1 m.

In contrast, soil, litter, and microbial variables were more widely and positively correlated to ST than SM in the top 1 m (Fig. 4.16). Correlations of ST (0-1 m) with HR and SR were similar in spatial pattern. We observed significant positive correlations of HR and SR with ST (0-1 m) at middle and high latitudes of North America, Europe, and Asia, central Africa, northeast South America, and southern edge of Asia, South America, and Australia/Oceania (Fig. 4.16a and c). While negative correlations of HR and SR with ST (0-1 m) were found in southwest Asia, southeast North America, central North America, central Africa, and central and northern Australia/Oceania. The FBC, BBC, DOC, and SOC in the top 1 m displayed similar spatial patterns (Fig. 4.16e, g, i, and k). We found significant and positive correlations of FBC, BBC, DOC, and SOC with ST in the top 1 m at middle and high latitudes of North America, Europe, and Asia, central Africa, northeast South America, and southern edge of Asia, South America, and Australia/Oceania. In addition, we also found some girds with negatives correlations scatterly distributed in central North America, Europe, Asia, South America, Africa, and Australia/Oceania. In contrast, correlations between LitC and ST in the top 1 m were equally found for being positive and negative (Fig. 4.16m). Significant positive correlations were observed in central Europe and Asia,

northeast South America, central and east coast of Africa, and southern and central Australia/Oceania. While significant negative correlations distributed in northeast Asia.

Correlations of HR, SR, and FBC, BBC, DOC, and SOC with SM in the top 1 m were similar in spatial patterns, with significant and positive correlations observed at high latitudes in North America, Europe, and Asia, some grids of central Africa, and central and northern Australia/Oceania and negative correlations at middle and low latitudes in North America, Europe, and Asia, east coast of South America and Africa, and southern Australia/Oceania (Fig. 4.16b, d, f, h, j, and l). In contrast, correlations between LitC and SM in the top 1 m were mostly negative, which reached the significance level of 0.05 at high latitudes of North America, Asia, and northwest Asia, southern and central Africa, and southern Australia/Oceania (Fig. 4.16n). In addition, some grids with significant and positive correlation coefficients were scattered throughout central Africa, southwest Asia, and central and northern Australia/Oceania.

Discussion

Comparison with previous studies

The CLM-Microbe model can well reproduce the latitudinal trends and grid-level distribution of GPP, NPP, HR, and SR (subfigures a-d of Figs. 4.1 and 4.3). Compared with the CLM4.5, the CLM-Microbe model was comparable or better at simulating the distribution of GPP, NPP, HR, and SR (subfigures a-d of Figs. 4.2 and 4.4). Plotting against the observational data, the CLM-Microbe model showed good performance in simulating GPP (R^2=0.78; P<0.0001) and NPP (R^2=0.63; P<0.0001) (Fig. 4.3a-b). Although the performance in simulating HR (R^2=0.23; P<0.0001) and SR (R^2=0.26; P<0.0001) was relatively poor (Fig. 4.3c-d), the model efficacy was comparable with that of the CLM4.5 (R^2=0.23;

P<0.0001 for HR and R^2=0.27; P<0.0001 for SR) (Fig. 4.4c-d). In line with our results, multiple models have reported the well-captured spatial variation of GPP, NPP, HR, and SR by ESMs (Kim et al. 2019, Delire et al. 2020, Zheng et al. 2020, Wiltshire et al. 2021). This may be due to the explicit representation of plant physiology and soil processes and their environmental control in the model (Mathieu and O'Neill 2008, Flato 2011).

The latitudinal trends and grid-level distribution of FBC and BBC in the top 30 cm and FBC, BBC, DOC, and SOC in the top 1 m were well-reproduced in the CLM-Microbe model (subfigures e-k of Figs. 4.1 and 4.3). Compared with the CLM4.5 (R^2=0.3 for 0-30 cm and R^2=0.24 for 0-1 m), the CLM-Microbe model performed better in simulating SOC in 0-30 cm (R^2=0.36) and 0-1 m (R^2=0.26) (Fig. 4.3g-h, Fig. 4.4e-f). In line with our results, Wieder et al. (2015) also reported a high spatial correlation (r = 0.46) of SOC (0-1 m) between MIMICS outputs and HWSD. In addition, Wang et al. (2017) observed the high consistency in SOC (0-1 m) (R^2=0.96; P<0.01) between the TRIPLEX-MICROBE model and HWSD by vegetation type. The well-developed soil biogeochemical module in those ESMs may explain the good performance of such models. However, the latitudinal trends and grid-level distribution of DOC, SOC, and MBC (sum of FBC and BBC) in the top 1 m were relatively worse reproduced than those in the top 30 cm (subfigures e-k of Figs. 4.1 and 4.3, subfigures e-f of Figs. 4.2 and 4.4), indicating that the vertical distribution of processes related to decomposition, microbial turnover, and plant C input needs further improvements. Although parameters classifying the active decomposition depth and biological function to perturbation were defined in the CLM-Microbe model, the gradual change of microbial turnover and activity defined along soil profile may need to be improved in future models (Preusser et al. 2019, Zhu et al. 2021). In addition, processes or parameters related to the active layer for decomposition and perturbation caused by biological (e.g., nematode) and abiotic (e.g., drying and rewetting) activities can cause uncertainties in the vertical distribution of C cycle, which needs further efforts and attention in

model development (Ettema and Wardle 2002, Gabet et al. 2003, Kuzyakov and Blagodatskaya 2015, Schimel 2018).

We estimated global annual averages of 129.5, 56.5, 99.8, and 49.8 PgC yr^{-1} for GPP, NPP, HR, and SR, respectively (Table 4.1). Consistent with our results, previous studies suggested similar simulations of GPP, NPP, HR, and SR (Cramer et al. 1999, Nemani et al. 2003, Hashimoto et al. 2015, Zhao et al. 2017, Huang et al. 2020, Zheng et al. 2020, Lu et al. 2021). The consistent simulation and good estimation of GPP, NPP, HR, and SR across model may indicate the convergent and well-defined plant physiology and soil processes in models. In addition, when comparing with observed data, the CLM-Microbe model produced more consistent NPP and HR but overestimated GPP and SR (Table 4.1). The overestimation of GPP and SR may be due to the lower ecosystem-scale C use efficiency (CUE) in the CLM-Microbe model. The vegetation physiology module in the CLM-Microbe model is adapted from CLM4.5. The ecosystem-scale CUEs between the CLM-Microbe model (0.44) and the CLM4.5 (0.43) were comparable, but lower than in MODIS (0.5). Correspondingly, we observed higher contribution of roots to total SR in the CLM-Microbe model (0.5) and the CLM4.5 (0.48) than in the observed SRDB dataset (0.43). Therefore, the well simulated NPP and HR but higher predicted GPP and SR in the CLM-Microbe model was attributed to the low ecosystem-scale CUE in the CLM-Microbe. Increasing ecosystem-scale CUE in the CLM-Microbe model will improve the modeling performance of GPP and SR in model development.

We estimated the global budget of FBC, BBC, and DOC in the top 30 cm and MBC and DOC in the top 1 m as 13.1, 4.2, 8.9, 40.2, and 22.6, respectively (Table 4.1). Compared with observed data, the CLM-Microbe model can reasonably predict FBC, BBC, and DOC in the top 30 cm well at the global level, indicating the well-represented microbial processes in surface soils. However, MBC and DOC in the top

1m were largely overestimated, with MBC and DOC in the top 1 m overestimated by 69.5% and 75.0%, respectively. Inconsistent with our results, previous studies suggested the underestimation of MBC (0-1 m). For example, Wang et al. (2017) estimated the global MBC as 21 Pg C. Wieder et al. (2015) suggested the steady-state MBC (0-1 m) of 16.3 Pg C in MIMICS. The relatively poor performance of the CLM-Microbe model in simulating DOC and MBC in the top 1 m and the discrepancy in MBC (0-1 m) among studies may result from several reasons. First, the active layer for decomposition in the CLM-Microbe model may not be sufficient to define soil microbial processes along soil profile. We observed better performance of the CLM-Microbe model in simulating FBC, BBC, and DOC in the top 30 cm relative to MBC and DOC in the top 1 m, indicating that the representation of microbial and soil processes along soil profile may need improvements. Second, the difference in calibration for MBC may cause the discrepancy between studies. The SOC in Wieder et al. (2015) was calibrated to observed data but not MBC, Wang et al. (2017) calibrated the MBC (0-1 m) in the TRIPLEX-MICROBE by vegetation type, while we calibrated both MBC (0-30 cm and 0-1 m) by grid in the CLM-Microbe model. The differences in variables and depths calibrated between studies can partly explain the difference. Third, the difference in simulated vegetation, litter, and soil C pools among studies can result in the discrepancy. Vegetation C as litter and volatile C input, DOC, and SOC are the C source for microbial C assimilation through decomposition (Fig. 4.S1). Consequently, the overestimation of SOC and DOC can partly explain the overestimation of MBC in the top 1 m (Table 4.1).

The CLM-Microbe model suggested pool sizes of 605.3 PgC in 0-30 cm and 1630.9 PgC in 0-1 m, indicating an underestimation of 8.5% for SOC (0-30 cm) and an overestimation of 32.4% for SOC (0-1 m) when comparing with observed data (Table 4.1). Compared with the CLM4.5, the CLM-Microbe predicted larger stocks of SOC (0-30 cm and 0-1 m). Previous studies suggest large variations in simulated SOC (0-1 m) among models. For example, Todd-Brown et al. (2013) reported the SOC (0-1 m) stock ranging from 510 to 3040 Pg C among 11 CMIP5 ESMs. The TRIPLEX-MICROBE modeled the

global SOC (0-1 m) stock as 1195 Pg C (Wang et al. 2017). Wieder et al. (2015) documented the steady-state SOC pool in the MIMICS as 1530 Pg C. Delire et al. (2020) reported the SOC (0-1 m) as 1611 PgC and 1520 PgC in the new (ISBA_bgc6) and old (ISBA_bgc5) versions, respectively, of ISBA-CTRIP. Given the wide range (510 to 3040 Pg C) of simulated SOC (0-1 m) in models, the CLM-Microbe model thus predicted reasonable SOC stocks.

Temporal trends of carbon fluxes and stocks

The area-weighted average of GPP, NPP, HR, and SR in the CLM-Microbe model increased by about 30, 15, 12, and 25 PgC yr^{-1}, respectively, from 1901 to 2016 (Fig. 4.5). Consistent with our findings, Wiltshire et al. (2021) also observed the increasing trends of GPP and NPP in the JULES model, with GPP and NPP increased by about 12 and 25 PgC yr^{-1} from 1901 to 2005. Bonan et al. (2019) observed the increase of about 20 PgC yr^{-1} of GPP, 10 PgC yr^{-1} of NPP, and 8 PgC yr^{-1} of HR in the CLM4.5 forced using CRUNCEP dataset from 1850 to 2014. The global increasing rate of SR was estimated as 0.04-0.14 Pg C $year^{-1}$ by Huang et al. (2020). Temperature, water, CO_2 concentration, and N are key factors determining plant photosynthesis, the increasing N deposition and rising CO_2 concentration and temperature may explain the enhancement of vegetation productivity under environmental change (Piñeiro et al. 2017, Dusenge et al. 2019). In this study, we observed significant and positive correlations of GPP and NPP with MAT and MAP (Fig. 4.S2a). Although the compounding effects of such environmental change factors also have positive effects on autotrophic respiration, but to a lesser extent, leading to increasing vegetation productivity in terrestrial ecosystems (Delire et al. 2020). Since ST (0-1 m) is positively correlated to HR, the rising ST (0-1 m) may explain the observed increase in HR (Fig. 4.14, Fig. 4.S2b). The increase of HR can partly explain the rising SR from 1901 to 2016 given its critical contribution to SR. In addition to HR, the increase in root respiration (RR) due to increasing C availability and rising temperature accounted for a crucial proportion of the SR increase (Bond-Lamberty and Thomson 2010, Hashimoto et al. 2015, Zhou et al. 2016, Piñeiro et al. 2017). Therefore, the increase

of GPP and NPP can be associated with environmental change (e.g., rising MAP and MAT), such increase of GPP and NPP together with rising ST and SM in the top 1 m enhanced HR and SR in the last century. Similar with GPP and NPP, by 2007-2016, both LitC (0-1 m) (5 PgC) and VegC (40 PgC) increased (Fig. 4.6g-h), which is consistent with previous study (Bonan et al. 2019). VegC indicates the C stock of vegetation biomass, while LitC is the C loss of vegetation biomass. Increasing water availability and temperature usually have negative impacts on maintenance of vegetation biomass and litter in the soil (Delire et al. 2020), while we observed positive correlations of VegC with MAT and MAP and of LitC with SM and ST in the top 1 m (Fig. 4.14). Therefore, the increase in GPP and NPP is primarily responsible for the increase of LitC (0-1 m) and VegC in the last century.

The area-weighted FBC and BBC in 0-30 cm increased by 1.0 and 0.4 PgC yr^{-1} and those in 0-1 m increased by 1.5 and 0.8 PgC yr^{-1}, respectively, in the CLM-Microbe model from 1901 to 2016 (Fig. 4.6a-d). In addition, both DOC (2.5 PgC) and SOC (40 PgC) in the top 1 m increased from 1901 to 2016 (Fig. 4.6e-f). Similarly, Bonan et al. (2019) also observed the increase of SOC (0-1 m) by about 30 PgC from 1850 to 2014 in the CLM4.5 forced using CRUNCEP dataset. Rising temperature has negative impacts on fungal and bacterial biomass due to its facilitating effects on microbial turnover (He and Xu 2021). Meanwhile, the observed increase in FBC and BBC in the top 30 cm and 1 m in the CLM-Microbe model, indicating the higher decomposition potential of soil microbial community (Fig. 4.S1). In addition, rising temperature and water availability promotes microbial decomposition (Wardle and Parkinson 1990, Qiu et al. 2005, Allison et al. 2010). Despite those negative impacts on microbial biomass maintenance and SOC stabilization, we observed increases in microbial and soil C pools from 1901 to 2016. Vegetation provides the major C source for soil C formation; therefore, increases in GPP and NPP can explain the increasing trends of soil C pools during 1901-2016. Litter, SOM, and DOC are three C sources for soil microbes in the CLM-Microbe model (Materials and Methods; Fig. 4.S1). The positive

temporal trends of DOC, LitC, and SOC can explain the increase in FBC and BBC in the CLM-Microbe model (Fig. 4.6).

The annual averages of fluxes (GPP, NPP, HR, and SR) and pools (FBC, BBC, DOC, LitC, and SOC in the top 1 m and VegC) exhibited more rapid increases since year 1980 (Fig. 4.5-6). Concurrently, we observed more rapid increase in MAT, MAP, and ST and SM in the top 1 m since year 1980 (Fig. 4.S2). In line with this study, Cheng et al. (2017) analyzed SM simulations during historical (1920–2005) and future (2006–2080) periods in the Community Earth System Model from CIMP5, they also found 1980 as a transition for a subsequent increase of variation during 1920-2005, indicating more rapid changes in SM after 1980. We observed significant associations of GPP, NPP, and VegC with MAT and MAP (Fig. 4.14a) and of HR, SR, and FBC, BBC, DOC, LitC, and SOC with ST and SM in the top 1 m (Fig. 4.14b). Therefore, more rapid increases in MAT, MAP, and ST and SM in the top 1 m after 1980 may explain the more rapid increases of such variables since year 1980.

Changes in carbon fluxes and stocks over the space and their controls

The GPP and NPP increased across latitudinal gradients and over continents from 1901-1910 to 2007-2016 (Fig. 4.7a-b, Table 4.2; Fig. 4.9a-f, Fig. 4.12a-b). Across the globe, absolute increases of GPP and NPP were the largest in Asia (particularly east Asia) and South America (particularly central and northern South America), while relative increases of GPP and NPP were the largest in Asia (particularly east Asia) and Europe (particularly southern Europe) at the continental scale (Table 4.2; Fig. 4.9a-f, Fig. 4.12a-b). Their largest increase of GPP and NPP was evidenced by the fastest increasing rate of GPP and NPP in those areas (Fig. 4.12a-b). The grids with fast increasing rate of GPP and NPP and the higher number of such grids were responsible for the largest absolute increase of GPP and NPP in Asia and South America. While grids with fast increasing rate of GPP and NPP and the higher proportion of such grids can explain

the largest relative increase of GPP and NPP in Asia and Europe. In line with this study, Zheng et al. (2020) reported that GPP in vegetated areas, particularly in temperate and humid regions (e.g., most of Asia and central and southern Africa), increased in the revised EC-LUE model from 1982 to 2017. Yue et al. (2015) observed distinguishing increases of GPP and NPP in central Africa, the Amazon, Europe, east Asia, and North America in the YIBs model. The broad increase of vegetation productivity may be due to the positive effects of elevated CO_2 and N deposition (Zheng et al. 2020). In addition, temperature and water availability have profound influence on plant growth and land C fluxes (Yue et al. 2015, Zheng et al. 2020). Our results showed significant correlations of GPP and NPP with MAT and MAP (Fig. 4.15a-d). The widely increase in MAP and MAT can partly explain the increase in GPP and NPP along latitudes and over continents (Fig. 4.S3a-b). Large increases in east Asia, central and northern South America, and southern Europe may be related to changes in MAT and MAP, considering their significant correlations from 1901-1910 to 2007-2016 (Fig. 4.S3a-b). Given the significant positive correlations of GPP and NPP with MAT and MAP in southern Europe, the large relative increase of GPP and NPP may be associated with the increasing MAT and MAP in that area. However, correlations of GPP and NPP with MAT and MAP varied with latitude in Asia, correlations of GPP and NPP with MAT and MAP were significant and positive at middle and high latitudes, but negative at low latitudes. Therefore, increases of GPP and NPP at middle and high latitudes may be related to rising MAT and those at low latitudes were associated with decreasing MAP. In central and northern South America, correlations between GPP and NPP and MAT and MAP were complex. Correlations of GPP and NPP with MAT were not consistent in such area, while GPP and NPP were consistently and positively correlated with MAP in central and northern South America. As a result, the increase of GPP and NPP in central and northern South America may be related to the increasing MAP. In addition, we also observed decreases of GPP and NPP in Middle East (Fig. 4.9a-f). The decreases of GPP and NPP can be explained by the increases in MAT and decreases in MAP (Fig. 4.15a-d, Fig. 4.S3a-b). In contrast to our results, Zheng et al. (2020) observed decreased GPP in tropical regions such as the Amazon Forest using the revised EC-LUE model. In addition to CO_2, N deposition, and meteorology, vegetation cover and type play an important role on GPP (Zheng et al.

2020). Land use and land cover change due to management practices have substantial effects on plant growth, such effects on leaf area index were considered in the revised EC-LUE model but not in our simulation. Therefore, the discrepancy between studies may be caused by land-use effects.

The HR and SR showed a widely increase from 1901-1910 to 2007-2016 along latitude, across the globe, and over continents (Table 4.2; Fig. 4.7c-d, Fig. 4.9k-l, Fig. 4.12c-d). Consistent with our findings, Huang et al. (2020) observed a globally significant increase of SR, particularly in boreal and tropical regions (e.g., northern Asia, central South America, and central and southern Africa) from 2000 to 2014. Bond-Lamberty et al. (2018) also observed the increase of HR in multiple biomes during 2000-2015. In addition, we observed the largest absolute increase of HR and SR in Asia and South America (e.g., east Asia and central and northern South America) and relative increase the largest in Asia and Europe (e.g., east Asia and southern and central Europe) at the continental scale, which was similar with GPP and NPP (Table 4.2; Fig. 4.9k-l, Fig. 4.12c-d). These results indicated that soil C fluxes were largely dependent on vegetation productivity, which can enhance soil C fluxes due to higher C allocation to belowground (Pendall et al. 2004, Prescott et al. 2020). Furthermore, soil C fluxes can be further increased due to facilitated decomposition in a warming world (Zhou et al. 2007, Noh et al. 2017). Temperature and water availability have profound influence on root respiration and HR (Bond-Lamberty and Thomson 2010, Hashimoto et al. 2015, Sinsabaugh et al. 2016). We also found significant correlations of HR and SR with ST and SM in the top 1 m (Fig. 4.16a-d). The large increases in east Asia, central and northern South America, and southern and central Europe may be related to changes in SM and ST in the top 1 m considering their significant correlations (Fig. 4.S3c-d). Given the significant positive correlations of HR and SR with ST (0-1 m) and negative correlations of HR and SR with SM (0-1 m) in southern and central Europe, the increases of HR and SR were related to the rising ST and decreasing SM in the top 1 m in that area. However, correlations of HR and SR with ST (0-1 m) varied with latitude in east Asia, with significant positive correlations of HR and SR with ST and SM in the top 1 m at middle and high latitudes

but negative correlations at low latitudes of east Asia. Therefore, increases of HR and SR at middle and high latitudes may be related to rising ST (0-1 m) and those at low latitudes were associated with decreasing SM (0-1 m). In central and northern South America, correlations of HR and SR with ST (0-1 m) were complex. The HR and SR were positively correlated to ST (0-1 m) in the east part, but negative correlations with SM (0-1 m) in central and northern South America. As a result, the increase of HR and SR in central and northern South America was associated with decreasing SM (0-1 m) and increasing ST (0-1 m). In addition, we also observed decreases of HR and SR in Middle East (Fig. 4.9c-d). The decreases of GPP and NPP in such region can explain the decrease of HR and SR (Fig. 4.9a-f).

The VegC and LitC (0-1 m) also increased across latitudinal gradients and the globe by 2007-2016 relative to 1901-1910 (Fig. 4.8g-h, Fig. 4.11g-l). The VegC and LitC (0-1 m) widely increased across continents, with the most distinct absolute increase in Asia (e.g., east Asia) and South America (e.g., central and northern South America) and relative increase in Europe (e.g., southern and central Europe) (Table 4.2; Fig. 4.13g-l). The VegC is the biomass C of vegetation, while LitC is the C loss of vegetation biomass. This can partly explain the similar spatial patterns of VegC and LitC (top 1 m) with GPP and NPP. In addition, VegC and LitC (0-1 m) are affected by environmental factors such as temperature and water availability. We found significant correlations of VegC with MAT and MAP (Fig. 4.15e-f) and of LitC with ST and SM in the top 1 m (Fig. 4.16m-n). Similar with GPP and NPP, the increase of VegC may be associated with the increasing MAT and MAP in southern and central Europe, increases of VegC at middle and high latitudes may be related to rising MAT and those at low latitudes associated with decreasing MAP in east Asia, while the increase of VegC in central and northern South America may be related to the increasing MAP. We observed significant negative correlations between SM and LitC in the top 1 m in east Asia, southern and central Europe, and central and northern South America (Fig. 4.16m-n). The LitC and ST in the top 1 m were weakly and negatively correlated in southern and central Europe, significantly and positively correlated in east parts but weakly and negatively correlated in rest areas of

central and northern South America, and weakly correlated in southern Europe. Temperature has positive impacts on decomposition processes, leading to the decrease in litter residue (Pendall et al. 2004, Pietikäinen et al. 2005, Qiu et al. 2005). Therefore, increasing LitC in the top 1 m in east Asia and in southern and central Europe was related to their increased GPP, NPP, and VegC, while increases in LitC at low latitudes of east Asia and in southern and central Europe may be also associated with the decreasing SM.

The DOC and SOC in the top 1 m also increased across latitude by 2007-2016 relative to 1901-1910 (Fig. 4.8e-f). In line with our results, Eglin et al. (2010) also recorded increasing soil C stock in Asia and South America in response to combined effects of atmospheric CO_2 concentration and climate simulated by ORCHIDEE–LUC from 1901 to 2002. In addition, DOC and SOC in the top 1m widely increased over continents, with the most prominent absolute increase in Asia (e.g., east Asia) and relative changes of DOC in Europe (e.g., central and northern Europe) and South America (e.g., east coast of South America) and of SOC in Africa (e.g., central Africa), but slight decreases of DOC (0-1 m) were found in Australia/Oceania (southern Australia/Oceania) (Table 4.2; Fig. 4.11a-c, Fig. 4.13e-f). As vegetation C input provides the major C source for SOC stabilization, the large increases in GPP, NPP, VegC, and LitC (0-1 m) in east Asia may partly explain the large absolute increase of SOC in those regions (Fig. 4.9a-f, Fig. 4.11g-l, Fig. 4.12a-b, Fig. 4.13g-h). The changes in environmental conditions can also affect SOC stock. Significant correlations of SOC with ST and SM in the top 1 m were observed (Fig. 4.16k-l). We found significant and positive correlations between ST and SOC in central and southern Africa and at middle and high latitudes of east Asia and between SM and SOC at low latitudes of east Asia, while significant and negative correlation between SM and SOC at low latitudes of east Asia were documented in the top 1 m. Since rising temperature exerts negative impacts on SOC stock, the increasing SOC in Africa, east Asia, and central Africa was associated with the increasing C input from vegetation, while increasing SOC at low latitudes of east Asia was also related to rising SM in the top 1 m (Fig. 4.12-b, Fig.

4.16k-l). However, contrary to our result, Eglin et al. (2010) found a slight decrease in soil C stock in Africa from 1901 to 2002. The decrease of SOC in Africa may be due to the missing temporal dynamics of N deposition in the ORCHIDEE–LUC. N has important impacts on plant growth and vegetation productivity and SOC formation, especially in N-limited areas such as arid and semiarid regions such as most African regions. The DOC is the balance among SOC and litter decomposition, microbial lysis, and DOC degradation (Fig. 4.S1). The large increase of GPP, NPP, VegC, LitC and SOC in the top 1 m in Asia, South America, and Europe can explain the increase of DOC (0-1 m) in those regions (Table 4.1; Fig. 4.7a-b, Fig. 4.8f-h, Fig. 4.9a-f, Fig. 4.11d-l, Fig. 4.12a-b, Fig. 4.13f-h). In addition, we observed significant and positive correlations between DOC and ST in the top 1 m in east Asia, central and northern Europe, and east coast of South America. Significant and positive correlations between DOC and SM in the top 1 m were observed in central and northern Europe and east Asia, while significant and negative correlations between DOC and SM in the top 1 m were observed at low latitudes of east Asia and along east coast of South America. Therefore, increasing DOC in Europe, South America, and east Asia were partly due to increasing C input from litter and SOC decomposition, while increases in DOC at low latitudes of east Asia and along east coast of South America were also related to decreasing SM in the top 1 m.

The FBC and BBC in the top 30 cm and 1 m increased across latitudes during 2007-2016 compared with 1901-1910 (Fig. 4.8a-d). The FBC and BBC in the top 30 cm and 1 m widely increased at the continental level, with the absolute increase largest in Asia (e.g., east Asia) and South America (e.g., central and northern South America) for FBC and BBC in the top 30 cm and 1 m and relative increase largest in South America (e.g., central and northern and east coast of South America) for FBC (0-30 cm and 0-1 m) and in Europe (e.g., central and northern Europe) for BBC (0-30 cm and 0-1 m). Vegetation is the major C source for soil microbes in terrestrial ecosystems, determining the total amount of C available for microbes through regulating microbial C assimilation through SOC, DOC, and litter (Schimel 1995,

Vance and Chapin 2001, Xu et al. 2014). This large increase of GPP and NPP in east Asia and central and northern South America could explain the largest absolute increase of FBC and BBC in the top 30 cm and 1 m in such areas. However, fungi and bacteria have different preferences in using those C sources, with fungi generally better at using recalcitrant C (e.g., SOC) and bacteria generally preferring labile C (e.g., DOC). The fast-increasing rate of SOC in South America and DOC in Europe can partly explain the highest relative change of BBC (0-30 cm and 0-1 m) in Europe and FBC (0-30 cm and 0-1 m) in South America (Fig. 4.13e-f). Moreover, microbial biomass is closely associated with environmental factors, which highly impact microbial processes such as lysis. Microbial turnover is negatively affected by rising temperature, with bacteria more affected than fungi due to the faster turnover rate of bacteria than fungi (Rousk and Bååth 2011, He and Xu 2021). The high air and soil temperature in central and northern and east coast of Southern America may cause the faster turnover of bacteria than fungi, leading to faster increase of bacteria in northern Europe and fungi in central and northern and east coast of South America. However, we also found slight decreases of FBC in the top 1 m in Europe (e.g., southern Europe) and decreases of FBC and BBC in the top 30 cm and 1 m in Australia/Oceania (e.g., southern Australia/Oceania) (Table 4.2; Fig. 4.10; Fig. 4.13a-d). The decrease of DOC (0-1 m) may explain the widespread decrease of FBC and BBC of 30 cm and 1 m in southern Europe and southern Australia/Oceania (Fig. 4.10, Fig. 4.13a-d). In addition, in the top 1 m, FBC and BBC were negatively correlated with ST and positively correlated to SM in southern Australia/Oceania (Fig. 4.16e-h). The increase of ST and SM in the top 1 m can also explain the decrease of FBC and BBC in 0-30 cm and 0-1 m in southern Australia/Oceania (Fig. 4.S3c-d).

Future improvements

Although the CLM-Microbe model can well reproduce the global distribution of vegetation, soil, and microbial variables, several aspects were identified as future work for our research. First, soil and microbial processes need to be better defined vertically. Soil and microbial variables such as DOC, SOC,

FBC, and BBC in 0-30 cm were better simulated than those in 0-1 m (Table 4.1; Figs. 4.1-3), indicating that soil and microbial processes along soil profile may not that well represented in the CLM-Microbe model. Therefore, better defining soil and microbial processes along soil profile can help improve the model efficacy in capturing soil and microbial processes, and further reduce uncertainties in future projections of the C cycle. Second, land use change needs to be considered in future work. In addition to meteorology, N deposition, aerosol, and elevated CO_2, land-use change also has profound influences on plant, soil, and microbial processes. Drastic changes in vegetation, soil, and microbial processes due to land-use change can occur at small scales, spatial pattern of those processes can also be changed (Pascual et al. 1997, Sampaio et al. 2007, Stevenson et al. 2016). Therefore, considering land-use change in the CLM-Microbe model can help improve the model efficiency in capturing spatial patterns of C density and stocks in terrestrial ecosystems. Lastly, factorial attribution of variations in terrestrial C fluxes and pools will be addressed in our future work. Variations in terrestrial C fluxes and pools are driven by multiple environmental change factors that contribute individually or in combination, attributing the variations in terrestrial C fluxes and pools to environmental change factors is important for understanding of terrestrial C fluxes and pools dynamics (Xu et al. 2010).

Conclusion

The ESMs incorporating microbial processes are expected to represent uncertainties in the terrestrial C cycle more comprehensively. The CLM-Microbe model can well reproduce the distribution of vegetation (GPP and NPP), soil (HR, SR, DOC, and SOC), and microbial (FBC, BBC, and MBC). In addition, fluxes (GPP and NPP) and pools (HR, SR, FBC and BBC in the top 30 cm, FBC, BBC, DOC, SOC, and LitC in the top 1 m, and VegC) increased from 1901 to 2016. We generally observed the largest absolute increases of such variables in Asia and South America, particularly in east Asia and central and northern South America. While relative increases of such variables varied over continents, with the largest relative

increases of GPP, NPP, HR, and SR in Asia and Europe (particularly east Asia and southern and central Europe), FBC (0-30 cm and 0-1 m) in South America (particularly central and east coast of South America), BBC (0-30 cm and 0-1 m) in Europe (particularly central and northern Europe), DOC (0-1 m) in South America and Europe (particularly east coast of South America and northern Europe), SOC (0-1 m) in Africa (particularly central and southern Africa), and VegC and LitC (0-1 m) in Europe (particularly southern and central Europe). Slight decreases of DOC (0-1 m) in Europe and FBC and BBC in the top 30 cm and FBC, BBC, and DOC in the top 1 m in Australia/Oceania were also observed. The increase in GPP, NPP, and VegC were significantly related to rising MAT and MAP, while increases in FBC and BBC in the top 30 cm and FBC, BBC, DOC, SOC, and LitC in the top 1 m were closely associated with increasing C input from vegetation and SM and ST in the top 1 m.

This study represents one of the first attempts to simulate the temporal trend and spatial distribution of soil, vegetation, litter, and microbial C fluxes and pools during the last century using the microbial-explicit model, i.e., the CLM-Microbe model. The historical trend and changes in spatial pattern of vegetation, soil, and microbial fluxes and pools and their controls have critical significance for understanding C dynamics in a changing world.

References

Allison, S. D., M. D. Wallenstein, and M. A. Bradford. 2010. Soil-carbon response to warming dependent on microbial physiology. Nature Geoscience **3**:336-340.

Bailey, V. L., J. L. Smith, and H. Bolton. 2002. Fungal-to-bacterial ratios in soils investigated for enhanced C sequestration. Soil Biology and Biochemistry **34**:997-1007.

Boer, W. d., L. B. Folman, R. C. Summerbell, and L. Boddy. 2005. Living in a fungal world: impact of fungi on soil bacterial niche development. FEMS Microbiology Reviews **29**:795-811.

Bonan, G. B., D. L. Lombardozzi, W. R. Wieder, K. W. Oleson, D. M. Lawrence, F. M. Hoffman, and N. Collier. 2019. Model structure and climate data uncertainty in historical simulations of the terrestrial carbon cycle (1850–2014). Global biogeochemical cycles **33**:1310-1326.

Bond-Lamberty, B., V. L. Bailey, M. Chen, C. M. Gough, and R. Vargas. 2018. Globally rising soil heterotrophic respiration over recent decades. Nature **560**:80-83.

Bond-Lamberty, B., and A. Thomson. 2010. Temperature-associated increases in the global soil respiration record. Nature **464**:579-582.

Cheng, S., J. Huang, F. Ji, and L. Lin. 2017. Uncertainties of soil moisture in historical simulations and future projections. Journal of Geophysical Research: Atmospheres **122**:2239-2253.

Cramer, W., D. W. Kicklighter, A. Bondeau, B. M. Iii, G. Churkina, B. Nemry, A. Ruimy, A. L. Schloss, and T. P. O. F. T. P. N. M. Intercomparison. 1999. Comparing global models of terrestrial net primary productivity (NPP): overview and key results. Global change biology **5**:1-15.

Delire, C., R. Séférian, B. Decharme, R. Alkama, J.-C. Calvet, D. Carrer, A.-L. Gibelin, E. Joetzjer, X. Morel, and M. Rocher. 2020. The global land carbon cycle simulated with ISBA-CTRIP: Improvements over the last decade. Journal of Advances in Modeling Earth Systems **12**:e2019MS001886.

Dusenge, M. E., A. G. Duarte, and D. A. Way. 2019. Plant carbon metabolism and climate change: elevated CO 2 and temperature impacts on photosynthesis, photorespiration and respiration. New Phytologist **221**:32-49.

Eglin, T., P. Ciais, S. L. Piao, P. Barré, V. Bellassen, P. Cadule, C. Chenu, T. Gasser, C. Koven, and M. Reichstein. 2010. Historical and future perspectives of global soil carbon response to climate and land-use changes. Tellus B: Chemical and Physical Meteorology **62**:700-718.

Ettema, C. H., and D. A. Wardle. 2002. Spatial soil ecology. Trends in ecology & evolution **17**:177-183.

Flato, G. M. 2011. Earth system models: an overview. Wiley Interdisciplinary Reviews: Climate Change **2**:783-800.

Gabet, E. J., O. J. Reichman, and E. W. Seabloom. 2003. The effects of bioturbation on soil processes and sediment transport. Annual Review of Earth and Planetary Sciences **31**:249-273.

Galloway, J. N., A. R. Townsend, J. W. Erisman, M. Bekunda, Z. Cai, J. R. Freney, L. A. Martinelli, S. P. Seitzinger, and M. A. Sutton. 2008. Transformation of the nitrogen cycle: recent trends, questions, and potential solutions. Science **320**:889-892.

Gomez-Casanovas, N., R. Matamala, D. R. Cook, and M. A. Gonzalez-Meler. 2012. Net ecosystem exchange modifies the relationship between the autotrophic and heterotrophic components of soil respiration with abiotic factors in prairie grasslands. Global change biology **18**:2532-2545.

Guo, Z., Y. Wang, Z. Wan, Y. Zuo, L. He, D. Li, F. Yuan, N. Wang, J. Liu, and Y. Song. 2020. Soil dissolved organic carbon in terrestrial ecosystems: Global budget, spatial distribution and controls. Global Ecology and Biogeography.

Hashimoto, S., N. Carvalhais, A. Ito, M. Migliavacca, K. Nishina, and M. Reichstein. 2015. Global spatiotemporal distribution of soil respiration modeled using a global database. Biogeosciences **12**:4121-4132.

He, L., C.-T. Lai, M. A. Mayes, S. Murayama, and X. Xu. 2021a. Microbial seasonality promotes soil respiratory carbon emission in natural ecosystems: a modeling study. Global change biology **27**:3035-3051.

He, L., D. A. Lipson, J. L. M. Rodrigues, M. Mayes, R. G. Björk, B. Glaser, P. Thornton, and X. Xu. 2021b. Dynamics of Fungal and Bacterial Biomass Carbon in Natural Ecosystems: Site-level Applications of the CLM-Microbe Model. Journal of Advances in Modeling Earth Systems **13**:e2020MS002283.

He, L., J. L. M. Rodrigues, N. A. Soudzilovskaia, M. Barceló, P. a. A. Olsson, C. Song, L. Tedersoo, F. Yuan, F. Yuan, and D. A. Lipson. 2020. Global biogeography of fungal and bacterial biomass carbon in topsoil. Soil Biology and Biochemistry:108024.

He, L., and X. Xu. 2021. Mapping soil microbial residence time at the global scale. Global change biology **27**:6484-6497.

Hršelová, H., I. Chvátalová, M. Vosátka, J. Klír, and M. Gryndler. 1999. Correlation of abundance of arbuscular mycorrhizal fungi, bacteria and saprophytic microfungi with soil carbon, nitrogen and phsophorus. Folia microbiologica **44**:683-687.

Huang, N., L. Wang, X.-P. Song, T. A. Black, R. S. Jassal, R. B. Myneni, C. Wu, L. Wang, W. Song, and D. Ji. 2020. Spatial and temporal variations in global soil respiration and their relationships with climate and land cover. Science advances **6**:eabb8508.

IPCC. 2001. Climate change 2001 : the scientific basis. Contribution of Working Group I to the Third Assessment Report of the Intergovernmental Panel on Climate Change, 2001.

IPCC. 2013. Summary for policymakers. Cambridge, United Kingdom and New York, NY, USA.

Kassambara, A., and M. A. Kassambara. 2019. Package 'ggcorrplot'. R package version 0.1 **3**.

Kim, D., M.-I. Lee, and E. Seo. 2019. Improvement of soil respiration parameterization in a dynamic global vegetation model and its impact on the simulation of terrestrial carbon fluxes. Journal of Climate **32**:127-143.

Koven, C. D., W. J. Riley, Z. M. Subin, J. Y. Tang, M. S. Torn, W. D. Collins, G. B. Bonan, D. M. Lawrence, and S. C. Swenson. 2013. The effect of vertically resolved soil biogeochemistry and alternate soil C and N models on C dynamics of CLM4. Biogeosciences **10**:7109.

Kuzyakov, Y., and E. Blagodatskaya. 2015. Microbial hotspots and hot moments in soil: Concept & review. Soil Biology and Biochemistry **83**:184-199.

Lal, R. 2004. Soil carbon sequestration to mitigate climate change. Geoderma **123**:1-22.

Lal, R. 2008. Promise and limitations of soils to minimize climate change. Journal of Soil and Water Conservation **63**:113A-118A.

Lu, H., S. Li, M. Ma, V. Bastrikov, X. Chen, P. Ciais, Y. Dai, A. Ito, W. Ju, and S. Lienert. 2021. Comparing machine learning-derived global estimates of soil respiration and its components with those from terrestrial ecosystem models. Environmental Research Letters **16**:054048.

Mathieu, P.-P., and A. O'Neill. 2008. Data assimilation: From photon counts to Earth System forecasts. Remote Sensing of Environment **112**:1258-1267.

Matson, P., K. A. Lohse, and S. J. Hall. 2002. The globalization of nitrogen deposition: consequences for terrestrial ecosystems. Ambio:113-119.

Meeran, K., J. Ingrisch, D. Reinthaler, A. Canarini, L. Müller, E. M. Pötsch, A. Richter, W. Wanek, and M. Bahn. 2021. Warming and elevated CO2 intensify drought and recovery responses of grassland carbon allocation to soil respiration. Global change biology **27**:3230-3243.

Mei, W., G. Yu, J. Lai, Q. Rao, and Y. Umezawa. 2018. basicTrendline: Add Trendline and Confidence Interval of Basic Regression Models to Plot, R package version 2.0.3, available at https://CRAN.R-project.org/package=basicTrendline.

Nemani, R. R., C. D. Keeling, H. Hashimoto, W. M. Jolly, S. C. Piper, C. J. Tucker, R. B. Myneni, and S. W. Running. 2003. Climate-driven increases in global terrestrial net primary production from 1982 to 1999. Science **300**:1560-1563.

Noh, N. J., M. Kuribayashi, T. M. Saitoh, and H. Muraoka. 2017. Different responses of soil, heterotrophic and autotrophic respirations to a 4-year soil warming experiment in a cool-temperate deciduous broadleaved forest in central Japan. Agricultural and Forest Meteorology **247**:560-570.

Pascual, J. A., C. García, T. Hernandez, and M. Ayuso. 1997. Changes in the microbial activity of an arid soil amended with urban organic wastes. Biology and Fertility of Soils **24**:429-434.

Pendall, E., S. Bridgham, P. J. Hanson, B. Hungate, D. W. Kicklighter, D. W. Johnson, B. E. Law, Y. Luo, J. P. Megonigal, M. Olsrud, M. G. Ryan, and S. Wan. 2004. Below-ground process responses to elevated CO2 and temperature: a discussion of observations, measurement methods, and models. New Phytologist **162**:311-322.

Pietikäinen, J., M. Pettersson, and E. Bååth. 2005. Comparison of temperature effects on soil respiration and bacterial and fungal growth rates. FEMS Microbiology Ecology **52**:49-58.

Piñeiro, J., R. Ochoa-Hueso, M. Delgado-Baquerizo, S. Dobrick, P. B. Reich, E. Pendall, and S. A. Power. 2017. Effects of elevated CO2 on fine root biomass are reduced by aridity but enhanced by soil nitrogen: A global assessment. Scientific reports **7**:1-9.

Prescott, C. E., S. J. Grayston, H.-S. Helmisaari, E. Kaštovská, C. Körner, H. Lambers, I. C. Meier, P. Millard, and I. Ostonen. 2020. Surplus carbon drives allocation and plant–soil interactions. Trends in ecology & evolution **35**:1110-1118.

Preusser, S., C. Poll, S. Marhan, G. Angst, C. W. Mueller, J. Bachmann, and E. Kandeler. 2019. Fungi and bacteria respond differently to changing environmental conditions within a soil profile. Soil Biology and Biochemistry **137**:107543.

Qiu, S., A. J. McComb, R. W. Bell, and J. A. Davis. 2005. Response of soil microbial activity to temperature, moisture, and litter leaching on a wetland transect during seasonal refilling. Wetlands Ecology and Management **13**:43-54.

Rousk, J., and E. Bååth. 2011. Growth of saprotrophic fungi and bacteria in soil. FEMS Microbiology Ecology **78**:17-30.

Sampaio, G., C. Nobre, M. H. Costa, P. Satyamurty, B. S. Soares-Filho, and M. Cardoso. 2007. Regional climate change over eastern Amazonia caused by pasture and soybean cropland expansion. Geophysical Research Letters **34**.

Schimel, D. S. 1995. Terrestrial ecosystems and the carbon cycle. Global change biology **1**:77-91.

Schimel, J. P. 2018. Life in dry soils: effects of drought on soil microbial communities and processes. Annual review of ecology, evolution, and systematics **49**:409-432.

Sinsabaugh, R. L., B. L. Turner, J. M. Talbot, B. G. Waring, J. S. Powers, C. R. Kuske, D. L. Moorhead, and J. J. Follstad Shah. 2016. Stoichiometry of microbial carbon use efficiency in soils. Ecological Monographs **86**:172-189.

Soong, J. L., C. Castanha, C. E. H. Pries, N. Ofiti, R. C. Porras, W. J. Riley, M. W. I. Schmidt, and M. S. Torn. 2021. Five years of whole-soil warming led to loss of subsoil carbon stocks and increased CO_2 efflux. Science advances **7**:eabd1343.

Stevenson, B. A., A. K. Sarmah, R. Smernik, D. W. F. Hunter, and S. Fraser. 2016. Soil carbon characterization and nutrient ratios across land uses on two contrasting soils: Their relationships to microbial biomass and function. Soil Biology and Biochemistry **97**:50-62.

Thornton, P. E., and N. A. Rosenbloom. 2005. Ecosystem model spin-up: Estimating steady state conditions in a coupled terrestrial carbon and nitrogen cycle model. Ecological Modelling **189**:25-48.

Todd-Brown, K. E. O., J. T. Randerson, W. M. Post, F. M. Hoffman, C. Tarnocai, E. A. G. Schuur, and S. D. Allison. 2013. Causes of variation in soil carbon simulations from CMIP5 Earth system models and comparison with observations. Biogeosciences **10**:1717-1736.

Van Damme, M., L. Clarisse, B. Franco, M. A. Sutton, J. W. Erisman, R. Wichink Kruit, M. van Zanten, S. Whitburn, J. Hadji-Lazaro, D. Hurtmans, C. Clerbaux, and P.-F. Coheur. 2021. Global, regional and national trends of atmospheric ammonia derived from a decadal (2008–2018) satellite record. Environmental Research Letters **16**:055017.

Vance, E. D., and I. F. S. Chapin. 2001. Substrate limitations to microbial activity in taiga forest floors. Soil Biology and Biochemistry **33**:173-188.

Viovy, N. 2018. CRUNCEP Version 7 - Atmospheric Forcing Data for the Community Land Model. Research Data Archive at the National Center for Atmospheric Research, Computational and Information Systems Laboratory, Boulder, CO.

Wang, G., S. Jagadamma, M. A. Mayes, C. W. Schadt, J. M. Steinweg, L. Gu, and W. M. Post. 2015. Microbial dormancy improves development and experimental validation of ecosystem model. The ISME Journal **9**:226-237.

Wang, K., C. Peng, Q. Zhu, X. Zhou, M. Wang, K. Zhang, and G. Wang. 2017. Modeling global soil carbon and soil microbial carbon by integrating microbial processes into the ecosystem process model TRIPLEX-GHG. Journal of Advances in Modeling Earth Systems **9**:2368-2384.

Wang, Y., F. Yuan, F. Yuan, B. Gu, M. S. Hahn, M. S. Torn, D. M. Ricciuto, J. Kumar, L. He, and D. Zona. 2019. Mechanistic modeling of microtopographic impacts on CO2 and CH4 Fluxes in an Alaskan tundra ecosystem using the CLM-Microbe model. Journal of Advances in Modeling Earth Systems **11**:17.

Wardle, D. A., and D. Parkinson. 1990. Interactions between microclimatic variables and the soil microbial biomass. Biology and Fertility of Soils **9**:273-280.

Wieder, W. R., G. B. Bonan, and S. D. Allison. 2013. Global soil carbon projections are improved by modelling microbial processes. Nature Climate Change **3**:909-912.

Wieder, W. R., A. S. Grandy, C. M. Kallenbach, P. G. Taylor, and G. B. Bonan. 2015. Representing life in the Earth system with soil microbial functional traits in the MIMICS model. Geoscientific Model Development **8**:1789-1808.

Wiltshire, A. J., E. J. Burke, S. E. Chadburn, C. D. Jones, P. M. Cox, T. Davies-Barnard, P. Friedlingstein, A. B. Harper, S. Liddicoat, and S. Sitch. 2021. JULES-CN: a coupled terrestrial carbon–nitrogen scheme (JULES vn5. 1). Geoscientific Model Development **14**:2161-2186.

Xu, X., D. A. Elias, D. E. Graham, T. J. Phelps, S. L. Carroll, S. D. Wullschleger, and P. E. Thornton. 2015. A microbial functional group-based module for simulating methane production and consumption: Application to an incubated permafrost soil. Journal of Geophysical Research: Biogeosciences **120**:1315-1333.

Xu, X., J. P. Schimel, P. E. Thornton, X. Song, F. Yuan, and S. Goswami. 2014. Substrate and environmental controls on microbial assimilation of soil organic carbon: a framework for Earth system models. Ecology letters **17**:547-555.

Xu, X., P. E. Thornton, and W. M. Post. 2013. A global analysis of soil microbial biomass carbon, nitrogen and phosphorus in terrestrial ecosystems. Global Ecology and Biogeography **22**:737-749.

Xu, X. F., H. Q. Tian, C. Zhang, M. L. Liu, W. Ren, G. S. Chen, C. Q. Lu, and L. Bruhwiler. 2010. Attribution of spatial and temporal variations in terrestrial methane flux over North America. Biogeosciences **7**:3637-3655.

Yue, X., N. Unger, and Y. Zheng. 2015. Distinguishing the drivers of trends in land carbon fluxes and plant volatile emissions over the past 3 decades. Atmospheric Chemistry and Physics **15**:11931-11948.

Zhang, Q., H.-M. Lei, and D.-W. Yang. 2013. Seasonal variations in soil respiration, heterotrophic respiration and autotrophic respiration of a wheat and maize rotation cropland in the North China Plain. Agricultural and Forest Meteorology **180**:34-43.

Zhao, Z., C. Peng, Q. Yang, F.-R. Meng, X. Song, S. Chen, T. E. Epule, P. Li, and Q. Zhu. 2017. Model prediction of biome-specific global soil respiration from 1960 to 2012. Earth's Future **5**:715-729.

Zheng, Y., R. Shen, Y. Wang, X. Li, S. Liu, S. Liang, J. M. Chen, W. Ju, L. Zhang, and W. Yuan. 2020. Improved estimate of global gross primary production for reproducing its long-term variation, 1982–2017. Earth System Science Data **12**:2725-2746.

Zhou, L., X. Zhou, J. Shao, Y. Nie, Y. He, L. Jiang, Z. Wu, and S. Hosseini Bai. 2016. Interactive effects of global change factors on soil respiration and its components: a meta-analysis. Global change biology **22**:3157-3169.

Zhou, X., S. Wan, and Y. Luo. 2007. Source components and interannual variability of soil CO2 efflux under experimental warming and clipping in a grassland ecosystem. Global change biology **13**:761-775.

Zhu, X., L. Zhang, Y. Zuo, J. Liu, J. Yu, F. Yuan, N. Wang, L. He, Y. Wang, Z. Guo, Y. Sun, Y. Song, C. Song, D. Guo, and X. Xu. 2021. Wetland reclamation homogenizes microbial properties along soil profiles. Geoderma **395**:115075.

Figures and tables

Fig. 4.1. Comparison between observed (black line) and the CLM-Microbe-simulated (red line) latitudinal gradients of (a) GPP, (b) NPP, (c) HR, (d) SR, (e) DOC in the top 30 cm, (f) DOC in the top 1 m, (g) SOC in the top 30 cm, (h) SOC in the top 1 m, (i) FBC in the top 30 cm, (j) BBC in the top 30 cm, and (k) MBC (0-1 m). GPP, gross primary productivity; NPP, net primary productivity; HR, heterotrophic respiration; SR, soil respiration; DOC, dissolved organic carbon; SOC, soil organic carbon; FBC, fungal biomass carbon; BBC, bacterial biomass carbon; MBC, microbial biomass carbon.

Fig. 4.2. Comparison between observed (black line) and the CLM4.5-simulated (red line) latitudinal gradients of (a) GPP, (b) NPP, (c) HR, (d) SR, (e) SOC in the top 30 cm, and (f) SOC in the top 1 m. GPP, gross primary productivity; NPP, net primary productivity; HR, heterotrophic respiration; SR, soil respiration; SOC, soil organic carbon.

Fig. 4.3. Comparison between observed and the CLM-Microbe-simulated grid cells of (a) GPP, (b) NPP, (c) HR, (d) SR, (e) DOC in the top 30 cm, (f) DOC in the top 1 m, (g) SOC in the top 30 cm, (h) SOC in the top 1 m, (i) FBC in the top 30 cm, (j) BBC in the top 30 cm, and (k) MBC (0-1 m). Black lines are linear regressions, red lines are 1:1 lines. GPP, gross primary productivity; NPP, net primary productivity; HR, heterotrophic respiration; SR, soil respiration; DOC, dissolved organic carbon; SOC, soil organic carbon; FBC, fungal biomass carbon; BBC, bacterial biomass carbon; MBC, microbial biomass carbon.

Fig. 4.4. Comparison between observed and the CLM4.5-simulated grid cells of (a) GPP, (b) NPP, (c) HR, (d) SR, (e) SOC in the top 30 cm, and (f) SOC in the top 1 m. Black lines are linear regressions, red lines are 1:1 lines. GPP, gross primary productivity; NPP, net primary productivity; HR, heterotrophic respiration; SR, soil respiration; SOC, soil organic carbon.

Fig. 4.5. Evolution of annual carbon flux of area-weighted (a) GPP, (b) NPP, (c) HR, and (d) SR

simulated by the CLM-Microbe model since 1901. The baseline was the ten-year average of corresponding variables during 1901-1910. GPP, gross primary productivity; NPP, net primary productivity; HR, heterotrophic respiration; SR, soil respiration.

Fig. 4.6. Evolution of global carbon stocks of area-weighted (a) FBC in the top 30 cm, (b) FBC in the top 1 m, (c) BBC in the top 30 cm, (d) BBC in the top 1 m, (e) DOC in the top 1 m, (f) SOC in the top 1 m, and (g) VegC, and (h) LitC in the top 1 m simulated by the CLM-Microbe model since 1901. The baseline was the ten-year average of corresponding variables during 1901-1910. DOC, dissolved organic carbon; SOC, soil organic carbon; FBC, fungal biomass carbon; BBC, bacterial biomass carbon; MBC, microbial biomass carbon; VegC, vegetation carbon; LitC, litter carbon.

Fig. 4.7. Latitudinal gradients of the CLM-Microbe model simulated ten-year averages of (a) GPP, (b) NPP, (c) HR, and (d) SR during 1901-1910 and 2007-2016. GPP, gross primary productivity; NPP, net primary productivity; HR, heterotrophic respiration; SR, soil respiration.

Fig. 4.8. Latitudinal gradients of the CLM-Microbe model simulated ten-year averages (a) FBC in the top 30 cm, (b) FBC in the top 1 m, (c) BBC in the top 30 cm, (d) BBC in the top 1 m, (e) DOC in the top 1 m, (f) SOC in the top 1 m, and (g) VegC, and (h) LitC in the top 1 m during 1901-1910 and 2007-2016. DOC, dissolved organic carbon; SOC, soil organic carbon; FBC, fungal biomass carbon; BBC, bacterial biomass carbon; MBC, microbial biomass carbon; VegC, vegetation carbon; LitC, litter carbon.

Fig. 4.9. Ten-year averages of (a-b) GPP, (d-e) NPP, (g-h) HR, and (j-k) SR during (a, d, g, and j) 1901-1910 and (b, e, h, and k) 2007-2016 and relative changes of (c) GPP, (f) NPP, (i) HR, and (l) SR by 2007-2016 relative to 1901-1910. GPP, gross primary productivity; NPP, net primary productivity; HR, heterotrophic respiration; SR, soil respiration.

Fig. 4.10. Ten-year averages of (a-b) FBC in the top 30 cm, (d-e) FBC in the top 1 m, (g-h) BBC in the top 30 cm, and (j-k) BBC in the top 1 m during (a, d, g, and j) 1901-1910 and (b, e, h, and k) 2007-2016 and relative changes of (c) GPP, (f) NPP, (i) HR, and (l) SR by 2007-2016 relative to 1901-1910. FBC, fungal biomass carbon; BBC, bacterial biomass carbon.

Fig. 4.11. Ten-year averages of (a-b) DOC in the top 1 m, (d-e) SOC in the top 1 m, (g-h) VegC, and (j-k) LitC in the top 1 m during (a, d, g, and j) 1901-1910 and (b, e, h, and k) 2007-2016 and relative changes of (c) DOC in the top 1 m, (f) SOC in the top 1 m, (i) VegC, and (l) LitC in the top 1 m by 2007-2016 relative to 1901-1910. DOC, dissolved organic carbon; SOC, soil organic carbon; VegC, vegetation carbon; LitC, litter carbon.

Fig. 4.12. Changing rates of the CLM-Microbe model simulated (a) GPP, (b) NPP, (c) HR, and (d) SR from 1901 to 2016. GPP, gross primary productivity; NPP, net primary productivity; HR, heterotrophic respiration; SR, soil respiration. DOC, dissolved organic carbon; SOC, soil organic carbon; FBC, fungal biomass carbon; BBC, bacterial biomass carbon; MBC, microbial biomass carbon; VegC, vegetation carbon; LitC, litter carbon. Black dots indicate significant regression coefficients (P<0.05).

Fig. 4.13. Changing rates of the CLM-Microbe model simulated (a) FBC in the top 30 cm, (b) FBC in the top 1 m, (c) BBC in the top 30 cm, (d) BBC in the top 1 m, (e) DOC in the top 1 m, (f) SOC in the top 1 m, and (g) VegC, and (h) LitC in the top 1 m from 1901 to 2016. DOC, dissolved organic carbon; SOC, soil organic carbon; FBC, fungal biomass carbon; BBC, bacterial biomass carbon; MBC, microbial biomass carbon; VegC, vegetation carbon; LitC, litter carbon. Black dots indicate significant regression coefficients (P<0.05).

Fig. 4.14. Heatmap showing Pearson's correlation between the CLM-Microbe model simulated (a) GPP, NPP, and VegC and MAT and MAP and (b) HR, SR, FBC in the top 1 m, BBC in the top 1 1m, DOC in the top 1 m, SOC in the top 1 m, and LitC in the top 1 m and SM and ST in the top 1 m from 1901 to 2016. GPP, gross primary productivity; NPP, net primary productivity; HR, heterotrophic respiration; SR, soil respiration; DOC, dissolved organic carbon; SOC, soil organic carbon; FBC, fungal biomass carbon; BBC, bacterial biomass carbon; VegC, vegetation carbon; LitC, litter carbon; MAT, mean annual temperature; MAP, mean annual precipitation; ST, soil temperature; SM, soil moisture. Black stars indicate significant correlates (P<0.05).

Fig. 4.15. Pearson's correlation between the CLM-Microbe model simulated (a-b) GPP, (c-d) NPP, and (e-f) VegC and (a, c, and e) MAT and (b, d, and f) MAP from 1901 to 2016. GPP, gross primary productivity; NPP, net primary productivity; VegC, vegetation carbon; MAT, mean annual temperature; MAP, mean annual precipitation. Black dots indicate significant correlates (P<0.05).

Fig. 4.16. Pearson's correlation between the CLM-Microbe model simulated (a-b) HR, (c-d) SR, (e-f) FBC in the top 1 m, (g-h) BBC in the top 1 m, (i-j) DOC in the top 1 m, (k-l) SOC in the top 1 m, and (m-n) LitC and (a, c, e, g, i, k, and m) ST and (b, d, f, h, j, l, and n) SM in the top 1 m from 1901 to 2016. HR, heterotrophic respiration; SR, soil respiration; DOC, dissolved organic carbon; SOC, soil organic carbon; FBC, fungal biomass carbon; BBC, bacterial biomass carbon; VegC, vegetation carbon; LitC, litter carbon; ST, soil temperature; SM, soil moisture. Black dots indicate significant correlates (P<0.05).

Table 4.1. Annual flux of GPP, NPP, HR, and SR and carbon stocks of FBC in the top 30 cm, BBC in the top 30 cm, MBC (0-1 m), DOC in the top 30 cm, SOC in the top 30 cm, and SOC in the top 1 m by observed datasets and by simulations of the CLM-Microbe model and CLM4.5 at the global scale

Table 4.2. Ten-year averages of GPP, NPP, HR, and SR and carbon stocks of FBC in the top 30 cm, FBC in the top 1 m, BBC in the top 30 cm, BBC in the top 1 m, DOC in the top 1 m, and SOC in the top 1 m and their absolute and relative changes by simulations of the CLM-Microbe model at the continental scale

Table 4.3. Carbon stock of vegetation, litter, and soil pools and absolute and relative changes from 1901-1910 to 2007-2016

Table 4.1. Annual flux of GPP, NPP, HR, and SR and carbon stocks of FBC in the top 30 cm, BBC in the top 30 cm, MBC (0-1 m), DOC in the top 30 cm, SOC in the top 30 cm, and SOC in the top 1 m by observed datasets and by simulations of the CLM-Microbe model and CLM4.5 at the global scale

Variables	Unit	Global estimation		
		Observed	CLM-Microbe	CLM4.5
GPP	PgC yr^{-1}	111.94	129.53	120.13
NPP		55.76	56.49	51.26
SR		86.34	99.80	89.79
HR		49.01	49.84	46.87
FBC (0-30 cm)	PgC	13.57	13.12	--
BBC (0-30 cm)		3.29	4.17	--
MBC (0-1 m)		23.70	40.18	--
DOC (0-30 cm)		7.16	8.94	--
DOC (0-1 m)		12.90	22.57	--
SOC (0-30 cm)		661.71	605.27	513.40
SOC (0-1 m)		1231.99	1630.90	967.87

GPP, gross primary productivity; NPP, net primary productivity; HR, heterotrophic respiration; SR, soil respiration; DOC, dissolved organic carbon; SOC, soil organic carbon; FBC, fungal biomass carbon; BBC, bacterial biomass carbon; MBC, microbial biomass carbon. -- denoted not available. The SOC (0-1 m) data were from the Harmonized World Soil Database (HWSD, https://daac.ornl.gov/cgi-bin/dsviewer.pl?ds_id=1247); the SOC (0-30 cm) data were from the Global Soil Organic Carbon Map (GSOCmap) version 1.5; GPP and NPP data were from MODIS gridded datasets (http://files.ntsg.umt.edu/data/NTSG_Products/); the SR and HR data were from Global Gridded 1-km Annual Soil Respiration Database (SRDB) version 3 (https://daac.ornl.gov/CMS/guides/CMS_Global_Soil_Respiration.html); the FBC and BBC in the top 30 cm were from He et al. (2020); MBC (0-1 m) was compared with Xu et al. (2013); the DOC (0-30 cm and 0-1 m) was derived from Guo et al. (2020). Output of the CLM-Microbe model during 2000-2009 (ten-year average) were used to compare with observational data.

Table 4.2. Ten-year averages of GPP, NPP, HR, and SR and carbon stocks of FBC in the top 30 cm, FBC in the top 1 m, BBC in the top 30 cm, BBC in the top 1 m, DOC in the top 1 m, and SOC in the top 1 m and their absolute and relative changes by simulations of the CLM-Microbe model at the continental scale

	Variables	Unit	Continent					
			Asia	North America	Europe	Africa	South America	Australia/Oceania
1901-1910	GPP	PgC yr^{-1}	28.7	16.6	9.2	20.8	31.0	3.3
	NPP		12.2	7.3	4.3	9.4	12.3	1.5
	HR		11.1	6.7	4.0	8.0	11.1	1.3
	SR		22.1	13.7	7.7	15.3	21.7	2.7
	FBC (0-30 cm)	PgC	4.5	3.5	1.3	1.5	1.9	0.4
	FBC (0-1 m)		10.3	7.8	2.7	3.6	5.5	0.9
	BBC (0-30 cm)		1.4	1.0	0.4	0.4	0.7	0.1
	BBC (0-1 m)		3.6	2.3	0.9	1.2	2.5	0.2
	DOC (0-1 m)		7.5	6.5	2.6	1.9	2.7	0.6
	SOC (0-1 m)		563.8	415.9	206.4	170.8	311.3	29.6
	VegC		49.9	23.3	12.5	34.6	69.8	3.2
	LitC (0-1 m)		8.5	3.1	1.1	5.6	13.5	0.7
2007-2016	GPP	PgC yr^{-1}	38.1	20.9	12.4	25.8	38.3	4.1
	NPP		16.3	9.2	5.8	11.6	15.3	1.8
	HR		14.7	8.3	5.4	9.8	13.8	1.7
	SR		30.1	17.2	10.4	19.4	27.5	3.4
	FBC (0-30 cm)	PgC	4.8	3.8	1.4	1.6	2.1	0.4
	FBC (0-1 m)		10.7	8.0	2.7	3.8	5.9	0.9
	BBC (0-30 cm)		1.6	1.1	0.5	0.5	0.8	0.1
	BBC (0-1 m)		3.7	2.4	1.0	1.3	2.6	0.2
	DOC (0-1 m)		8.3	7.2	3.0	2.1	3.1	0.6
	SOC (0-1 m)		572.8	421.4	212.3	176.5	318.9	30.3
	VegC		58.7	29.0	16.5	39.0	83.2	3.9
	LitC (0-1 m)		9.6	3.5	1.3	6.3	15.0	0.8
Absolute change from 1901-1910 to 2007-2016	GPP	PgC yr^{-1}	9.39	4.23	3.20	4.98	7.32	0.86
	NPP		4.11	1.91	1.55	2.21	2.99	0.34
	HR		3.61	1.62	1.43	1.79	2.70	0.31
	SR		8.02	3.48	2.76	4.03	5.83	0.74
	FBC (0-30 cm)	PgC	0.35	0.21	0.10	0.13	0.22	0.00
	FBC (0-1 m)		0.37	0.26	-0.01	0.21	0.38	-0.04
	BBC (0-30 cm)		0.11	0.07	0.06	0.05	0.09	0.00
	BBC (0-1 m)		0.18	0.11	0.10	0.09	0.18	-0.01
	DOC (0-1 m)		0.75	0.67	0.40	0.21	0.41	-0.04
	SOC (0-1 m)		8.96	5.46	5.90	5.67	7.65	0.69
	VegC		8.82	5.71	4.06	4.46	13.39	0.68
	LitC (0-1 m)		1.06	0.45	0.26	0.75	1.42	0.10
Relative change from 1901-1910 to 2007-2016	GPP	%	32.7	25.4	34.9	23.9	23.6	26.4
	NPP		33.6	26.3	36.0	23.6	24.4	23.0
	HR		32.5	24.2	36.0	22.3	24.4	23.1
	SR		36.2	25.5	36.0	26.2	26.9	27.9
	FBC (0-30 cm)		7.8	6.0	7.6	8.7	12.0	-0.9
	FBC (0-1 m)		3.6	3.3	-0.3	5.7	6.8	-4.2
	BBC (0-30 cm)		7.9	6.5	14.9	11.0	13.2	-1.9
	BBC (0-1 m)		5.0	4.9	11.5	7.4	7.3	-2.7
	DOC (0-1 m)		10.0	10.2	15.1	11.1	15.1	-7.2
	SOC (0-1 m)		1.6	1.3	2.9	3.3	2.5	2.3
	VegC		17.7	24.5	32.5	12.9	19.2	21.2
	LitC (0-1 m)		12.4	14.5	23.4	13.4	10.5	14.5

GPP, gross primary productivity; NPP, net primary productivity; HR, heterotrophic respiration; SR, soil respiration; DOC, dissolved organic carbon; SOC, soil organic carbon; FBC, fungal biomass carbon; BBC, bacterial biomass carbon.

Table 4.3. Carbon stock of vegetation, litter, and soil pools and absolute and relative changes from 1901-1910 to 2007-2016

Pool	Total Carbon stock (PgC)		Change from 1901-1910 to 2007-2016	
	1901-1910	2007-2016	Absolute change (PgC)	Relative change (%)
Soil	4527	4564	37.0	0.8
Litter	63	68	5.1	8.0
Vegetation	193	230	37.1	19.2

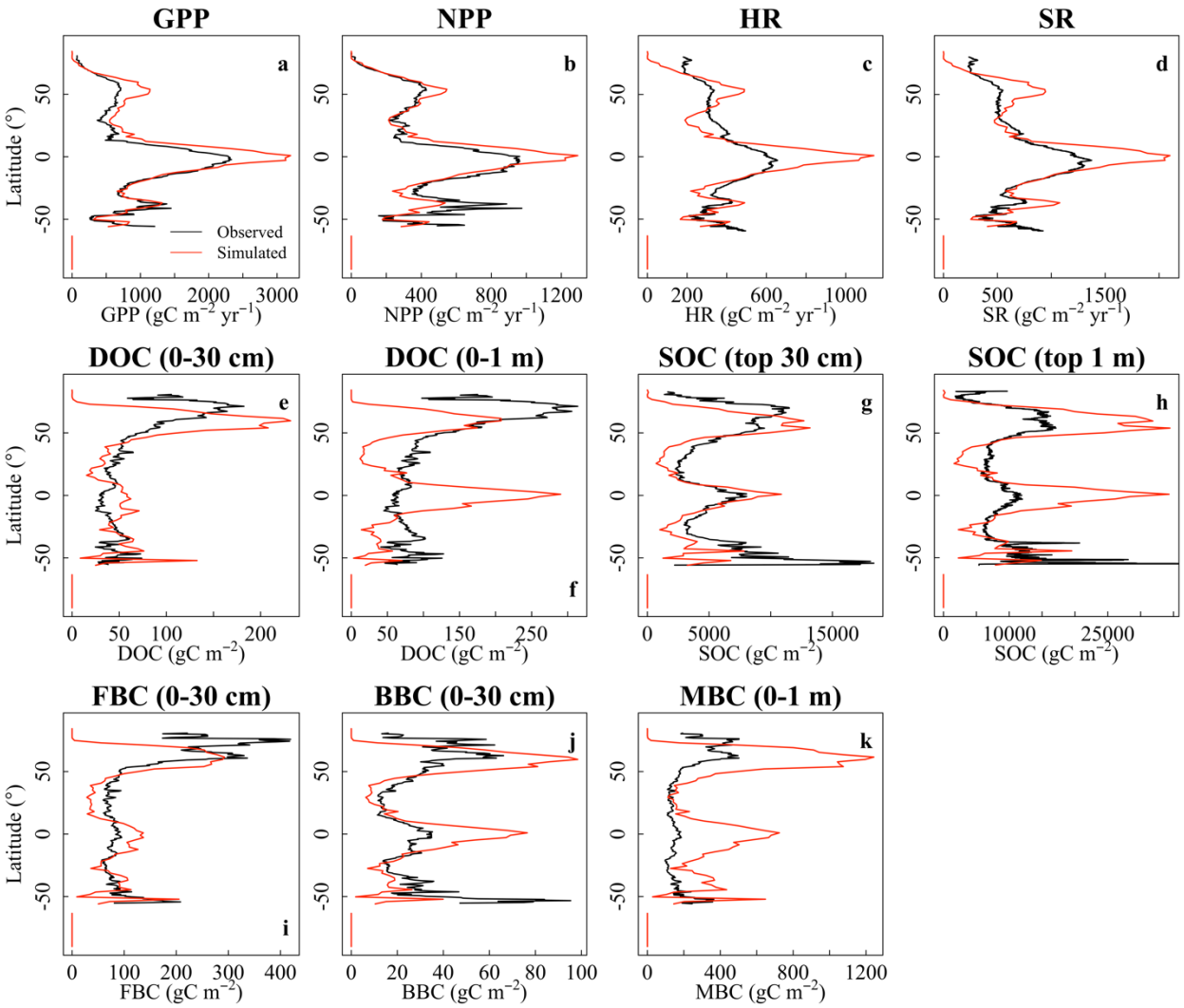

Fig. 4.1. Comparison between observed (black line) and the CLM-Microbe-simulated (red line) latitudinal gradients of (a) GPP, (b) NPP, (c) HR, (d) SR, (e) DOC in the top 30 cm, (f) DOC in the top 1 m, (g) SOC in the top 30 cm, (h) SOC in the top 1 m, (i) FBC in the top 30 cm, (j) BBC in the top 30 cm, and (k) MBC (0-1 m). GPP, gross primary productivity; NPP, net primary productivity; HR, heterotrophic respiration; SR, soil respiration; DOC, dissolved organic carbon; SOC, soil organic carbon; FBC, fungal biomass carbon; BBC, bacterial biomass carbon; MBC, microbial biomass carbon.

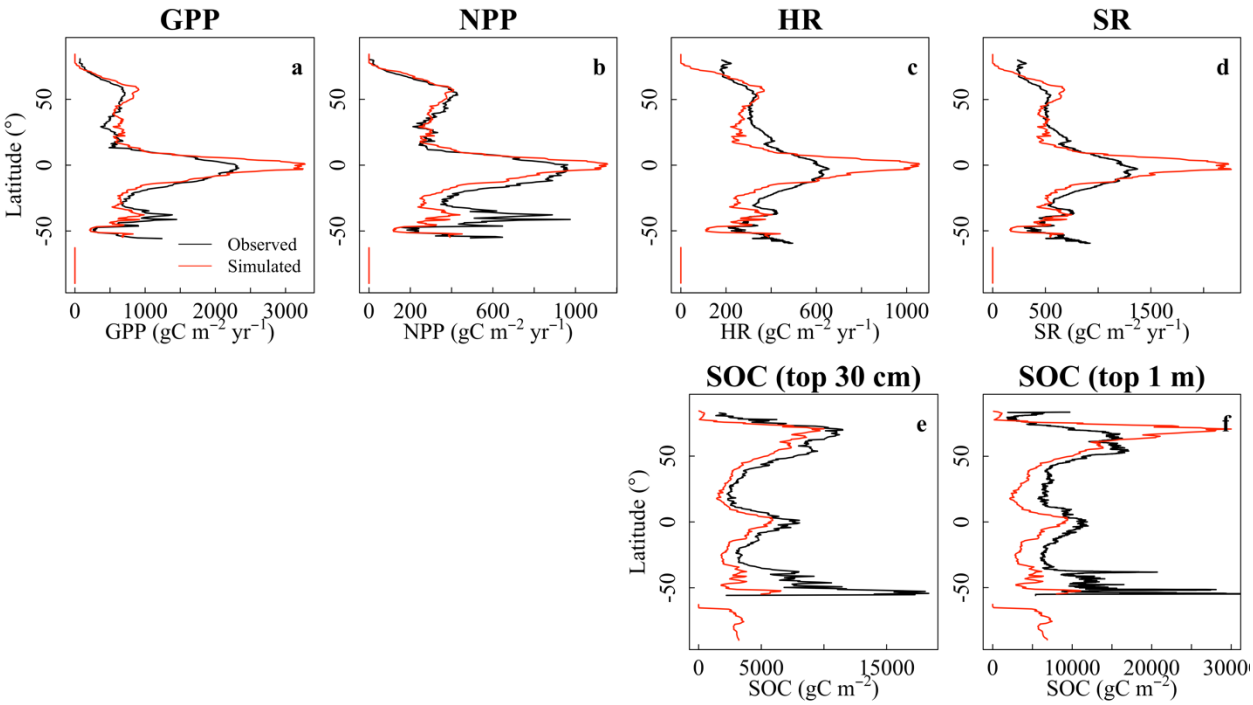

Fig. 4.2. Comparison between observed (black line) and the CLM4.5-simulated (red line) latitudinal gradients of (a) GPP, (b) NPP, (c) HR, (d) SR, (e) SOC in the top 30 cm, and (f) SOC in the top 1 m. GPP, gross primary productivity; NPP, net primary productivity; HR, heterotrophic respiration; SR, soil respiration; SOC, soil organic carbon.

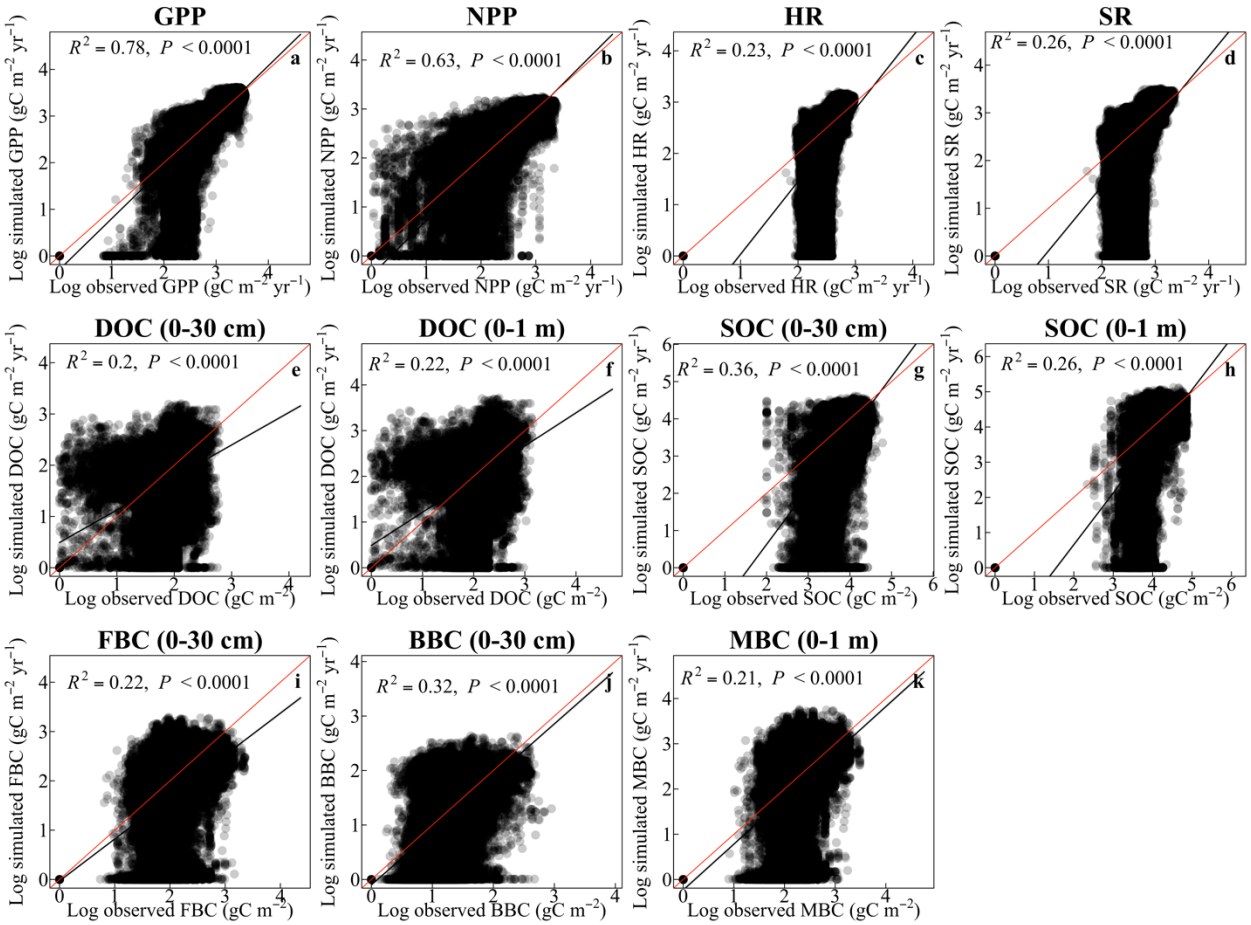

Fig. 4.3. Comparison between observed and the CLM-Microbe-simulated grid cells of (a) GPP, (b) NPP, (c) HR, (d) SR, (e) DOC in the top 30 cm, (f) DOC in the top 1 m, (g) SOC in the top 30 cm, (h) SOC in the top 1 m, (i) FBC in the top 30 cm, (j) BBC in the top 30 cm, and (k) MBC (0-1 m). Black lines are linear regressions, red lines are 1:1 lines. GPP, gross primary productivity; NPP, net primary productivity; HR, heterotrophic respiration; SR, soil respiration; DOC, dissolved organic carbon; SOC, soil organic carbon; FBC, fungal biomass carbon; BBC, bacterial biomass carbon; MBC, microbial biomass carbon.

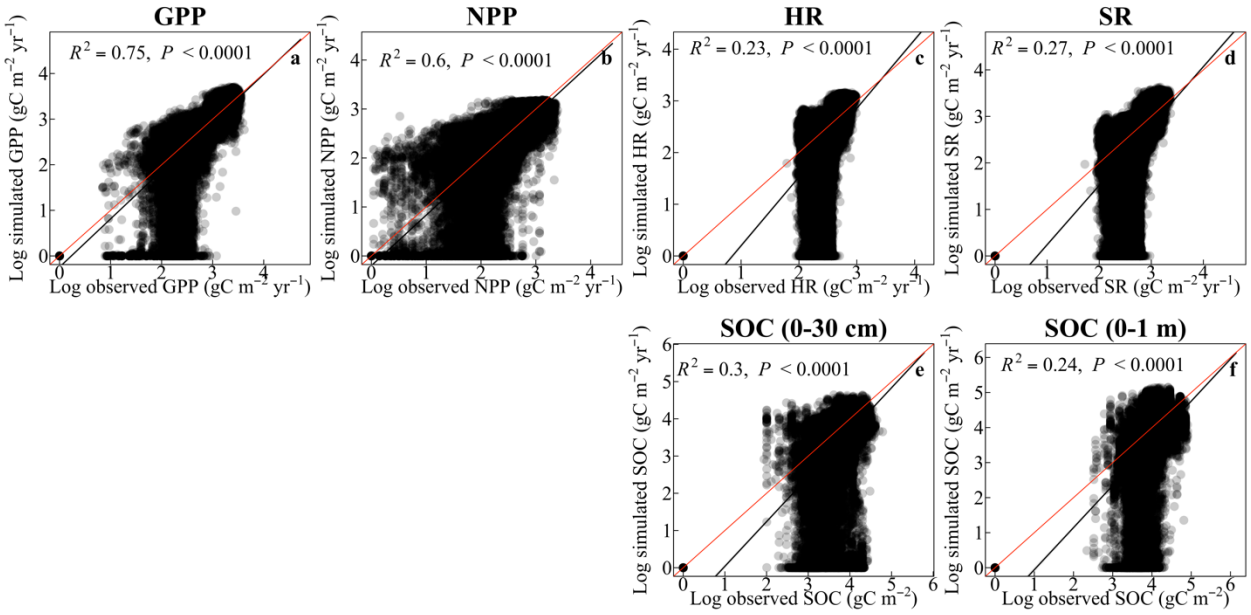

Fig. 4.4. Comparison between observed and the CLM4.5-simulated grid cells of (a) GPP, (b) NPP, (c) HR, (d) SR, (e) SOC in the top 30 cm, and (f) SOC in the top 1 m. Black lines are linear regressions, red lines are 1:1 lines. GPP, gross primary productivity; NPP, net primary productivity; HR, heterotrophic respiration; SR, soil respiration; SOC, soil organic carbon.

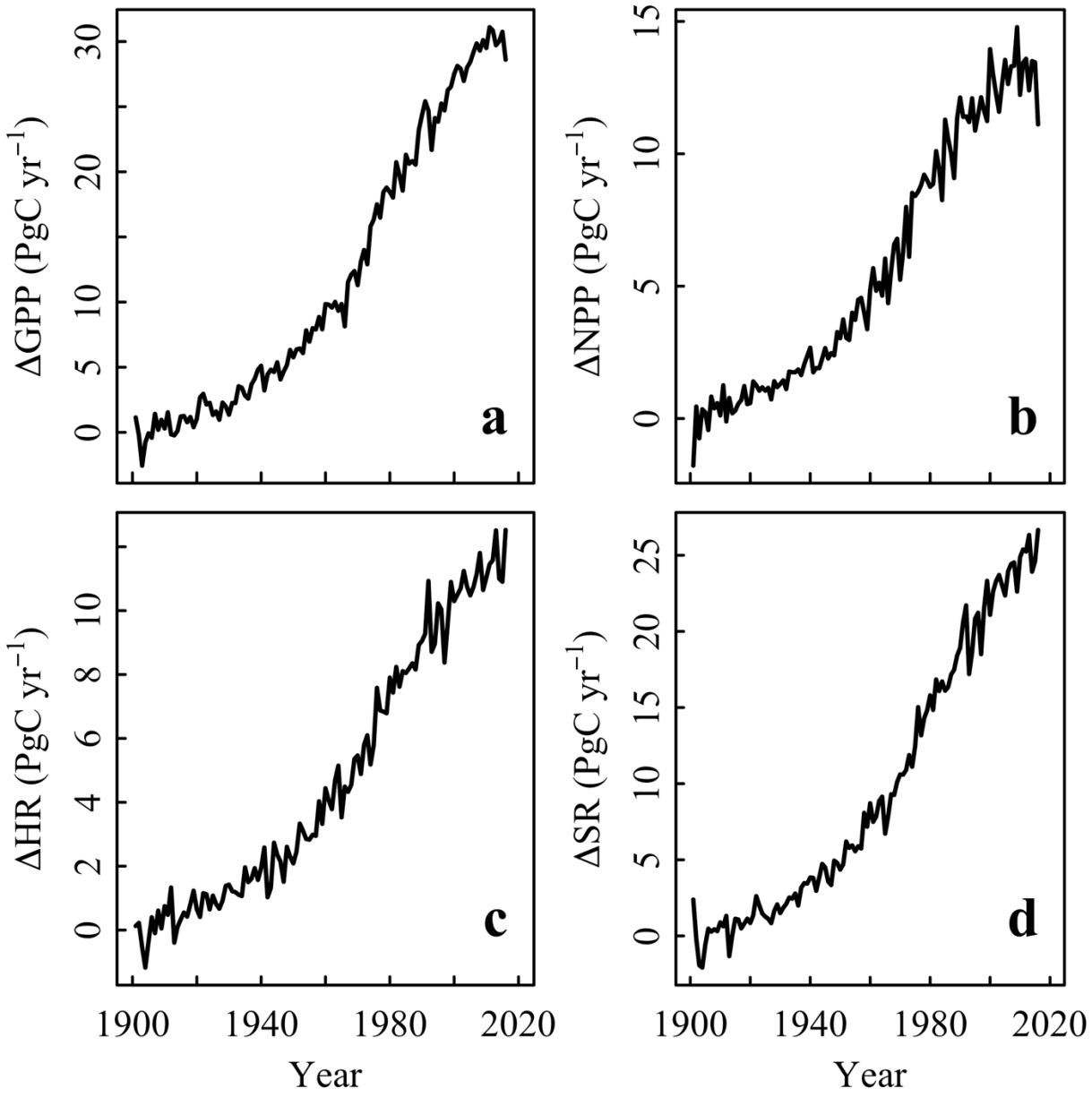

Fig. 4.5. Evolution of annual carbon flux of area-weighted (a) GPP, (b) NPP, (c) HR, and (d) SR simulated by the CLM-Microbe model since 1901. The baseline was the ten-year average of corresponding variables during 1901-1910. GPP, gross primary productivity; NPP, net primary productivity; HR, heterotrophic respiration; SR, soil respiration.

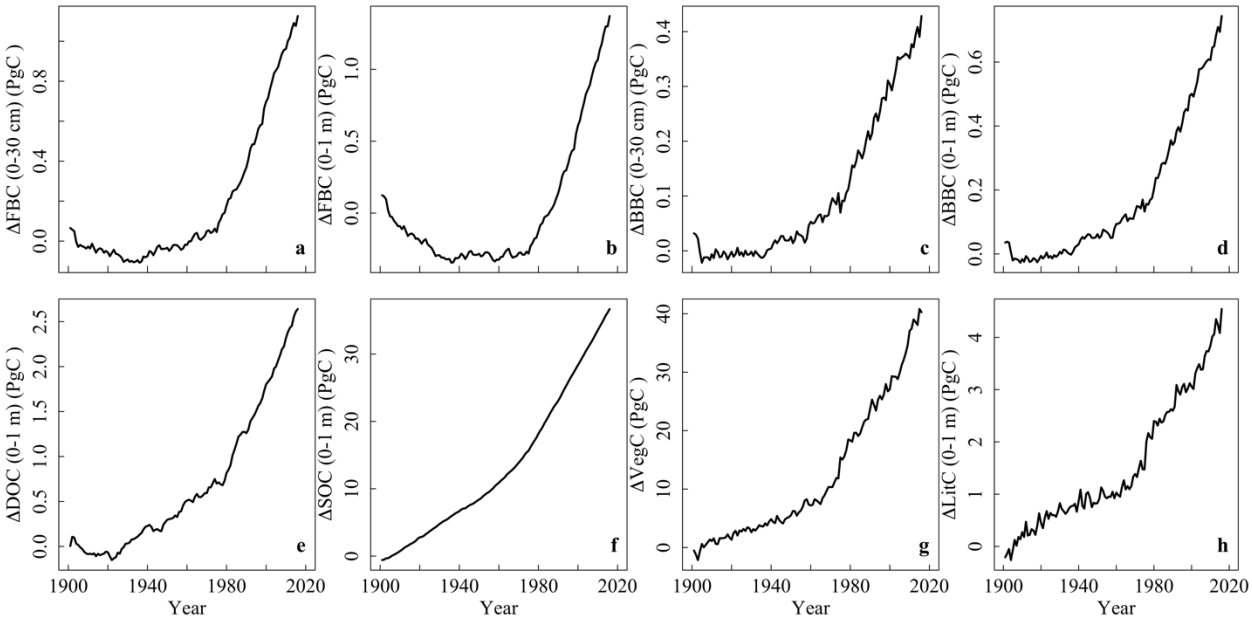

Fig. 4.6. Evolution of global carbon stocks of area-weighted (a) FBC in the top 30 cm, (b) FBC in the top 1 m, (c) BBC in the top 30 cm, (d) BBC in the top 1 m, (e) DOC in the top 1 m, (f) SOC in the top 1 m, and (g) VegC, and (h) LitC in the top 1 m simulated by the CLM-Microbe model since 1901. The baseline was the ten-year average of corresponding variables during 1901-1910. DOC, dissolved organic carbon; SOC, soil organic carbon; FBC, fungal biomass carbon; BBC, bacterial biomass carbon; MBC, microbial biomass carbon; VegC, vegetation carbon; LitC, litter carbon.

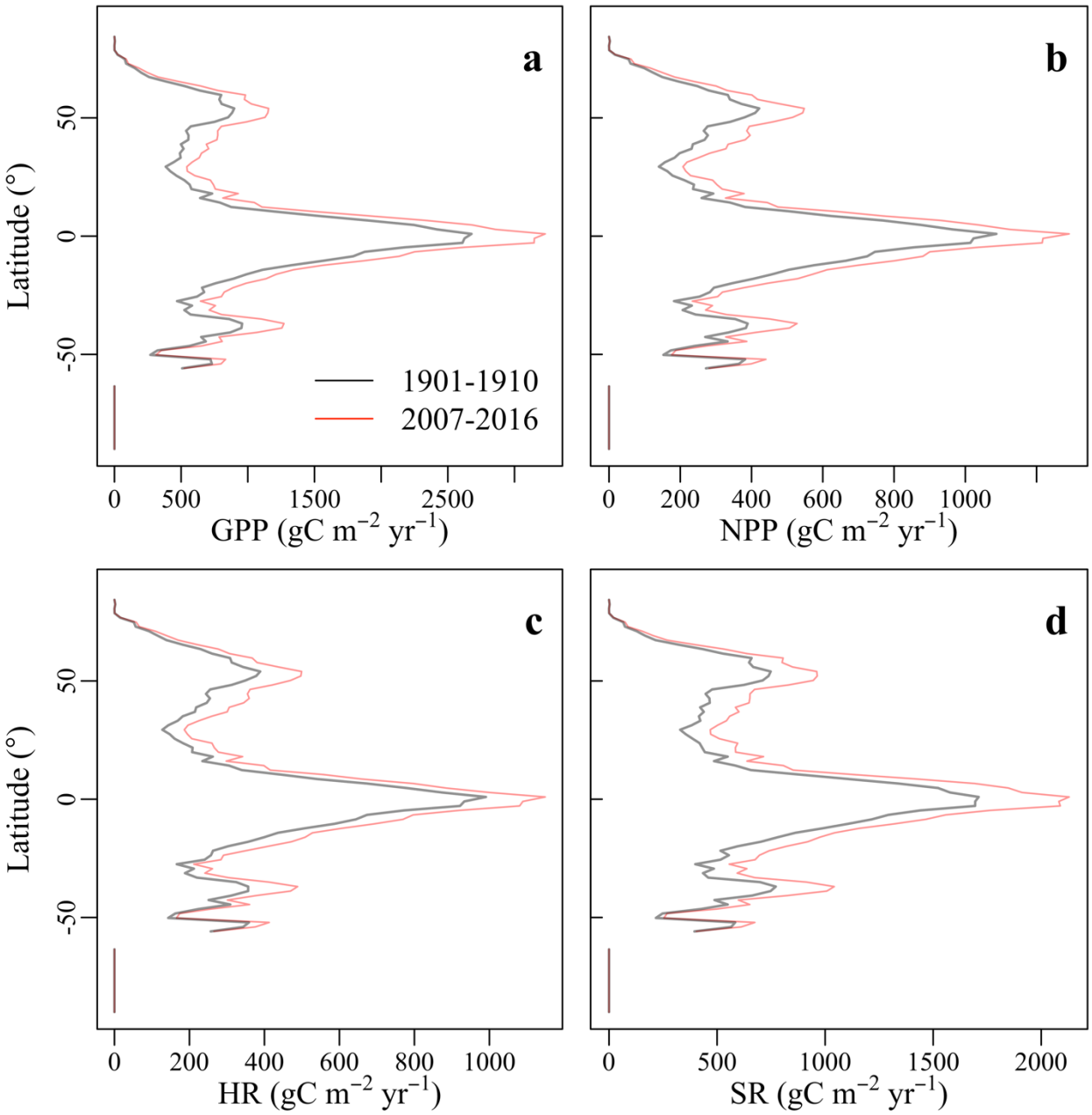

Fig. 4.7. Latitudinal gradients of the CLM-Microbe model simulated ten-year averages of (a) GPP, (b) NPP, (c) HR, and (d) SR during 1901-1910 and 2007-2016. GPP, gross primary productivity; NPP, net primary productivity; HR, heterotrophic respiration; SR, soil respiration.

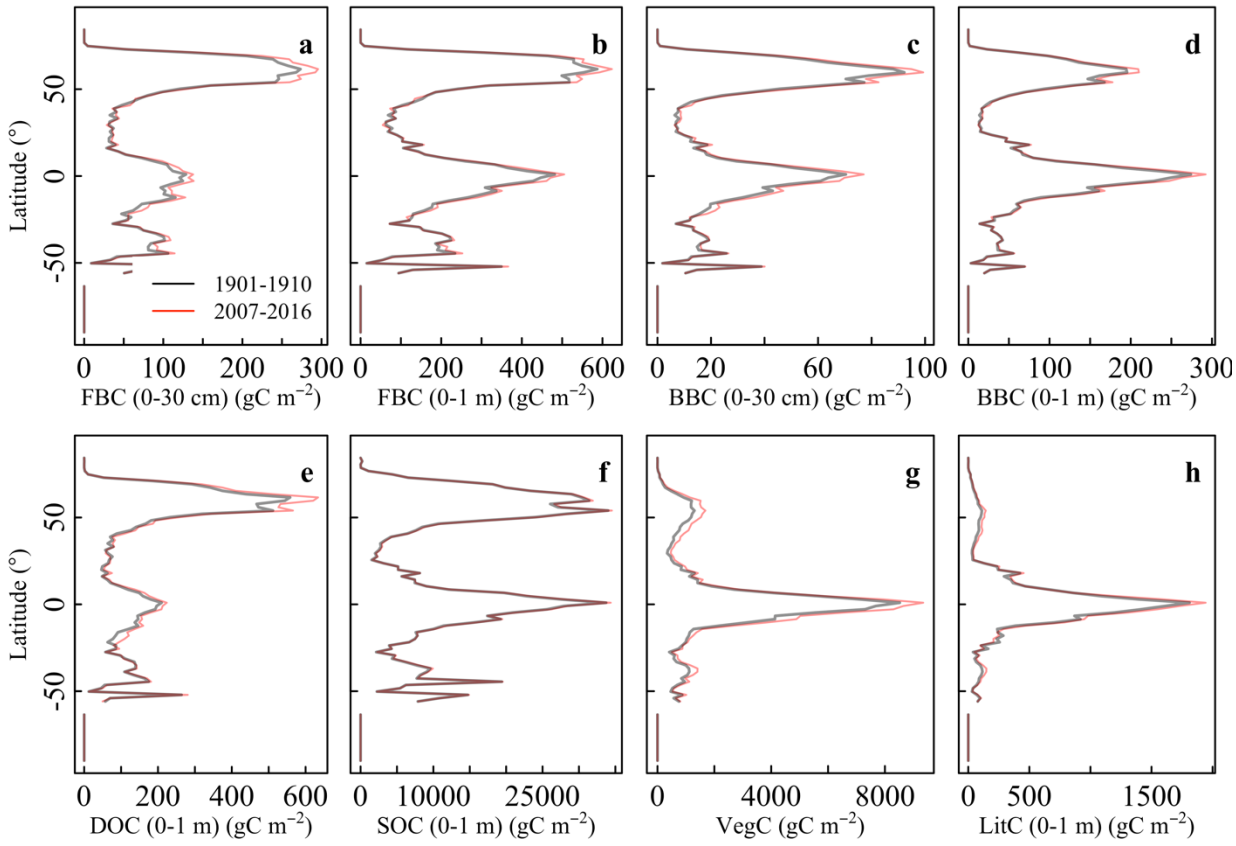

Fig. 4.8. Latitudinal gradients of the CLM-Microbe model simulated ten-year averages (a) FBC in the top 30 cm, (b) FBC in the top 1 m, (c) BBC in the top 30 cm, (d) BBC in the top 1 m, (e) DOC in the top 1 m, (f) SOC in the top 1 m, and (g) VegC, and (h) LitC in the top 1 m during 1901-1910 and 2007-2016. DOC, dissolved organic carbon; SOC, soil organic carbon; FBC, fungal biomass carbon; BBC, bacterial biomass carbon; MBC, microbial biomass carbon; VegC, vegetation carbon; LitC, litter carbon.

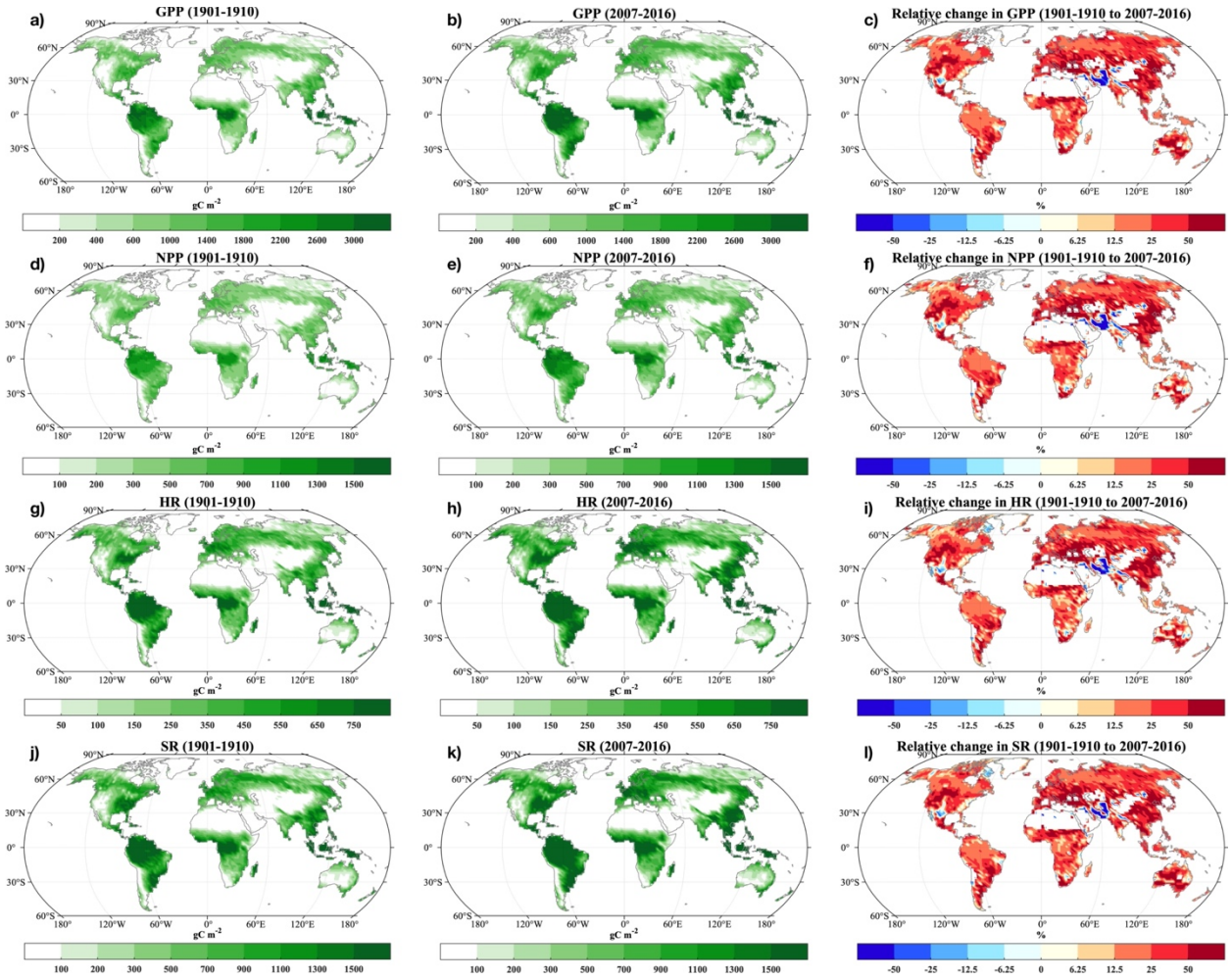

Fig. 4.9. Ten-year averages of (a-b) GPP, (d-e) NPP, (g-h) HR, and (j-k) SR during (a, d, g, and j) 1901-1910 and (b, e, h, and k) 2007-2016 and relative changes of (c) GPP, (f) NPP, (i) HR, and (l) SR by 2007-2016 relative to 1901-1910. GPP, gross primary productivity; NPP, net primary productivity; HR, heterotrophic respiration; SR, soil respiration.

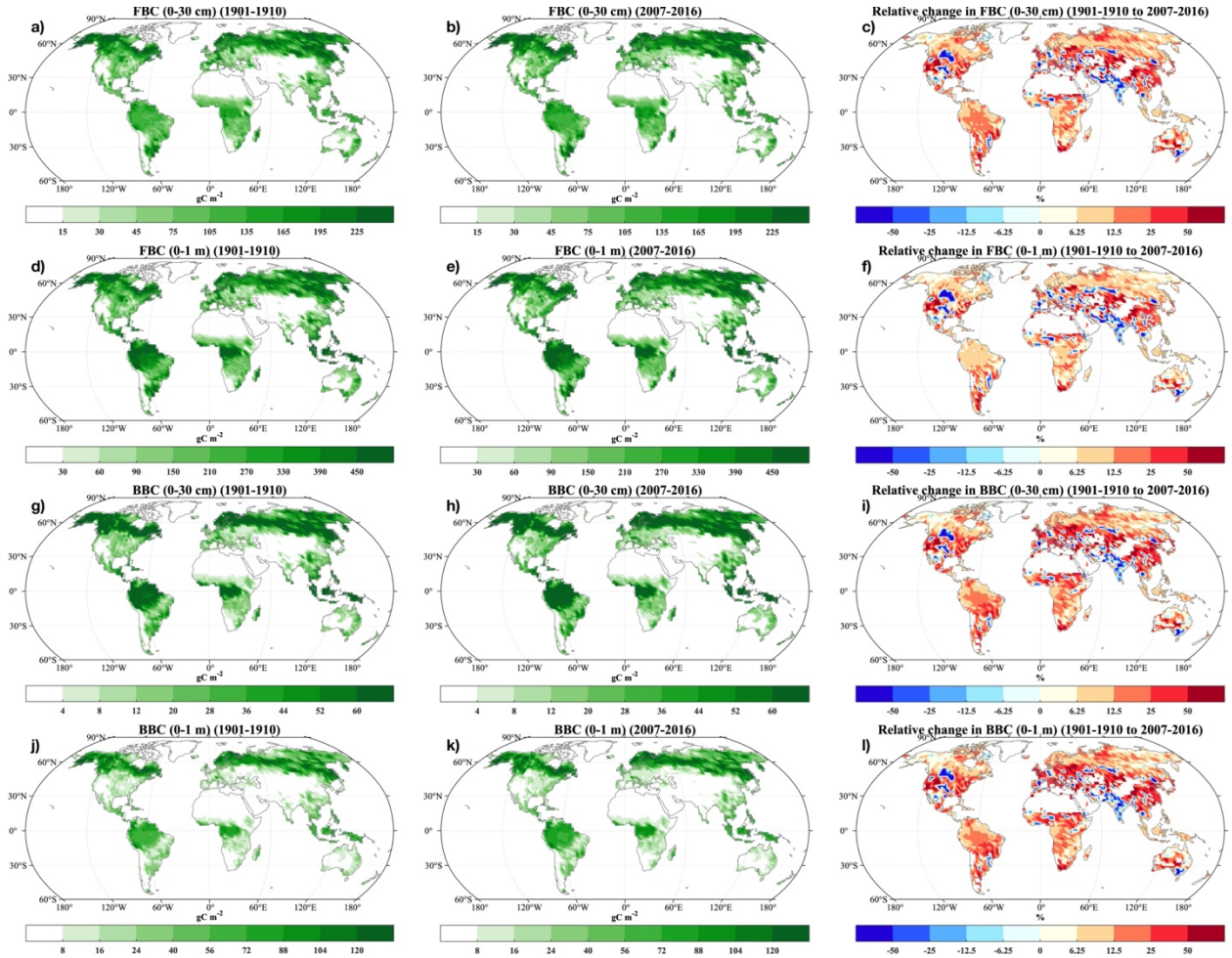

Fig. 4.10. Ten-year averages of (a-b) FBC in the top 30 cm, (d-e) FBC in the top 1 m, (g-h) BBC in the top 30 cm, and (j-k) BBC in the top 1 m during (a, d, g, and j) 1901-1910 and (b, e, h, and k) 2007-2016 and relative changes of (c) GPP, (f) NPP, (i) HR, and (l) SR by 2007-2016 relative to 1901-1910. FBC, fungal biomass carbon; BBC, bacterial biomass carbon.

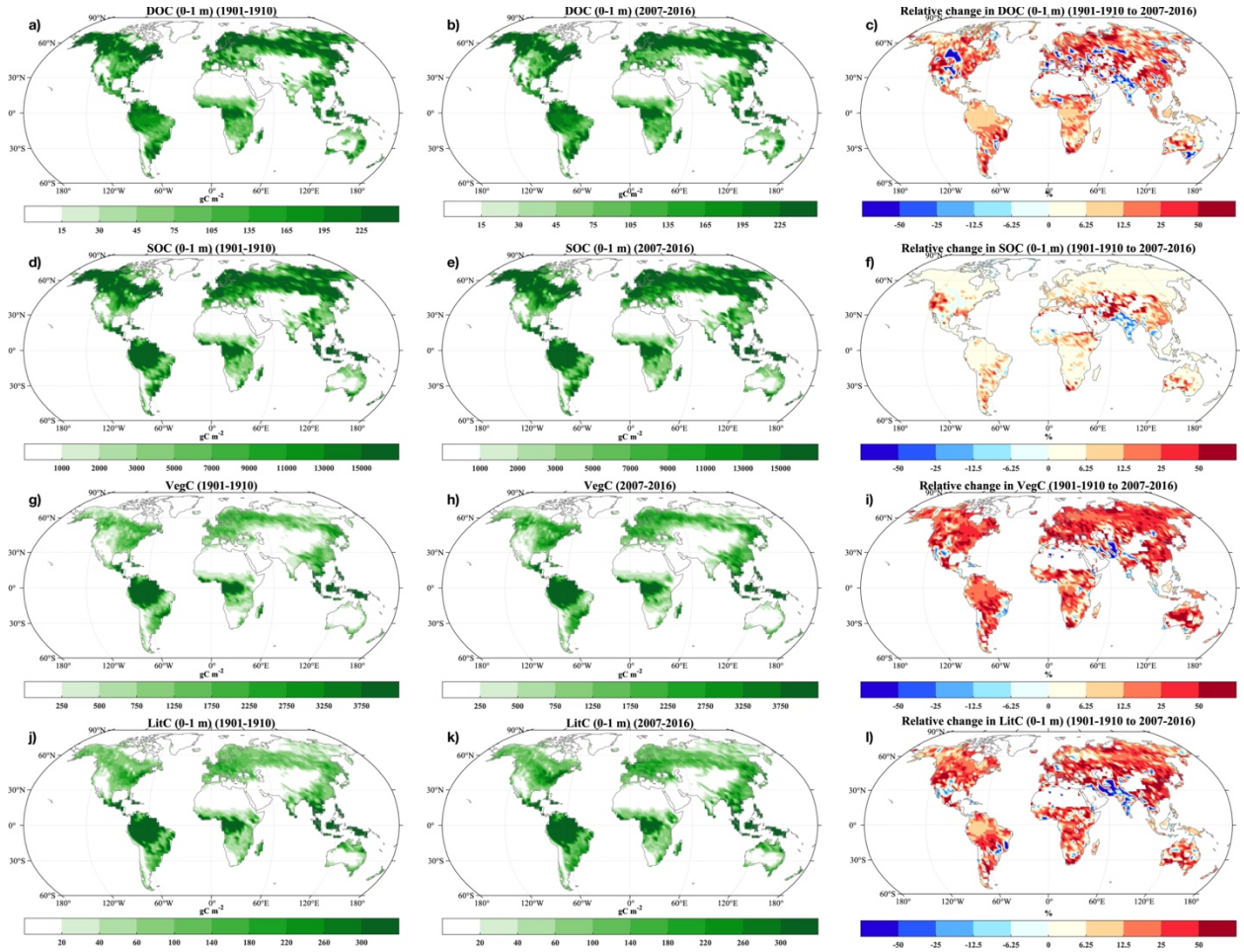

Fig. 4.11. Ten-year averages of (a-b) DOC in the top 1 m, (d-e) SOC in the top 1 m, (g-h) VegC, and (j-k) LitC in the top 1 m during (a, d, g, and j) 1901-1910 and (b, e, h, and k) 2007-2016 and relative changes of (c) DOC in the top 1 m, (f) SOC in the top 1 m, (i) VegC, and (l) LitC in the top 1 m by 2007-2016 relative to 1901-1910. DOC, dissolved organic carbon; SOC, soil organic carbon; VegC, vegetation carbon; LitC, litter carbon.

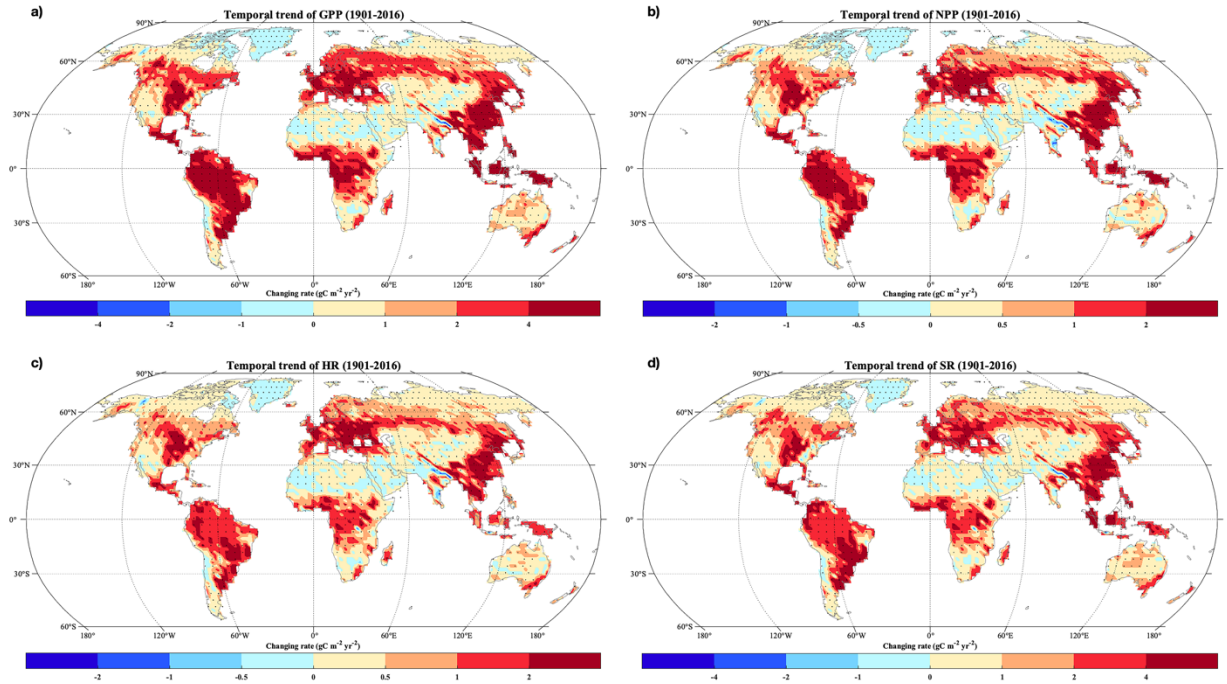

Fig. 4.12. Changing rates of the CLM-Microbe model simulated (a) GPP, (b) NPP, (c) HR, and (d) SR from 1901 to 2016. GPP, gross primary productivity; NPP, net primary productivity; HR, heterotrophic respiration; SR, soil respiration. DOC, dissolved organic carbon; SOC, soil organic carbon; FBC, fungal biomass carbon; BBC, bacterial biomass carbon; MBC, microbial biomass carbon; VegC, vegetation carbon; LitC, litter carbon. Black dots indicate significant regression coefficients (P<0.05).

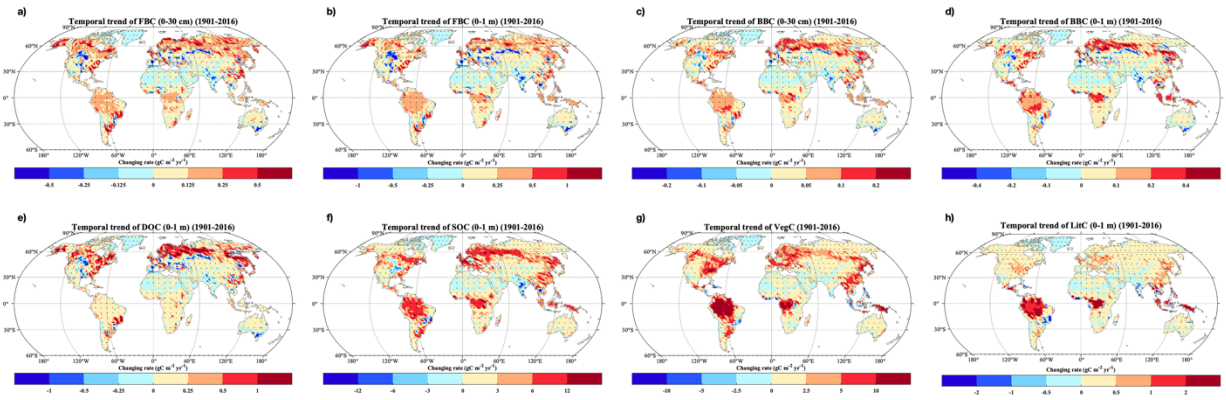

Fig. 4.13. Changing rates of the CLM-Microbe model simulated (a) FBC in the top 30 cm, (b) FBC in the top 1 m, (c) BBC in the top 30 cm, (d) BBC in the top 1 m, (e) DOC in the top 1 m, (f) SOC in the top 1 m, and (g) VegC, and (h) LitC in the top 1 m from 1901 to 2016. DOC, dissolved organic carbon; SOC, soil organic carbon; FBC, fungal biomass carbon; BBC, bacterial biomass carbon; MBC, microbial biomass carbon; VegC, vegetation carbon; LitC, litter carbon. Black dots indicate significant regression coefficients (P<0.05).

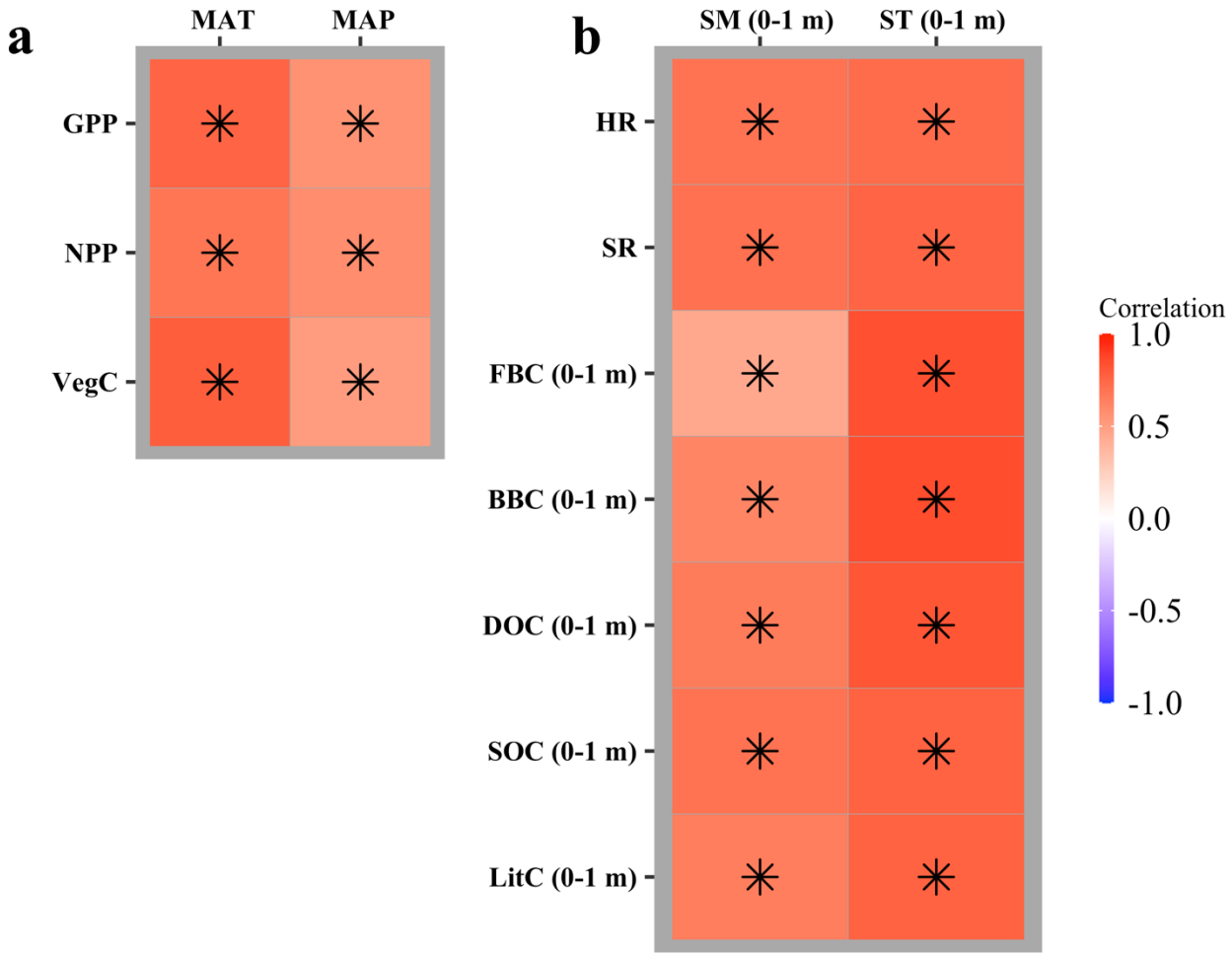

Fig. 4.14. Heatmap showing Pearson's correlation between the CLM-Microbe model simulated (a) GPP, NPP, and VegC and MAT and MAP and (b) HR, SR, FBC in the top 1 m, BBC in the top 1 1m, DOC in the top 1 m, SOC in the top 1 m, and LitC in the top 1 m and SM and ST in the top 1 m from 1901 to 2016. GPP, gross primary productivity; NPP, net primary productivity; HR, heterotrophic respiration; SR, soil respiration; DOC, dissolved organic carbon; SOC, soil organic carbon; FBC, fungal biomass carbon; BBC, bacterial biomass carbon; VegC, vegetation carbon; LitC, litter carbon; MAT, mean annual temperature; MAP, mean annual precipitation; ST, soil temperature; SM, soil moisture. Black stars indicate significant correlates (P<0.05).

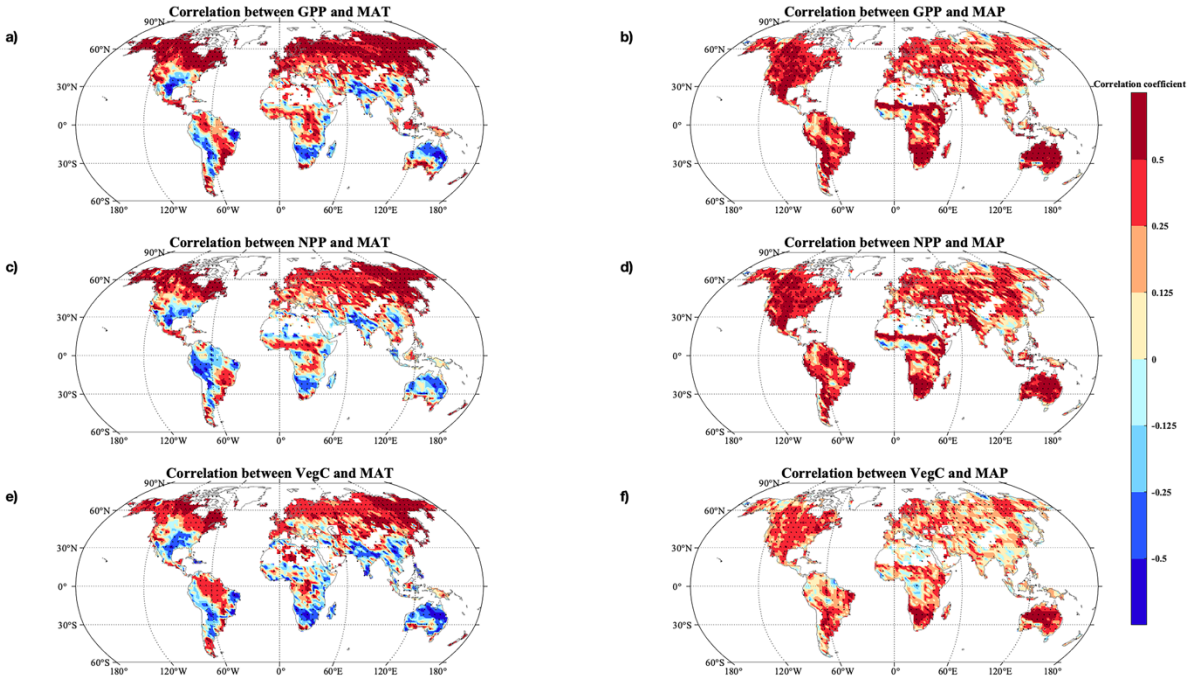

Fig. 4.15. Pearson's correlation between the CLM-Microbe model simulated (a-b) GPP, (c-d) NPP, and (e-f) VegC and (a, c, and e) MAT and (b, d, and f) MAP from 1901 to 2016. GPP, gross primary productivity; NPP, net primary productivity; VegC, vegetation carbon; MAT, mean annual temperature; MAP, mean annual precipitation. Black dots indicate significant correlates (P<0.05).

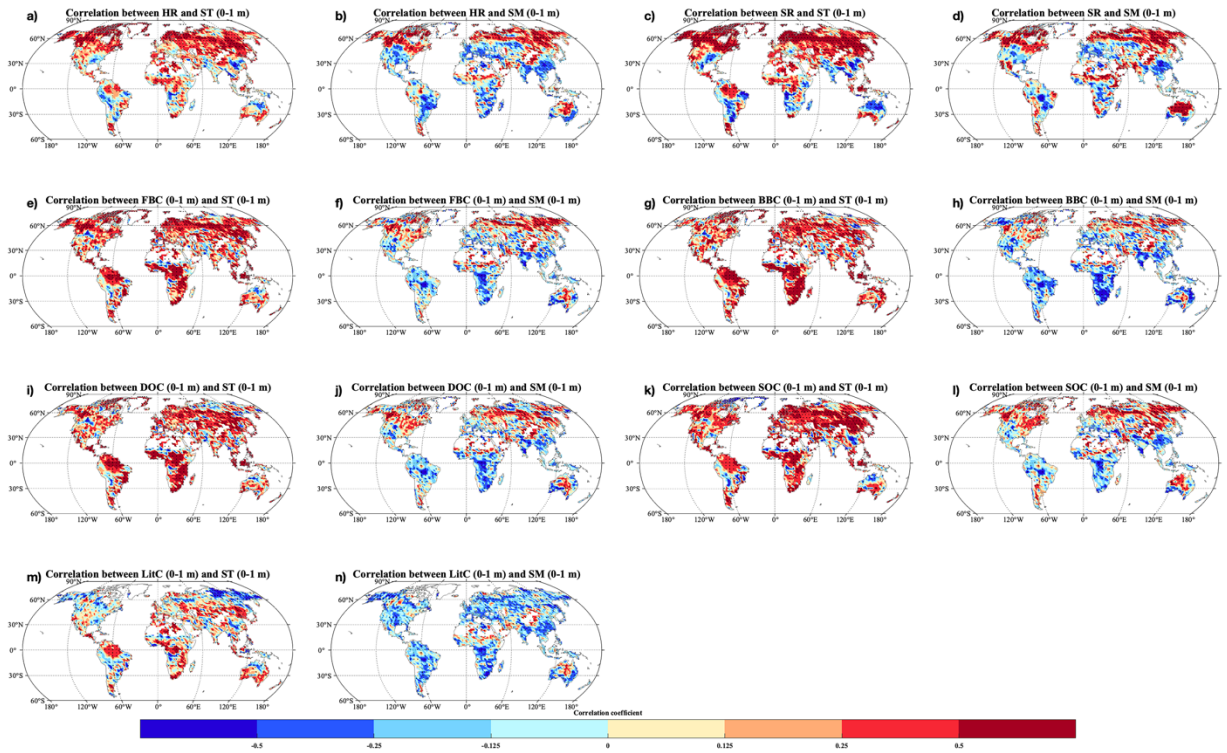

Fig. 4.16. Pearson's correlation between the CLM-Microbe model simulated (a-b) HR, (c-d) SR, (e-f) FBC in the top 1 m, (g-h) BBC in the top 1 m, (i-j) DOC in the top 1 m, (k-l) SOC in the top 1 m, and (m-n) LitC and (a, c, e, g, i, k, and m) ST and (b, d, f, h, j, l, and n) SM in the top 1 m from 1901 to 2016. HR, heterotrophic respiration; SR, soil respiration; DOC, dissolved organic carbon; SOC, soil organic carbon; FBC, fungal biomass carbon; BBC, bacterial biomass carbon; VegC, vegetation carbon; LitC, litter carbon; ST, soil temperature; SM, soil moisture. Black dots indicate significant correlates (P<0.05).

Supplementary material for chapter 4

Fig. 4.S1. Conceptual diagram showing the key processes and the roles of fungi and bacteria in the CLM-Microbe model. CWD, coarse woody debris; SOM, soil organic matter; B, bacteria; F, fungi; DOM, dissolved organic matter. In the CLM-Microbe model, number in the box means turnover time of each pool. Black solid lines indicate transitions in the CLM-Microbe model, which generally represents processes such as 1) decomposition of coarse woody debris, 2) litter 1 decomposition, 3) litter 2 decomposition, 4) litter 3 decomposition, 5) soil organic matter 1 decomposition, 6) soil organic matter 2 decomposition, 7) soil organic matter 3 decomposition, 8) soil organic matter 4 decomposition, 9) fungal and bacterial lysis, 10) dissolved organic matter adsorption, 11) dissolved organic matter uptake by fungal and bacterial, and 12) fungal and bacterial respiration. Red dash lines represent regulatory role of fungi and bacteria on the process, including fungi and bacteria regulation on 13) litter 1, 14) litter 2, 15) litter 3, 16) soil organic matter 1, 17) soil organic matter 2, 18) soil organic matter 3, and 19) soil organic matter 4 decomposition (He et al. 2021).

Fig. 4.S2. Evolution of annual averages of (a) MAT, (b) MAP, (c) ST of top 1m, and (d) SM of top 1m weighted by area in the CLM-Microbe model since 1901. The baseline was the ten-year average of corresponding variables during 1901-1910. MAT, mean annual temperature; MAP, mean annual precipitation; ST, soil temperature; SM, soil moisture.

Fig. 4.S3. Changes of (a) MAT, (b) MAP, (c) ST (0-1 m), and (d) SM (0-1 m) by 2007-2016 relative to 1901-1910. MAT, mean annual temperature; MAP, mean annual precipitation; ST, soil temperature; SM, soil moisture.

Table 4.S1. Key model parameters in processes involving fungal and bacterial biomass

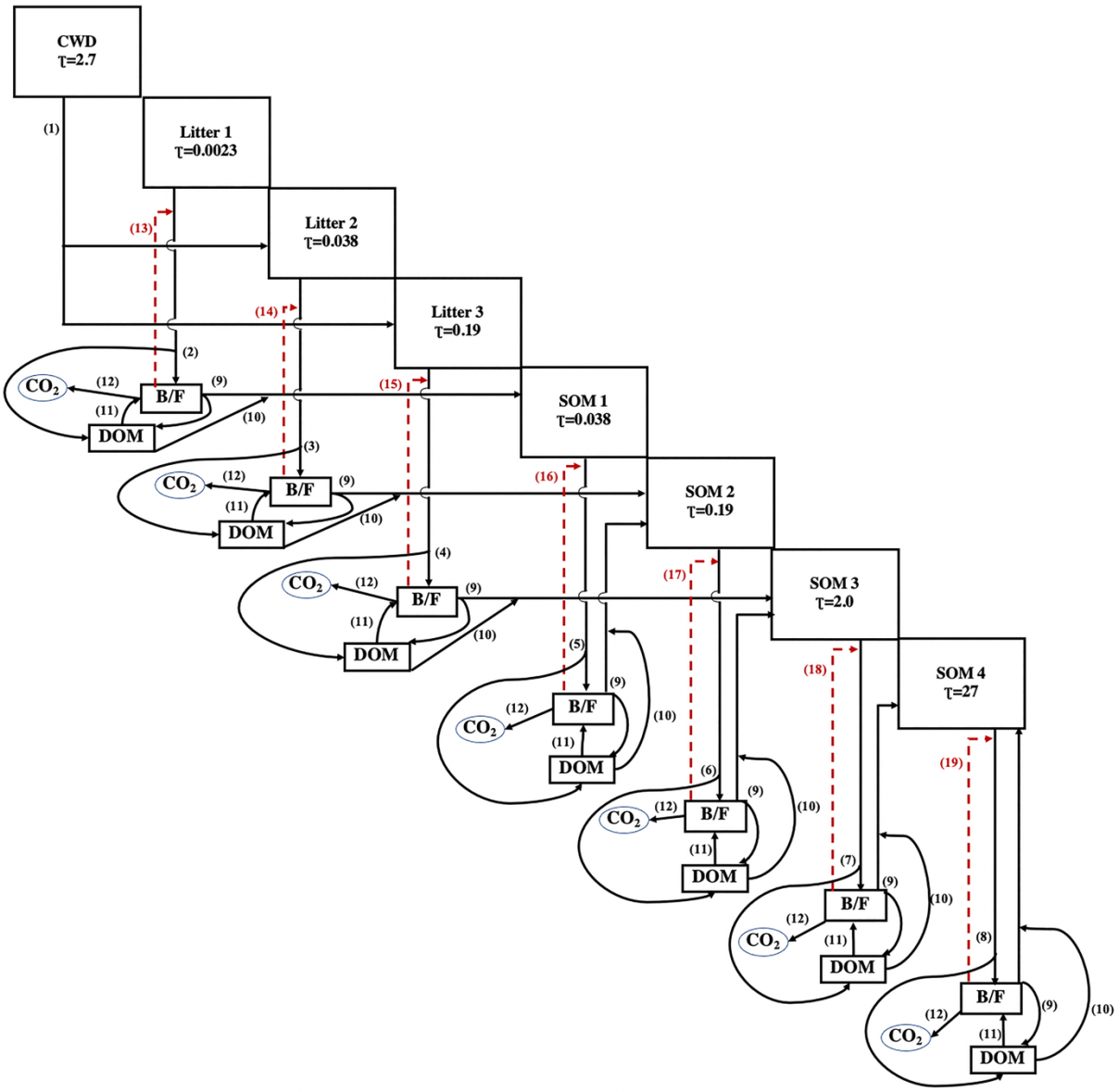

Fig. 4.S1. Conceptual diagram showing the key processes and the roles of fungi and bacteria in the CLM-Microbe model. CWD, coarse woody debris; SOM, soil organic matter; B, bacteria; F, fungi; DOM, dissolved organic matter. In the CLM-Microbe model, number in the box means turnover time of each pool. Black solid lines indicate transitions in the CLM-Microbe model, which generally represents processes such as 1) decomposition of coarse woody debris, 2) litter 1 decomposition, 3) litter 2 decomposition, 4) litter 3 decomposition, 5) soil organic matter 1 decomposition, 6) soil organic matter 2 decomposition, 7) soil organic matter 3 decomposition, 8) soil organic matter 4 decomposition, 9) fungal and bacterial lysis, 10) dissolved organic matter adsorption, 11) dissolved organic matter uptake by fungal and bacterial, and 12) fungal and bacterial respiration. Red dash lines represent regulatory role of fungi and bacteria on the process, including fungi and bacteria regulation on 13) litter 1, 14) litter 2, 15) litter 3, 16) soil organic matter 1, 17) soil organic matter 2, 18) soil organic matter 3, and 19) soil organic matter 4 decomposition (He et al. 2021).

Table 4.S1. Key model parameters in processes involving fungal and bacterial biomass

Symbol	Range [a]	Uni	Description	Reference
k_dom	0.0025-0.5	d^{-1}	decomposition rate constant of DOM	(Cherrier et al., 1996; Kirchman et al., 1991; Wheeler et al., 1996)
k_bacteria	0.00143-2	d^{-1}	lysis rate constant of bacteria	(Moore et al., 2005; Rousk & Bååth, 2007, 2011; Schippers et al., 2005)
k_fungi	0.00027-0.05	d^{-1}	lysis rate constant of fungi	(Moore et al., 2005; Rousk & Bååth, 2011; Thornton & Rosenbloom, 2005; Wallander et al., 2004)
m_rf_s1m	0-1		fraction factor quantifying carbon from SOM1 to microbes	Calibrated
m_rf_s2m	0-1		fraction factor quantifying carbon from SOM2 to microbes	Calibrated
m_rf_s3m	0-1		fraction factor quantifying carbon from SOM3 to microbes	Calibrated
m_rf_s4m	0-1		fraction factor quantifying carbon from SOM4 to microbes	Calibrated
m_batm_f	0-1		fraction factor quantifying carbon respired by bacteria	Calibrated
m_bdom_f	0-1		fraction factor quantifying carbon from DOM to bacteria	Calibrated
m_bs1_f	0-1		fraction factor quantifying carbon from bacteria to SOM1	Calibrated
m_bs2_f	0-1		fraction factor quantifying carbon from bacteria to SOM2	Calibrated
m_bs3_f	0-1		fraction factor quantifying carbon from bacteria to SOM3	Calibrated
m_fatm_f	0-1		fraction factor quantifying carbon respired by fungi	Calibrated
m_fdom_f	0-1		fraction factor quantifying carbon from DOM to fungi	Calibrated
m_fs1_f	0-1		fraction factor quantifying carbon from fungi to SOM1	Calibrated
m_fs2_f	0-1		fraction factor quantifying carbon from fungi to SOM2	Calibrated
m_fs3_f	0-1		fraction factor quantifying carbon from fungi to SOM3	Calibrated
m_domb_f	0-1		fraction factor quantifying carbon from DOM to bacteria	Calibrated
m_domf_f	0-1		fraction factor quantifying carbon from DOM to fungi	Calibrated
m_doms1_f	0-1		fraction factor quantifying carbon from DOM to SOM1	Calibrated
m_doms2_f	0-1		fraction factor quantifying carbon from DOM to SOM2	Calibrated
m_doms3_f	0-1		fraction factor quantifying carbon from DOM to SOM3	Calibrated
cn_bacteria	3-12		C:N ratio of bacteria	(Strickland & Rousk, 2010)
cn_fungi	3-60		C:N ratio of fungi	(Strickland & Rousk, 2010)
cn_dom	4.2-185		C:N ratio of DOM	(Sinsabaugh et al., 2016)
CUEmax	0.46-0.9		maximum carbon use efficiency of microbes	(Gommers et al., 1988; Sinsabaugh et al., 2013; Sinsabaugh et al., 2016)

[a]The values may not be the same as those from literature sources due to unit conversion.

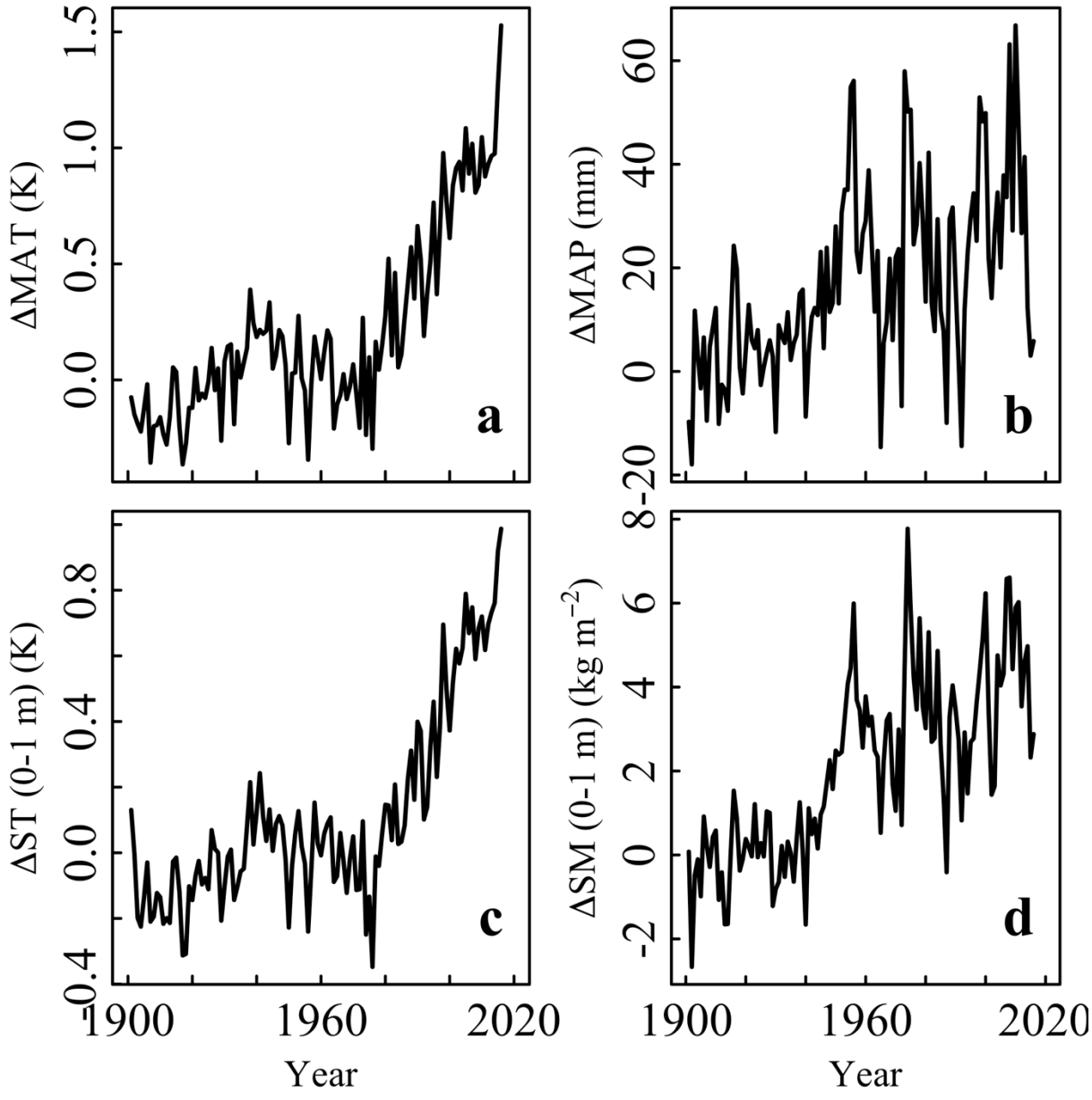

Fig. 4.S2. Evolution of annual averages of (a) MAT, (b) MAP, (c) ST of top 1m, and (d) SM of top 1m weighted by area in the CLM-Microbe model since 1901. The baseline was the ten-year average of corresponding variables during 1901-1910. MAT, mean annual temperature; MAP, mean annual precipitation; ST, soil temperature; SM, soil moisture.

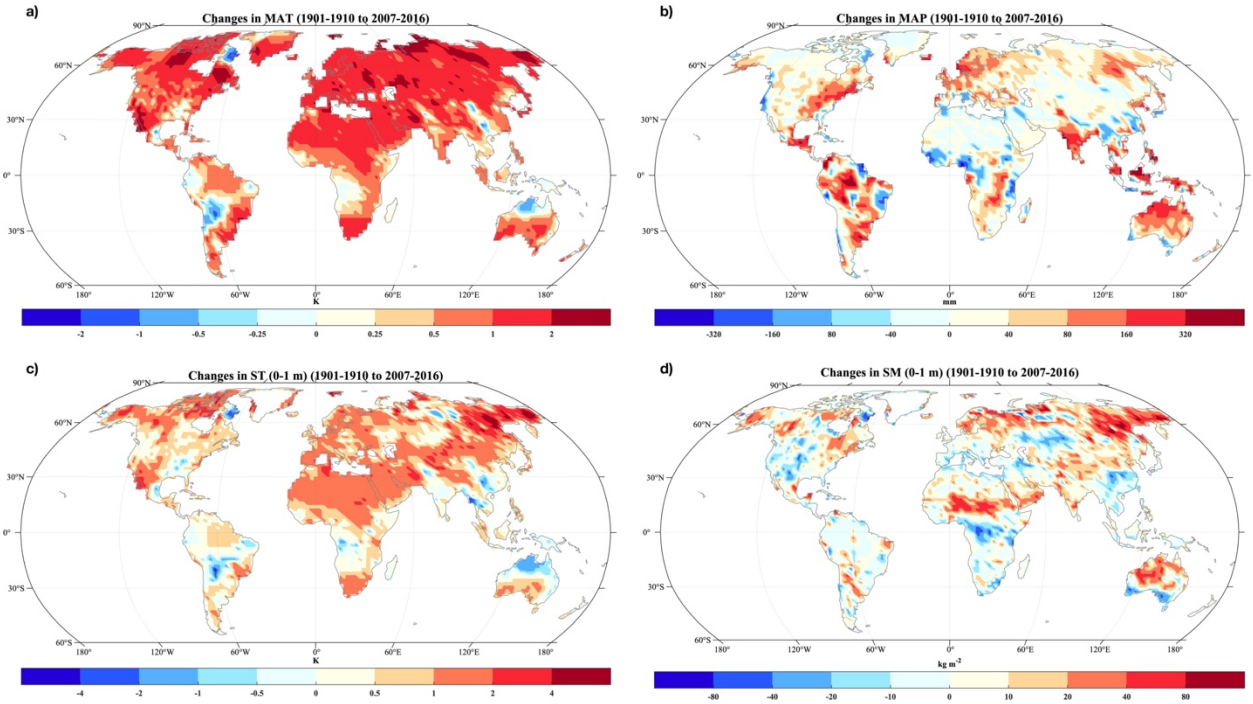

Fig. 4.S3. Changes of (a) MAT, (b) MAP, (c) ST (0-1 m), and (d) SM (0-1 m) by 2007-2016 relative to 1901-1910. MAT, mean annual temperature; MAP, mean annual precipitation; ST, soil temperature; SM, soil moisture.

References for supplementary materials in chapter 4

Cherrier, J., J. Bauer, and E. Druffel. 1996. Utilization and turnover of labile dissolved organic matter by bacterial heterotrophs in eastern North Pacific surface waters. Marine Ecology Progress Series **139**:267-279.

Gommers, P. J. F., B. J. v. Schie, J. P. v. Dijken, and J. G. Kuenen. 1988. Biochemical limits to microbial growth yields: An analysis of mixed substrate utilization. Biotechnology and Bioengineering **32**:86-94.

He, L., D. A. Lipson, J. L. M. Rodrigues, M. Mayes, R. G. Björk, B. Glaser, P. Thornton, and X. Xu. 2021. Dynamics of Fungal and Bacterial Biomass Carbon in Natural Ecosystems: Site-level Applications of the CLM-Microbe Model. Journal of Advances in Modeling Earth Systems **13**:e2020MS002283.

Kirchman, D. L., Y. Suzuki, C. Garside, and H. W. Ducklow. 1991. High turnover rates of dissolved organic carbon during a spring phytoplankton bloom. Nature **352**:612-614.

Moore, J. C., K. McCann, and P. C. de Ruiter. 2005. Modeling trophic pathways, nutrient cycling, and dynamic stability in soils. Pedobiologia **49**:499-510.

Rousk, J., and E. Bååth. 2007. Fungal biomass production and turnover in soil estimated using the acetate-in-ergosterol technique. Soil Biology and Biochemistry **39**:2173-2177.

Rousk, J., and E. Bååth. 2011. Growth of saprotrophic fungi and bacteria in soil. FEMS Microbiology Ecology **78**:17-30.

Schippers, A., L. N. Neretin, J. Kallmeyer, T. G. Ferdelman, B. A. Cragg, R. John Parkes, and B. B. Jørgensen. 2005. Prokaryotic cells of the deep sub-seafloor biosphere identified as living bacteria. Nature **433**:861-864.

Sinsabaugh, R. L., S. Manzoni, D. L. Moorhead, and A. Richter. 2013. Carbon use efficiency of microbial communities: stoichiometry, methodology and modelling. Ecology Letters **16**:930-939.

Sinsabaugh, R. L., B. L. Turner, J. M. Talbot, B. G. Waring, J. S. Powers, C. R. Kuske, D. L. Moorhead, and J. J. F. Shah. 2016. Stoichiometry of microbial carbon use efficiency in soils. Ecological Monographs **86**:172-189.

Strickland, M. S., and J. Rousk. 2010. Considering fungal: bacterial dominance in soils–methods, controls, and ecosystem implications. Soil Biology and Biochemistry **42**:1385-1395.

Thornton, P. E., and N. A. Rosenbloom. 2005. Ecosystem model spin-up: Estimating steady state conditions in a coupled terrestrial carbon and nitrogen cycle model. Ecological Modelling **189**:25-48.

Wallander, H. a., H. Göransson, and U. Rosengren. 2004. Production, standing biomass and natural abundance of 15 N and 13 C in ectomycorrhizal mycelia collected at different soil depths in two forest types. Oecologia **139**:89-97.

Wheeler, P. A., M. Gosselin, E. Sherr, D. Thibaultc, D. L. Kirchman, R. Benner, and T. E. Whitledge. 1996. Active cycling of organic carbon in the central Arctic Ocean. Nature **380**:697-699.

Conclusion

This dissertation investigated microbial controls on the terrestrial C cycle at multiple scales. I first investigated the biogeographical patterns of fungal and bacterial biomass C and their controls based on a synthesized global dataset. Second, I parameterized the CLM-Microbe model using the time-series FBC and BBC data from nine major natural terrestrial biomes. Then, I further conducted the model sensitivity analysis for simulating C cycling with a focus on microbial mechanisms. Third, I applied the CLM-Microbe model to assess the effects of seasonality on the soil C cycle in terrestrial ecosystems. Lastly, I investigated the historical dynamics of terrestrial C fluxes and pools using the CLM-Microbe model. The key conclusions are listed as below,

1. The FBC, BBC, and F:B ratio showed clear biogeographic patterns at a global scale.
2. The FBC and BBC were primarily determined by edaphic properties, whereas F:B ratio is primarily driven by climatic variables.
3. We produced the first global maps of BBC and FBC in 0-30 cm topsoil and estimated global FBC and BBC as 12.56 (6.64 ~ 16.42) PgC and 4.34 (0.47 ~ 10.26) PgC, respectively, in 0-30 cm topsoil.
4. Model parameterization suggested the reasonable performance of the CLM-Microbe model in capturing the seasonal variation of FBC and BBC and good performance in simulating FBC and BBC across biomes.
5. Sensitivity analysis showed that microbial turnover rates, biomass carbon-to-nitrogen ratio, and carbon assimilation efficiency were the most critical parameters regulating FBC and BBC dynamics.
6. Removing soil microbial biomass seasonality underestimated soil respiratory fluxes across biomes, leading to overestimated soil organic C pool size in the CLM-Microbe model.
7. The CLM-Microbe model can well reproduce the distribution of vegetation (GPP and NPP), soil (HR, SR, DOC, and SOC), and microbial (FBC, BBC, and MBC) C variables.

8. Vegetation (GPP, NPP, and VegC), litter (LitC in 0-1 m), soil (HR, SR, and DOC and SOC in the top 1 m), and microbial (FBC and BBC in the top 30 cm and 1 m) C variables increased from 1901 to 2016.
9. The absolute increases of C fluxes and pools were generally the largest in Asia and South America, particularly in east Asia and central and northern South America.
10. Relative changes of C fluxes and pools at the continental level varied among variables, with the largest relative increases of GPP, NPP, HR, and SR in Asia and Europe (particularly east Asia and southern and central Europe), FBC (0-30 cm and 0-1 m) in South America (particularly central and east coast of South America), BBC (0-30 cm and 0-1 m) in Europe (particularly central and northern Europe), DOC (0-1 m) in South America and Europe (particularly east coast of South America and northern Europe), SOC (0-1 m) in Africa (particularly central and southern Africa), and VegC and LitC (0-1 m) in Europe (particularly southern and central Europe).
11. The increase in GPP, NPP, and VegC were significantly related to rising MAT and MAP, while increases in FBC and BBC in the top 30 cm and FBC, BBC, DOC, SOC, and LitC in the top 1 m were closely associated with increasing C input from vegetation and SM and ST in the top 1 m.

This dissertation represents one of the first attempts to investigate microbial control over the terrestrial C cycle at multiple scales. The improvements in understanding fungal and bacterial biogeography and microbial role in the terrestrial C cycle will broaden our knowledge of microbial contributions to climate change and rethink the functional role of soil microbes in the C cycle. The explicit representation of microbial processes will likely bring more robust abilities to ESMs to better simulate and project the climate system.